

PETROLEUM SYSTEM MODELLING OF POTENTIAL LOWER
JURASSIC SOURCE ROCKS ALONG THE SCOTIAN MARGIN

by

Juan Carlos Wong

Submitted in partial fulfilment of the requirements
for the degree of Master of Science

at

Dalhousie University
Halifax, Nova Scotia
August 2018

© Copyright by Juan Carlos Wong, 2018

Dedication Page

I am dedicating this thesis to my father and brother. Although they no longer in this world, their memories continue in my life. First and foremost, to my father that taught me the values of hard work and perseverance, who always kept pushing me to study and learn more in life and school. Now that I have completed this thesis is an outcome from that perseverance and hard work.

Next, to my brother whose life was cut short, whom I believe his knowledge was vast; I would never be able to share all of my accomplishments to him.

Thank you.

Table of Contents

Dedication Page	ii
List of Tables	v
List of Figures	vi
Abstract	xi
List of Abbreviations Used	xii
Acknowledgements	xiii
Chapter 1: Introduction	1
1.1 Introduction	1
1.2 Problem Statement, Objective and Hypothesis.....	5
1.3 Thesis Organization.....	6
1.4 Background Geology	6
1.5 Previous Studies.....	11
1.6 Source Rock.....	12
Chapter 2: Data and Methods	15
2.1 Introduction	15
2.2 Data.....	15
2.3 Methods.....	18
2.3.1 Input.....	19
2.3.2 Simulation	24
2.3.3 Salt modelling.....	25
2.3.4 Calibration.....	27
2.3.5 Uncertainty	27
Chapter 3: Results	29
3.1 Introduction	29
3.2 Paleo Water Depth (PWD)	29
3.3 Sediment-Water Interface Temperature (SWIT)	30
3.4 Uncertainty Tests	31
3.5 1D Models Calibrations.....	32
3.6 2D NovaSPAN Models	50
3.7 Summary of the Base Case 2D Models	94
3.7.1 NovaSPAN 1100	94
3.7.2 NovaSPAN 1400	97
3.7.3 NovaSPAN 1800	99
3.7.4 NovaSPAN 2000	101
3.7.5 Extrapolation of the Lower Jurassic source rock interval	102
3.8 Sensitivities to Base Case Model.....	114
Chapter 4: Discussion	130
4.1 Source Rock Parameters	130

4.2	The Impact of Salt Tectonics	134
4.3	Challenges	138
4.4	Distribution of the Lower Jurassic Source Rock Maturity of the Scotian Basin ...	140
4.5	Lower Jurassic Source Rock Maturity on the Conjugate Margin	143
4.6	Key Sensitivities.....	144
Chapter 5: Conclusion.....		145
5.1	Future Work	146
References		148
Appendix A: Borehole Information.....		155
Appendix B: Borehole Temperature & Vitrinite Reflectance.....		160
Appendix C: Python Code.....		179
Appendix D: Uncertainty Tests with Petro Risk		182
D.1	Calibration.....	182
D.2	NovaSPAN 1100	183
D.3	NovaSPAN 1400	185
D.4	NovaSPAN 1800	188
D.5	NovaSPAN 2000	191
Appendix E: 2D Modelling Results.....		Supplemental File
E.1	NovaSPAN 1100	Supplemental File
E.2	NovaSPAN 1400	Supplemental File
E.3	NovaSPAN 1800	Supplemental File
E.4	NovaSPAN 2000	Supplemental File
Appendix F: Composite Maps.....		Supplemental File
F.1	Base Case Scenario.....	Supplemental File
F.2	Sensitivity Maps	Supplemental File

List of Tables

Table 1.1: Source rock geochemical properties used as the parameter inputs for the Lower Jurassic Source Rock interval in PetroMod (Wach et al., 2018).....	3
Table 2.1: List of offshore boreholes used in this study for each model, this data was collected from the Basin Database (http://basin.gdr.nrcan.gc.ca/index_e.php).....	16
Table 2.2: Description of the 2D models built in this study, with the offshore boreholes associated for each model, and the run type and migration method of simulation run in these models.	19
Table 2.3: Latitude of the offshore borehole location used to calculate the paleo sediment-water interface temperature trend in PetroMod.....	22
Table 2.4: Input Value used for McKenzie Crustal Model.	24
Table 3.1: Summary of maturity of the Lower Jurassic rocks for the model 1100.	95
Table 3.2: Summary of maturity of the Lower Jurassic rocks for the model 1400.	97
Table 3.3: Summary of maturity of the Lower Jurassic rocks for the model 1800.	99
Table 3.4: Summary of maturity of the Lower Jurassic rocks for the model 2000 in the slope region.....	101
Table 4.1: Summary the Lower Jurassic rocks maturity for the models 1100, 1400, 1600, 1800, and 2000.	140
Table 4.2: Modelling outcomes comparison between this study and the PFA (2011).....	143

List of Figures

Figure 1.1: Location of the Study Area.	2
Figure 1.2: Rock-Eval Pyrolysis graph from the data collected at Aït Moussa, Morocco.	4
Figure 1.3: Paleogeographic reconstruction of the Lower Jurassic (Wach et al., 2018) showing the location of Aït Moussa.....	9
Figure 1.4: Composite comparison of two stratigraphic charts.	9
Figure 2.1: Composite map of sediment thickness map of the Scotian Basin, with contrasting salt tectonic styles.....	17
Figure 2.2: Flowchart of methodology.....	18
Figure 2.3: Depositional environments for a continental margin setting, modified after Veecken and Moerkerken (2013).....	21
Figure 2.4: Normal Gauss distribution for the uncertainty parameter of heat flow and heat flow Time Shift.....	28
Figure 3.1: Paleo water depth of each NovaSPAN 1800.....	30
Figure 3.2: White line is the paleo sea level temperature at 43°N modern latitude in the Northern hemisphere near the Northern American continent, based on Wygrala (1989).31	31
Figure 3.3: 1D models results for Bonnet P-23.	34
Figure 3.4: 1D models results for Glooscap C-63.....	36
Figure 3.5: 1D models results for Moheida P-15.	37
Figure 3.6: 1D models results for Mohican I-100.....	38
Figure 3.7: 1D models results for Torbrook C-15.....	39
Figure 3.8: 1D models results for Bluenose G-47.	41
Figure 3.9: 1D models results for Bluenose G-47.	42
Figure 3.10: 1D models results for Missisauga H-54.....	43
Figure 3.11: 1D models results for Wyandot E-53.....	44
Figure 3.12: 1D models results for Bluenose G-47.	46
Figure 3.13: 1D models results for Bluenose G-47.	47
Figure 3.14: 1D models results for Sachem D-76.....	48
Figure 3.15: 1D models results for South Griffin J-13.....	49
Figure 3.16: Model of heat flow distribution for NovaSPAN 1100 line.	51
Figure 3.17: Model of temperature distribution for NovaSPAN 1100 line.....	52
Figure 3.18: Model of vitrinite reflectance distribution for NovaSPAN 1100.....	54

Figure 3.19: Model of transformation ratio for Pliensbachian source rock (Type III) for NovaSPAN 1100 line.	55
Figure 3.20: Model of transformation ratio for Pliensbachian source rock (Type II) for NovaSPAN 1100 line.	56
Figure 3.21: Model of transformation ratio for Pliensbachian source rock (Type I) for NovaSPAN 1100 line.	57
Figure 3.22: Model of the critical moment for the Pliensbachian source rock (Type III) for NovaSPAN 1100 line.	58
Figure 3.23: Model of the critical moment for the Pliensbachian source rock (Type II) for NovaSPAN 1100 line.	59
Figure 3.24: Model of the critical moment for the Pliensbachian source rock (Type I) for NovaSPAN 1100 line.	60
Figure 3.25: Model of heat flow distribution for NovaSPAN 1400 line.	62
Figure 3.26: Model of temperature distribution for NovaSPAN 1400 line.	63
Figure 3.27: Model of vitrinite reflectance distribution for NovaSPAN 1400 line.	65
Figure 3.28: Model of transformation ratio for Pliensbachian source rock (Type III) for NovaSPAN 1400 line.	66
Figure 3.29: Model of transformation ratio for Pliensbachian source rock (Type II) for NovaSPAN 1400 line.	67
Figure 3.30: Model of transformation ratio for Pliensbachian source rock (Type I) for NovaSPAN 1400 line.	68
Figure 3.31: Model of the critical moment for the Pliensbachian source rock (Type III) for NovaSPAN 1400 line.	69
Figure 3.32: Model of the critical moment for the Pliensbachian source rock (Type III) for NovaSPAN 1400 line.	70
Figure 3.33: Model of the critical moment for the Pliensbachian source rock (Type I) for NovaSPAN 1400 line.	71
Figure 3.34: Model of heat flow distribution for NovaSPAN 1800 line.	73
Figure 3.35: Model of temperature distribution for NovaSPAN 1800 line.	74
Figure 3.36: Model of vitrinite reflectance distribution for NovaSPAN 1800 line.	76
Figure 3.37: Model of transformation ratio for Pliensbachian source rock (Type III) for NovaSPAN 1800 line.	77
Figure 3.38: Model of transformation ratio for Pliensbachian source rock (Type II) for NovaSPAN 1800 line.	78
Figure 3.39: Model of transformation ratio for Pliensbachian source rock (Type I) for NovaSPAN 1800 line.	79
Figure 3.40: Model of the critical moment for the Pliensbachian source rock (Type III) for NovaSPAN 1800 line.	80

Figure 3.41: Model of the critical moment for the Pliensbachian source rock (Type II) for NovaSPAN 1800 line.	81
Figure 3.42: Model of the critical moment for the Pliensbachian source rock (Type I) for NovaSPAN 1800 line.	82
Figure 3.43: Model of heat flow distribution for NovaSPAN 2000 line.	84
Figure 3.44: Model of temperature distribution for NovaSPAN 2000 line.	85
Figure 3.45: Model of vitrinite reflectance distribution for NovaSPAN 2000 line.	87
Figure 3.46: Model of transformation ratio for Pliensbachian source rock (Type III) for NovaSPAN 2000 line.	88
Figure 3.47: Model of transformation ratio for Pliensbachian source rock (Type II) for NovaSPAN 2000 line.	89
Figure 3.48: Model of transformation ratio for Pliensbachian source rock (Type I) for NovaSPAN 2000 line.	90
Figure 3.49: Model of the critical moment for the Pliensbachian source rock (Type III) for NovaSPAN 2000 line.	91
Figure 3.50: Model of the critical moment for the Pliensbachian source rock (Type II) for NovaSPAN 2000 line.	92
Figure 3.51: Model of the critical moment for the Pliensbachian source rock (Type I) for NovaSPAN 2000 line.	93
Figure 3.52: This a 1D model extraction from the 2D NovaSPAN 1100 model at the slope region (50 Km).	96
Figure 3.53: This a 1D model extraction from the 2D NovaSPAN 1100 model in the abyssal region (110 Km).	96
Figure 3.54: This a 1D model extraction from the 2D NovaSPAN 1400 model at the slope region (80 Km)	98
Figure 3.55: This a 1D model extraction from the 2D NovaSPAN 1400 model in the abyssal region (140 Km).	98
Figure 3.56: This a 1D model extraction from the 2D NovaSPAN 1800 model at the slope region (180 Km).	100
Figure 3.57: This a 1D model extraction from the 2D NovaSPAN 1800 model in the abyssal region (245 Km).	100
Figure 3.58: This a 1D model extraction from the 2D NovaSPAN 2000 model at the slope region (125 Km).	102
Figure 3.59: Map of depth below sea level of the Pliensbachian source rock (1 km by 1 km smooth gridded) based on NovaSPAN 1100, 1400, 1600, 1800 and 2000 models.	104
Figure 3.60: Temperature map (1 km by 1 km smooth gridded) at the top of the Pliensbachian source rock based on NovaSPAN 1100, 1400, 1600, 1800 and 2000 models.	105
Figure 3.61: Heat flow map (1 km by 1 km smooth gridded) at the top of the Pliensbachian source rock based on NovaSPAN 1100, 1400, 1600, 1800 and 2000 models.	106

Figure 3.62: Vitrinite reflectance map (1 km by 1 km smooth gridded) at the top of the Pliensbachian source rock based on NovaSPAN 1100, 1400, 1600, 1800 and 2000 models.	107
Figure 3.63: Transformation Ratio map (1 km by 1 km smooth gridded) of the Pliensbachian source rock of kerogen Type I.	108
Figure 3.64: Transformation Ratio map (1 km by 1 km smooth gridded) of the Pliensbachian source rock of kerogen Type II.	109
Figure 3.65: Transformation Ratio map (1 km by 1 km smooth gridded) of the Pliensbachian source rock of kerogen Type III.	110
Figure 3.66: Critical Moment map (1 km by 1 km smooth gridded) of the Pliensbachian source rock of kerogen Type I.	111
Figure 3.67: Critical Moment map (1 km by 1 km smooth gridded) of the Pliensbachian source rock of kerogen Type II.	112
Figure 3.68: Critical Moment map (1 km by 1 km smooth gridded) of the Pliensbachian source rock of kerogen Type III.	113
Figure 3.69: Magnetic grid of the NW Central Atlantic Ocean (Dehler, 2010; PFA 2011, PL. 2.1.2).	115
Figure 3.70: Vitrinite reflectance map with COB boundary outboard of the ECMA.	118
Figure 3.71: Stretching Beta factor (β) map calculated to best fit crustal inversion process by PetroMod.	119
Figure 3.72: Digitized surface map of the Moho from georeferenced refraction lines from Louden et al. (2010) in Petrel.	120
Figure 3.73: Depth of the basement from sea level based on the models from this study. NovaSPAN line are in black lines.	121
Figure 3.74: Stretching Beta factor (β) map calculated using the depth of the Moho from Louden et al. (2010) and depth to sedimentary basement as defined in this project, with an initial depth of crustal lithosphere of 32 Km.	122
Figure 3.75: Beta factor using Moho depth from refraction data divided by Beta factor from inversion within PetroMod.	123
Figure 3.76: Vitrinite reflectance map based on models with calculated crustal stretching factors from refraction data (Figure 3.74).	124
Figure 3.77: Vitrinite reflectance difference map: VR via beta from refraction data minus VR via beta from inversion in PetroMod.	125
Figure 3.78: A comparison of temperature and vitrinite reflectance testing the models with salt and no salt.	126
Figure 3.79: Thermal effect on the vitrinite reflectance map without salt deposition in the Basin.	127
Figure 3.80: This map show the change in temperature if the salt was not present in the model.	128

Figure 3.81: This vitrinite reflectance difference map shows the amount of %Ro that the is affected by the influence of salt in the model.	129
Figure 4.1: This panoramic photograph of the outcrop of the Aït Moussa section.	132
Figure 4.2: Rock-Eval Pyrolysis graph from the data collected at Aït Moussa, Morocco.	133
Figure 4.3: As salt is deposited it does not move until some force/weight like sediment loading is applied.	136
Figure 4.4: On left salt diapirs and the right a salt canopy structure, in pink.....	136
Figure 4.5: Description of salt movement through time (salt in blue layer).	137
Figure 4.6: Depth smooth gridded map at the top of the Pliensbachian source rock based on NovaSPAN 1100, 1400, 1600, 1800 and 2000 models.	138
Figure 4.7: Comparison between the transformation ratio results from the PFA (OERA, 2011)(top) and this study (bottom).....	142

Abstract

A mature source rock is the key element in a petroleum system and it is the critical risk when exploring in undrilled areas where there are very few direct indications of hydrocarbons (either from surface seeps or seismic data). On the Scotian Margin, there are proven offshore commercial hydrocarbon fields in Jurassic and Cretaceous reservoirs that have geochemical characteristics consistent with proven Upper Jurassic source rocks - but the unequivocal linkage between source and reservoir has not been demonstrated. (Silva, Wong and Wach, 2015; Fowler, Webb, Obermajer et al., 2016). Below this proven interval, in rocks of Lower and Middle Jurassic age, source rocks are abundant globally, related to restricted marine and lacustrine depositional environments associated with the break-up of Pangea, although it is uncertain whether source rocks of this age are present on the Scotian Margin. If they are, and they have a suitable thermal history, then there is the potential for commercial petroleum systems that are currently undiscovered. The objective of this study is to address this technical problem through 2D thermal modelling. This study integrates source rock geochemistry and depositional history from proven source rocks in Morocco (the conjugate margin) with basin modelling of the Scotian Margin in a more detailed approach than previous studies, such as the 2011 Play Fairway Analysis (PFA). These models test the Lower Jurassic source rocks by testing the kerogen type and demonstrating the thermal maturity range of each kerogen type in the Scotian Basin.

This thesis presents the results from the construction and testing of 2D Petroleum System models on four shelf-to-slope regional seismic lines (NovaSPAN 1100, 1400, 1800 and 2000) using PetroMod software, together with new data from the 2011, 2015 and 2016 Nova Scotia Department of Energy sponsored Play Fairway Analysis, and outcrop data from Aït Moussa in the Middle Atlas, Morocco. Several organic-rich intervals have been identified along the Mesozoic conjugate margins of the Central and North Atlantic. The similarity of the depositional environments and paleogeography of the Scotian margin with the conjugate Western European and Northwest African domains, which contain proven Lower Jurassic source rock successions, suggests the presence of a similar interval in the offshore Scotian margin. If present, there is uncertainty in the source rock characteristics (quantity, quality, and maturity). With ongoing and future petroleum exploration offshore Nova Scotia, resolving these uncertainties is necessary to reduce the risks associated with exploration. In this study, the software PetroMod version 2018.1 (Schlumberger) was used to construct 2D models of source rock maturation of potential Lower Jurassic rocks on the Scotian Margin using dip lines of the ION NovaSPAN geophysical dataset (NVR1-1100, NVR1-1400, NVR1-1600, NVR1-2000). In each model, different source rock variables (hydrogen index and total organic carbon) were used based on data from the High and Middle Atlas Basins (Morocco). Results suggest potential Lower Jurassic source rocks in the Scotian Basin are within the oil maturity window in the south, and transition to the gas maturity window to the north, due to burial depth and salt mobilization. The Lower Jurassic interval has a range of maturity and potential for generation of hydrocarbons. The transformation ratio (organic matter to hydrocarbons) varies throughout the Scotian Basin when modelled with different types of kerogen. Data limitations are recognized as only five 2D seismic lines are used to map the maturity of the Scotian Basin.

List of Abbreviations Used

1D	1 Dimension
2D	2 Dimension
C	Celsius
CNSOPB	Canada-Nova Scotia Offshore Petroleum Board
CM	Critical Moment
COB	Continental Oceanic Boundary
DSDP	Deep Sea Drilling Project
ENARS	Eastern North America Rift System
HI	Hydrogen Index
km	Kilometres
m	Metre
Ma	Millions of years
mg	Milligrams
PFA	Play Fairway Analysis
PSM	Petroleum Systems Modelling
PWD	Paleo Water Depth
SR	Source Rock
SWIT	Sediment-Water Interface Temperature
RT	Rotatory Table
TOC	Total Organic Carbon
TD	Total Depth
TR	Transformation Ratio
TVD	Total Vertical Depth
UWI	Unique Well Identifier
WD	Water Depth

Acknowledgements

I would first like to thank the people who encourage me and support me throughout my graduate research.

I want to thank my supervisor and committee members, Professor Grant Wach, Professor Marcos Zentilli, and Mr. Bill Richards, of the Department of Earth Science at Dalhousie University. I want to thank them for the opportunity and encouragement to pursue research on the Scotian Basin. Their knowledge, supervision, patience, and positive feedback showed to be endless, without their support and persistence, I could not imagine completing this thesis without them.

I would like to thank the experts at Schlumberger for providing the software donation and technical support: Mr. Charlie James, Mr. Tayo Akintokunbo, and Dr. Thomas Hantschel. I would also like to thank Dr. Ricardo Silva and Dr. P. K. Mukhodahyay (Muki) for their encouragement and positive feedback throughout my graduate research. Also, want to thank the people at Canada-Nova Scotia Offshore Petroleum Board and Natural Resources Canada for maintaining the databases which were essential to the success of the study.

I would also like to acknowledge Dr. Steve Ings from ExxonMobil Canada as the external reader of this thesis, and I am grateful to my friends and colleagues that I meet through my years at Dalhousie University: Carla, Taylor, Trevor, Natasha, Emma, Kenny, Darragh, Anne, Rachel, Erin, Laura, Bryan, Trudy, Charlie and Johnathan. You all have helped me reach the finish line.

Finally, I must express my very profound gratitude to my family for encouraging me throughout these past years of this thesis. Thank you

Chapter 1: Introduction

1.1 Introduction

A mature source rock is the key element in a petroleum system and is often the critical risk when exploring undrilled areas – particularly in areas like Eastern Canada offshore where there are few direct indications of hydrocarbons from geophysics or surface seeps. On the Scotian Margin (Figure 1.1), the presence of Upper Jurassic petroleum source rocks and active petroleum systems are proven by drilling and commercial production in the Sable Sub-Basin. Below this proven interval, in rocks of Lower and Middle Jurassic age, source rocks are abundant globally (Wach, Silva, O'Connor et al., 2018), related to restricted marine and lacustrine depositional environments associated with the break-up of Pangea. It is uncertain whether source rocks of this age are present on the Scotian Margin. This study integrates source rock geochemistry and depositional history from proven source rocks in Morocco (the conjugate margin) with basin modelling of the Scotian Margin to produce a more detailed approach than existing studies, such as the Play Fairway Analysis (OERA, 2011).

“Petroleum system modelling” (PSM) is a method for evaluation of source rock maturity. This method is used here to investigate the thermal maturity of Lower Jurassic sediments containing possible source rocks in the Scotian Basin (there are only a few penetrations at the updip margin of the basin). The study is based on five shelf-slope regional seismic lines (ION Geophysical) (Figure 1.1). Four of these were modelled in this study; the other line interpretation was provided by a colleague (Xinyue Hu, research assistant at Basin and Reservoir, Dalhousie University). Geological knowledge of subsurface thermal conductivity and crustal heat production are used to predict geotherms and thus temperature spatially away from control points (borehole and seismic data). The presence of Lower Jurassic source rocks is

addressed by considering depositional environments in the Scotian Basin and its conjugate, the Moroccan Margin, where source rocks of this age are exposed - specifically at Aït Moussa in the Middle Atlas. These organic-rich sediments are interpreted to be deposited in an oxygen depleted depositional environment, resulting in a high-quality source rock of Pliensbachian age (Sachse, Leythaeuser, Grobe et al., 2012).

In addition to Aït Moussa, proven Lower Jurassic petroleum source rocks in Morocco occur in the Prerif Basin and Middle Atlas (Sachse et al., 2012); and several oils in the Tarfaya and Essaouira Basins (Morocco) are thought to be sourced from Jurassic age carbonates (Morabet, Bouchta and Jabour, 1998; Sachse et al., 2012). The Jurassic organic-rich intervals observed on the Western European and African conjugate margins suggest that exploration for hydrocarbons in Atlantic Canada can test new and alternative play concepts (Silva et al., 2015).

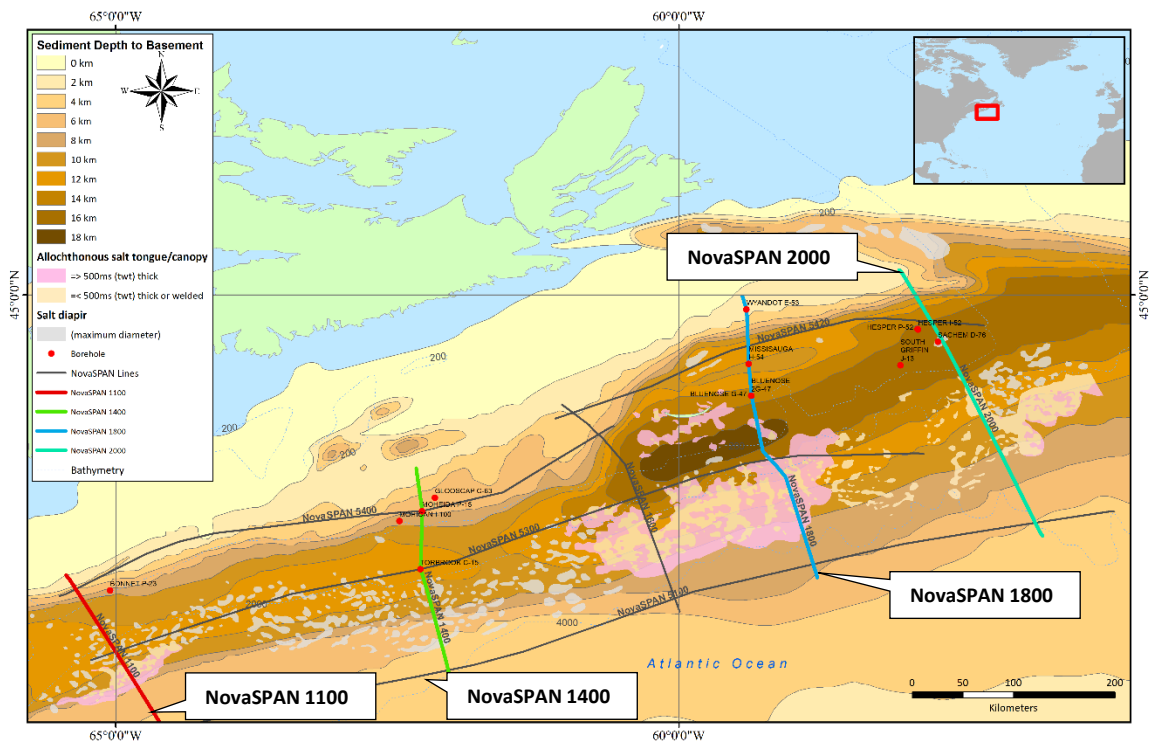


Figure 1.1: Location of the Study Area. The coloured lines are the NovaSPAN lines, and the red dots are the offshore boreholes used for this study. This project is a contributing part of the Source Rock & Geochemistry of the Central Atlantic Margins study. The 2D petroleum systems models in this study are NovaSPAN 1100 (Red Line), NovaSPAN 1400 (Green Line), NovaSPAN 1800 (Blue Line), and NovaSPAN 2000 (Teal Line).

This study complements and expands previous petroleum systems models (PFA;(OERA, 2011, 2015, 2016)); it presents a series of 1D and 2D models of the potential Lower Jurassic source rock in the Scotian Basin, testing multiple scenarios, using the commercial software package PetroMod version 2018.1, (courtesy of Schlumberger Limited). In Morocco, geochemical and organic petrographic analysis of the Upper Pliensbachian organic-rich outcrop in the Middle Atlas region suggest high productivity conditions, with oxygen-depleted, but not anoxic, bottom waters (Sachse et al., 2012). This organic matter is mostly associated with marine-derived organic matter (algal/bacterial) (Sachse et al., 2012), and are also known from other regions around the world such as Portugal (Silva and Duarte, 2015).

The models presented here predict the level of thermal maturity of potential Lower Jurassic source rocks in the Sable Sub-Basin. Based on Ait Moussa, Morocco outcrop data this study uses a broader range of parameters for the Lower Jurassic source rocks than previous studies (Figure 1.2 and Table 1.1), and also considers source rocks of kerogen Type I, Type II and Type III. These parameters are based on fieldwork at Ait Moussa (Figure 1.3).

Table 1.1: Source rock geochemical properties used as the parameter inputs for the Lower Jurassic Source Rock interval in PetroMod (Wach et al., 2018).

Lower Jurassic Source Rock Properties			
Kerogen	HI (mgHC/gTOC)	TOC	Source Rock Kinetic
Type I	800	5%	Behar et al. (1997)_TI(GRS)-cs
Type II	400	3%	Behar et al. (1997)_TII(PB)-cs
Type III	200	3%	Vandenbroucke et al. (1999)_TIII(NorthSea)-cs

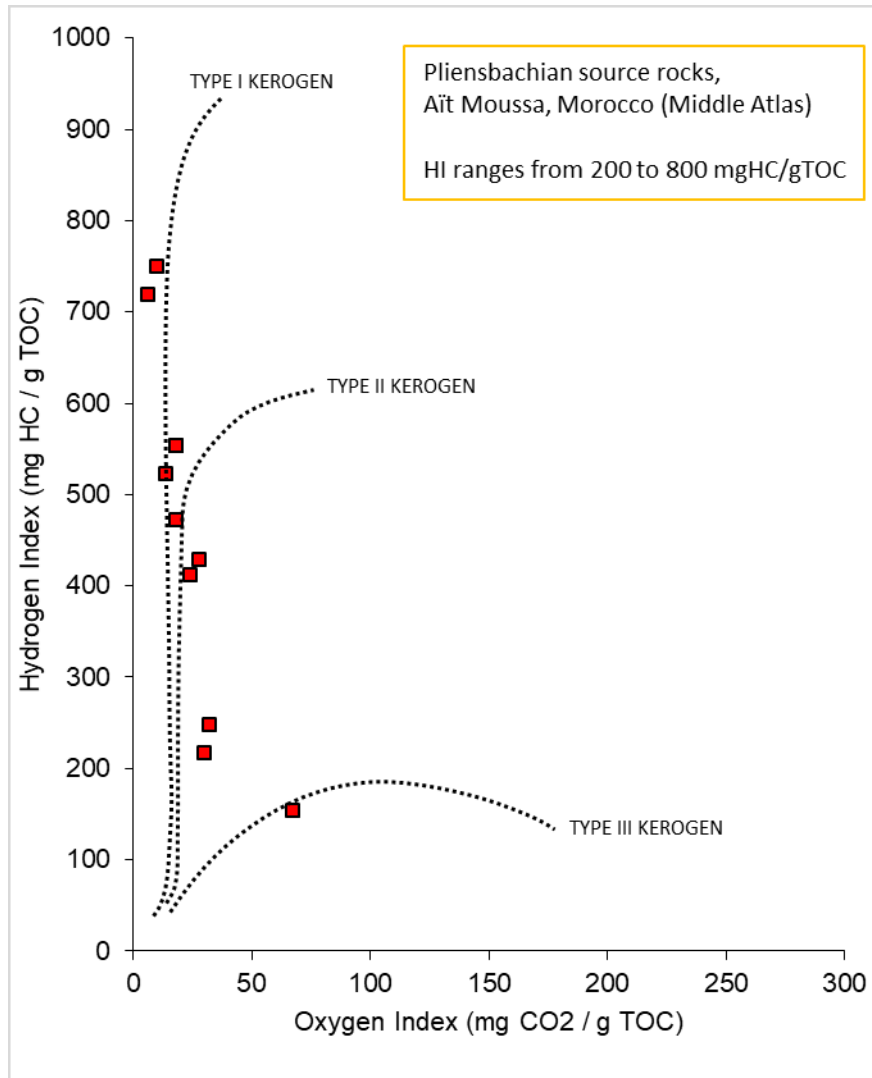


Figure 1.2: Rock-Eval Pyrolysis graph from the data collected at Aït Moussa, Morocco. This graph shows data points (red), ranging from hydrogen index (HI) of 200-800 mgHC/gTOC, Type I-Type III kerogen (Silva, Duarte, Gómez et al., 2017b).

For comparison, a similar study referred to as the Play Fairway Analysis (PFA) (OERA, 2011, 2015, 2016) used a hydrogen index of 600 mg CO₂/g TOC with a TOC of 3% or 5%. The source rock analysis of the PFA study was based on a data set extrapolated from offshore boreholes Venture B-13 and Weymouth A-45 (Nova Scotia), M-02 and DSDP 547B (Morocco), and Heron H-73 (Newfoundland), and outcrops at Peniche (Portugal) and Sidi Rhalem Essaouira oils (Morocco). However, they did not consider depositional environment variations or different sources of the organic materials. The Deep Sea Drilling Project Leg 79, site 547B (offshore Morocco) showed several immature Lower Jurassic organic-rich levels kerogen Type III (Wach et

al., 2018). In the Play Fairway Analysis, the Early Jurassic Source Complex was “inferred by analogy to source rocks recognized on the conjugate margins of Newfoundland and Nova Scotia, in Portugal and Morocco” (OERA, 2011).

This thesis is part of a more extensive research program, “Source Rock & Geochemistry of the Central Atlantic Margins”, led by the Basin and Reservoir Lab, Dalhousie University, under the direction of Professor Grant Wach (Wach et al., 2018).

1.2 Problem Statement, Objective and Hypothesis

There are proven commercial hydrocarbons offshore Nova Scotia in Jurassic and Cretaceous reservoirs that have geochemical characteristics consistent with proven Upper Jurassic source rocks, but the unequivocal linkage between source and reservoir has not been demonstrated (Silva et al., 2015; Fowler et al., 2016). Lower Jurassic source rocks are proven in the conjugate margin in Morocco, and it is possible that similar Lower Jurassic source rocks are present on the Scotian Margin and may contribute to proven hydrocarbons systems, or, may be the source of undiscovered hydrocarbon systems on the Scotian Basin. However, they have not been confirmed through drilling. Even if similar Lower Jurassic source rocks could be demonstrated on the Scotian margin, their effectiveness would be dependent on the thermal history of the margin. The objective of this study is to address this technical problem through 2D thermal modelling. Products from modelling include a series of maps showing thermal maturity, current temperature and heat flow (impacted by salt), and critical moment and hydrocarbon generation of Type I, Type II and Type III kerogen for rocks of Lower Jurassic age.

The initial hypothesis in this study is that Lower Jurassic source rocks on the Scotian Margin, if present, will be sufficiently mature to generate an effective hydrocarbon system. To

test this hypothesis, it is necessary to determine if there is a similar tectonic history, heat flow, and sediment thickness for both (Scotian and Moroccan) conjugate margins.

1.3 Thesis Organization

This thesis is organized into the following chapters. Chapter 1 comprises the introduction, problem statement, objective, geological background and previous studies. Chapter 2 introduces previous data and the methods used in this study. Chapter 3 contains the results of each 2D model and subsequent maps. This study results in multiple thermal models constructed from NovaSPAN 1100, NovaSPAN 1400, NovaSPAN 1800 and NovaSPAN 2000 seismic lines (and NovaSPAN 1600 in subsequent maps). The 2D results comprise a set of cross-sections that model heat flow, temperature, maturity, and critical moment. Accompanying these 2D results, there are 1D model extractions which comprise transformation ratio plots at specific locations on the continental margin, and temperature and vitrinite reflectance plots that are compared to borehole data. These results are discussed in Chapter 4 for each 2D modelled line and 1D extraction and then summarized and synthesized for the study area, which covers a major portion of the Scotian Basin. Chapter 5 presents the conclusions and future work from this study. Appendices present larger format figures and videos (supplemental files), tables of data, calibration and uncertainty tests for the 2D models and Python code for this study.

1.4 Background Geology

Scotian Basin

A series of preserved Permo-Triassic rift basins extend along the conjugate Atlantic margins of eastern North America, northwestern Africa, and Europe. These basins formed during the Permian to Triassic breakup of the Pangean supercontinent (Olsen, 1997; Withjack, Schlische and Olsen, 2012; Leleu, Hartley, van Oosterhout et al., 2016). The basins along the

eastern margin of North America are collectively known as the Eastern North American Rift System (ENARS). These buried and exposed rift basins extend over 3000 km from Florida to the eastern Grand Banks, offshore Newfoundland. Based on the tectonic style and sedimentary deposition within these basins, the ENARS was divided into the southern, central, and northern segments (Withjack et al., 2012 and references within).

The Scotian Basin, located in the Atlantic offshore region of Nova Scotia, comprises the northernmost part of the ENARS central segment (Withjack et al., 2012). The Scotian Basin contains a record of 250 Ma of episodic sedimentation, comprises a maximum sedimentary thickness of about 15 km, and covers an area of approximately 280,000 km² (Wade and MacLean, 1990). The basin comprises several sub-basins, from southwest to northeast: Shelburne, Sable, Abenaki, and Laurentian Sub-Basins (Wade and MacLean, 1990; Withjack et al., 2012).

The Scotian Basin stratigraphy is a classic record of the transition from rift to passive margin, with syn-rift phase punctuated by a breakup unconformity followed by a post-rift and thermal sag phases. Notable additional features include the continental scale Abenaki carbonate bank in Middle to Late Jurassic which was effectively terminated by Late Cretaceous Sable Delta clastic influx that resulted from the Avalon uplift to the (Jansa and Wade, 1975; Wade and MacLean, 1990).

The earliest sediments deposited in the Scotian Basin comprise Triassic to Early Jurassic alluvial, fluvial, lacustrine, and evaporitic successions deposited in continental lowlands and shallow marine environments under arid to semi-arid climatic conditions (Figure 1.3) (Jansa and Wade, 1975; Wade and MacLean, 1990). The break-up unconformity is marked by the bottom of the Jurassic (Figure 1.4). From the Lower to the Upper Jurassic, the basin was filled by marine

transgressions, depositing carbonates and clastic sediments in two phases. The first phase is the continental and marine clastics of the Mohican Formation located inboard of the marine dolomites of the Iroquois Formation. The second phase is the marine clastics of the Mohawk and Mic Mac Formations which transition seaward to carbonates of the Abenaki Formation at the shelf margin (the Abenaki Carbonate Bank) (Figure 1.4). Distal shale equivalents of these lithostratigraphic formations are found in the Verrill Canyon Formation. In the Late Jurassic, sea-floor spreading continued, the ocean became broader and deeper but, in addition, the Avalon uplift to the north caused a massive influx of clastic sediment that diluted the Abenaki Carbonate Bank, and led to sediment loading, salt movement and deposition of successive thick clastic intervals (Sable and Shelburne deltas) that prograded into the basin. Salt moved both vertically and laterally forming diapirs, pillows, and canopies (Jansa and Wade, 1975; Wade and MacLean, 1990; Ings and Shimeld, 2006; Campbell, 2010). This influx of clastics continued until late Cretaceous. At that time, prolific deltaic sedimentation (Missisauga Formation) was interrupted by a major marine transgression in the Aptian (Naskapi Member of Logan Canyon Formation) and then a return to deltaic and progressively more estuarine depositional settings (Logan Canyon Formation) (Figure 1.4). Transgression and deepening culminated in shales of the Dawson Canyon Formation, which was subsequently overlain by marls and chalky mudstones of the Wyandot Formation in response sea level rise at the end of the Cretaceous (Wade and MacLean, 1990). During the Cenozoic, and above the Wyandot Formation, a progradational system of sandstones, mudstones and marls (Banquereau Formation) deposited (McIver, 1972). During the Quaternary glacial drift and stratified proglacial material of the Laurentian Formation overlain the Banquereau Formation (Jansa and Wade, 1975)(Figure 1.4).

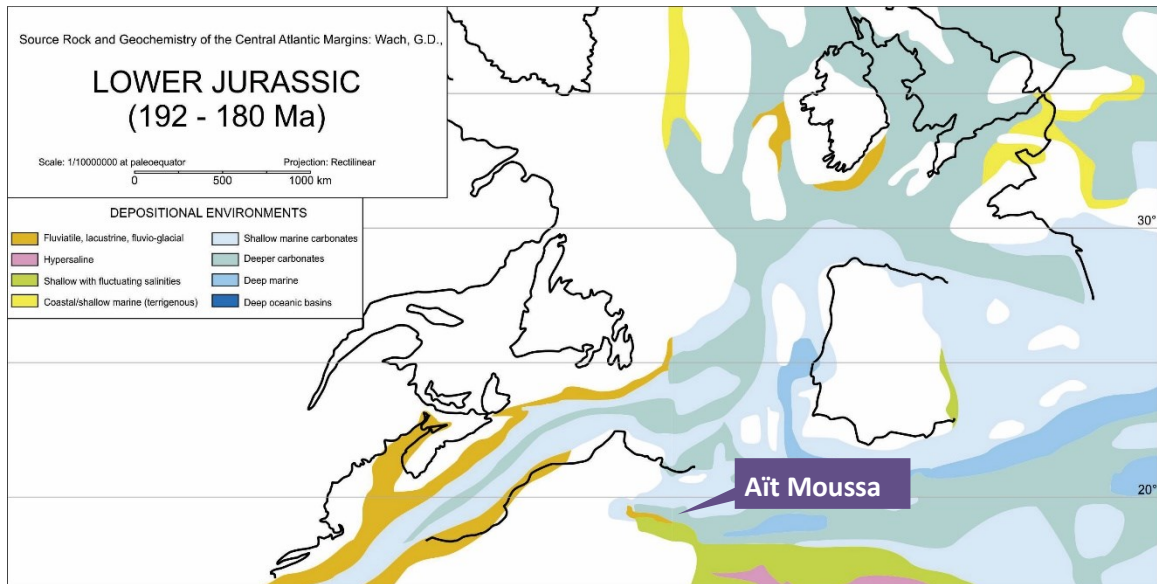


Figure 1.3: Paleogeographic reconstruction of the Lower Jurassic (Wach et al., 2018) showing the location of Ait Moussa.

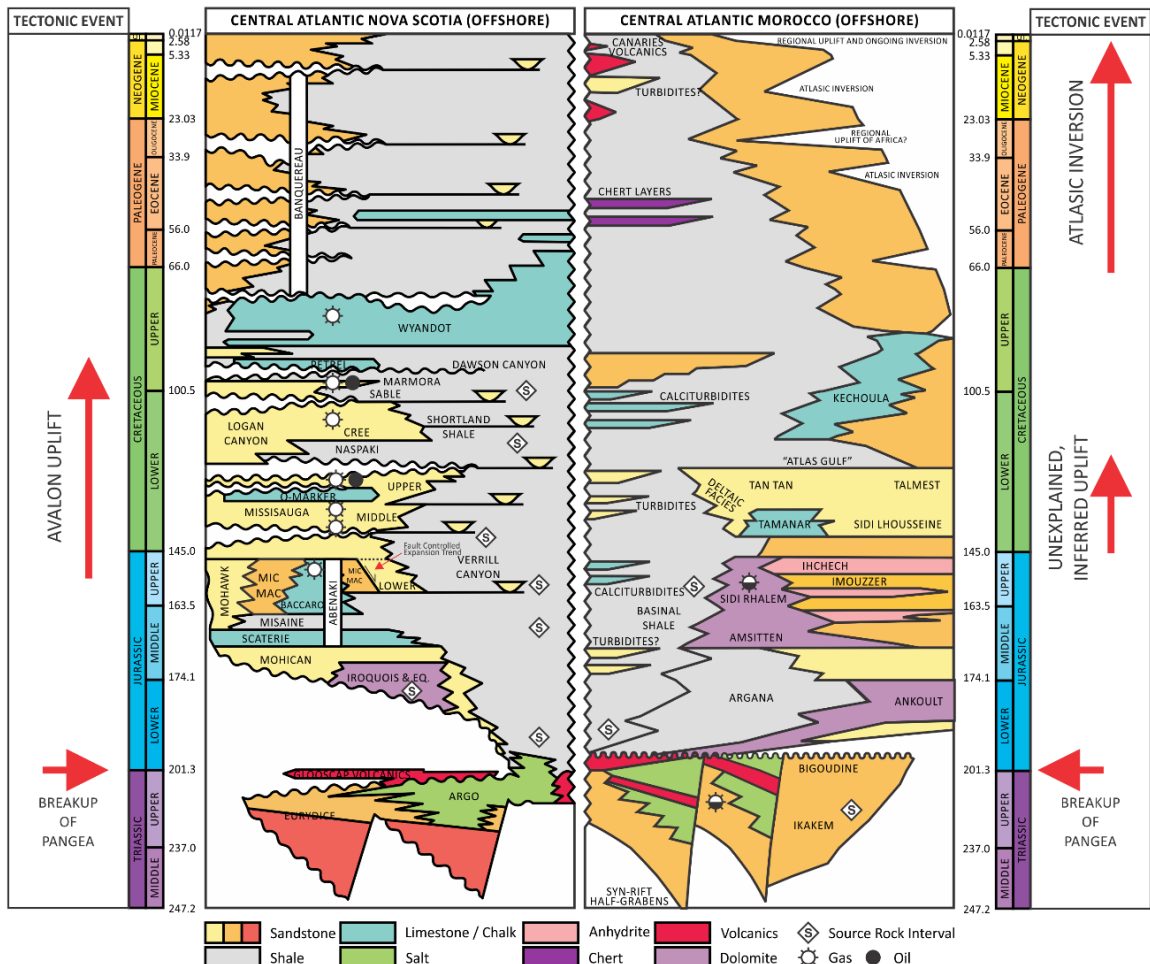


Figure 1.4: Composite comparison of two stratigraphic charts. On the left is the Central Atlantic Nova Scotia stratigraphy modified after Olsen (1997); Weston, MacRae, Ascoli et al. (2012); (Campbell, 2018). On the right is the stratigraphy of the conjugate margin of Central Atlantic Morocco modified after Tari and Jabour (2013).

Conjugate Margin – Morocco

Depositional history on the conjugate margin of Morocco is similar to the Scotian margin (Figure 1.4). The oldest Mesozoic sediments in the Tarfaya Basin, Morocco are of Lower Triassic Age. During the opening of the North Atlantic (Late Triassic – Early Jurassic), the Scotian and Moroccan margins developed grabens and half-grabens caused by an extension. The Triassic Age sediments in the Tarfaya Basin are similar to the Scotian Basin (boreholes Eurydice P-36 and Mohican I-100) and composed of red conglomerates and sandstones (Hafid, Tari, Bouhadioui et al., 2008). During extension, syn-rift clastic sediments were deposited on both the Scotian and Moroccan margins. The breakup of Africa from North America took place during the Lower Jurassic forming the proto-Atlantic Ocean (Figure 1.3).

After the breakup similar deposits are seen on both stratigraphic charts. On the Moroccan Margin carbonates (Ankoul Formation) transition into distal clastic sediments, similar to the Scotian Basin, where the Iroquois Formation (carbonates) transition into the Mohican Formation and distally into the Verrill Canyon Formation (clastics) (Figure 1.4). During the Upper Jurassic to Lower Cretaceous, the Moroccan Basin had sediment input from the Tan Tan deltaic system (Hafid et al., 2008). Along the Scotian Margin, several deltaic systems developed during the Cretaceous (Wade and MacLean, 1990). Salt mobilization was initiated by the thickening of the Moroccan Basin deposits (Tari and Jabour, 2013). Similarly, thick clastic sediment packages in the Scotian Basin (Missisauga, Logan Canyon, Verrill Canyon formations) induced salt mobilization in the Scotian Basin (Ings and Shimeld, 2006; Deptuck and Kendell, 2012; Deptuck and Kendell, 2017). A noteworthy difference between the Scotian and Moroccan Margin depositional history occurred during the Cretaceous (Figure 1.4). On the Scotian Margin the Late Jurassic Avalon Uplift event is associated with the start of seafloor spreading between North America (Grand Banks) and Western Europe (Iberia) (Wade and MacLean, 1990). On the

Moroccan Margin, the Atlasic Uplift during the Late Cretaceous and deposited siliciclastics in the basin (Louden, Wu and Tari, 2013) (Figure 1.4).

1.5 Previous Studies

The Scotian Basin has been actively studied since 1959 by government agencies, academia and industry to understand the tectonic, depositional, and hydrocarbon history. The stratigraphy of the Scotian Basin has been described in detail by Jansa and Wade (1975), Wade and MacLean (1990), MacLean and Wade (1993), and recently by Weston et al. (2012) (Figure 1.4).

Regional thermal history is a crucial component of hydrocarbon exploration as hydrocarbons require sufficient heat and time to transform the organic matter (Magoon and Dow, 1994; Allen and R., 2013). Previous studies of the thermal history of the Scotian Basin were limited to the effects of rifting and subsidence on the thermal evolution of the Scotian Margin (Royden and Keen, 1980; Beaumont, Keen and Boutilier, 1982; Keen and Beaumont, 1990; Williamson, Courtney, Keen et al., 1995; Goteti, Beaumont and Ings, 2013). Additional studies suggest that salt can influence the thermal history and maturity of source rocks (Mukhopadhyay, 2006; Goteti et al., 2013). The Scotian Basin has basal deposits of salt (Argo Formation), with the subsequent development of mini-basins due to sediment loading and salt mobilization. The salt also created thermal variations which impact the maturity of a source rock (Ings, 2006; MacDonald, 2009; Goteti, Ings and Beaumont, 2012; Goteti et al., 2013).

Seismic inversion studies for the source rock evaluation on the organic-rich intervals of the Scotian Basin indicate that low acoustic impedance may provide indirect evidence of source rock presence and active or late-stage hydrocarbon generation from below borehole penetrations or from outside the study area (Morrison, 2017).

Petroleum System Models from other studies suggest that Lower Jurassic source rocks (if present) in the Scotian Basin are within the oil window (50 – 150 °C) and base this conclusion on data collected from the Scotian margin (condensate and fluid inclusions from offshore boreholes), the Moroccan margin (offshore and onshore oil samples and offshore collected core), Peniche in Portugal (outcrop), and offshore Newfoundland (oil samples from boreholes) (OERA, 2011, 2015, 2016). Other approaches to model the thermal history include work by Negulic (2010); Negulic and Louden (2017) who used seafloor temperature data and predicted the maturation of a hypothetical Late Jurassic source rock within the oil window.

A study by Mukhopadhyay (2006) speculated that Early Jurassic rocks in the Scotian Basin comprise lacustrine / marine kerogens (Type I – II) which were subjected to high heat flow owing to sediment loading and salt mobilization.

1.6 Source Rock

Source rocks are defined as organic-rich sediments that originate in various sedimentary environments and are one of the essential elements of a petroleum system and must often a key risk element when exploring new frontier areas (Magoon and Dow, 1994). The term source rock is applied to any rock unit containing sufficient organic matter with an appropriate chemical composition to generate and expel hydrocarbons via biogenic or thermal processes, irrespective of the degree of maturation (e.g. Tissot and Welte, 1984; Suarez-Ruiz, Flores, Mendonca et al., 2012 and references therein). A source rock is characterized by 1) amount of organic matter preserved (preservation is mainly controlled by oxygen content which is related to depositional environment); 2) quality and type of organic matter capable of yielding hydrocarbons (mainly controlled by the depositional environment); and 3) thermal maturity of organic matter (dependent on burial history) (e.g. Tissot and Welte, 1984).

The slope and deep water have significant unproven reserves of hydrocarbon potential although major exploration investments in 2D and 3D seismic, regional studies, and drilling (OERA, 2011) have not resulted in commercial discoveries. There are 121 exploratory offshore boreholes across the entire Scotian Basin, mostly concentrated in the productive Sable Sub-Basin which has been extensively explored (73 boreholes). Historically, drilling focused on the successful rollover anticlinal structures (gas) in the Sable sub-Basin, yet the source rock and timing of hydrocarbon generation and migration pathways are not fully understood (Silva et al., 2015). Identifying source rocks on the Scotian Margin has been a considerable challenge for both known and suspected intervals (Barss, Bujak, Wade et al., 1980; Powell, 1985; Mukhopadhyay and Wade, 1990; Wade and MacLean, 1990; Bell and Campbell, 1990; Kidston, Brown, Altheim et al., 2002; OERA, 2011). None of these studies proved a Lower Jurassic source rock due to a lack of borehole data in the Lower Jurassic intervals of interest (located deeper in subsurface than has been drilled).

The PFA constructed a petroleum systems models, based on observations (oils and condensates) and data from neighbouring basins such as Morocco (Sachse et al., 2012) and Portugal (Silva, Duarte, Comas-Rengifo et al., 2011), suggesting Lower Jurassic source rocks may exist. Although their presence is unproven in the Scotian Basin, they should be considered based on the conjugate Morocco margin data. However, when modelling the Scotian Basin, their initial parameters were on a limited data set extrapolated from offshore boreholes (Nova Scotia and Morocco) and few outcrops (Morocco and Portugal). Recent research and fieldwork from the Basin and Reservoir Lab refined these initial source rock parameters by providing better constraints on hydrogen indices, total organic carbon and organic matter types (Campbell, 2010; Morrison, 2017; Silva, Carlisle and Wach, 2017a). In Morocco, geochemical and organic petrography analyses of the Upper Pliensbachian organic-rich outcrop in the Middle Atlas region

suggest high productivity conditions, with oxygen-depleted, but not anoxic, bottom waters (Sachse et al., 2012). Further discussion of source rock parameters are in 3.8section 4.1 Source Rock Parameters.

Chapter 2: Data and Methods

2.1 Introduction

The following sections outline the data and methods used in this study. This project uses a combination of seismic and borehole data along with and previous seismic and borehole interpretations from various sources (Figure 2.1). This data is used to produce thermal maturation models for offshore Nova Scotia using petroleum system modelling software PetroMod.

2.2 Data

Data and interpretations from 13 offshore boreholes from the Scotian Basin were used as input parameters and calibration of the models (Table 2.1). The deepest penetrations of these offshore boreholes reached the Middle Jurassic section. The borehole selection emphasized proximity to the NovaSPAN lines modelled in this study (Table 2.1). Borehole data includes formation picks, deviation, biostratigraphy, geological age, total organic carbon (TOC), hydrogen index (HI), and vitrinite reflectance (VR). These data were accessed from an online repository known as the BASIN Database maintained by the Geological Survey of Canada (<http://basin.gdr.nrcan.gc.ca/>) (Appendix A and Appendix B). Digital lithology logs were provided by Canstrat Ltd (kindly donated to Dalhousie University). These Canstrat lithology logs, includes interpretations of facies from both cuttings and cores collected during the drilling of each borehole.

Table 2.1: List of offshore boreholes used in this study for each model, this data was collected from the Basin Database (http://basin.gdr.nrcan.gc.ca/index_e.php).

Borehole Name	Associated NS line	Projection offset (km)	Temperature	Vitrinite Reflectance	Deviation
Bonnet P-23	NS 1100	22.13	Yes	Yes	No
Glooscap C-63	NS 1400	10.30	Yes	Yes	Yes
Moheida P-15	NS 1400	0.20	Yes	No	No
Mohican I-100	NS 1400	16.50	Yes	Yes	Yes
Torbrook C-15	NS 1400	0.10	Yes	Yes	Yes
Mississauga H-54	NS 1800	0.17	Yes	Yes	Yes
Wyandot E-53	NS 1800	0.04	Yes	Yes	Yes
Bluenose G-47	NS 1800	0.27	Yes	Yes	Yes
Bluenose 2G-47	NS 1800	0.16	Yes	Yes	Yes
Hesper I-52	NS 2000	11.75	Yes	Yes	No
Hesper P-52	NS 2000	11.93	Yes	No	Yes
Sachem D-76	NS 2000	3.58	Yes	Yes	No
South Griffin J-13	NS 2000	36.49	Yes	Yes	Yes

Seismic data for this study includes four seismic lines from the NovaSPAN 2D regional study of the offshore Scotian Basin. The seismic lines included in this study are NovaSPAN 1100, 1400, 1800, and 2000. These are regional dip seismic lines that extend outbound from the inner parts of the shelf to beyond the continental slope. ION Geophysical provided this dataset to Dalhousie University and Professor Grant Wach, principal investigator. These seismic lines are pre-processed ION's RTM technology and were collected in 2003 by the ION/GXT Corp. Previously completed interpretations of these lines by ION and the PFA were used as a basis for this study.

2.3 Methods

This study used the Petroleum System Modelling software PetroMod (Schlumberger) to model the maturation of possible source rocks of Lower Jurassic age from the offshore regions of Nova Scotia. PetroMod enables integration of seismic, well-log, and geological data to model the evolution of a sedimentary basin. The software package predicts the timing of hydrocarbon generation from organic-rich intervals. These models were based on the burial and thermal history, giving outputs of hydrocarbon generation (Figure 2.2) (Hantschel and Kauerauf, 2009). In this study, four 2D models were constructed to test different regions of the Scotian Basin and are based on the NovaSPAN seismic lines 1100, 1400, 1800 and 2000 (Figure 2.1, Table 2.2).

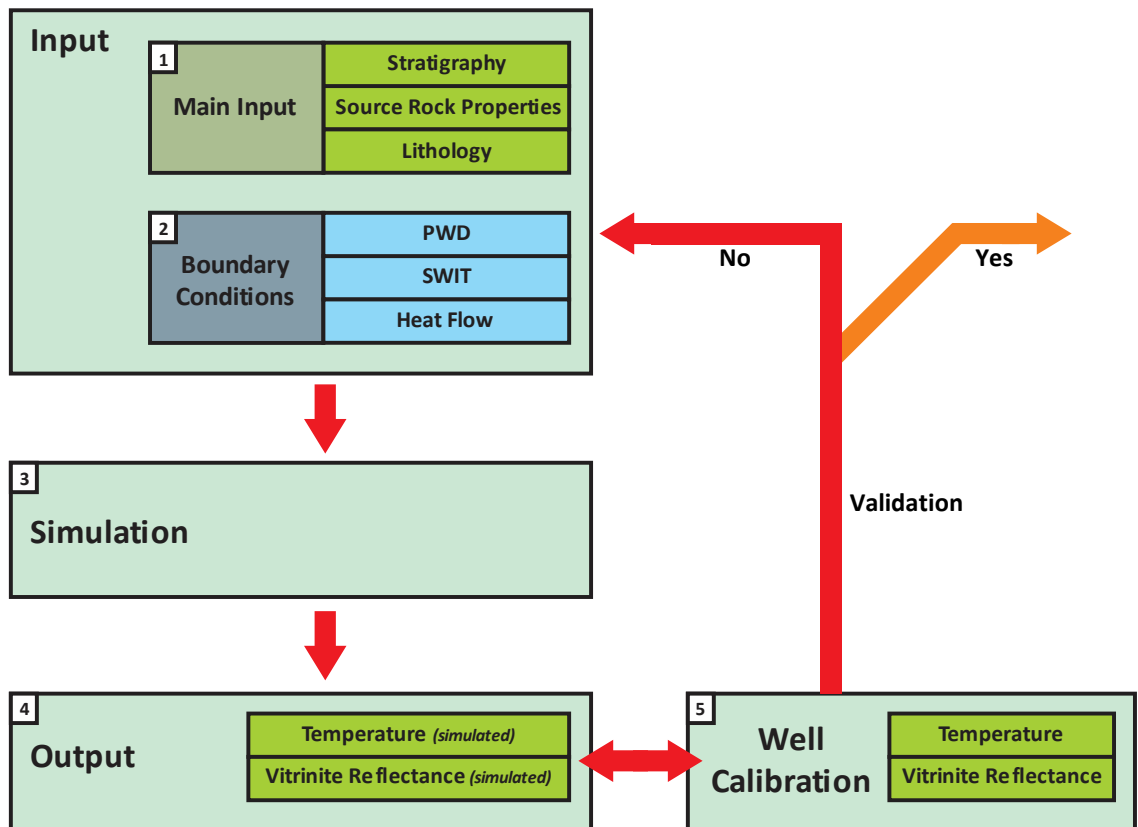


Figure 2.2: Flowchart of methodology. The model construction starts by inputting known geological data in the following categories. 1) Main inputs, with stratigraphy, source rock properties and lithology properties. 2) Boundary conditions, paleo-water depth (PWD), sediment-water interface temperature (SWIT), and heat flow. Once the model is built it can be simulated (3), each simulation has an output (4) depending on the inputs values (1), and (2). With the output (4) the model must be validated with measured data from the borehole (5), and if it fails validation, the process must start over again in the input (1) and (2) and go through the process again. If the validation is in the acceptable ranges, then we have a possible valid solution.

Table 2.2: Description of the 2D models built in this study, with the offshore boreholes associated for each model, and the run type and migration method of simulation run in these models.

Line I.D.	NovaSPAN 1100	NovaSPAN 1400	NovaSPAN 1800	NovaSPAN 2000
Length (km)	184.8	215	283.9	281.0
Depth min/max (m)	45 - 9173	29 - 13000	33 - 15000	35 - 16070
Fine grid points	1850	2150	1426	1413
Sample grid points	1850	2150	1426	1413
Valid elements	46588	68571	39439	38604
Cells in Depth	28	35	29	28
Layers	28	35	29	28
Run type	2D/3D temperature and pressure			
Migration Method	generation only			
Boreholes used in calibration of the model	Bonnet P-23	Glooscap C-63 Moheida P-15 Mohican I-100 Torbrook C-15	Missisauga H-54 Wyandot E-53 Bluenose G-47 Bluenose 2G-47	Hesper I-52 Hesper P-52 Sachem D-76 South Griffin J-13

2.3.1 Input

Before modelling, data sets were assembled for input into PetroMod to create the 2D petroleum system models. The following list describes these data sets (Figure 2.2):

1. **Previous seismic interpretations and borehole data:** existing horizon interpretations from previous studies were used as a basis for this study (OERA, 2011). These horizons were imported into PetroMod as depth horizons for each NovaSPAN lines except for NovaSPAN 1800, which they (PFA 2011) do not model in their report. Geologic horizons of the seismic line NovaSPAN 1800 were interpreted in Petrel and then imported into PetroMod. Between each horizon, a layer is inferred which is representative of a specific

geologic interval. The borehole data were then added. Each geologic layer was populated with lithological properties from boreholes using a custom program written in python (Appendix C), to populate the lithology of each layer. The final product was a 2D model framework which consisted of interpreted seismic lines with age data, lithological data, and thickness of each layer.

2. **Source rock parameters:** These data included hydrogen index (HI) and total organic carbon (TOC) and were collected from the outcrop at Aït Moussa, Middle Atlas, Morocco (Table 1.1). These data were added to a specific layer in the 2D model which corresponds to the Lower Jurassic layer.
3. **Paleo water depth (PWD):** Paleo water depths were estimated from biostratigraphic interpretations of inner neritic, outer neritic, bathyal and abyssal environments in the BASIN database, combined with paleo-bathymetry ranges defined by Veeken and Moerkerken (2013) (Figure 2.3). Estimates were cross-referenced to eustatic sea level curves (Haq, Hardenbol and Vail, 1987; Haq and Schutter, 2008) (Figure 3.1). The PWD allowed PetroMod to constrain sedimentation rate, sediment-water interface temperature (SWIT), and compaction of the sediments during model simulation.

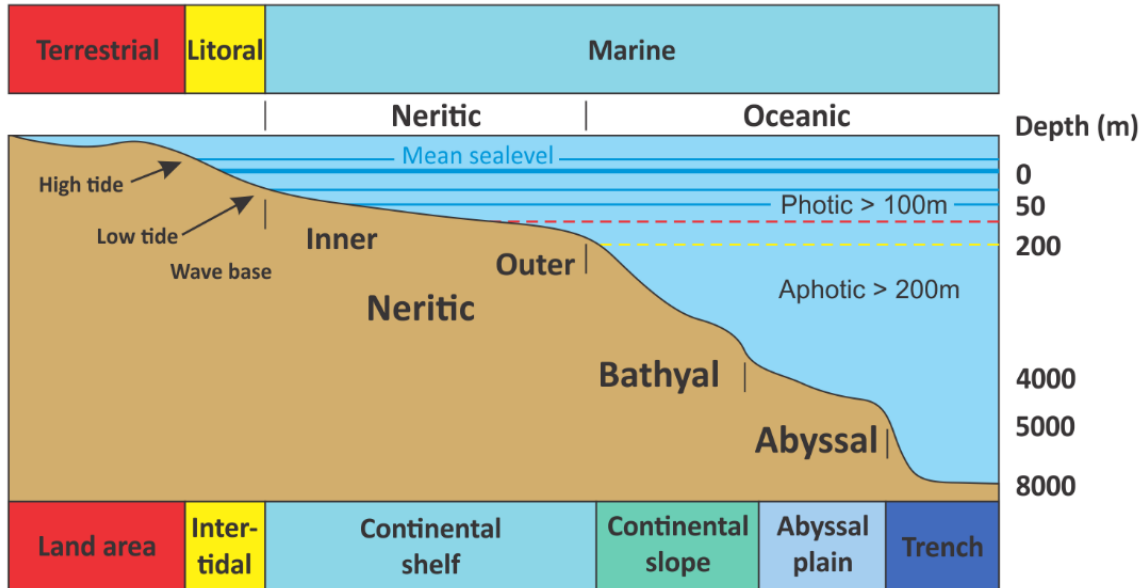


Figure 2.3: Depositional environments for a continental margin setting, modified after Veeken and Moerkerken (2013).

4. **Sediment-Water Interface Temperature (SWIT):** is a required control that constrains the thermal influence between the sediments and water during the deposition of sediments. The SWIT was calculated based on the global mean temperature at sea level using the method by Wygrala (1989) and the PWD. The SWIT interface in PetroMod calculates the SWIT based on present-day latitude of the model. In this study, the latitude is based on one offshore borehole for each 2D model as input (Table 2.3). The SWIT interface in PetroMod calculates the paleolatitude of the offshore borehole, based on the present-day latitude. With the paleolatitude, PetroMod calculates the SWIT based on the paleo global mean temperature at sea level and the PWD using the Wygrala (1989) method. The resulting output is a paleo SWIT map that is used as a boundary condition in the model. Together the SWIT and the PWD are used to constrain the boundary conditions of the model when running the simulation.

Table 2.3: Latitude of the offshore borehole location used to calculate the paleo sediment-water interface temperature trend in PetroMod

Model	Reference Well	Latitude (degree)
1100	Bonnet P-23	42°
1400	Glooscap C-63	43°
1800	Bluenose G-47	44°
2000	Sachem D-76	44°

1. Thermal History (paleo-heat flow): To calculate the temperatures in the sediments

throughout the geological time it is essential to define the thermal history of the basin.

The thermal history is the most vital portion of petroleum system modelling. Heat flow is

the movement of heat from the mantle to the surface. It is measured in the units of

mWatts/m² (Hantschel and Kauerauf, 2009; Goteti et al., 2013). The calculation of the

paleo-heat flow is based on the knowledge of the thickness of the lithospheric layer

through time. The heat flow from the base of the lithosphere is mainly controlled by the

base temperature of the crust, which is the Moho (1333°C), the thickness of the

lithospheric layers and their thermal conductivities. Compaction and stretching of the

layers during the basin history creates subsidence in turn creating accommodation space

(McKenzie, 1978; White and McKenzie, 1988).

To define the thermal history, two boundary conditions are specified 1) the SWIT and 2)

the basal heat flow. Using multiple 1D heat flow trends from offshore boreholes is a

method to calculate the heat flow map for a 2D model. This method generates heat flow

maps that implement the McKenzie stretching model at a specific location (1D model

from offshore boreholes). The heat flow may vary at locations along a 2D or 3D model

(shelf, slope and abyssal). This method is useful when there are multiple 1D models along

with a single 2D line. Unfortunately, the sparsity of the offshore boreholes in the slope

and abyssal regions in this study limits the ability to create a 2D heat flow maps. PetroMod

has two alternative methods to calculate the paleo heat flow for 2D and 3D models, both

based on the McKenzie Crustal Model for rift basins (McKenzie, 1978; Jarvis and Mckenzie, 1980). This method is applied by using the “McKenzie Crustal Model” process in PetroMod.

The McKenzie Crustal Model process uses the McKenzie model to calculate the heat flow history of 2D models. Heat flow trends are usually based on the knowledge of lithospheric layer thickness through geological time. The ascending heat flow from the base of the lithosphere is mainly controlled by the mantle isotherm, the thickness of the layers and their thermal conductivity. The compaction of layers (layer thickness) and lithospheric stretching (McKenzie, 1978; White and McKenzie, 1988) affects basin subsidence. It is essential to combine subsidence, lithospheric stretching and heat flow to calculate basal heat flow maps throughout geological time. This process implements the timing, subsidence and crustal parameters as inputs to calculate stretching factors and to generate paleo heat flow maps for the 2D or 3D model. This enhanced method produces more optimal stretching factors and better heat flow maps for each model.

Within this McKenzie Crustal Model, there are two methods to calculate subsidence inversion for basal heat flow through geological time: 1) subsidence inversion by lithospheric layer thickness and 2) inversion to heat flow. Both methods use model inputs including pre-rift basement layer, the age of sediment deposition, lithology distribution, and paleowater depth.

- a. **Inversion to a lithospheric layer thickness:** this method calculates the heat flow at the base of the sediments taking into consideration the boundary conditions (SWIT and PWD). The calculation uses a two-phase inversion. The first phase inverts the post-rift tectonic subsidence to a mantle stretching map (i.e. inverting the post-rift tectonic subsidence which was purely driven by cooling of upwelled asthenosphere).

The second phase uses the result of the first phase and then inverts the stretching of the lithosphere and cooling in the asthenosphere during syn-rift of the basin. These inversions together allows the modelling software to match the crustal stretching and tectonic subsidence of the mantle and crustal thickness through time. During the simulation, the basal heat flow is calculated based on basin evolution throughout geological time. The advantage of this method is that the heat flow is calculated throughout geological time taking into consideration the sediment deposits which will produce thermal effects. The disadvantage of this method requires a full simulation to get the basal heat flow.

- b. **Inversion to heat flow:** it produces a more simplistic geological model. However, it does not take into consideration the SWIT and ignores the thermal effects of the sediments.

For this study, the Inversion to a lithospheric layer thickness process was used for 2D modelling (Table 2.4), because of the sparse density of offshore boreholes along each of the NovaSPAN lines.

Table 2.4: Input Value used for McKenzie Crustal Model.

Syn-Rift Period (Ma)		Post-Rift Period (Ma)
225 -200		180 - 0
Thickness Crust (m)	Thickness Mantle (m)	Base Lithosphere Temperature (°C)
32000	93000	1333
Crustal Thickness Ratio		
Upper Crust Ratio		Lower Crust Ratio
62.5		37.5

2.3.2 Simulation

The simulation process starts by restoring the original thickness for each lithostratigraphic unit, defined by the lithostratigraphic picks, using the back-stripping method of Watts and Ryan

(1976). This method quantitatively estimates the depth that the basement would have been in the absence of sediment and water loading. Once the original thickness for each layer is calculated, PetroMod simulates basin subsidence by applying compaction, and thermal properties through the geological time. The resulting calculated output from this process includes 2D temperature and vitrinite reflectance along each of the NovaSPAN models.

The output generated by the simulation process contains information about burial history, thermal maturation history, the timing of hydrocarbon generation, and the timing of hydrocarbon expulsion. Although each model has outputs from the simulation, each model must be calibrated and validated with the offshore borehole data (temperature and vitrinite reflectance) as respective input values significantly influence each output. For this study which focuses on the maturity of the Lower Jurassic source rocks, the simulation outputs are as follow the burial history, thermal maturation history, timing of hydrocarbon generation, and timing of hydrocarbon expulsion.

2.3.3 Salt modelling

Salt reconstruction through time is essential as the salt affects the structures, sediment dispersal along the Scotian Basin, and the thermal maturity of the source rocks (Ings and Shimeld, 2006; Goteti et al., 2013). To recreate the movement of the salt we need to discern the salt movement history: where the salt was deposited initially, when did the salt start and cease movement. This study tested both methods of salt modelling that can be used to recreate the salt mobilization through time. These methods are the “Salt Reconstruction” workflow and the “Salt Piercing” tool component that is built into PetroMod.

1) Salt Reconstruction workflow

Salt reconstruction is an advanced modelling workflow. This method reconstructs salt movement incrementally through geological time, modifying the salt shape, but preserving salt volume (or area in a 2D cross section) and it is repeated for every time event in the model. The key assumption is that the salt volume remains constant throughout the geological time interval. This method requires simulation, calculation of compaction, and reshaping of salt at each stage and is very iterative and time-consuming. The salt reconstruction workflow was tested only on the NovaSPAN 1400 model.

2) “Salt Piercing” Tool

This salt modelling tool models salt mobilization by estimating discrete times when the salt moved and pierced overlying layers, and so is a more efficient modelling technique. It also has the advantage that canopy structures, or sloping diapirs thrust onto younger sediments can be modelled. The key step in this approach is that a minimum thickness of overburden that is deposited prior to salt movement must be estimated. This was estimated to be 1.5-2.5 km based on numerical models (Warsitzka, Kukowski and Kley, 2017).

2.3.4 Calibration

The calibration of a PSM is needed to validate the results of the 2D petroleum systems models. This validation was done by comparing calculated and measured data available for the offshore boreholes (vitrinite reflectance and temperature). If the calculated data is not within the range of the measured borehole data, the model inputs must be changed, and the simulation must be rerun (or the data must be challenged). Vitrinite reflectance is a key method for identifying the maximum temperature history of sediments in sedimentary basins (Dow, 1977). It is assumed in this work that the vitrinite reflectance is representative of the thermal history of individual boreholes, however limitations to this methods have been described in Bustin (1996).

This process cannot be automated since there are too many variables, such as thermal heat flow from rifting or impact from salt tectonics, lithology (limestone, shale, sandstone), thickness, and quality of borehole data. These variables can impact the result of the model (Hantschel and Kauerauf, 2009). Once there is a satisfactory result, the model is a reasonable solution for understanding petroleum systems of the basin.

2.3.5 Uncertainty

To further validate the confidence of a model, each model was tested with a Monte Carlo simulation. Probability distributions of heat flow amount and heat flow timing were defined and Monte Carlo simulation (100 trials) then enabled a range of uncertainty in the models to be estimated (see Appendix D for results).

Each model was tested for uncertainties, PetroMod has a module called PetroRisk. PetroRisk is a risk management module that runs as a controlling framework on PetroMod models. This module allows uncertainties in geologic input data that are used as part of the

construction of the model (e.g. lithofacies properties and distributions, heat flow, source rocks, and boundary conditions such as erosion and tectonic influences) to be defined and the effects of these uncertainties on the outcome of the model. An uncertainty test was run on each model based on the highest uncertainty parameter, heat flow and time, in our model with these two parameters (Figure 2.4):

1. **Heat flow uncertainty:** Values are drawn from a probability distribution shift the heat flow trend of the model. In this study, a normal distribution was used with a confidence interval of 10% and 90% with uncertainty time frame of 225 Ma to 0 Ma, and with a 10 and 90 percentile.
2. **Heat flow time shift uncertainty:** The heat flow trend of the model is shifted in geological time according to a probability distribution. For this study, a normal distribution was used with a set the time shift to be a 10 and 90 percentile of a normal distribution (-6.4 Ma to 6.4 Ma).

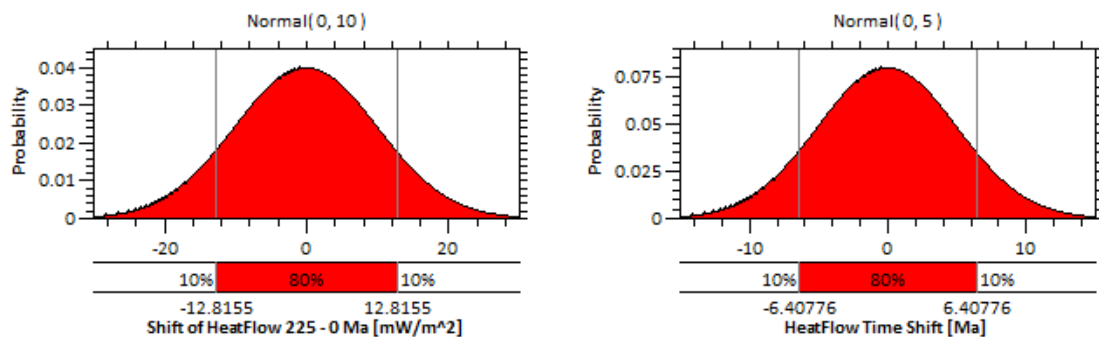


Figure 2.4: Normal Gauss distribution for the uncertainty parameter of heat flow and heat flow Time Shift.

Chapter 3: Results

3.1 Introduction

This study performed thermal modelling along four shelf-to-slope seismic lines. Each model comprises a seismically-derived 2D structural framework, rock properties in each layer (from wells and analogue outcrops) and input parameters that address heat generation and escape (heat flow) progressively through time. The modelling process requires progressive estimation of water depth and compaction in a simulation process. The outputs for each model are: paleo-water depth history, sediment-water interface temperature history, 1D temperature and vitrinite reflectance plots calibrated to borehole data; then 2D modelling results which comprise heat flow distribution, temperature distribution, maturation based on Sweeney & Burnham EASY%Ro (1990) method, transformation ratio, and critical moment (20% of potential hydrocarbons produced from source rock). In these model outputs, the Lower Jurassic source rock is of Pliensbachian age.

3.2 Paleo Water Depth (PWD)

The following Paleo water depth cross-sections created using PetroMod were based on extrapolation of seismic data in conjunction with biostratigraphic data from selected offshore boreholes, and paleowater depth based on eustatic sea level curves (Haq et al., 1987; Haq and Schutter, 2008). Figure 3.1 shows the paleowater depth used as a boundary condition for NovaSPAN 1800 model. Each line within each of the images corresponds to a PWD at a geologic time. The darkest blue line at the top of each image shows the PWD at 200 Ma. Each subsequent line represents a PWD at a younger geologic age up until present day.

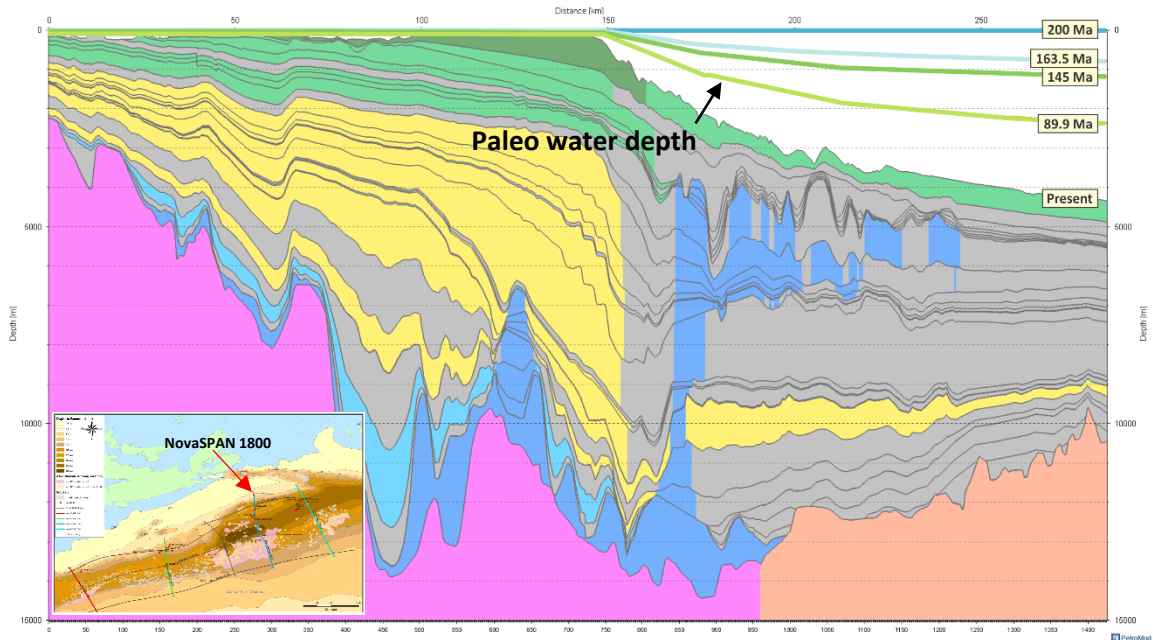


Figure 3.1: Paleo water depth of each NovaSPAN 1800. Each line represents the water depth profile at a given geological time. These colours between the layers are lithologies assigned to the models. Inset is the Scotian Basin map pointing the location of NovaSPAN 1800 (red arrow).

3.3 Sediment-Water Interface Temperature (SWIT)

To calculate the SWIT the contemporaneous latitude of an offshore borehole was used. These trends are based on the paleolatitude of an offshore borehole (Table 2.3). The resulting maps are for the global mean temperature for the Northern American hemisphere. The paleolatitude is shown as a white line based on the offshore borehole location for each model (Figure 3.2).

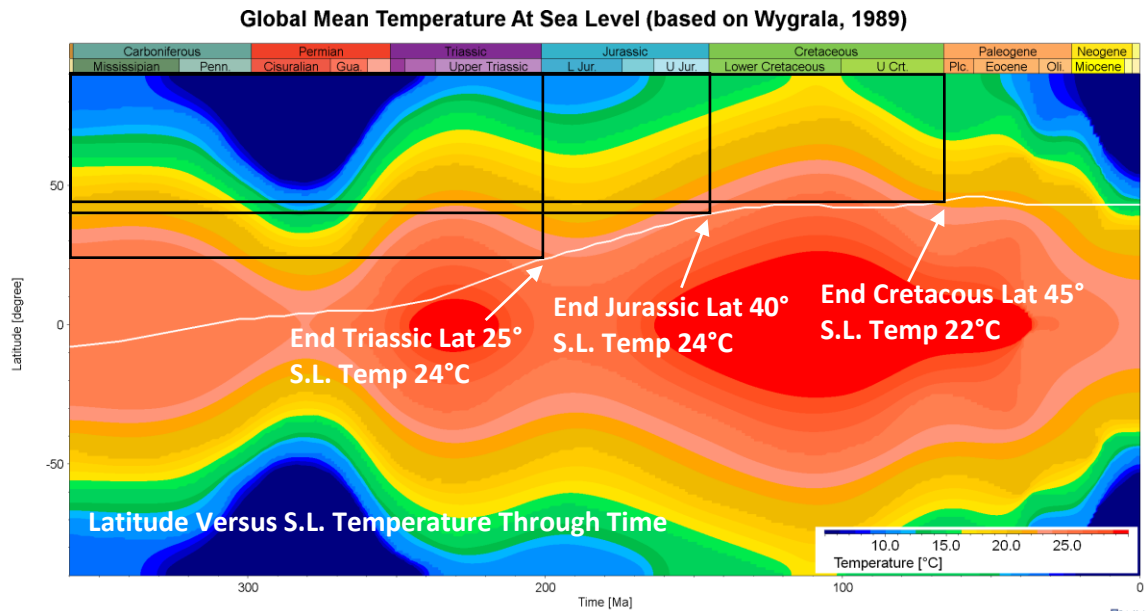


Figure 3.2: White line is the paleo sea level temperature at 43°N modern latitude in the Northern hemisphere near the Northern American continent, based on Wygrala (1989).

3.4 Uncertainty Tests

Each model was run with a Monte Carlo (MC) simulation 100 times. Sample points are selected without considering previously generated sample points sampling distribution, which is a random sampling (See Appendix D).

The diagram below illustrates the potential uncertainty in depth versus temperature and depth versus vitrinite reflectance at one of the most uncertain wells Torbrook C-15. The green line is the modelled depth temperature relationship, and the pink lines are the P10 and P90 depth-temperature lines from the Monte Carlo simulation described above. What this illustrates is that at a depth of Lower Jurassic source rock below the Torbrook C-15 well (7000 m) there is uncertainty in temperature (calculated temperature of 127°C with +29°C to -40°C) and vitrinite reflectance (calculated 0.82 %R_o with +0.44%R_o to -0.27%R_o). While the models presented here estimates the temperature and timing of heat flow based on McKenzie Models, there can be considerable uncertainties in some instances (for example where the potential source is considered deeper than the control well). See Appendix D for more details.

Torbrook C-15

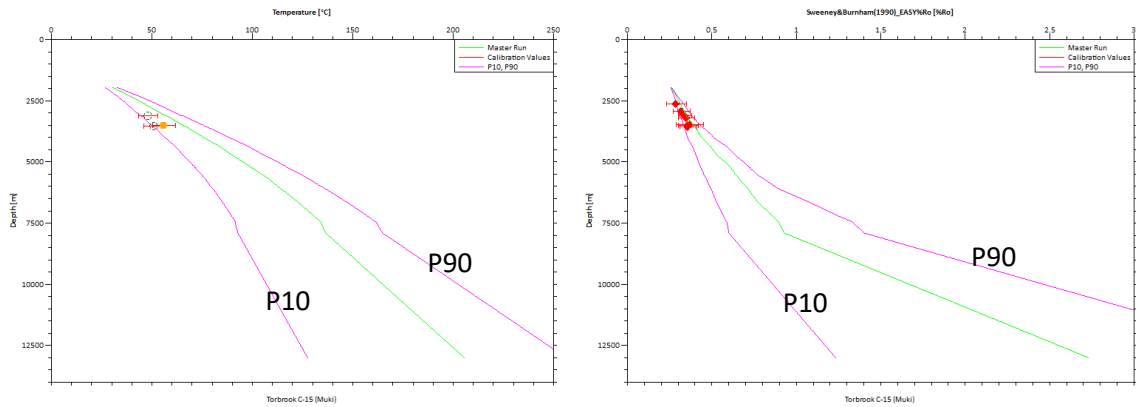


Figure A.1: Uncertainty test results from Monte Carlo simulation for Torbrook C-15. The green line is the modelled line, and pink lines are P10 and P90.

3.5 1D Models Calibrations

It is necessary to calibrate and to validate the model by plotting the model data against borehole data. The following plots are of temperature versus depth, and vitrinite reflectance versus depth. These plots compare model results against borehole data from Basin Database (See Appendix B).

Temperature data are recorded during log runs and typically requires a +10% to +30% adjustment to the actual formation temperatures (PetroMod training course). These adjustments are indicated in the temperature plots as horizontal bars from the data point. Vitrinite reflectance is the measurement of the incident light reflected on organic particles (macerals) in the sedimentary rocks (Tissot and Welte, 1984). Vitrinite reflectance is a method for identifying the maximal thermal history of sediments. Vitrinite reflectance interpretations can be misleading (Bustin, 1996) for a variety of reasons that include: oxidation, borehole caving, reworking, staining, improper vitrinite particles identification and drilling mud additives. Measurements often vary depending on individual workers and date.

1. Bonnet P-23

The Bonnet P-23 is the only borehole that is close to the NovaSPAN 1100. This borehole is about 22.13 km offset from the NovaSPAN 1100, and this presented a challenge when calibrating the model. The comparison between the measured data and model output results of temperature and vitrinite reflectance (Figure 3.3), shows that the correlation between the model and the borehole data are within a reasonable confidence for both temperature and vitrinite reflectance plots.

NovaSPAN 1100 - Bonnet P-23

34

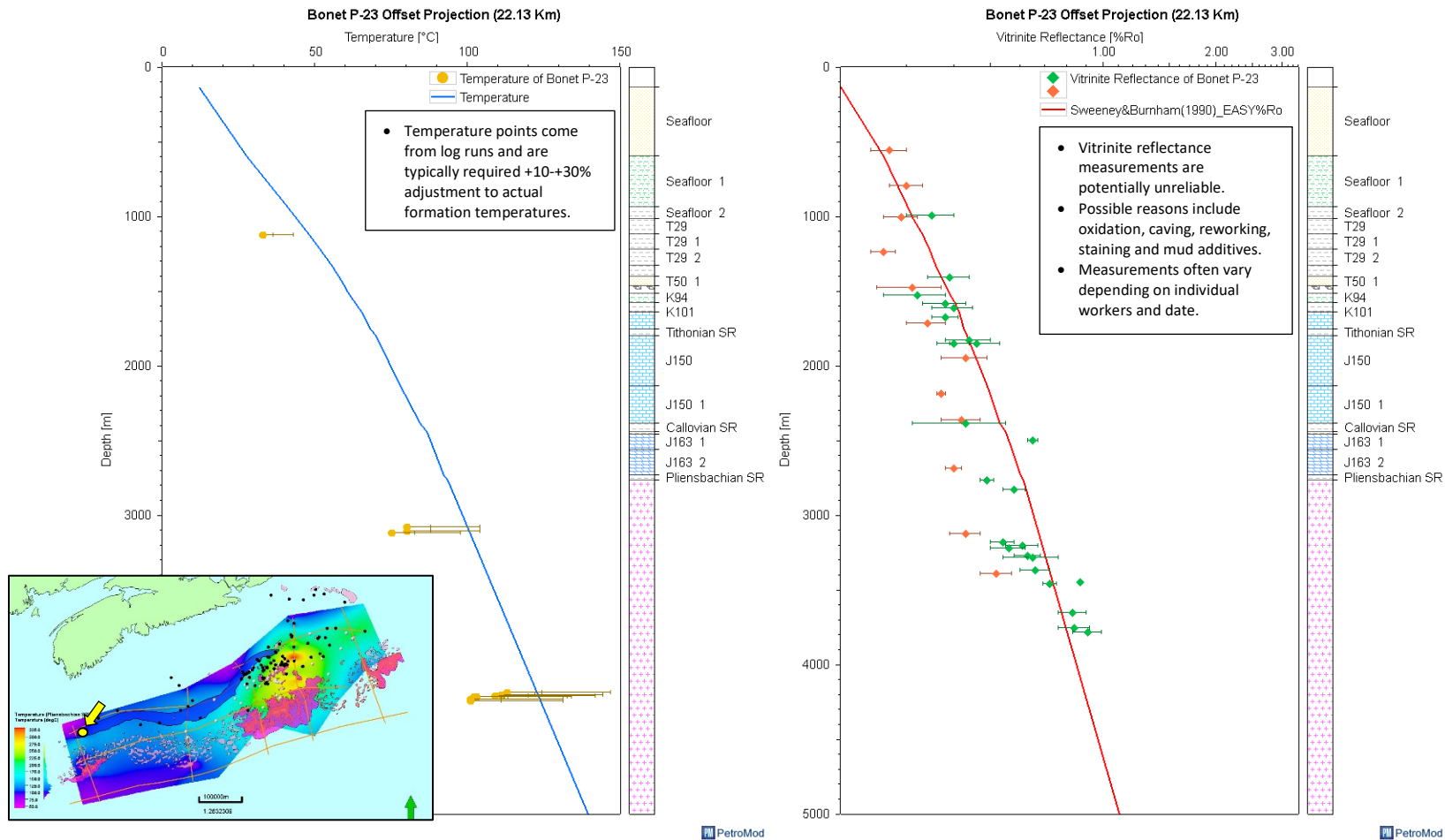


Figure 3.3: 1D models results for Bonnet P-23. The left plot is the temperature model, and the right plot is the vitrinite reflectance plot. The solid blue line is the modelled temperature results; the yellow circles are the data points collected at the borehole (Appendix B). The red line is the vitrinite reflectance modelled result based on Sweeney & Burnham (1990). The orange and green diamonds are the vitrinite reflectance data points measured at the borehole (Appendix B).

2. Glooscap C-63, Moheida P-15, Mohican I-100 and Torbrook C- 15

The following plots (Figures 3.4 - 3.7) are the comparison plots for Glooscap C-63, Moheida P-15, Mohican I-100 and Torbrook C- 15 models. These plots were used to validate the NovaSPAN 1400 model. Glooscap C-63 (10.30 km) and Mohican I-100 (16.50 km) boreholes are offset from the NovaSPAN 1400. The Torbrook C-15 is a shallow borehole in the slope region that only penetrates the Banquereau Formation. The only borehole that is on the NovaSPAN 1400 is Moheida P-15, and for this borehole, there is no vitrinite reflectance data.

The following temperature plots for these four boreholes show that is a reasonable fit, on the other hand, the vitrinite reflectance plots, the only borehole that the vitrinite reflectance matches is the Torbrook C-63. For Glooscap C-63 the plot models lower vitrinite reflectance, but it follows the same trending of the data, this is possible due to the misleading errors that the vitrinite reflectance may have. For Mohican I-100 the vitrinite reflectance plots higher than the data points , this could be for either rework of the samples or caving of the samples.

NovaSPAN 1400 - Glooscap C-63

36

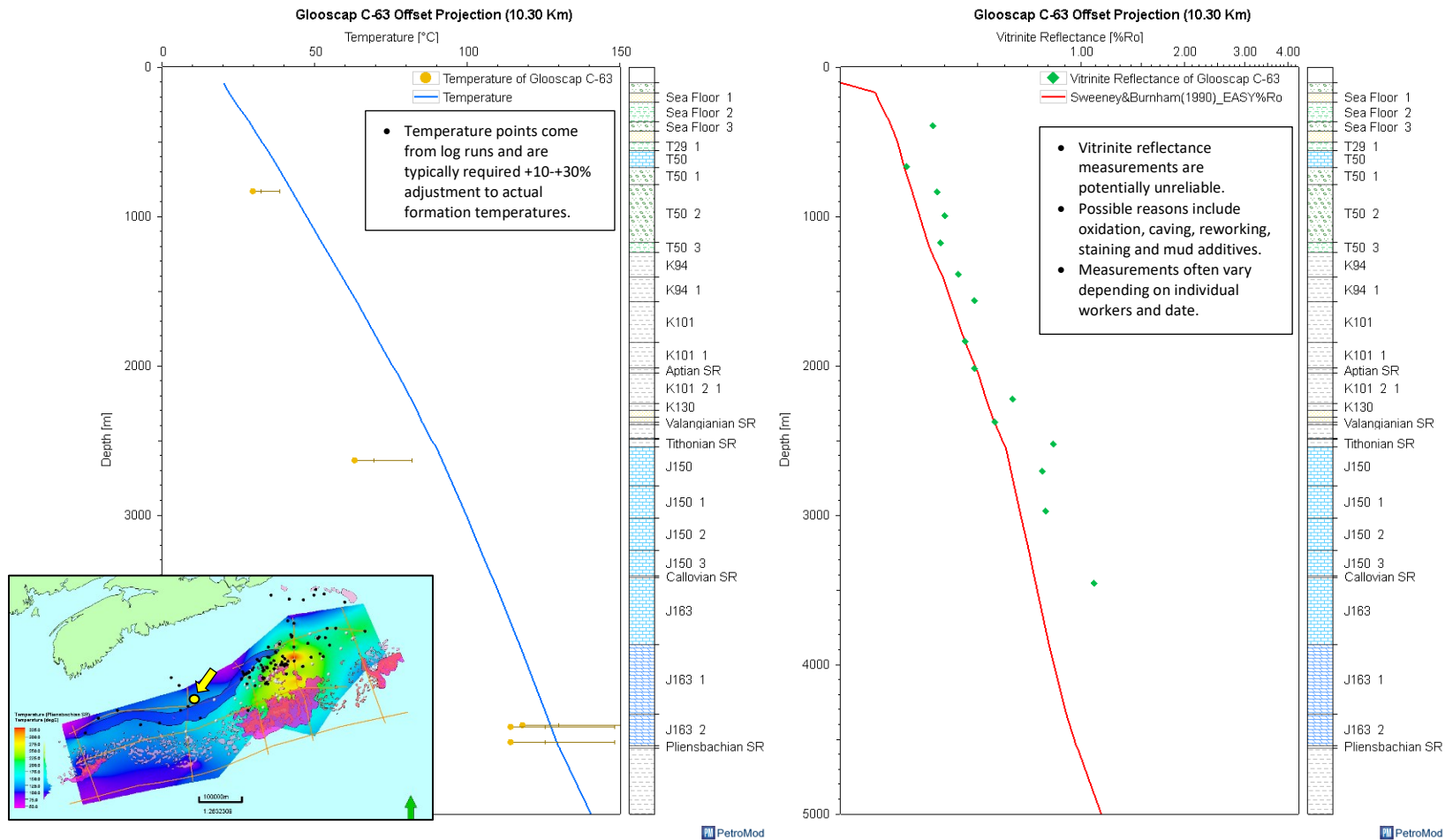


Figure 3.4: 1D models results for Glooscap C-63. The left plot is the temperature model, and the right plot is the vitrinite reflectance plot. The solid blue line is the modelled temperature results; the yellow circles are the data points collected at the borehole (Appendix B). The red line is the vitrinite reflectance modelled result based on Sweeney & Burnham (1990). The green diamonds are the vitrinite reflectance data points measured at the borehole (Appendix B).

NovaSPAN 1400 - Moheida P-15

37

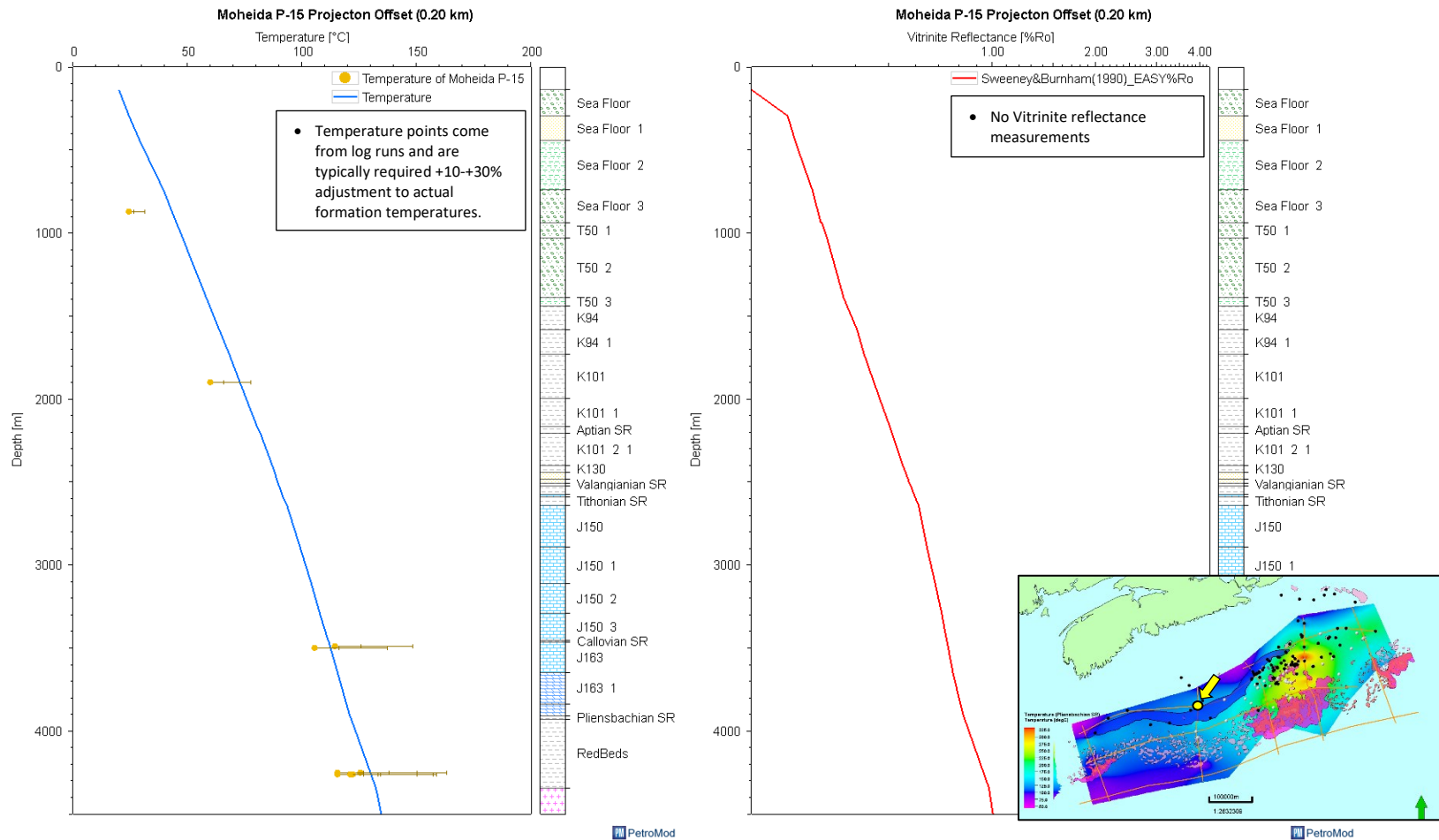


Figure 3.5: 1D models results for Moheida P-15. The left plot is the temperature model, and the right plot is the vitrinite reflectance plot. The solid blue line is the modelled temperature results; the yellow circles are the data points collected at the borehole (Appendix B). The red line is the vitrinite reflectance modelled result based on Sweeney & Burnham (1990). There were no vitrinite reflectance measurements from this borehole available (Appendix B).

NovaSPAN 1400 - Mohican I-100

38

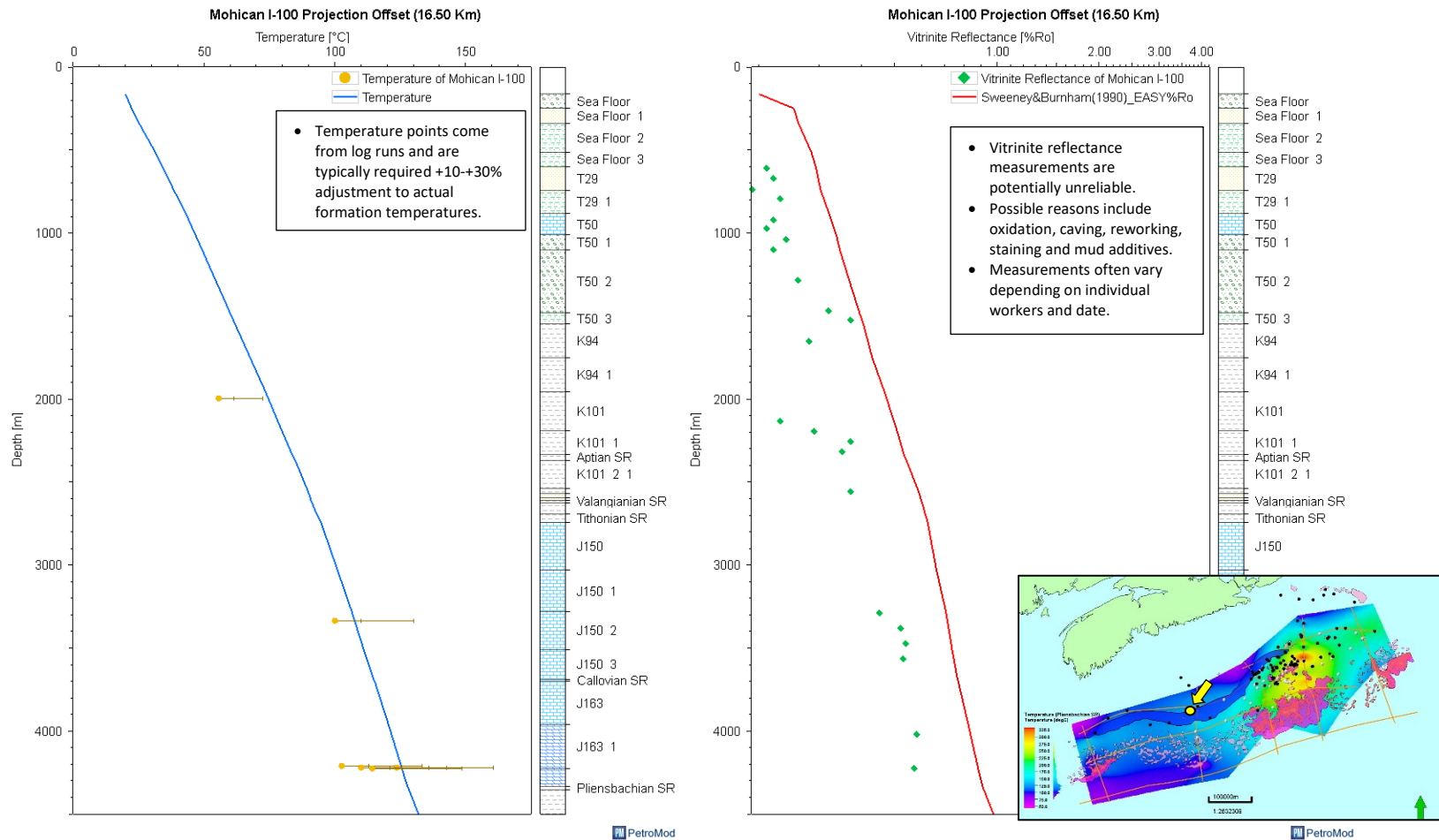


Figure 3.6: 1D models results for Mohican I-100. The left plot is the temperature model, and the right plot is the vitrinite reflectance plot. The solid blue line is the modelled temperature results; the yellow circles are the data points collected at the borehole (Appendix B). The red line is the vitrinite reflectance modelled result based on Sweeney & Burnham (1990). The green diamonds are the vitrinite reflectance data points measured at the borehole (Appendix B).

NovaSPAN 1400 - Torbrook C-15

39

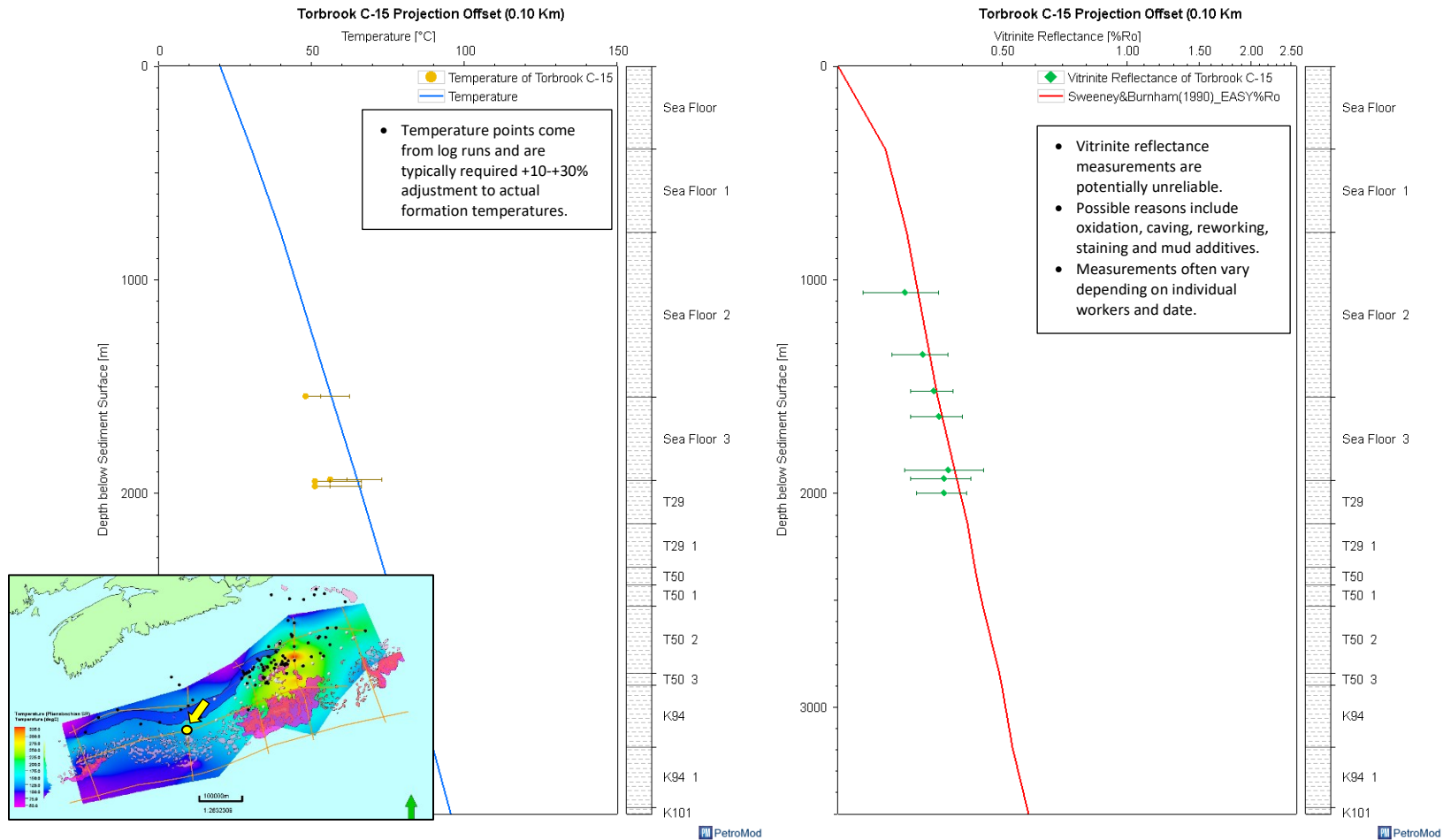


Figure 3.7: 1D models results for Torbrook C-15. The left plot is the temperature model, and the right plot is the vitrinite reflectance plot. The solid blue line is the modelled temperature results; the yellow circles are the data points collected at the borehole (Appendix B). The red line is the vitrinite reflectance modelled result based on Sweeney & Burnham (1990). The green diamonds are the vitrinite reflectance data points measured at the borehole (Appendix B).

3. Bluenose G-47, Bluenose 2G-47, Missisauga H-54 and Wyandot E-53

The following plots (Figures 3.8 - 3.11) are the comparison plots for Bluenose G-47, Bluenose 2G-47, Missisauga H-54 and Wyandot E-53 models. These plots were used to validate the NovaSPAN 1800 model. The Missisauga H-54 and Wyandot E-53 plots does not match the borehole data comfortably. The vitrinite reflectance data points from these offshore boreholes were collected in 1973 (See Appendix B), at that time the data control was not to standards of the present day, and vitrinite reflectance interpretations can be misleading (Bustin, 1996) for a variety of reasons that include: oxidation, borehole caving, reworking, staining, improper vitrinite particles identification and drilling mud additives. Measurements often vary depending on individual. Bluenose G-47 and Bluenose 2G-47, are reasonable plots for the temperature and vitrinite reflectance. In Bluenose 2G-47, it is observed two different data sets and comparing both datasets in this plot shows that the vitrinite reflectance data can be misleading. The validation of this model was based on Bluenose G-47 and Bluenose 2G-47. These boreholes were chosen as validation points for the model because they are in closest proximity and give the nearest control points to the slope and abyssal regions and, therefore, would most likely resemble any potential Lower Jurassic source rock material from these two distal regions within the basin.

NovaSPAN 1800 - Bluenose G-47

41

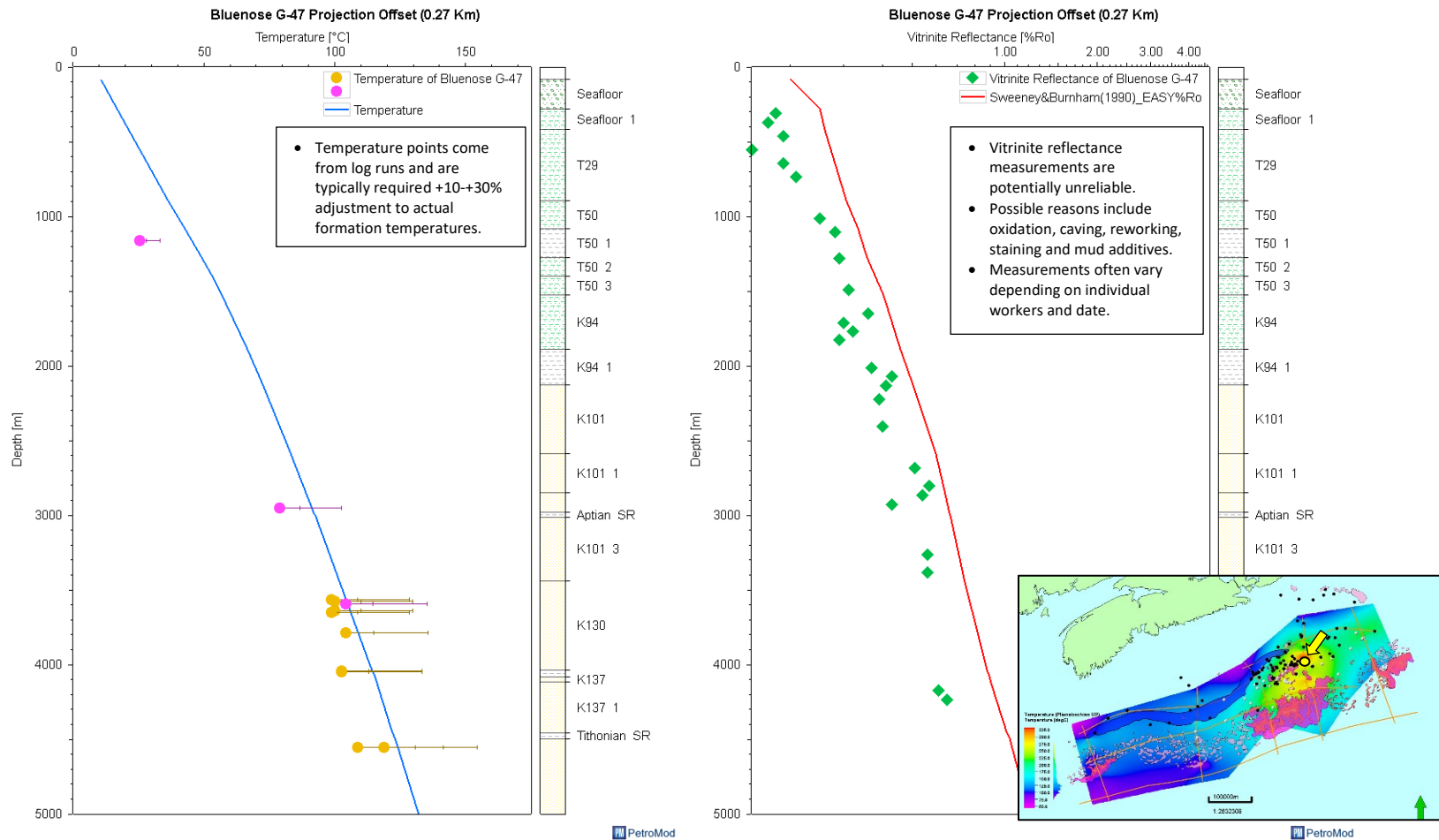


Figure 3.8: 1D models results for Bluenose G-47. The left plot is the temperature model, and the right plot is the vitrinite reflectance plot. The solid blue line is the modelled temperature results, the yellow and pink circles are the data points collected at the borehole (Appendix B). The red line is the vitrinite reflectance modelled result based on Sweeney & Burnham (1990). The green diamonds are the vitrinite reflectance data points measured at the borehole (Appendix B).

NovaSPAN 1800 - Bluenose 2G-47

42

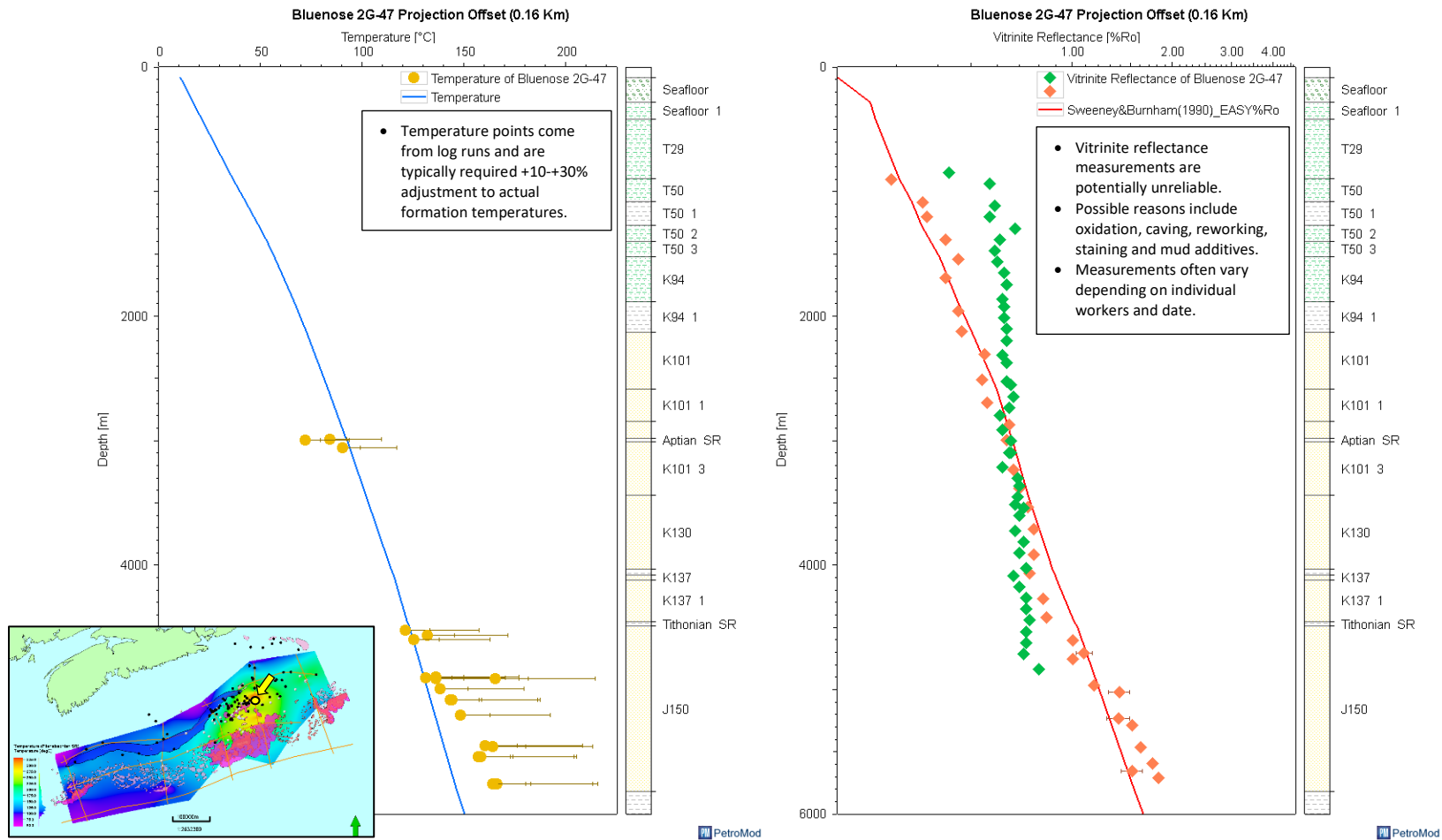


Figure 3.9: 1D models results for Bluenose G-47. The left plot is the temperature model, and the right plot is the vitrinite reflectance plot. The solid blue line is the modelled temperature results; the yellow circles are the data points collected at the borehole (Appendix B). The red line is the vitrinite reflectance modelled result based on Sweeney & Burnham (1990). The green diamonds are the vitrinite reflectance data points measured at the borehole (Appendix B).

NovaSPAN 1800 - Missisauga H-54

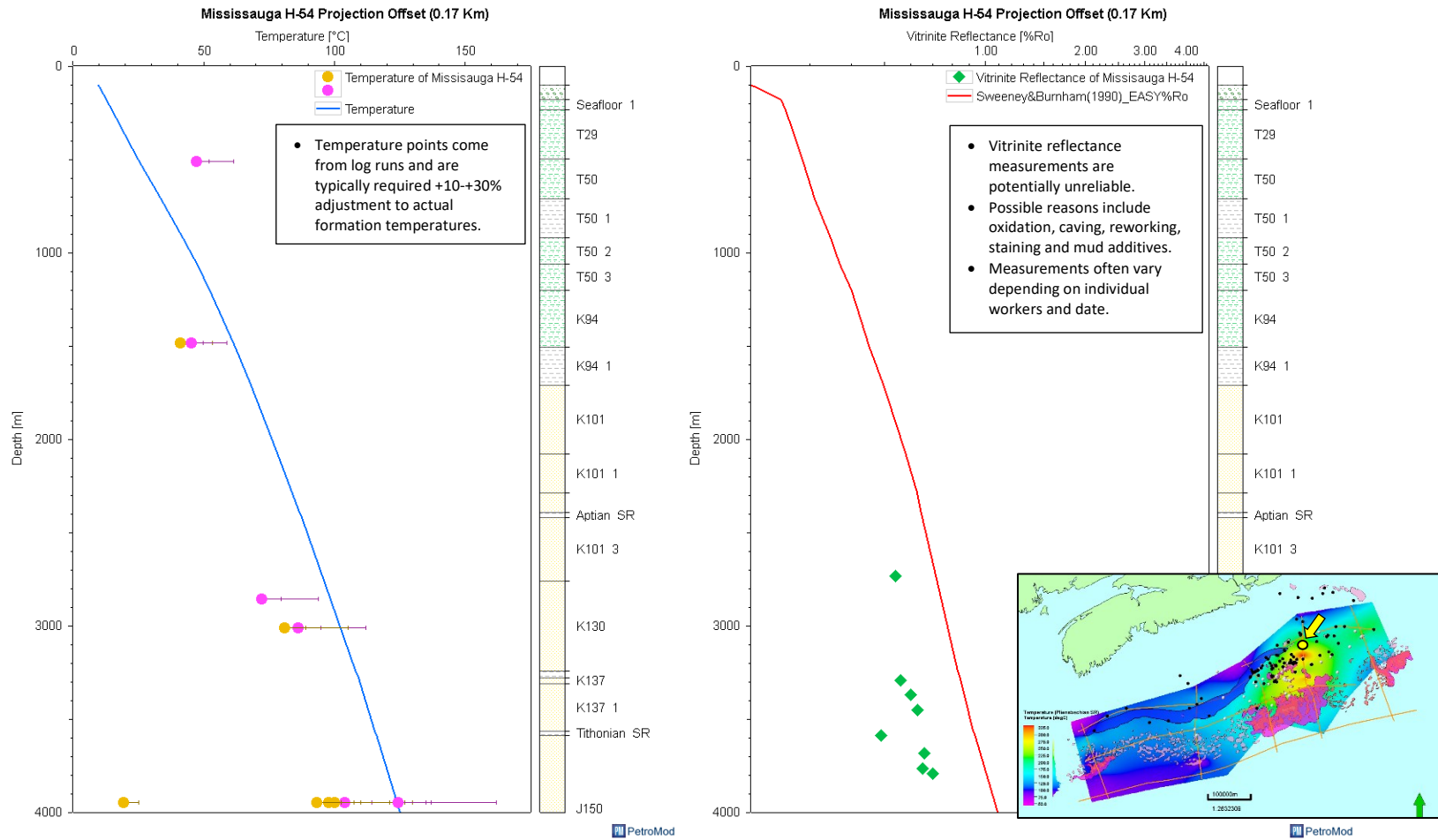


Figure 3.10: 1D models results for Missisauga H-54. The left plot is the temperature model, and the right plot is the vitrinite reflectance plot. The solid blue line is the modelled temperature results, the yellow and pink circles are the data points collected at the borehole (Appendix B). The red line is the vitrinite reflectance modelled result based on Sweeney & Burnham (1990). The green diamonds are the vitrinite reflectance data points measured at the borehole (Appendix B).

NovaSPAN 1800 - Wyandot E-53

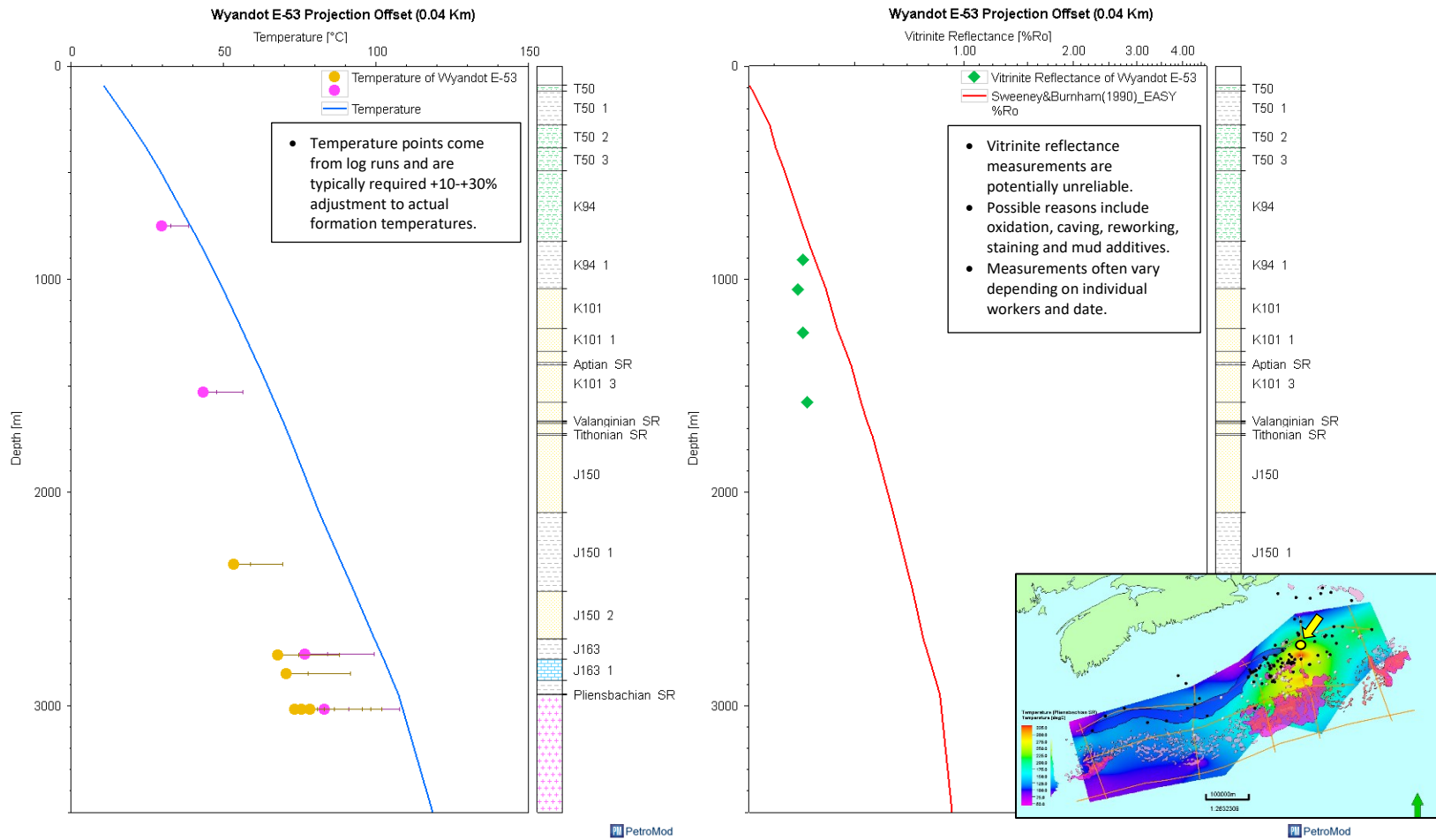


Figure 3.11: 1D models results for Wyandot E-53. The left plot is the temperature model, and the right plot is the vitrinite reflectance plot. The solid blue line is the modelled temperature results, the yellow and pink circles are the data points collected at the borehole (Appendix B). The red line is the vitrinite reflectance modelled result based on Sweeney & Burnham (1990). The green diamonds are the vitrinite reflectance data points measured at the borehole (Appendix B).

4. Hesper I-52, Hesper P-52, Sachem D -76 and South Griffin J-13

The following plots (Figures 3.12 - 3.15) are comparison plots for Hesper I-52, Hesper P-52, Sachem D -76 and South Griffin J-13 models. These plots were used to validate the NovaSPAN 2000 model. The borehole South Griffin J-13 is an offset borehole, about 36.49 km. The South Griffin J-13 plots show to be a mismatch in the temperature plot. This mismatch is probably due to the cooling of the formation from the mud while drilling. The borehole of Hesper P-52 had no vitrinite reflectance data. Although the Hesper I-52, which is adjacent to Hesper P-52, the model plots for temperature and vitrinite reflectance matches reasonably. The Sachem D-76 borehole is along the NovaSPAN; the model plots are a reasonable fit for both temperature and vitrinite.

NovaSPAN 2000 - Hesper I-52

46

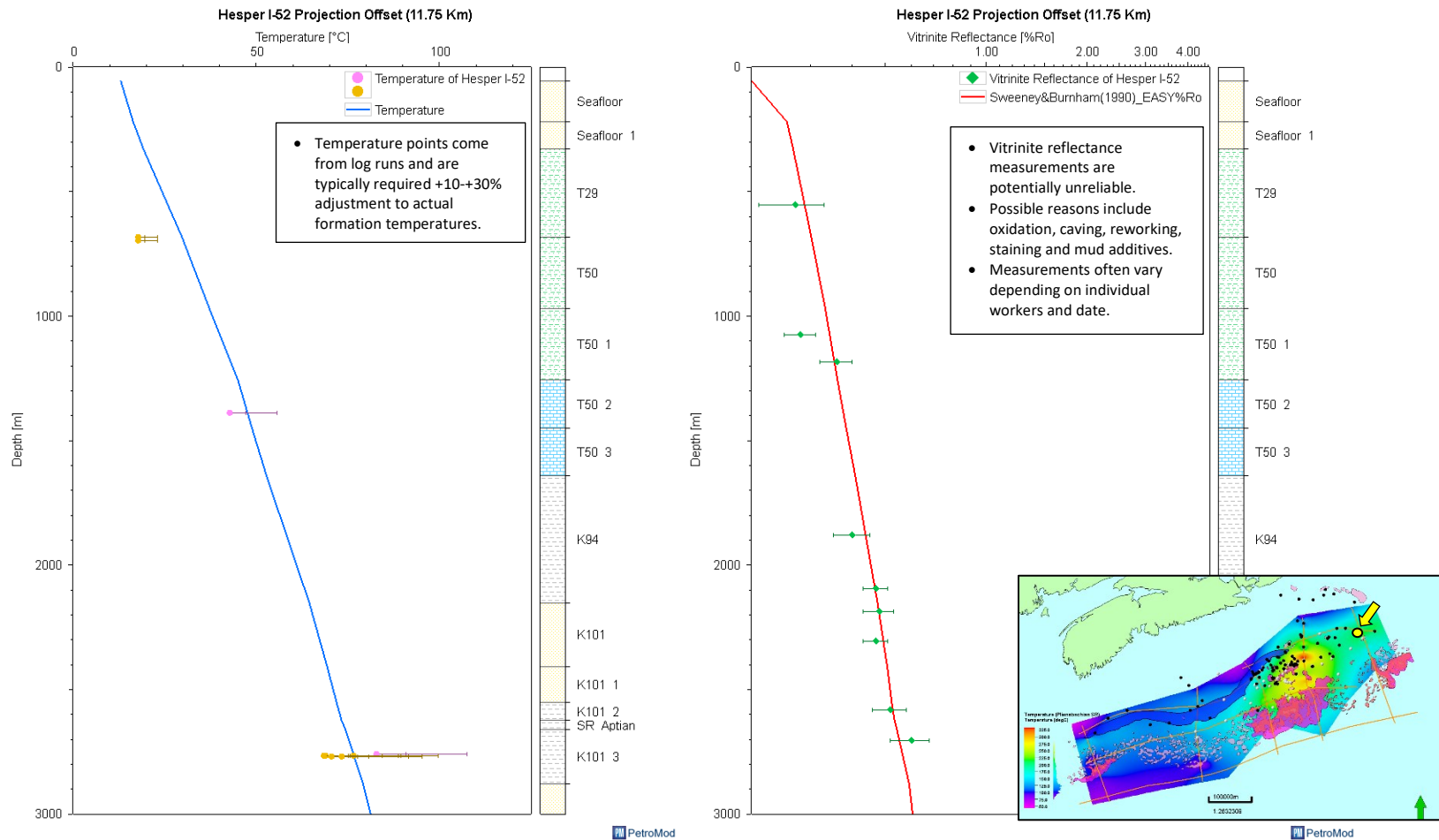


Figure 3.12: 1D models results for Hesper I-52. The left plot is the temperature model, and the right plot is the vitrinite reflectance plot. The solid blue line is the modelled temperature results, the yellow and pink circles are the data points collected at the borehole (Appendix B). The red line is the vitrinite reflectance modelled result based on Sweeney & Burnham (1990). The green diamonds are the vitrinite reflectance data points measured at the borehole (Appendix B).

NovaSPAN 2000 - Hesper P-52

47

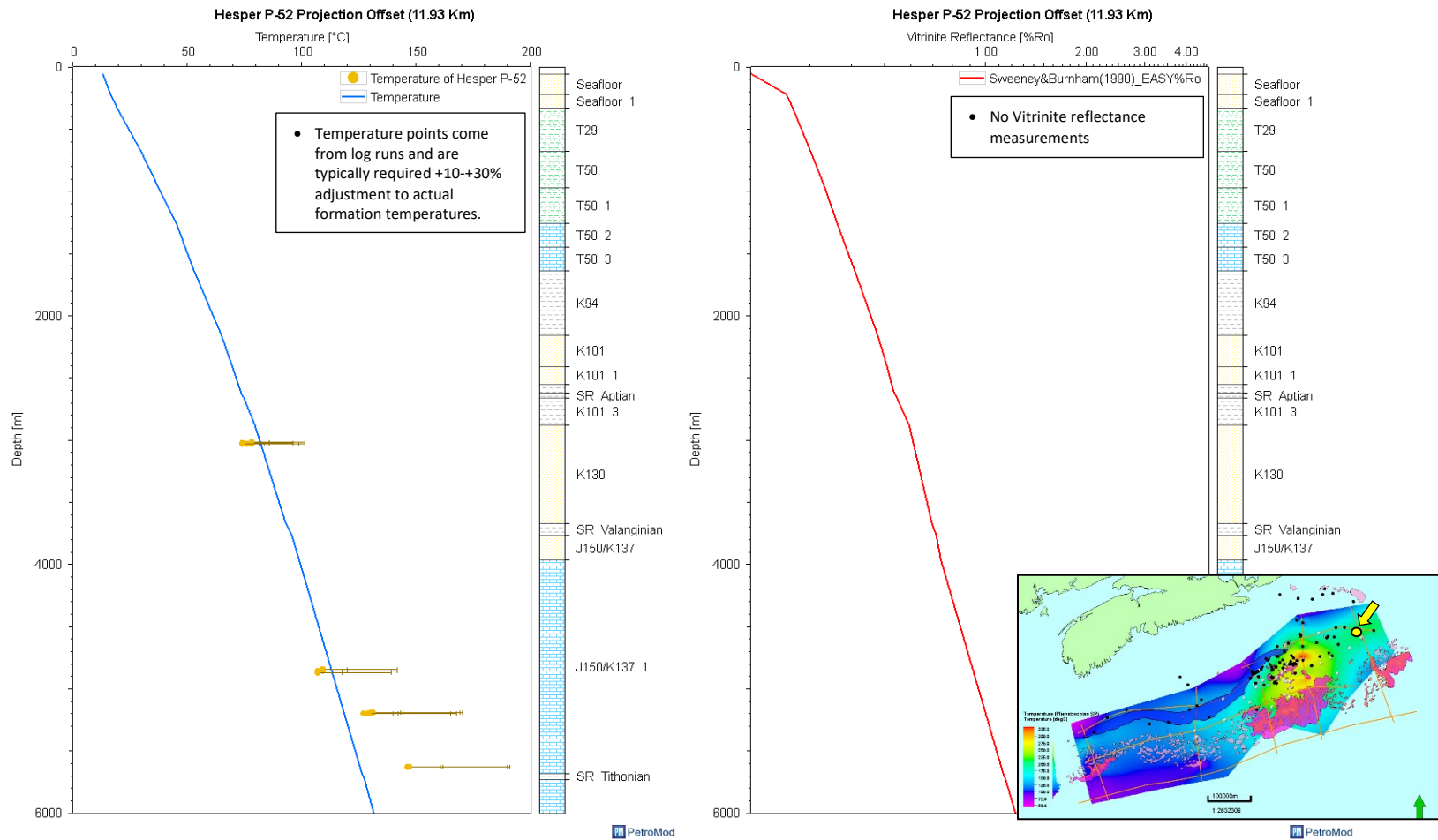


Figure 3.13: 1D models results for Bluenose G-47. The left plot is the temperature model, and the right plot is the vitrinite reflectance plot. The solid blue line is the modelled temperature results; the yellow is the data points collected at the borehole (Appendix B). The red line is the vitrinite reflectance modelled result based on Sweeney & Burnham (1990). There were no vitrinite reflectance measurements from this borehole available (Appendix B).

NovaSPAN 2000 - Sachem D-76

48

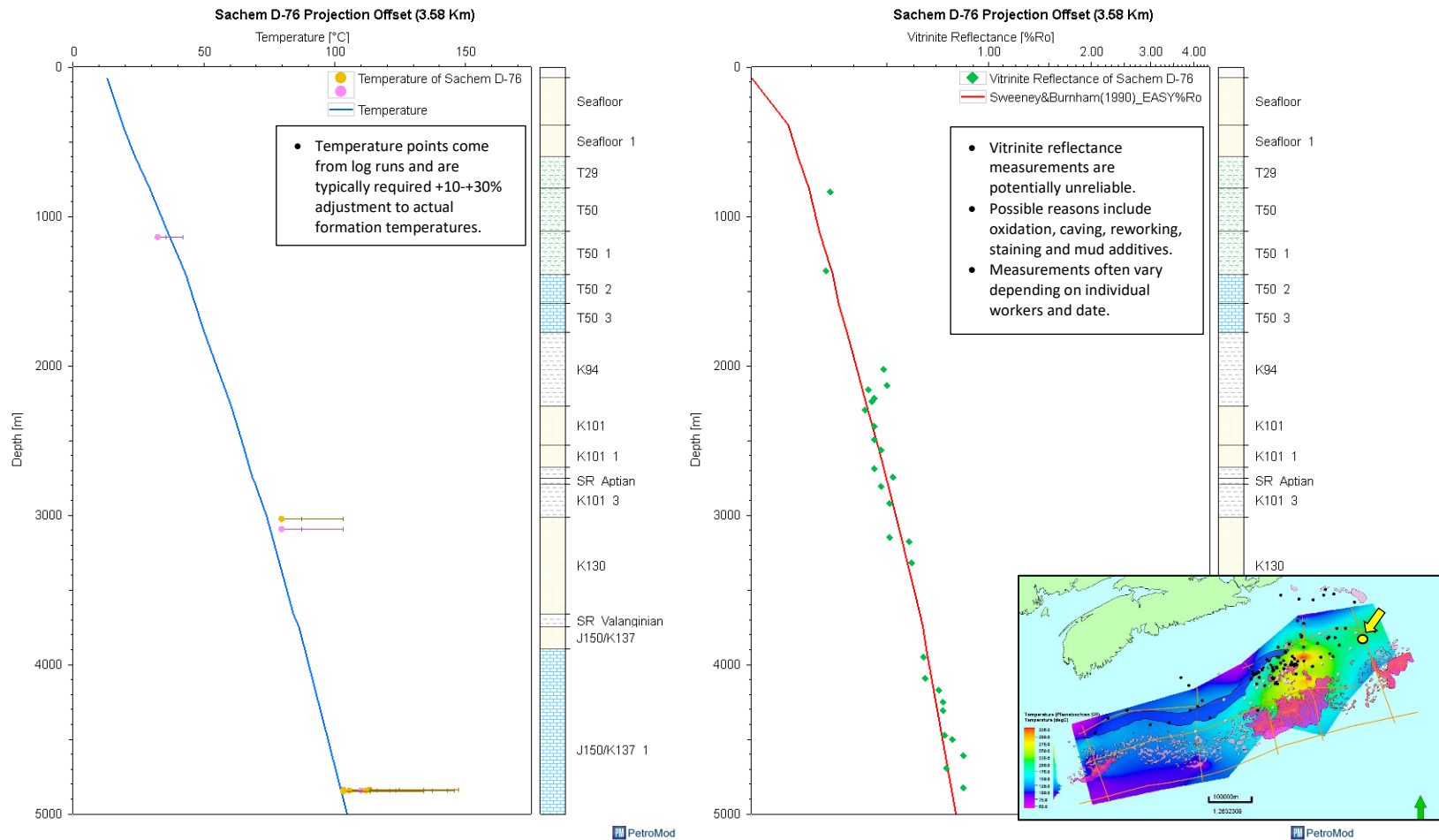


Figure 3.14: 1D models results for Sachem D-76. The left plot is the temperature model, and the right plot is the vitrinite reflectance plot. The solid blue line is the modelled temperature results; the yellow is the data points collected at the borehole (Appendix B). The red line is the vitrinite reflectance modelled result based on Sweeney & Burnham (1990). The green diamonds are the vitrinite reflectance data points measured at the borehole (Appendix B).

NovaSPAN 2000 - South Griffin J-13

49

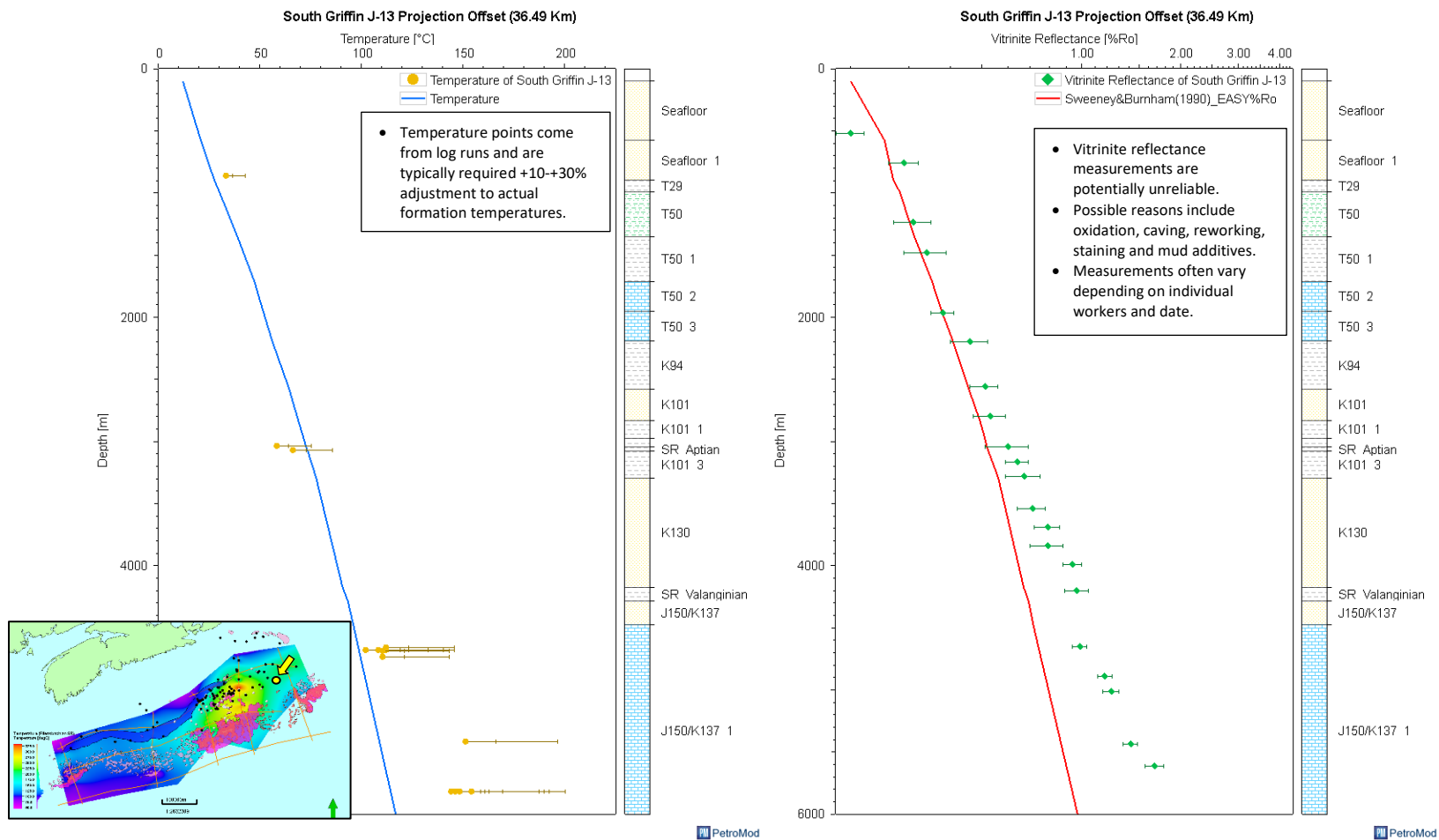


Figure 3.15: 1D models results for South Griffin J-13. The left plot is the temperature model, and the right plot is the vitrinite reflectance plot. The solid blue line is the modelled temperature results; the yellow is the data points collected at the borehole (Appendix B). The red line is the vitrinite reflectance modelled result based on Sweeney & Burnham (1990). The green diamonds are the vitrinite reflectance data points measured at the borehole (Appendix B).

3.6 2D NovaSPAN Models

The following cross-sections are the results from the 2D models of the NovaSPAN. These cross-sections show the heat flow, the temperature, the maturity, the transformation ratio and the critical moment of the potential Lower Jurassic source rock. The heat flow cross-section shows the distribution of vertical heat flow within the model. The temperature cross-section shows the temperature distribution within the model. The maturity cross-section displays vitrinite reflectance distribution using the EASY%Ro algorithm after Sweeney and Burnham (1990). The transformation ratio cross-section displays the percentage of the total potential primary generation of the potential Lower Jurassic source rock that has been generated. The critical moment cross-section presents the time when the Lower Jurassic source rock reached a 20% transformation ratio, which is an estimate of the time at which the petroleum system becomes effective regarding generation, migration and accumulation in this study.

1. NovaSPAN 1100

Heat Flow and Temperature

The heat flow cross-section shows the distribution of heat that is being transferred vertically within the model (Figure 3.16). The model takes into consideration the burial history and the crustal heat flow history, with the thermal conductivity from the lithology from the model. This cross-section displays the impact that the salt has on the model, creating hot spots on the cusp of the salt diapirs, these higher heat flows also impacts the temperature cross-section in the model. As observed in the model (Figure 3.17) the temperature gradient being pushed down at the bottom of the diapir and bumped up at in the top o the salt diapirs.

NovaSPAN 1100 – Heat Flow

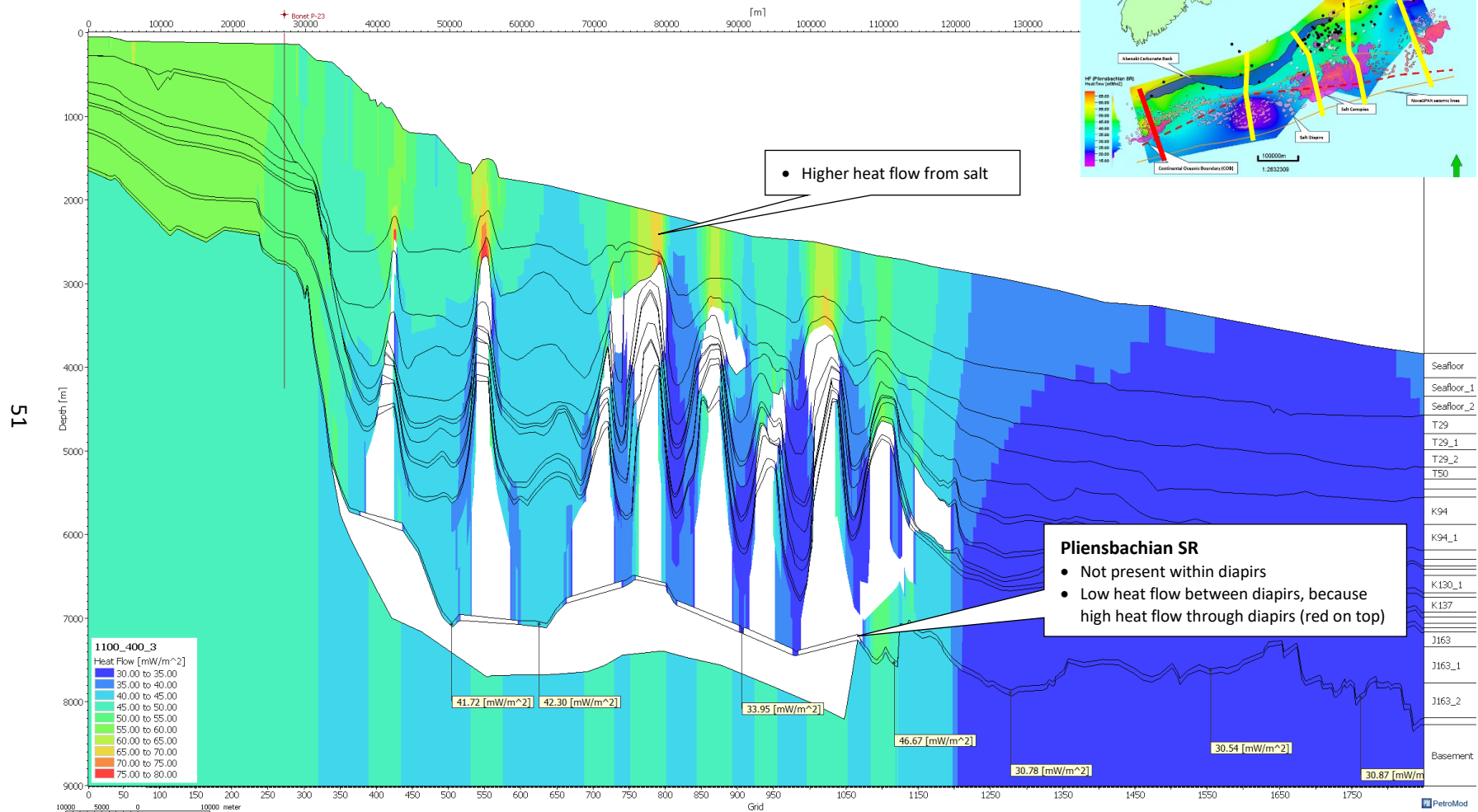


Figure 3.16: Model of heat flow distribution for NovaSPAN 1100 line. The data points indicate the heat flow value of the potential Lower Jurassic source rock layer. The white areas are the salt structures from the Argo Formation.

NovaSPAN 1100 – Temperature

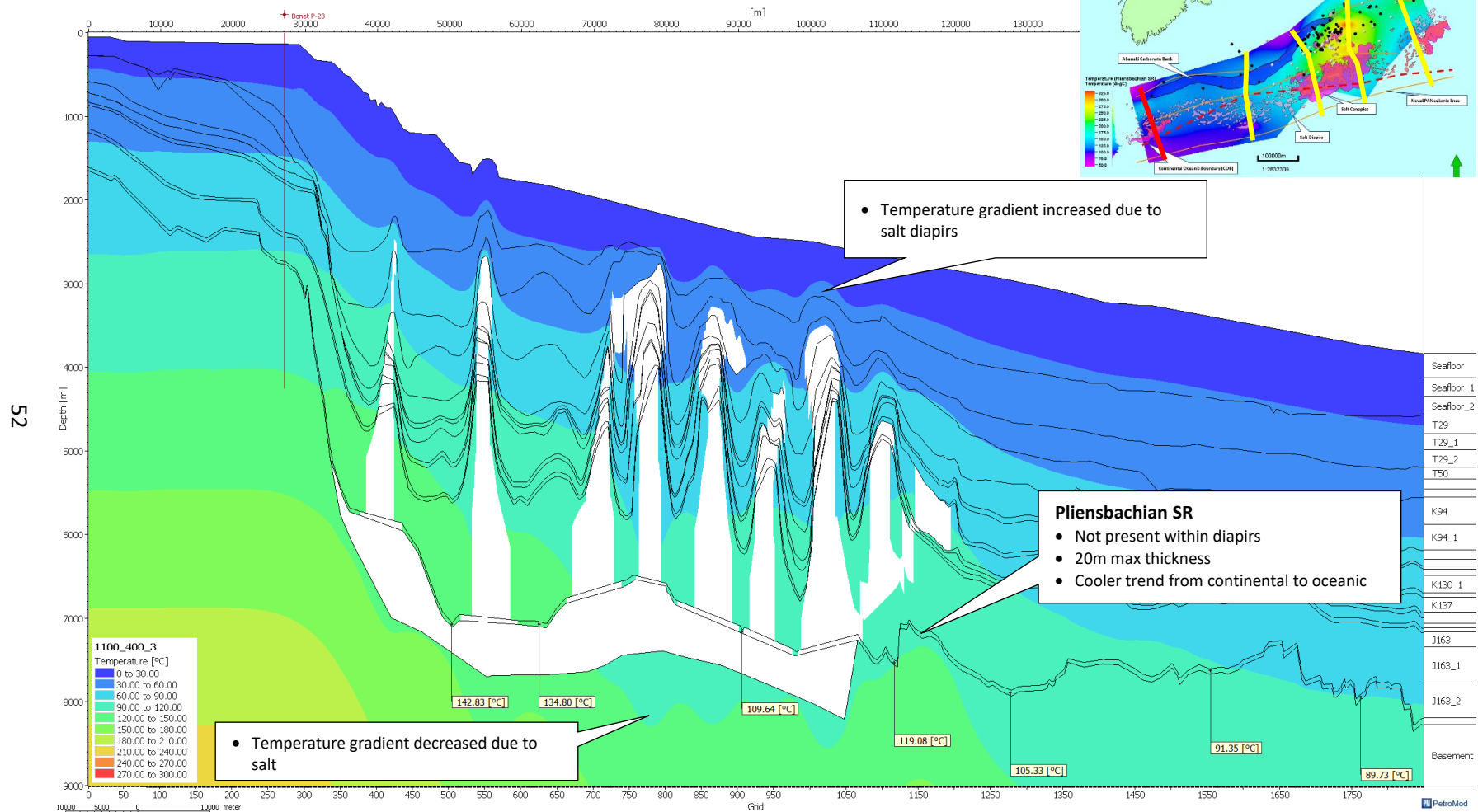


Figure 3.17: Model of temperature distribution for NovaSPAN 1100 line. The data points indicate the temperature value of the potential Lower Jurassic source rock layer. The white areas are the salt structures from the Argo Formation.

Maturity Range, Transformation Ratio and Critical Moment

The maturity cross-section is the vitrinite reflectance modelled after the EASY%Ro algorithm (Sweeney and Burnham, 1990). This cross-section demonstrates that the Lower Jurassic rocks are within the maturity oil window (Figure 3.18) and have the potential to be a source rock. Testing this model with the different kerogen types (Table 1.1), the model demonstrates a range of results depending upon the kerogen type of the Lower Jurassic source rock. The transformation ratio cross-section is a quantitative transformation measurement of organic material into hydrocarbons based on total organic carbon and hydrogen index in the organic-rich rock. In these cross-sections (Figures 3.19 - 3.21), five different source rock intervals can be observed, but the focus of this study is specifically the bottommost layer, which is the representative of the Lower Jurassic source rock. The Lower Jurassic source rock is also a close representation to the "Lower Jurassic Complex" that the PFA named for their source rock. These transformation ratio cross-sections demonstrate a broad range of results depending upon the source rock kerogen type and location along the line. The "critical moment cross-section" is the age when the source rock had generated 20% of the convertible kerogen, which is the age when the transformation ratio of the source rock was 20% (Figures 3.22 - 3.24). The following set of cross-sections demonstrates the critical moment for each modelled kerogen type (Table 1.1).

NovaSPAN 1100 – Maturity

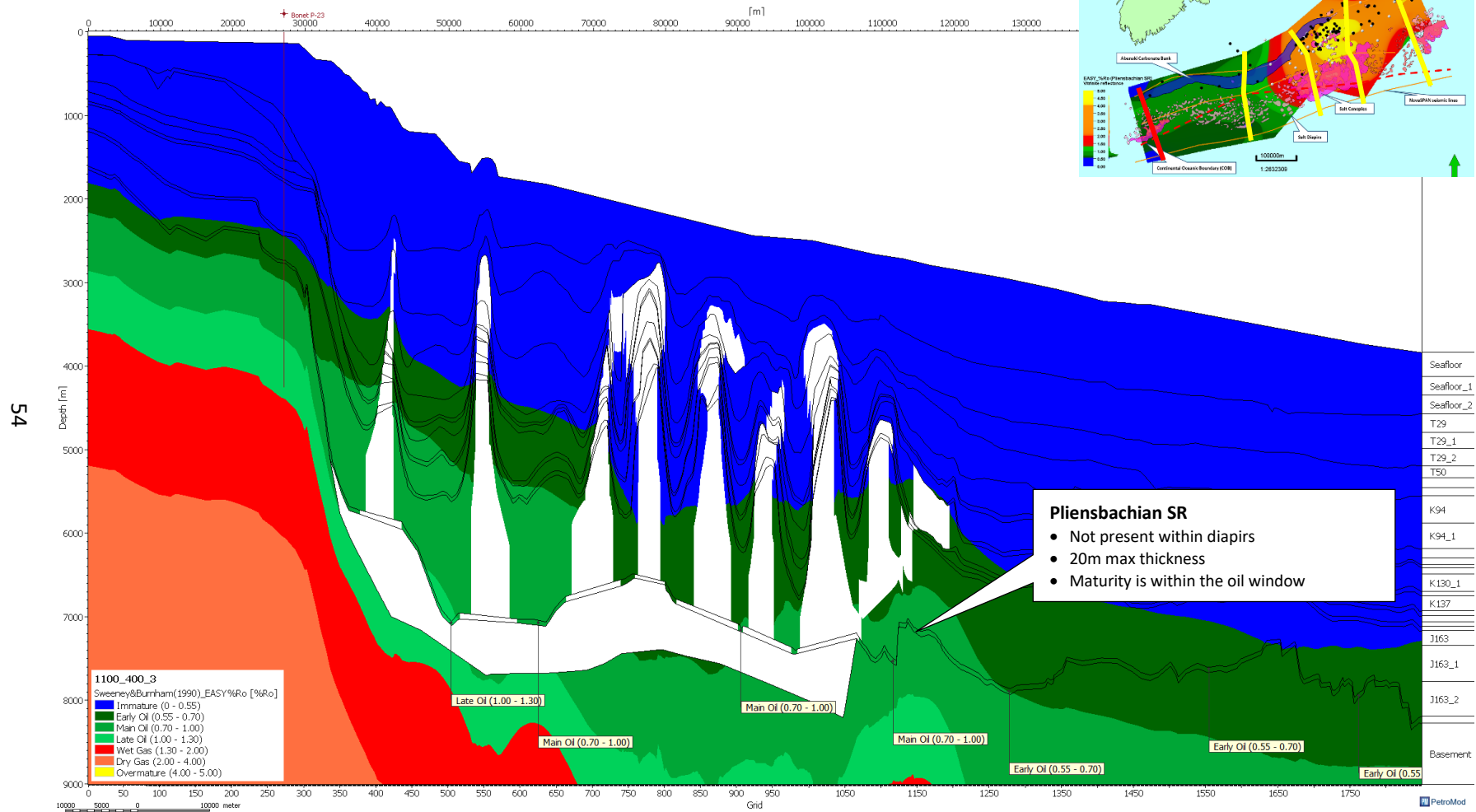


Figure 3.18: Model of vitrinite reflectance distribution for NovaSPAN 1100. The data points indicate the vitrinite reflectance value based on the Sweeney and Burnham (1990) algorithm for the potential Lower Jurassic source rock layer. The white areas are the salt structures from the Argo Formation. The potential Lower Jurassic source rock is in the oil window.

NovaSPAN 1100 – Transformation Ratio (Pliensbachian Source Rock -Type III)

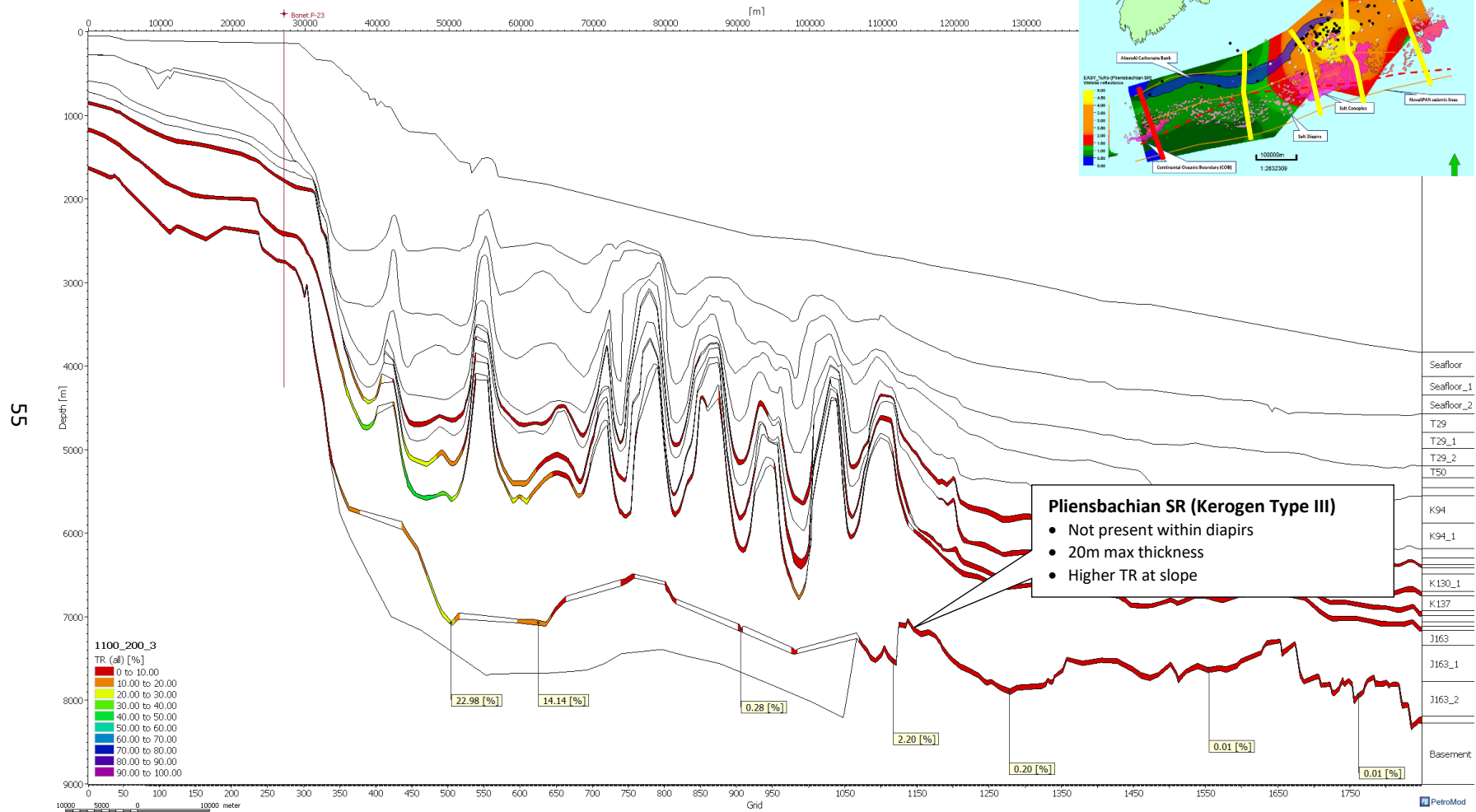


Figure 3.19: Model of transformation ratio for Pliensbachian source rock (Type III) for NovaSPAN 1100 line. Here we can observe the five different source rocks in the model; the Lower Jurassic source rock is the bottommost layer. The data points indicate the percentage of the value of hydrocarbons generated from the potential Lower Jurassic source rock layer.

NovaSPAN 1100 – Transformation Ratio (Pliensbachian Source Rock -Type II)

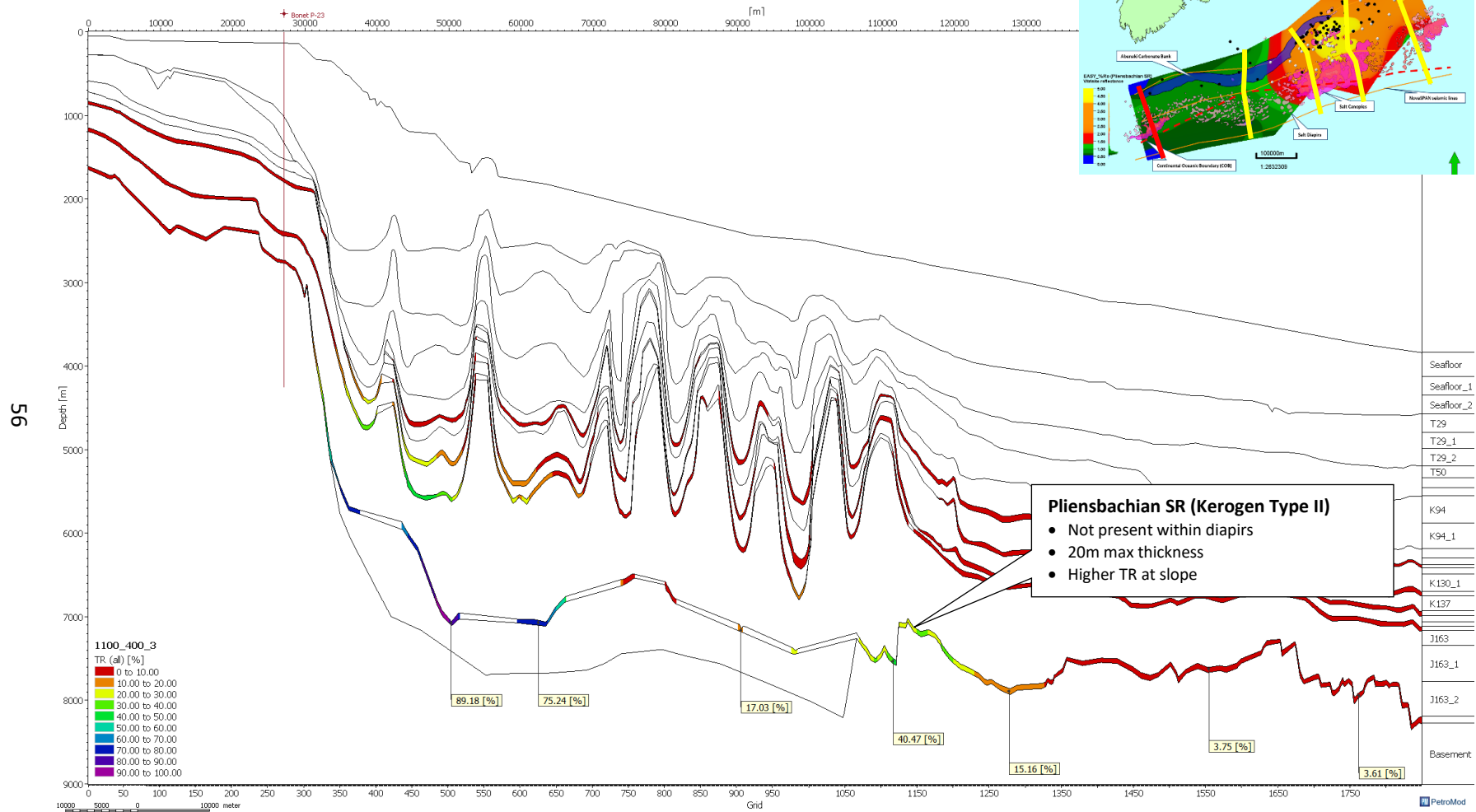


Figure 3.20: Model of transformation ratio for Pliensbachian source rock (Type II) for NovaSPAN 1100 line. Here we can observe the five different source rocks in the model; the Lower Jurassic source rock is the bottommost layer. The data points indicate the percentage of the value of hydrocarbons generated from the potential Lower Jurassic source rock layer.

NovaSPAN 1100 – Transformation Ratio (Pliensbachian Source Rock -Type I)

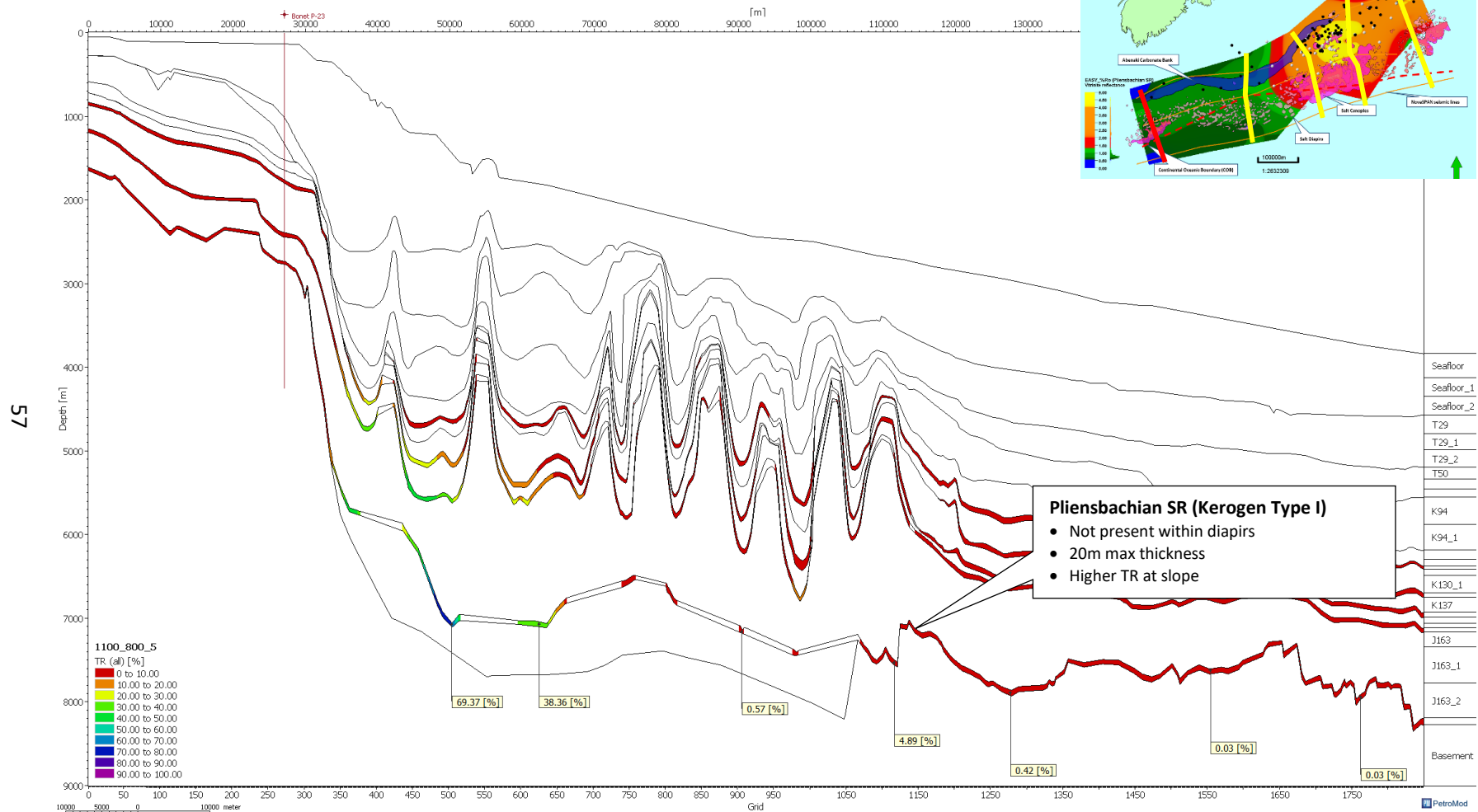


Figure 3.21: Model of transformation ratio for Pliensbachian source rock (Type I) for NovaSPAN 1100 line. Here we can observe the five different source rocks in the model; the Lower Jurassic source rock is the bottommost layer. The data points indicate the percentage of the value of hydrocarbons generated from the potential Lower Jurassic source rock layer.

NovaSPAN 1100 – Critical Moment (Pliensbachian Source Rock -Type II)

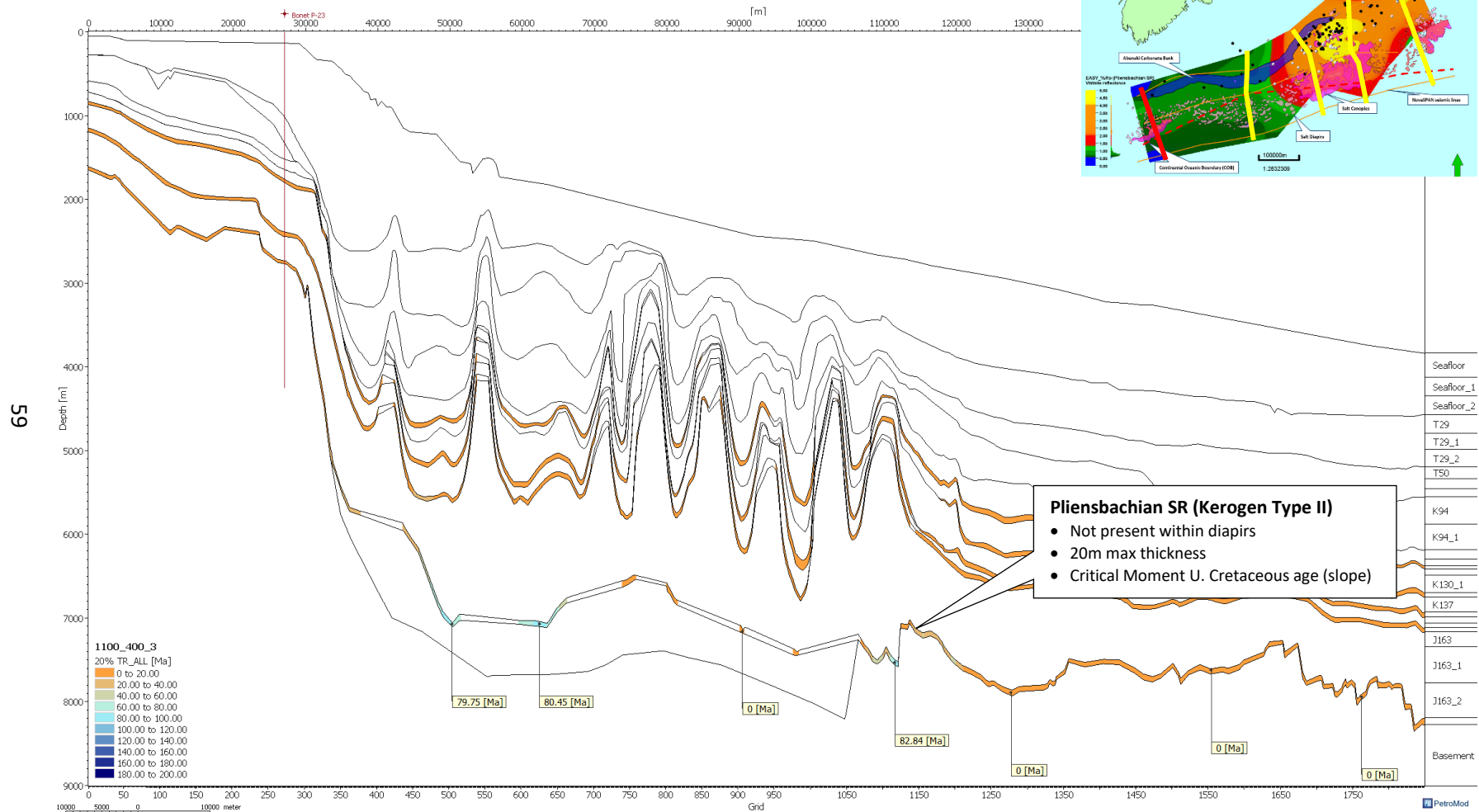


Figure 3.23: Model of the critical moment for the Pliensbachian source rock (Type II) for NovaSPAN 1100 line. Here we can observe the five different source rocks in the model; the Lower Jurassic source rock is the bottommost layer. The data points indicate the critical moment age that the potential Lower Jurassic had generated hydrocarbons exceeding the threshold.

NovaSPAN 1100 – Critical Moment (Pliensbachian Source Rock -Type I)

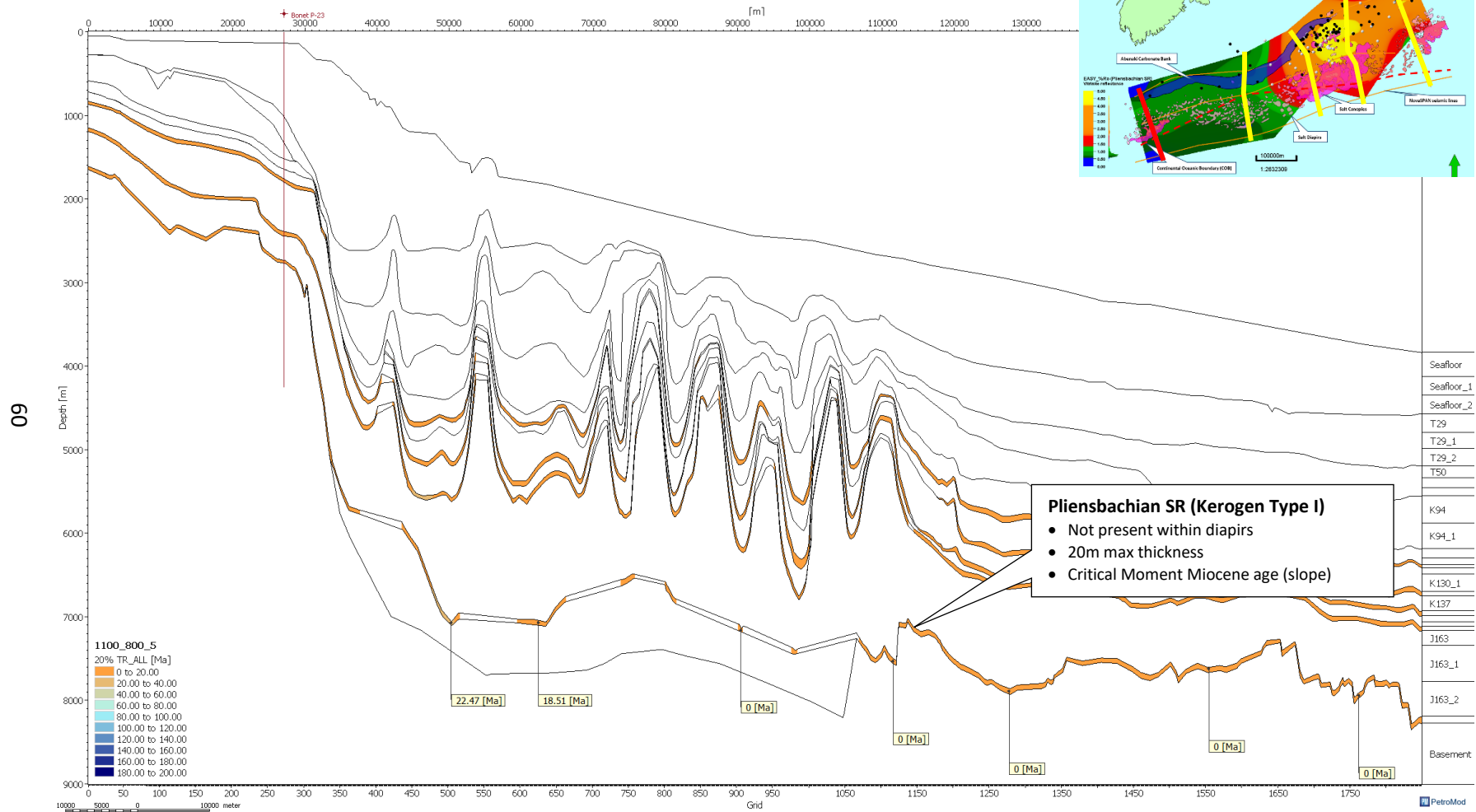


Figure 3.24: Model of the critical moment for the Pliensbachian source rock (Type I) for NovaSPAN 1100 line. Here we can observe the five different source rocks in the model; the Lower Jurassic source rock is the bottommost layer. The data points indicate the critical moment age that the potential Lower Jurassic had generated hydrocarbons exceeding the threshold.

2. NovaSPAN 1400

Heat Flow and Temperature

The heat flow cross-section shows the distribution of heat that is being transferred vertically within the model (Figure 3.25). The model takes into consideration the burial history and the crustal heat flow history, with the thermal conductivity from the lithology from the model. This cross-section displays the impact that the salt has on the model, creating hot spots on the cusp of the salt diapirs, these higher heat flows also impacts the temperature cross-section in the model. As observed in the model (Figure 3.26) the temperature gradient being pushed down at the bottom of the diapir and bumped up at in the top o the salt diapirs.

NovaSPAN 1400 – Heat Flow

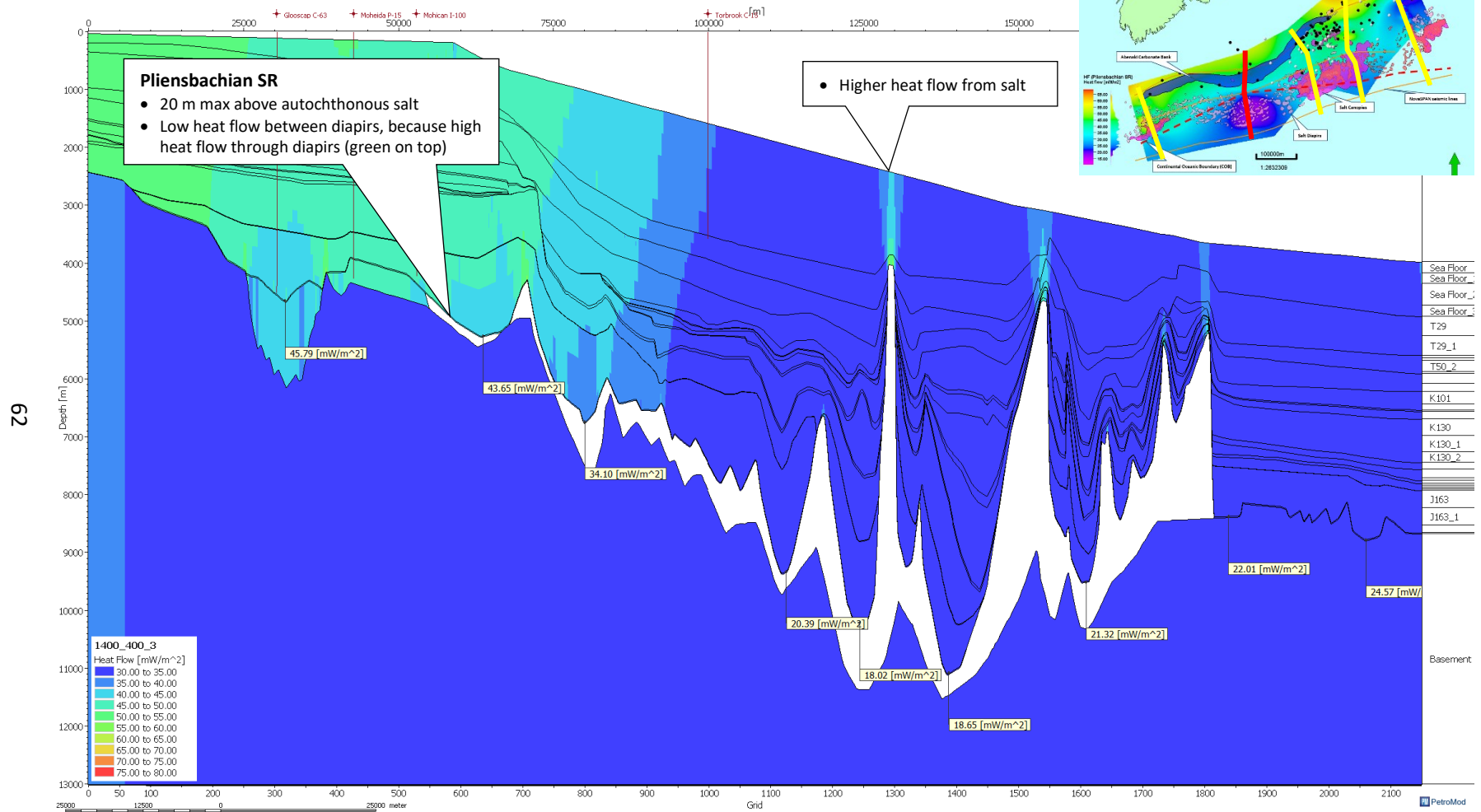


Figure 3.25: Model of heat flow distribution for NovaSPAN 1400 line. The data points indicate the heat flow value of the potential Lower Jurassic source rock layer. The white areas are the salt structures from the Argo Formation.

NovaSPAN 1400 – Temperature

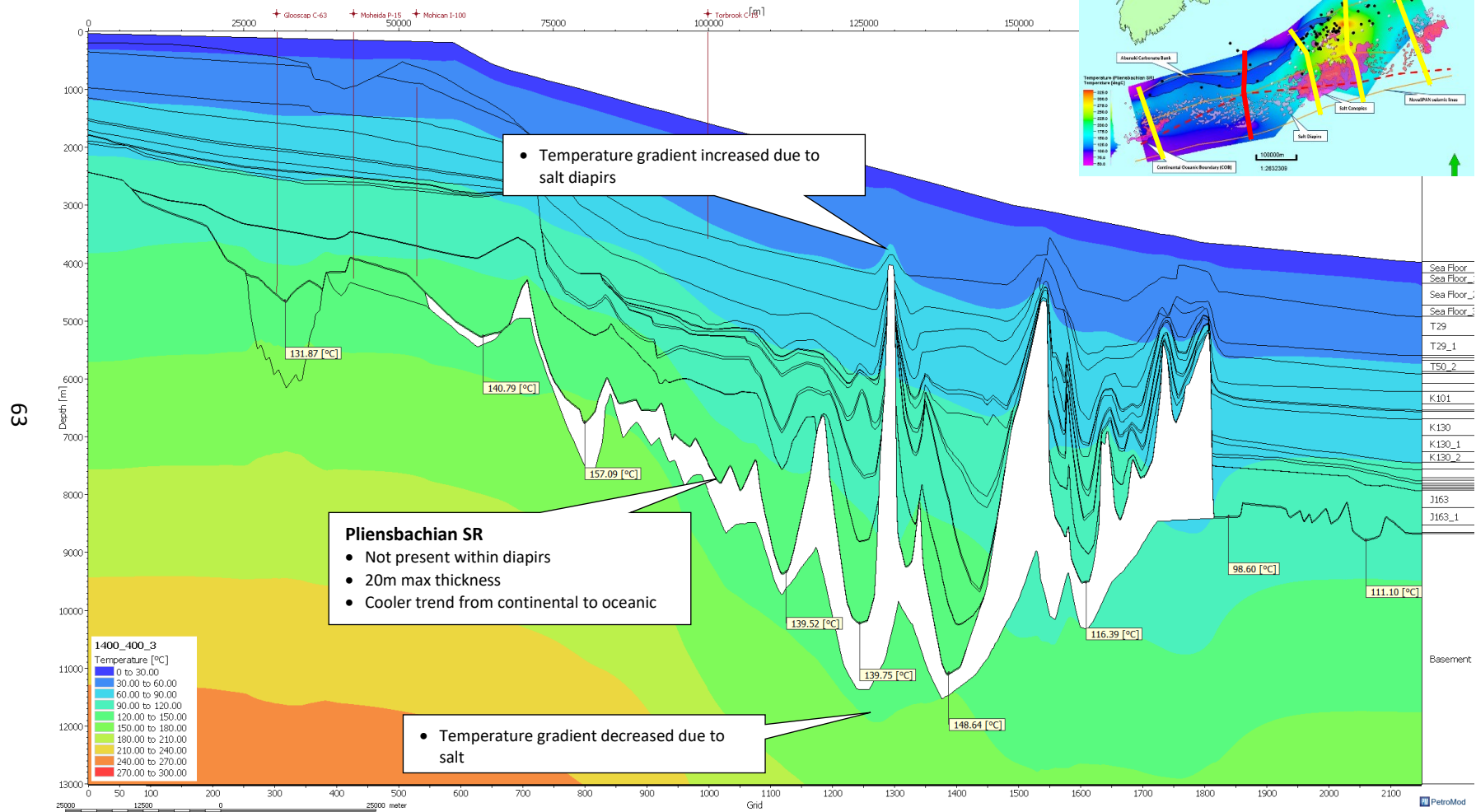


Figure 3.26: Model of temperature distribution for NovaSPAN 1400 line. The data points indicate the temperature value of the potential Lower Jurassic source rock layer. The white areas are the salt structures from the Argo Formation.

Maturity Range, Transformation Ratio and Critical Moment

The maturity cross-section is the vitrinite reflectance modelled after the EASY%Ro algorithm (Sweeney and Burnham, 1990). This cross-section demonstrates that the Lower Jurassic rocks are within the maturity oil window (Figure 3.27) and have the potential to be a source rock. Testing this model with the different kerogen types (Table 1.1), the model demonstrates a range of results depending upon the kerogen type of the Lower Jurassic source rock. The transformation ratio cross-section is a quantitative transformation measurement of organic material into hydrocarbons based on total organic carbon and hydrogen index in the organic-rich rock. In these cross-sections (Figures 3.28 - 3.30), five different source rock intervals can be observed, but the focus of this study is specifically the bottommost layer, which is the representative of the Lower Jurassic source rock. The Lower Jurassic source rock is also a close representation to the "Lower Jurassic Complex" that the PFA named for their source rock. These transformation ratio cross-sections demonstrate a broad range of results depending upon the source rock kerogen type and location along the line. The "critical moment cross-section" is the age when the source rock had generated 20% of the convertible kerogen, which is the age when the transformation ratio of the source rock was 20% (Figures 3.31 - 3.33). The following set of cross-sections illustrates the critical moment for each modelled kerogen type (Table 1.1).

NovaSPAN 1400 – Maturity

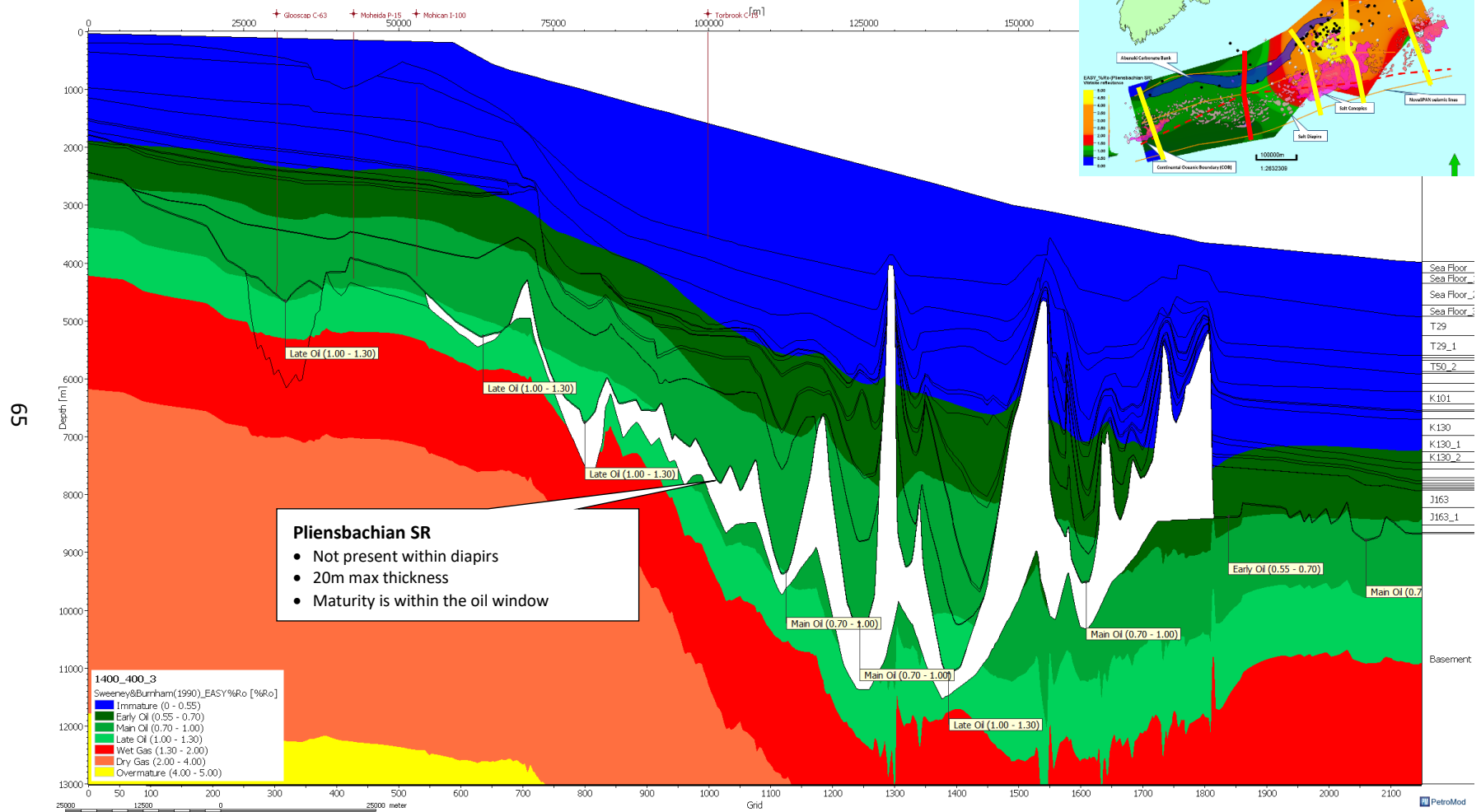


Figure 3.27: Model of vitrinite reflectance distribution for NovaSPAN 1400 line. The data points indicate the vitrinite reflectance value based on the Sweeney and Burnham (1990) algorithm for the potential Lower Jurassic source rock layer. The white areas are the salt structures from the Argo Formation. The potential Lower Jurassic source rock is in the oil window.

NovaSPAN 1400 – Transformation Ratio (Pliensbachian Source Rock -Type II)

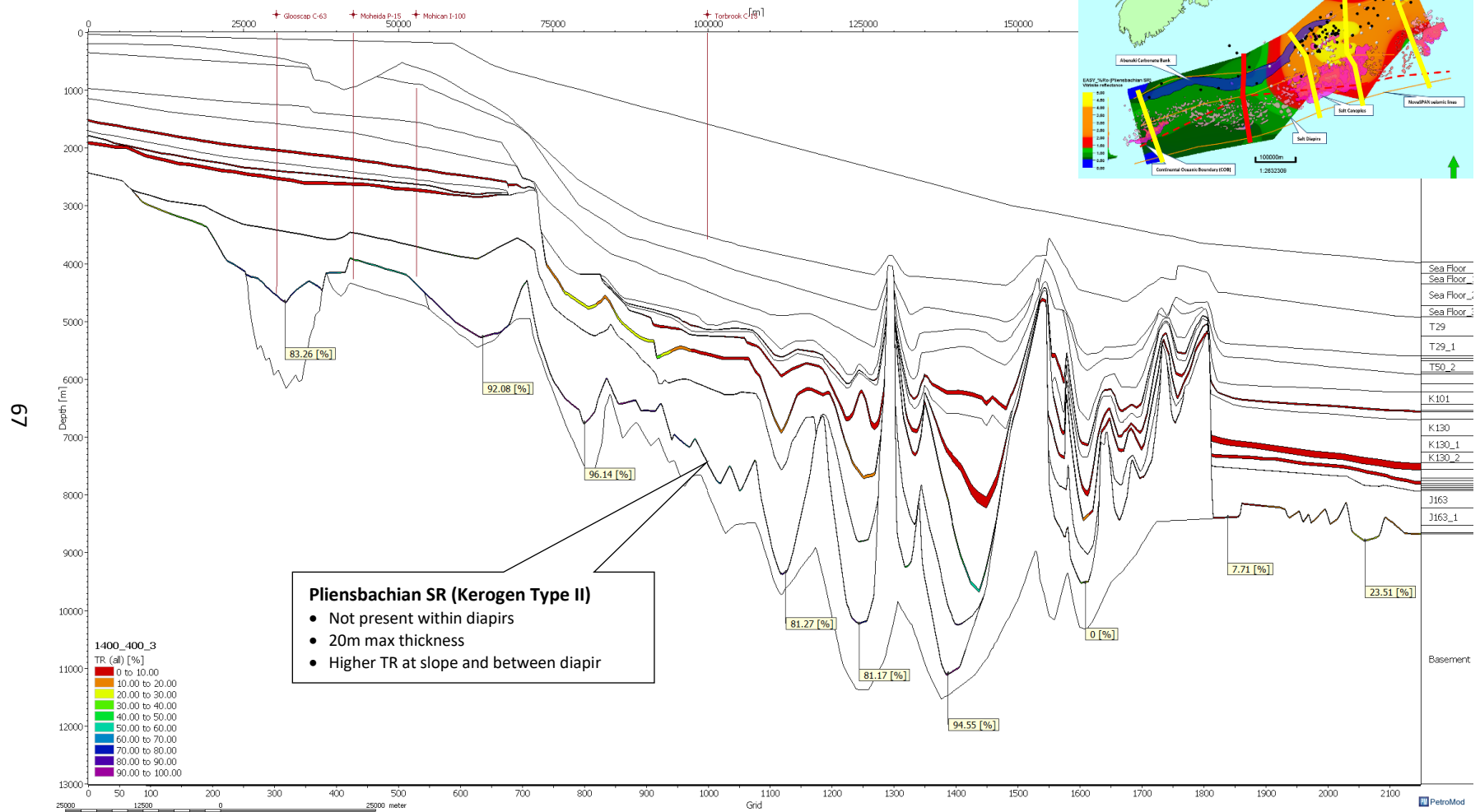


Figure 3.29: Model of transformation ratio for Pliensbachian source rock (Type II) for NovaSPAN 1400 line. Here we can observe the five different source rocks in the model; the Lower Jurassic source rock is the bottommost layer. The data points indicate the percentage of the value of hydrocarbons generated from the potential Lower Jurassic source rock layer.

NovaSPAN 1400 – Transformation Ratio (Pliensbachian Source Rock -Type I)

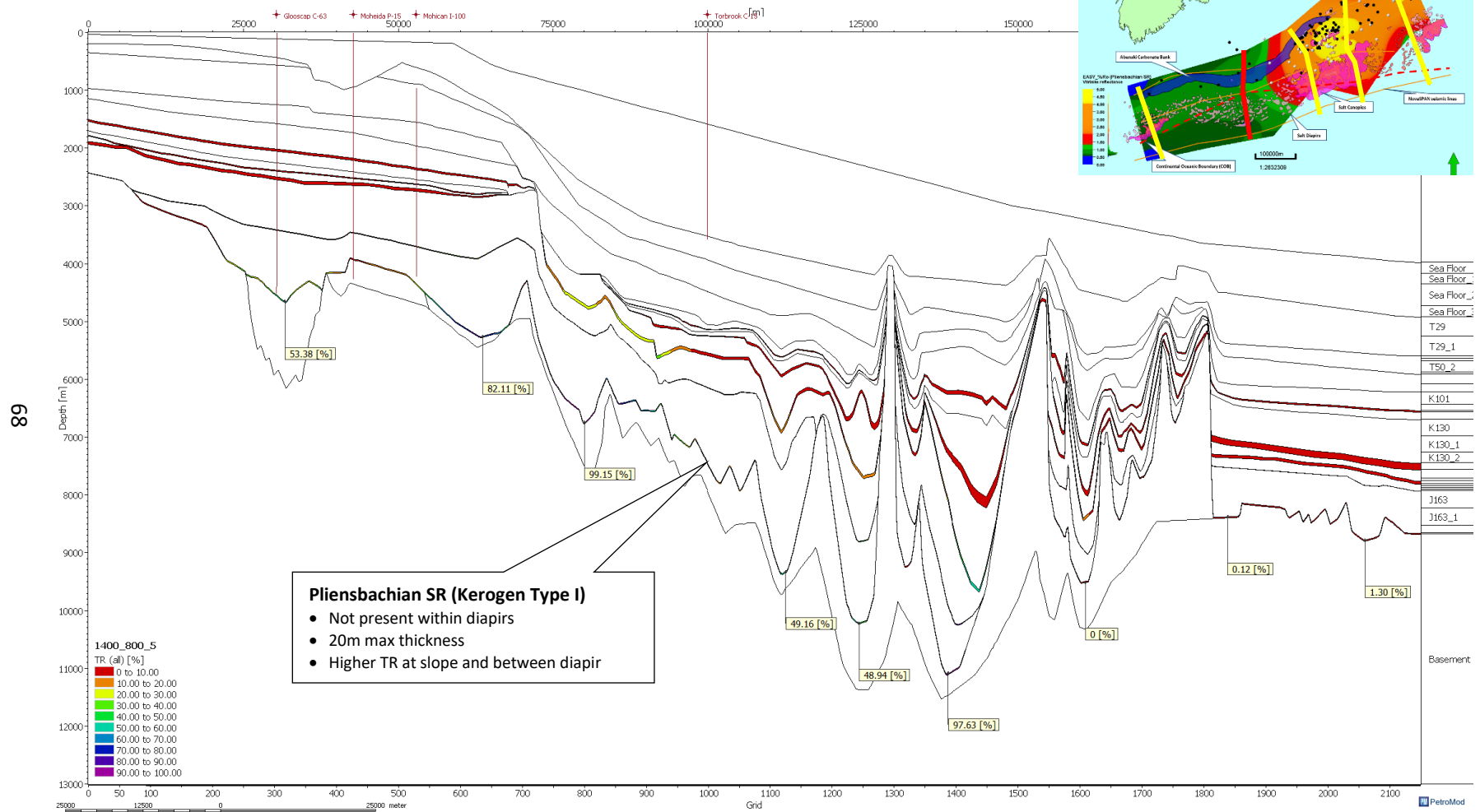


Figure 3.30: Model of transformation ratio for Pliensbachian source rock (Type I) for NovaSPAN 1400 line. Here we can observe the five different source rocks in the model; the Lower Jurassic source rock is the bottommost layer. The data points indicate the percentage of the value of hydrocarbons generated from the potential Lower Jurassic source rock layer.

NovaSPAN 1400 – Critical Moment (Pliensbachian Source Rock -Type III)

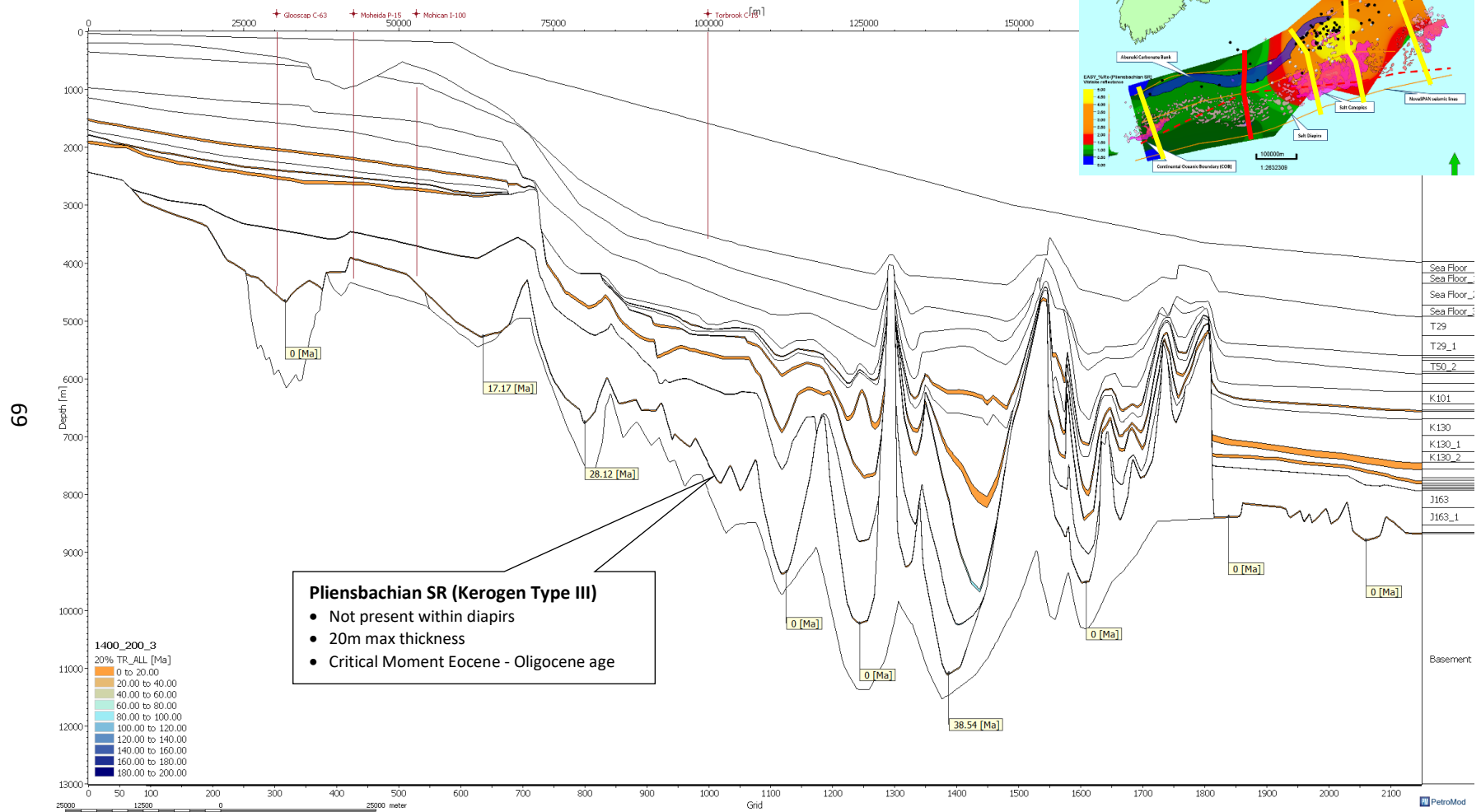


Figure 3.31: Model of the critical moment for the Pliensbachian source rock (Type III) for NovaSPAN 1400 line. Here we can observe the five different source rocks in the model; the Lower Jurassic source rock is the bottommost layer. The data points indicate the critical moment age that the potential Lower Jurassic had generated hydrocarbons exceeding the threshold.

NovaSPAN 1400 – Critical Moment (Pliensbachian Source Rock -Type II)

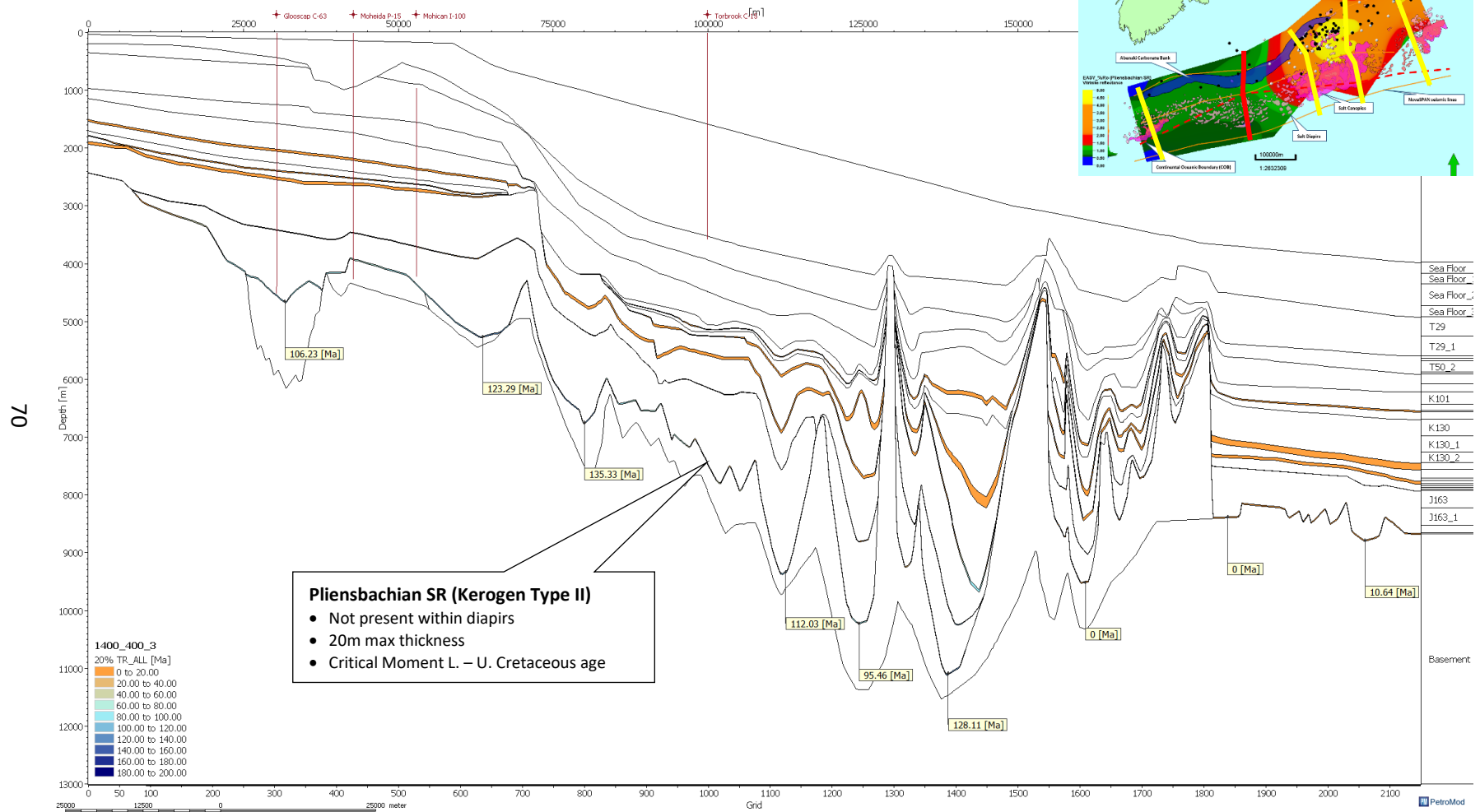


Figure 3.32: Model of the critical moment for the Pliensbachian source rock (Type III) for NovaSPAN 1400 line. Here we can observe the five different source rocks in the model; the Lower Jurassic source rock is the bottommost layer. The data points indicate the critical moment age that the potential Lower Jurassic had generated hydrocarbons exceeding the threshold.

NovaSPAN 1400 – Critical Moment (Pliensbachian Source Rock -Type I)

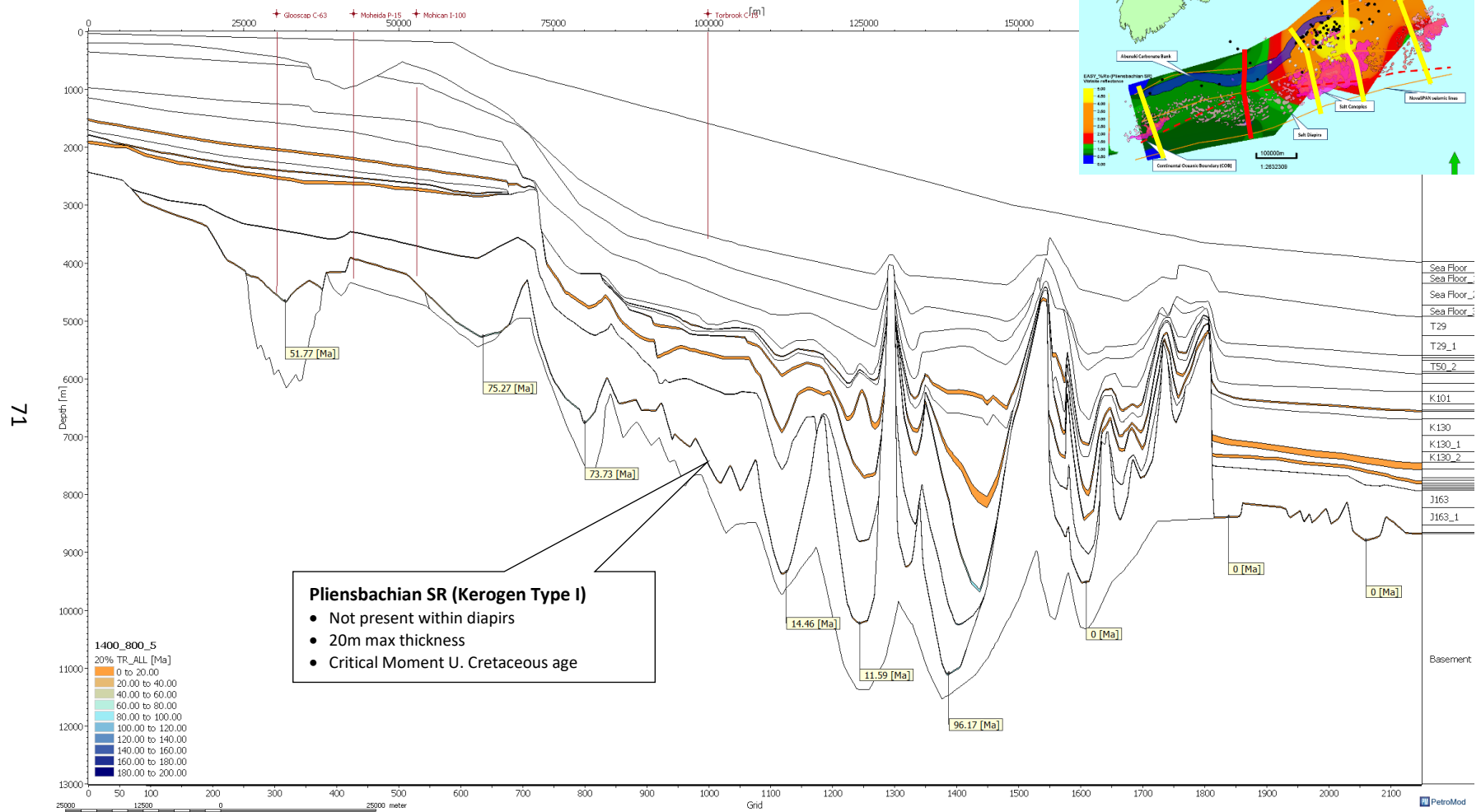


Figure 3.33: Model of the critical moment for the Pliensbachian source rock (Type I) for NovaSPAN 1400 line. Here we can observe the five different source rocks in the model; the Lower Jurassic source rock is the bottommost layer. The data points indicate the critical moment age that the potential Lower Jurassic had generated hydrocarbons exceeding the threshold.

3. NovaSPAN 1800

Heat Flow and Temperature

The heat flow cross-section shows the distribution of heat that is being transferred vertically within the model (Figure 3.34). The model takes into consideration the burial history and the crustal heat flow history, with the thermal conductivity from the lithology from the model. This cross-section displays the impact that the salt has on the model, creating hot spots on the cusp of the salt diapirs, these higher heat flows also impacts the temperature cross-section in the model. As observed in the model (Figure 3.35) the temperature gradient being pushed down at the bottom of the diapir and bumped up at in the top o the salt diapirs.

NovaSPAN 1800 – Heat Flow

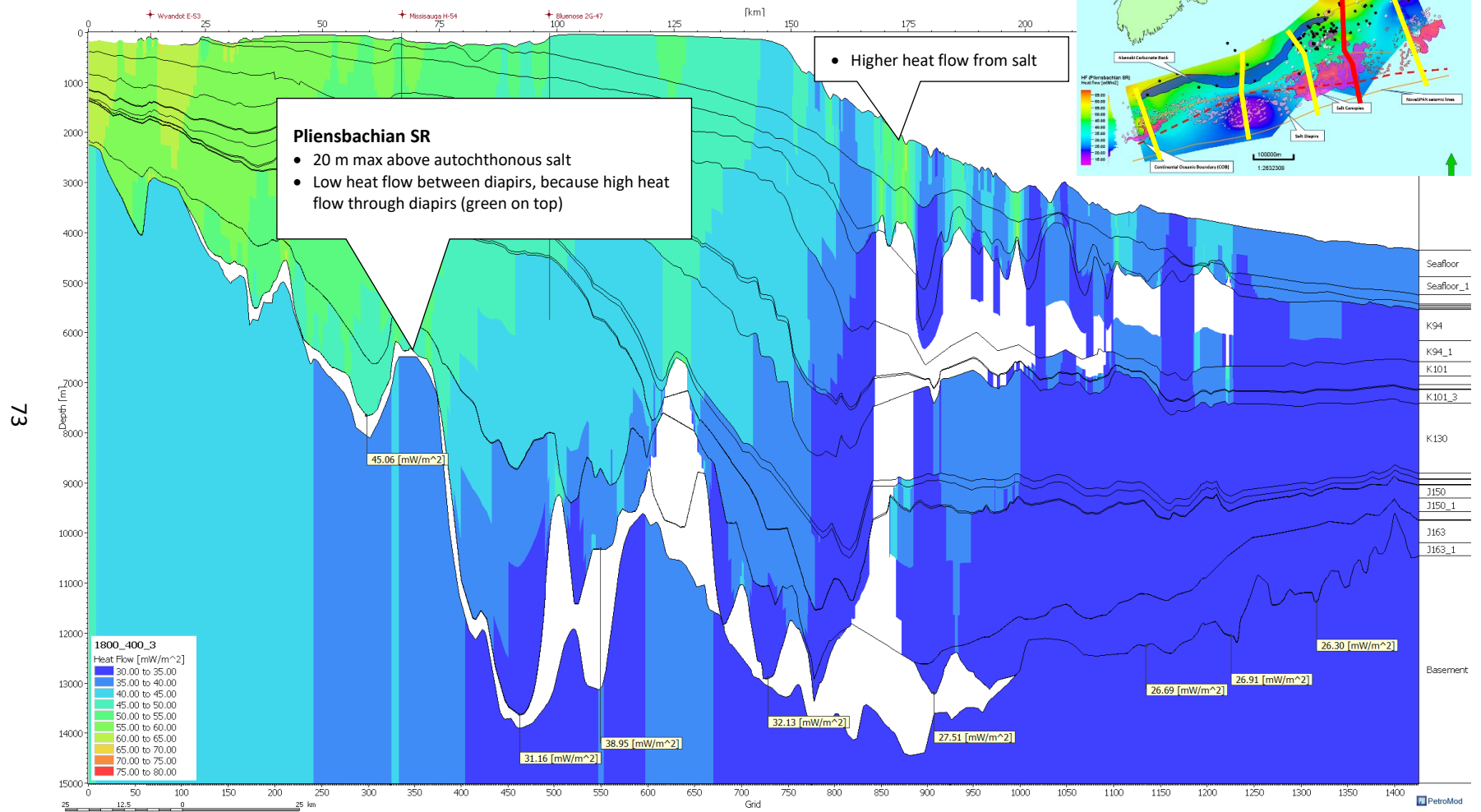


Figure 3.34: Model of heat flow distribution for NovaSPAN 1800 line. The data points indicate the heat flow value of the potential Lower Jurassic source rock layer. The white areas are the salt structures from the Argo Formation.

NovaSPAN 1800 – Temperature

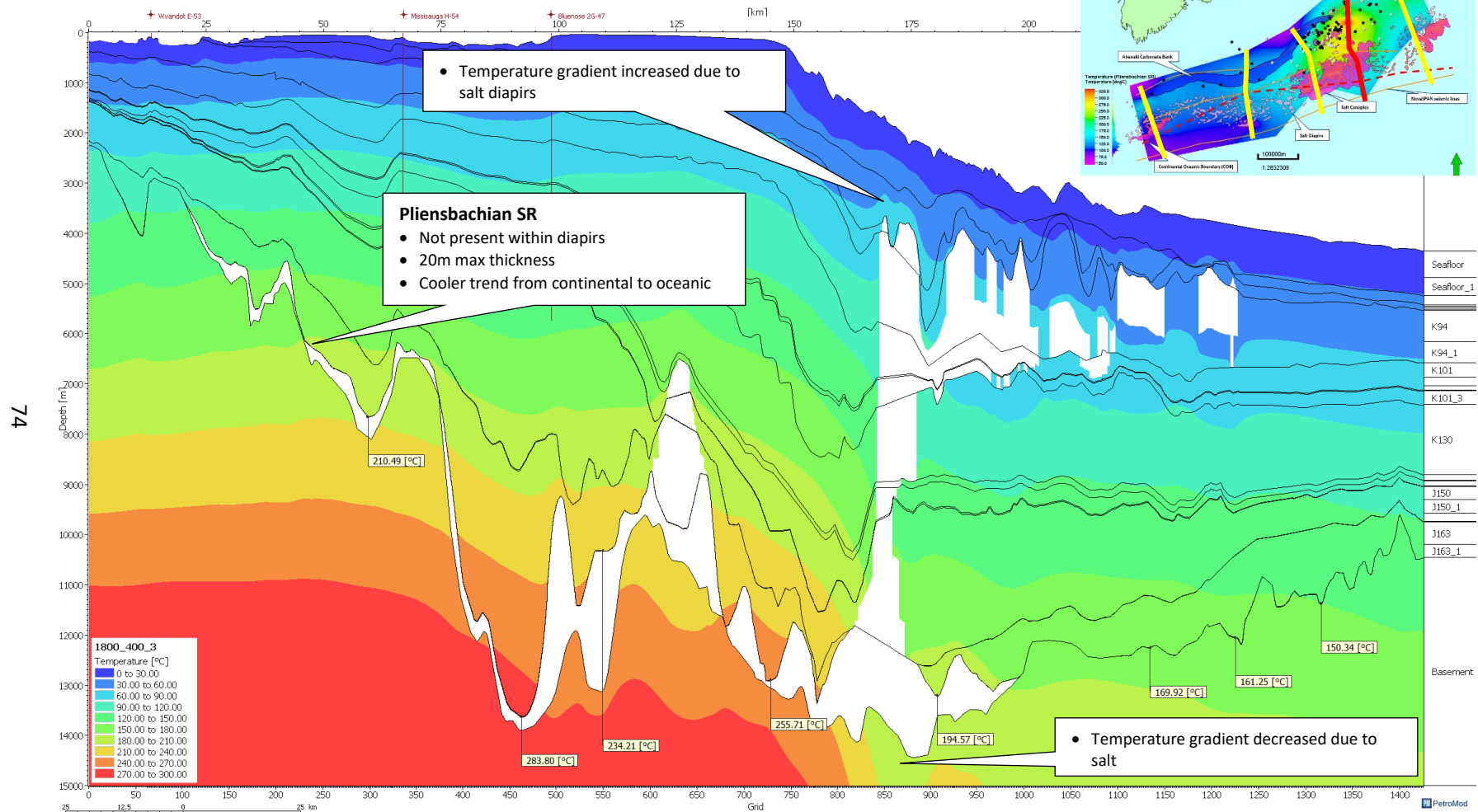


Figure 3.35: Model of temperature distribution for NovaSPAN 1800 line. The data points indicate the temperature value of the potential Lower Jurassic source rock layer. The white areas are the salt structures from the Argo Formation.

Maturity Range, Transformation Ratio and Critical Moment

The maturity cross-section is the vitrinite reflectance modelled after the EASY%Ro algorithm (Sweeney and Burnham, 1990). This cross-section demonstrates that the Lower Jurassic rocks are within the maturity oil window (Figure 3.36) and have the potential to be a source rock. Testing this model with the different kerogen types (Table 1.1), the model demonstrates a range of results depending upon the kerogen type of the Lower Jurassic source rock. The transformation ratio cross-section is a quantitative transformation measurement of organic material into hydrocarbons based on total organic carbon and hydrogen index in the organic-rich rock. In these cross-sections (Figures 3.37 - 3.39), five different source rock intervals can be observed, but the focus of this study is specifically the bottommost layer, which is the representative of the Lower Jurassic source rock. The Lower Jurassic source rock is also a close representation to the "Lower Jurassic Complex" that the PFA named for their source rock. These transformation ratio cross-sections demonstrate a broad range of results depending upon the source rock kerogen type and location along the line. The "critical moment cross-section" is the age when the source rock had generated 20% of the convertible kerogen, which is the age when the transformation ratio of the source rock was 20% (Figures 3.40 - 3.42). The following set of cross-sections demonstrates the critical moment for each modelled kerogen type (Table 1.1).

NovaSPAN 1800 – Maturity

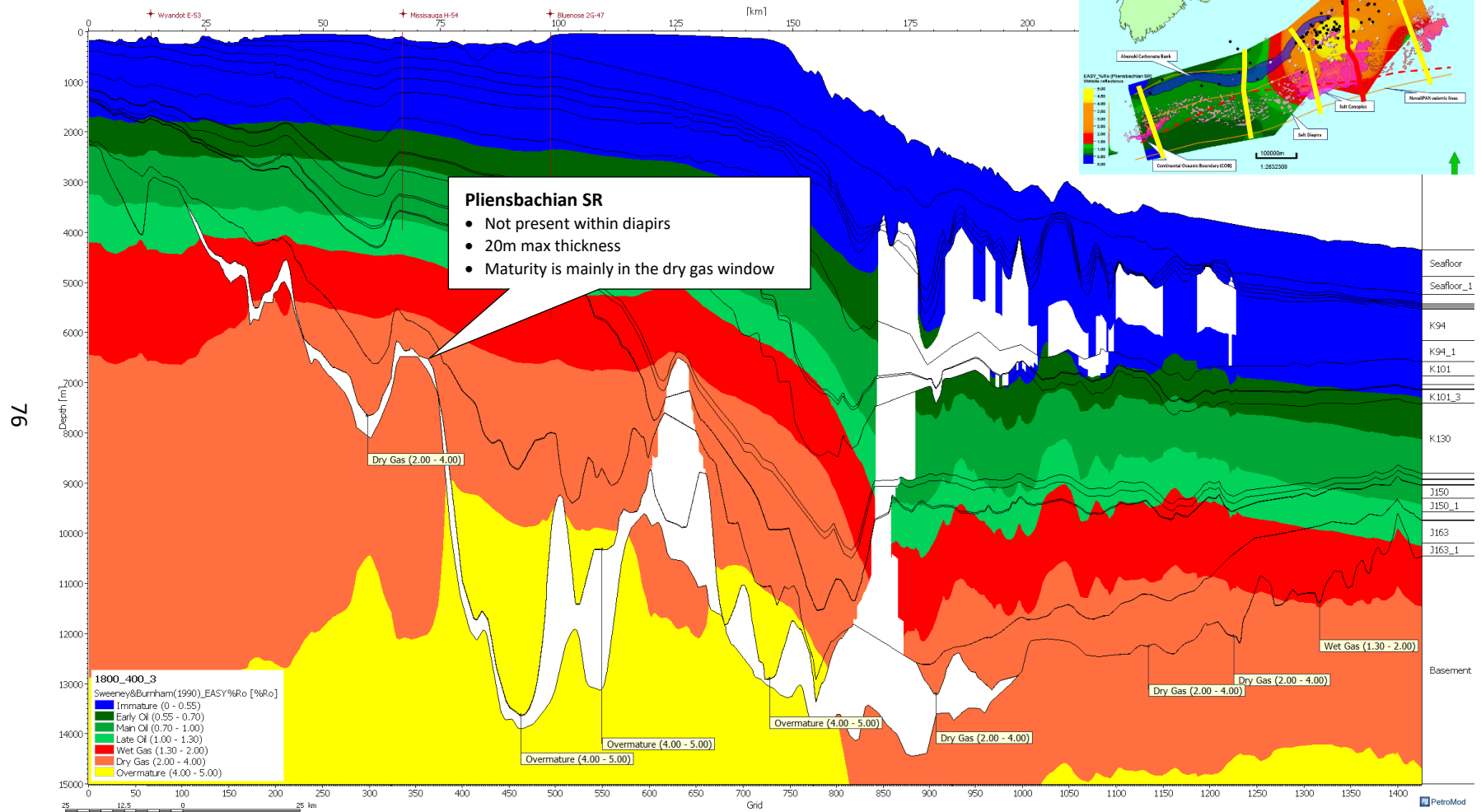


Figure 3.36: Model of vitrinite reflectance distribution for NovaSPAN 1800 line. The data points indicate the vitrinite reflectance value based on the Sweeney and Burnham (1990) algorithm for the potential Lower Jurassic source rock layer. The white areas are the salt structures from the Argo Formation. The potential Lower Jurassic source rock is in the oil.

NovaSPAN 1800 – Transformation Ratio (Pliensbachian Source Rock - Type III)

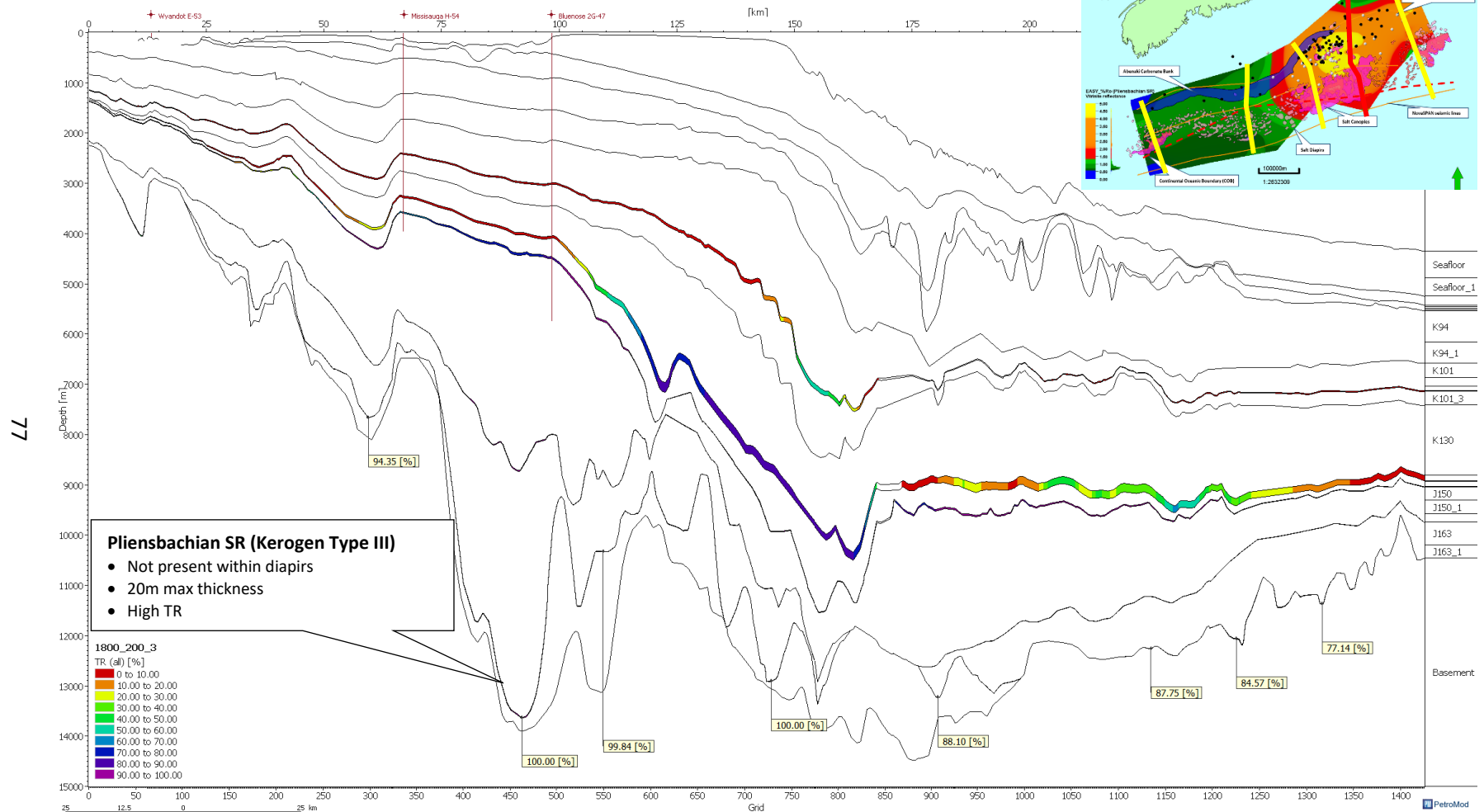


Figure 3.37: Model of transformation ratio for Pliensbachian source rock (Type III) for NovaSPAN 1800 line. Here we can observe the five different source rocks in the model; the Lower Jurassic source rock is the bottommost layer. The data points indicate the percentage of the value of hydrocarbons generated from the potential Lower Jurassic source rock layer.

NovaSPAN 1800 – Transformation Ratio (Pliensbachian Source Rock -Type II)

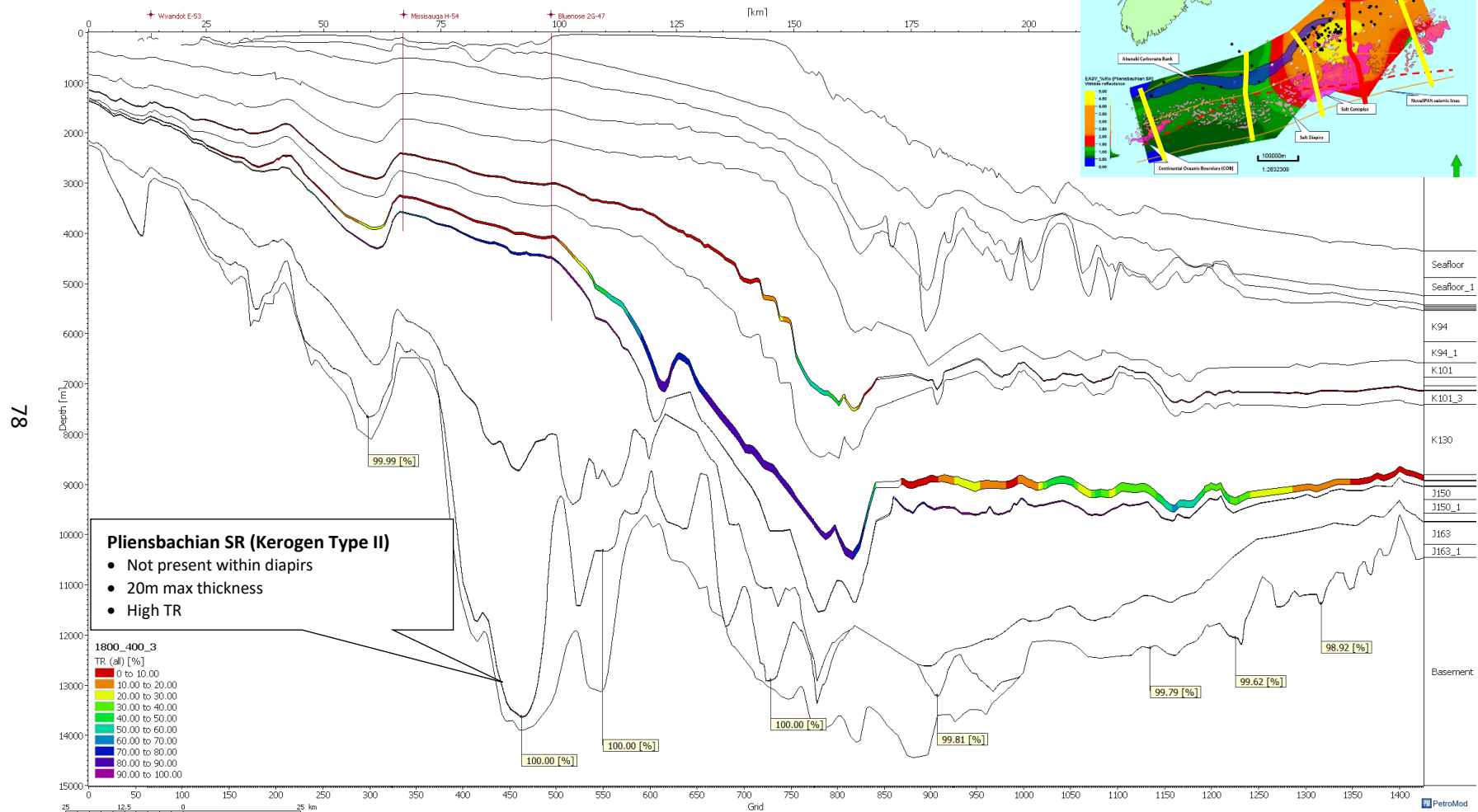


Figure 3.38: Model of transformation ratio for Pliensbachian source rock (Type II) for NovaSPAN 1800 line. Here we can observe the five different source rocks in the model; the Lower Jurassic source rock is the bottommost layer. The data points indicate the percentage of the value of hydrocarbons generated from the potential Lower Jurassic source rock layer.

NovaSPAN 1800 – Transformation Ratio (Pliensbachian Source Rock -Type I)

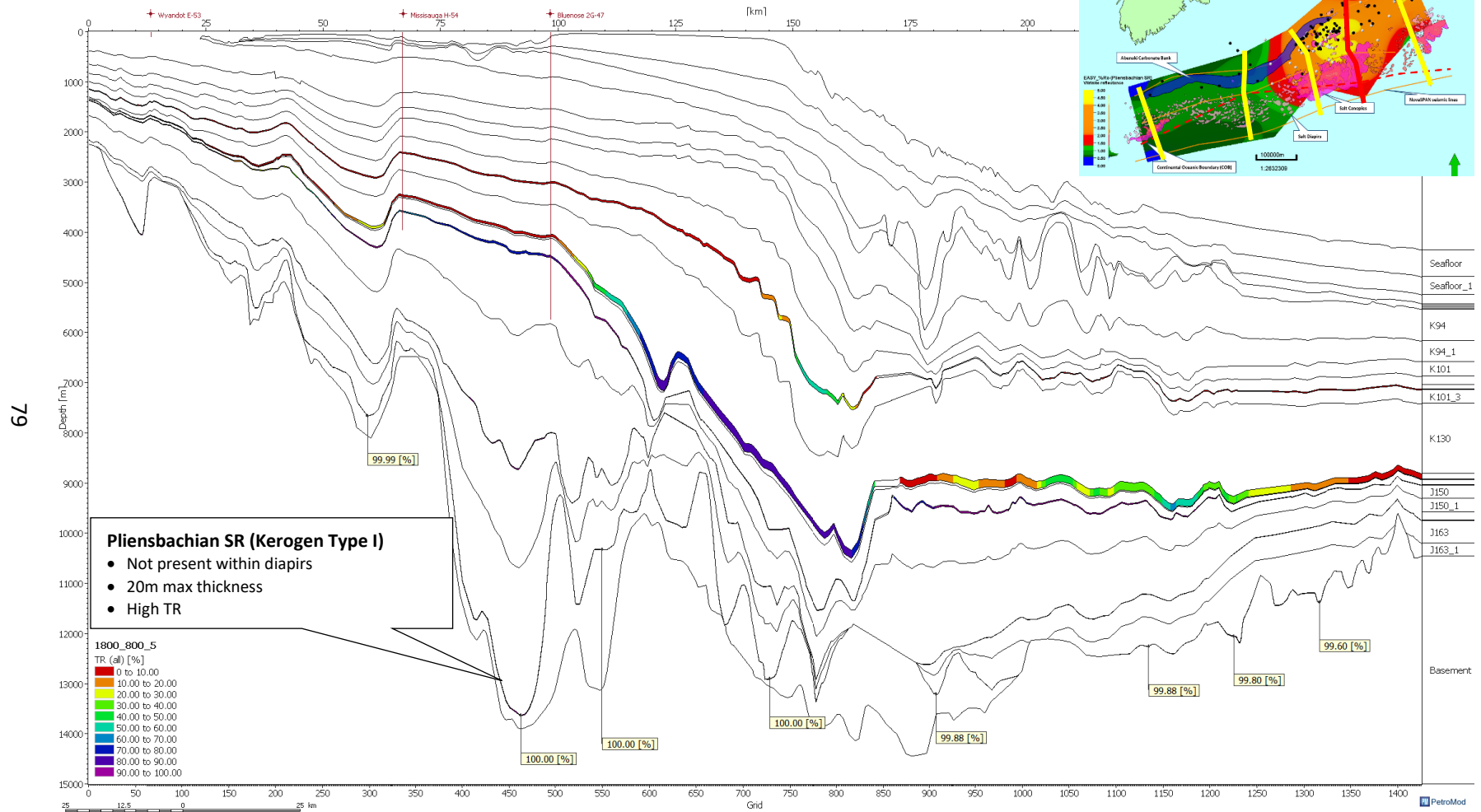


Figure 3.39: Model of transformation ratio for Pliensbachian source rock (Type I) for NovaSPAN 1800 line. Here we can observe the five different source rocks in the model; the Lower Jurassic source rock is the bottommost layer. The data points indicate the percentage of the value of hydrocarbons generated from the potential Lower Jurassic source rock layer.

NovaSPAN 1800 – Critical Moment (Pliensbachian Source Rock -Type II)

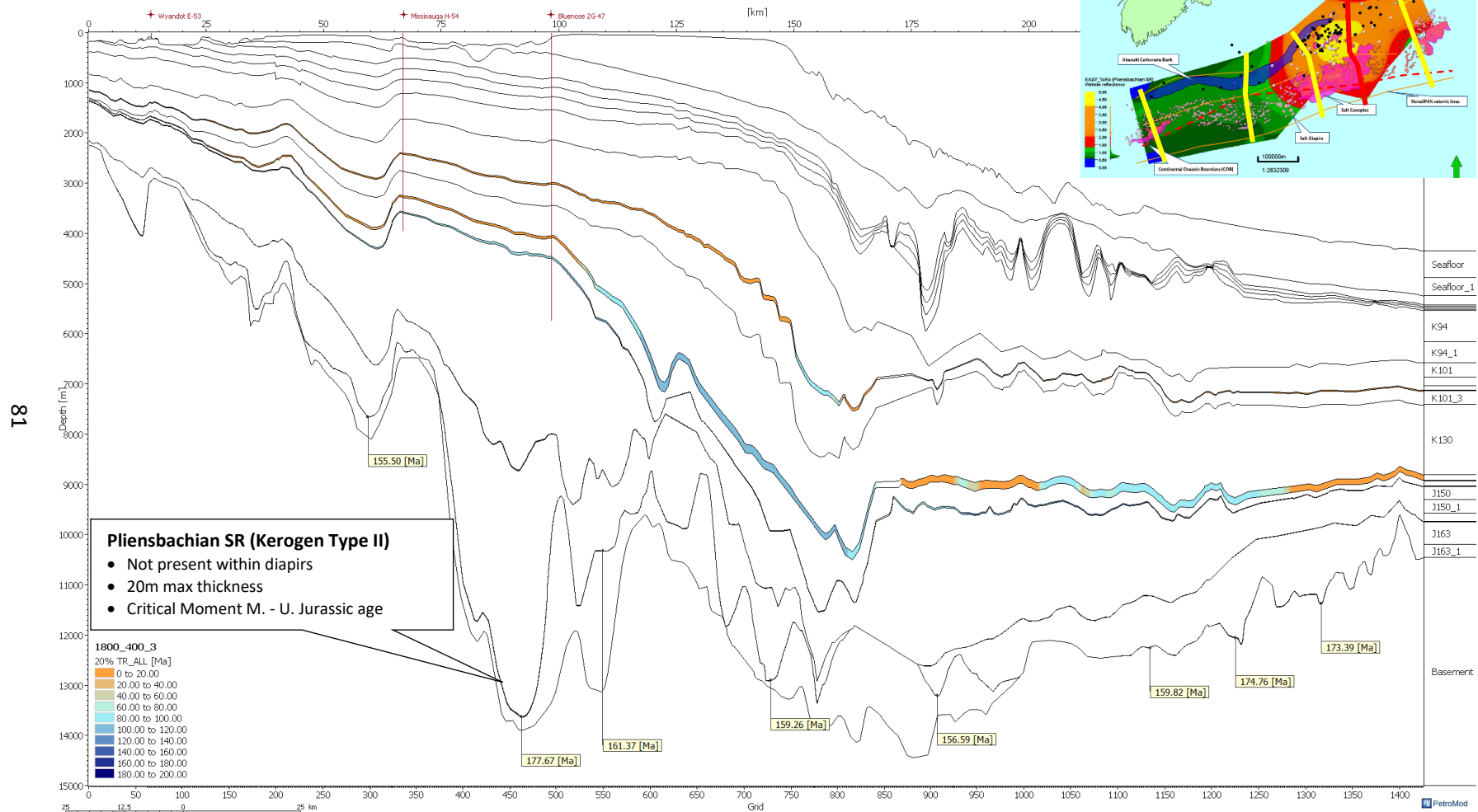


Figure 3.41: Model of the critical moment for the Pliensbachian source rock (Type II) for NovaSPAN 1800 line. Here we can observe the five different source rocks in the model; the Lower Jurassic source rock is the bottommost layer. The data points indicate the critical moment age that the potential Lower Jurassic had generated hydrocarbons exceeding the threshold.

NovaSPAN 1800 – Critical Moment (Pliensbachian Source Rock -Type I)

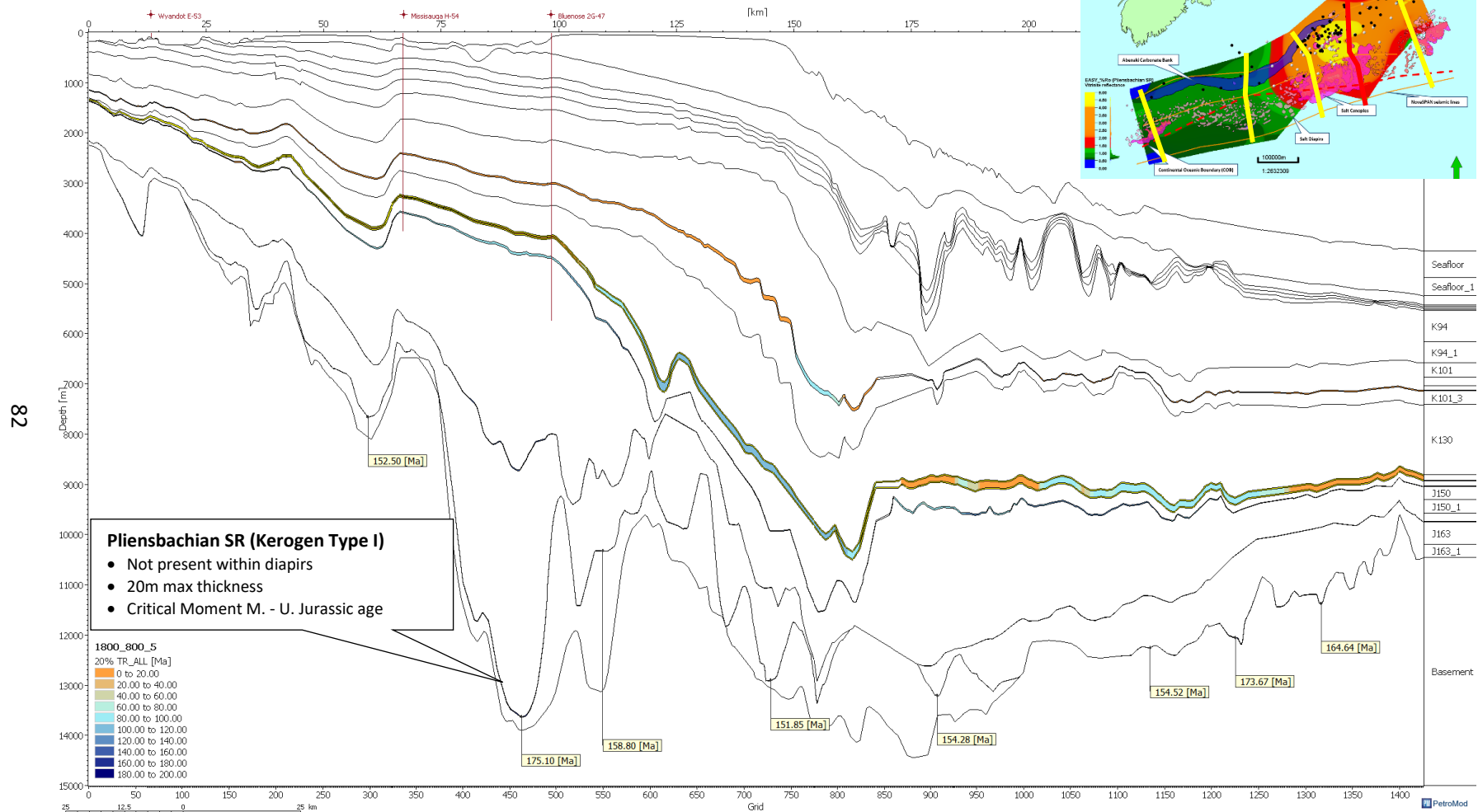


Figure 3.42: Model of the critical moment for the Pliensbachian source rock (Type I) for NovaSPAN 1800 line. Here we can observe the five different source rocks in the model; the Lower Jurassic source rock is the bottommost layer. The data points indicate the critical moment age that the potential Lower Jurassic had generated hydrocarbons exceeding the threshold.

4. NovaSPAN 2000

Heat Flow and Temperature

The heat flow cross-section shows the distribution of heat that is being transferred vertically within the model (Figure 3.43). The model takes into consideration the burial history and the crustal heat flow history, with the thermal conductivity from the lithology from the model. This cross-section displays the impact that the salt has on the model, creating hot spots on the cusp of the salt diapirs, these higher heat flows also impacts the temperature cross-section in the model. As observed in the model (Figure 3.44) the temperature gradient being pushed down at the bottom of the diapir and bumped up at in the top o the salt diapirs.

NovaSPAN 2000 – Heat Flow

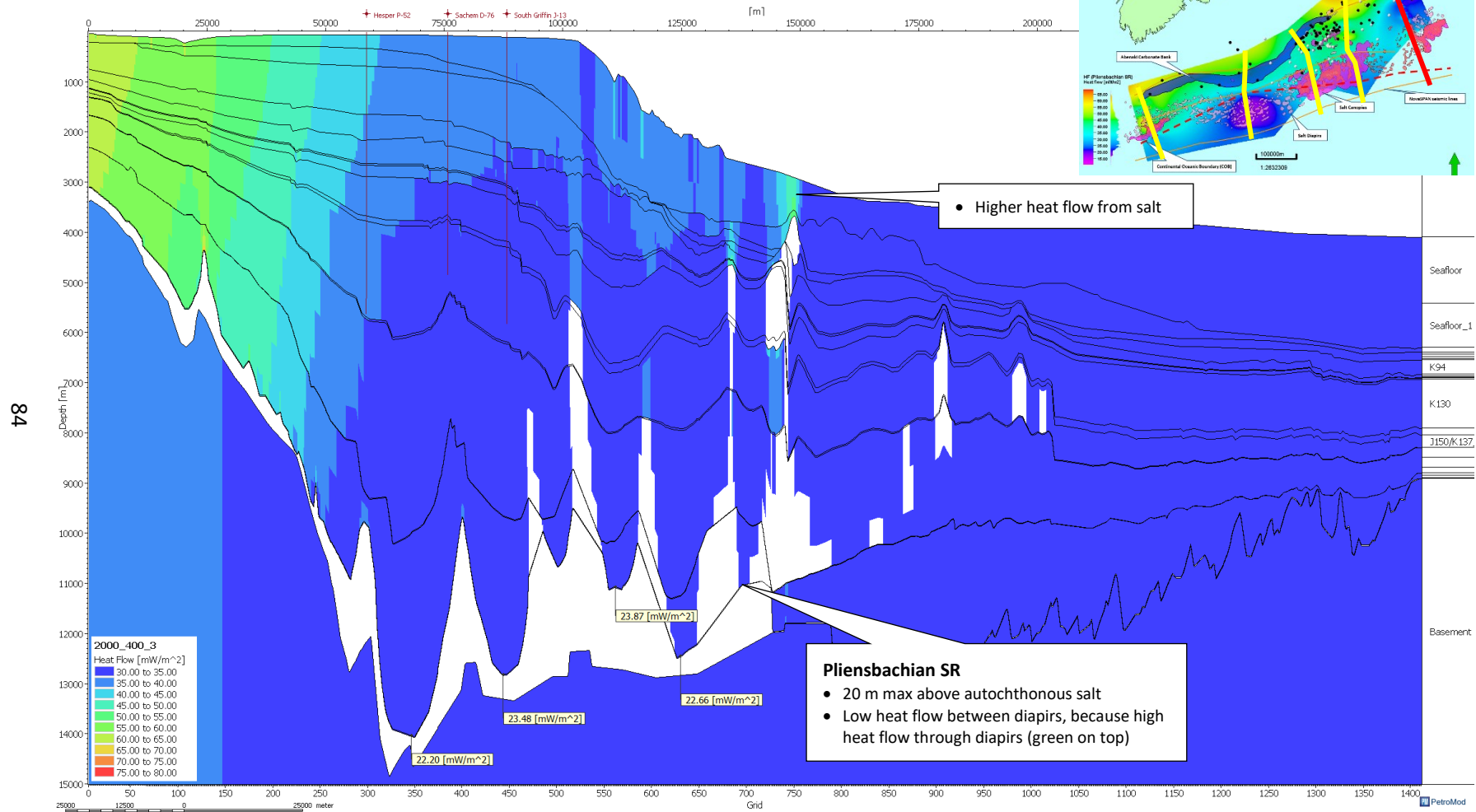


Figure 3.43: Model of heat flow distribution for NovaSPAN 2000 line. The data points indicate the heat flow value of the potential Lower Jurassic source rock layer. The white areas are the salt structures from the Argo Formation.

NovaSPAN 2000 – Temperature

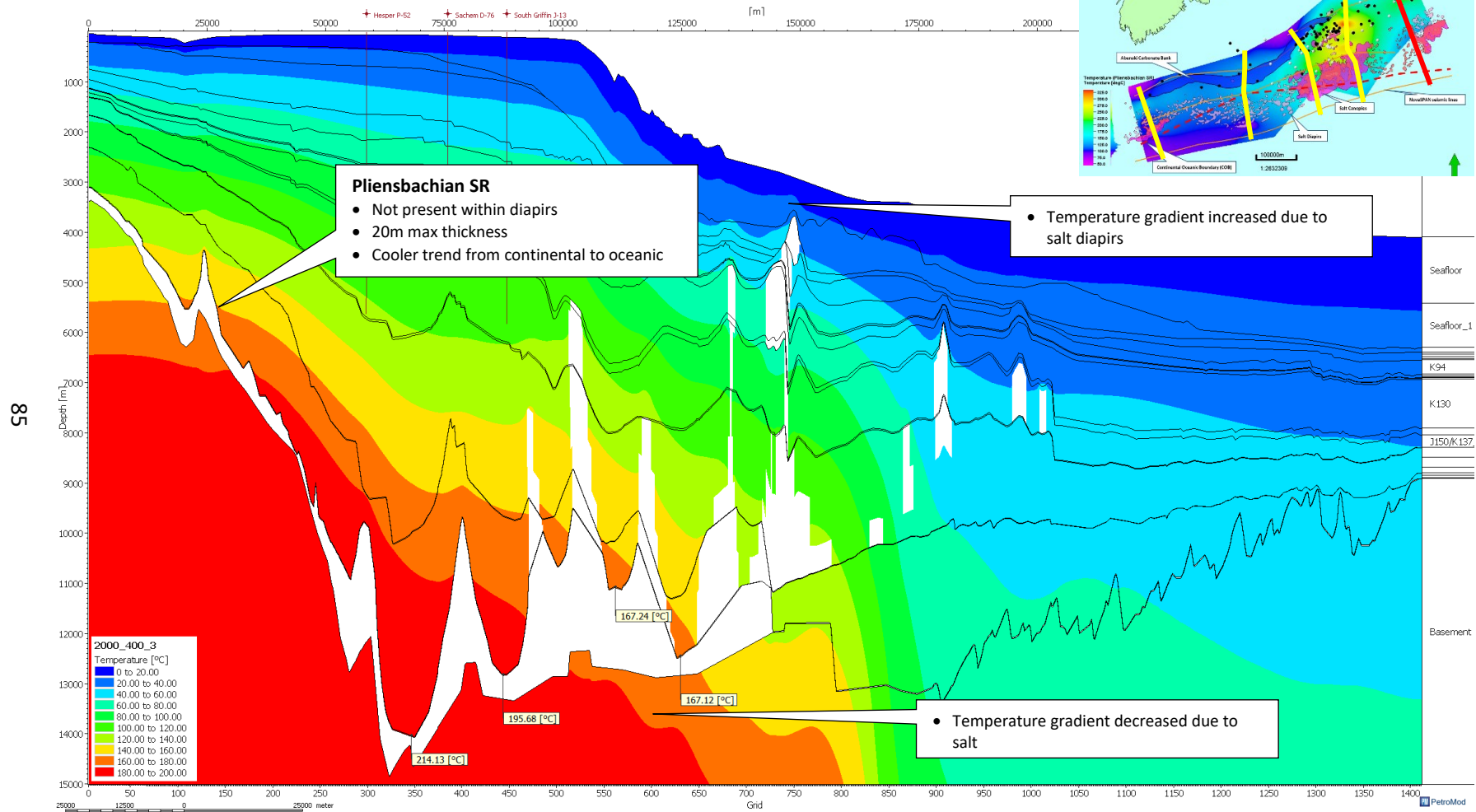


Figure 3.44: Model of temperature distribution for NovaSPAN 2000 line. The data points indicate the temperature value of the potential Lower Jurassic source rock layer. The white areas are the salt structures from the Argo Formation.

Maturity Range, Transformation Ratio and Critical Moment

The maturity cross-section is the vitrinite reflectance modelled after the EASY%Ro algorithm (Sweeney and Burnham, 1990) and have the potential to be a source rock. Testing this model with the different kerogen types (Table 1.1), the model demonstrates a range of results depending upon the kerogen type of the Lower Jurassic source rock. The transformation ratio cross-section is a quantitative transformation measurement of organic material into hydrocarbons based on total organic carbon and hydrogen index in the organic-rich rock. In these cross-sections (Figures 3.46 - 3.48), five different source rock intervals can be observed, but the focus of this study is specifically the bottommost layer, which is the representative of the Lower Jurassic source rock. The Lower Jurassic source rock is also a close representation to the “Lower Jurassic Complex” that the PFA named for their source rock. These transformation ratio cross-sections demonstrate a broad range of results depending upon the source rock kerogen type and location along the line. The “critical moment cross-section” is the age when the source rock had generated 20% of the convertible kerogen, which is the age when the transformation ratio of the source rock was 20% (Figures 3.49 - 3.51). The following set of cross-sections demonstrates the critical moment for each modelled kerogen type (Table 1.1).

NovaSPAN 2000 – Maturity

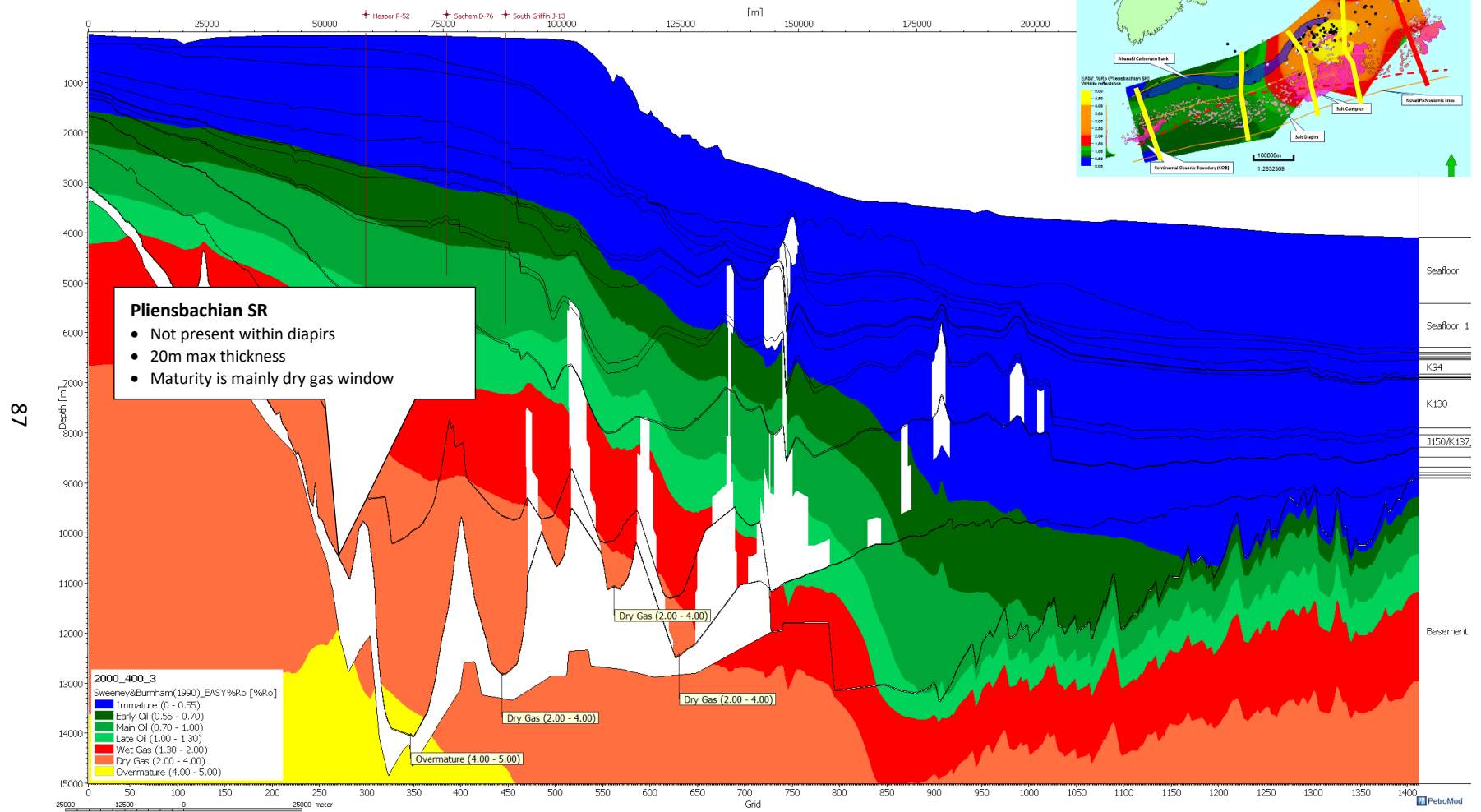


Figure 3.45: Model of vitrinite reflectance distribution for NovaSPAN 2000 line. The data points indicate the vitrinite reflectance value based on the Sweeney and Burnham (1990) algorithm for the potential Lower Jurassic source rock layer. The white areas are the salt structures from the Argo Formation. The potential Lower Jurassic source rock is in the oil window.

NovaSPAN 2000 – Transformation Ratio (Pliensbachian Source Rock -Type III)

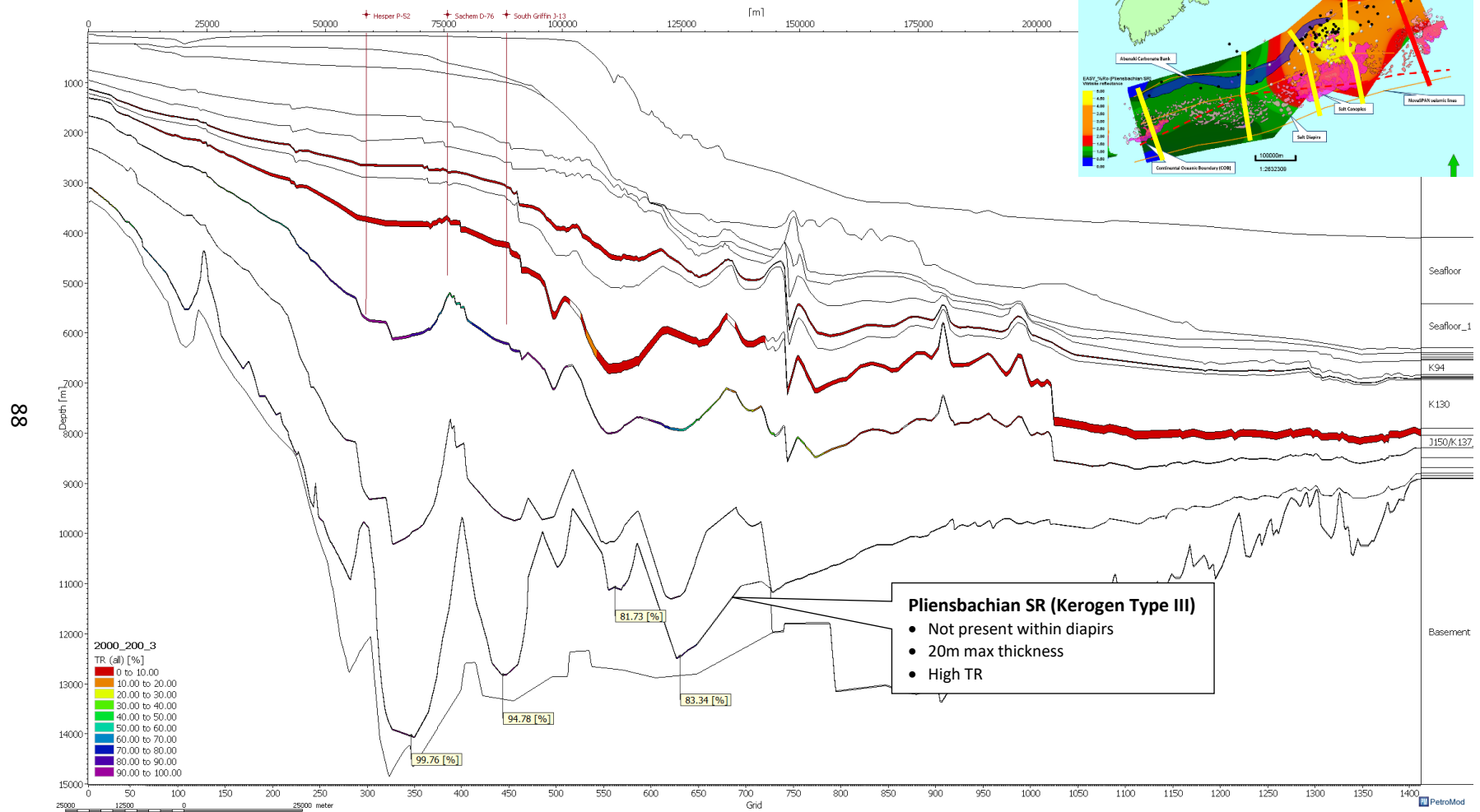


Figure 3.46: Model of transformation ratio for Pliensbachian source rock (Type III) for NovaSPAN 2000 line. Here we can observe the five different source rocks in the model; the Lower Jurassic source rock is the bottommost layer. The data points indicate the percentage of the value of hydrocarbons generated from the potential Lower Jurassic source rock layer.

NovaSPAN 2000 – Transformation Ratio (Pliensbachian Source Rock -Type II)

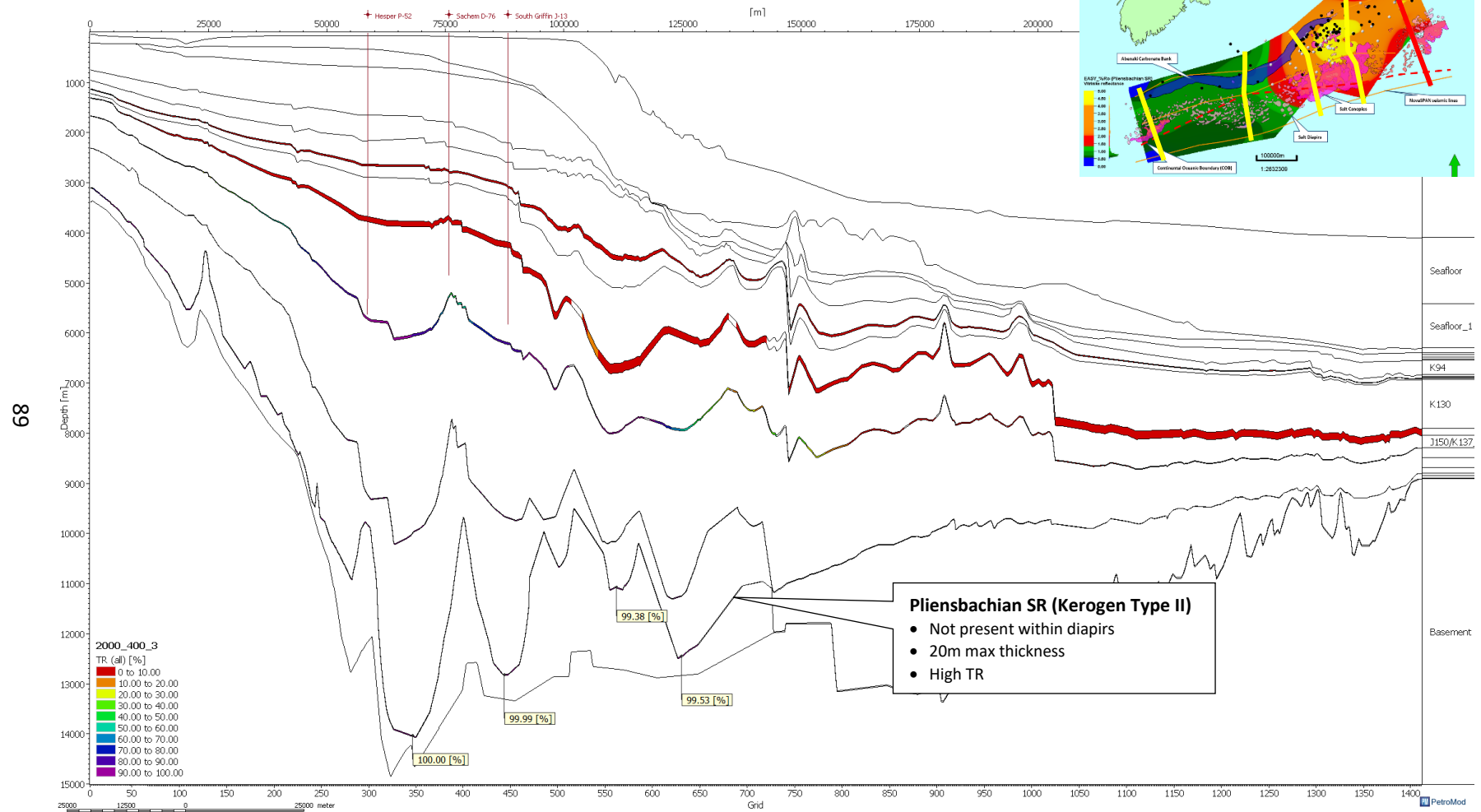


Figure 3.47: Model of transformation ratio for Pliensbachian source rock (Type II) for NovaSPAN 2000 line. Here we can observe the five different source rocks in the model; the Lower Jurassic source rock is the bottommost layer. The data points indicate the percentage of the value of hydrocarbons generated from the potential Lower Jurassic source rock layer.

NovaSPAN 2000 – Transformation Ratio (Pliensbachian Source Rock -Type I)

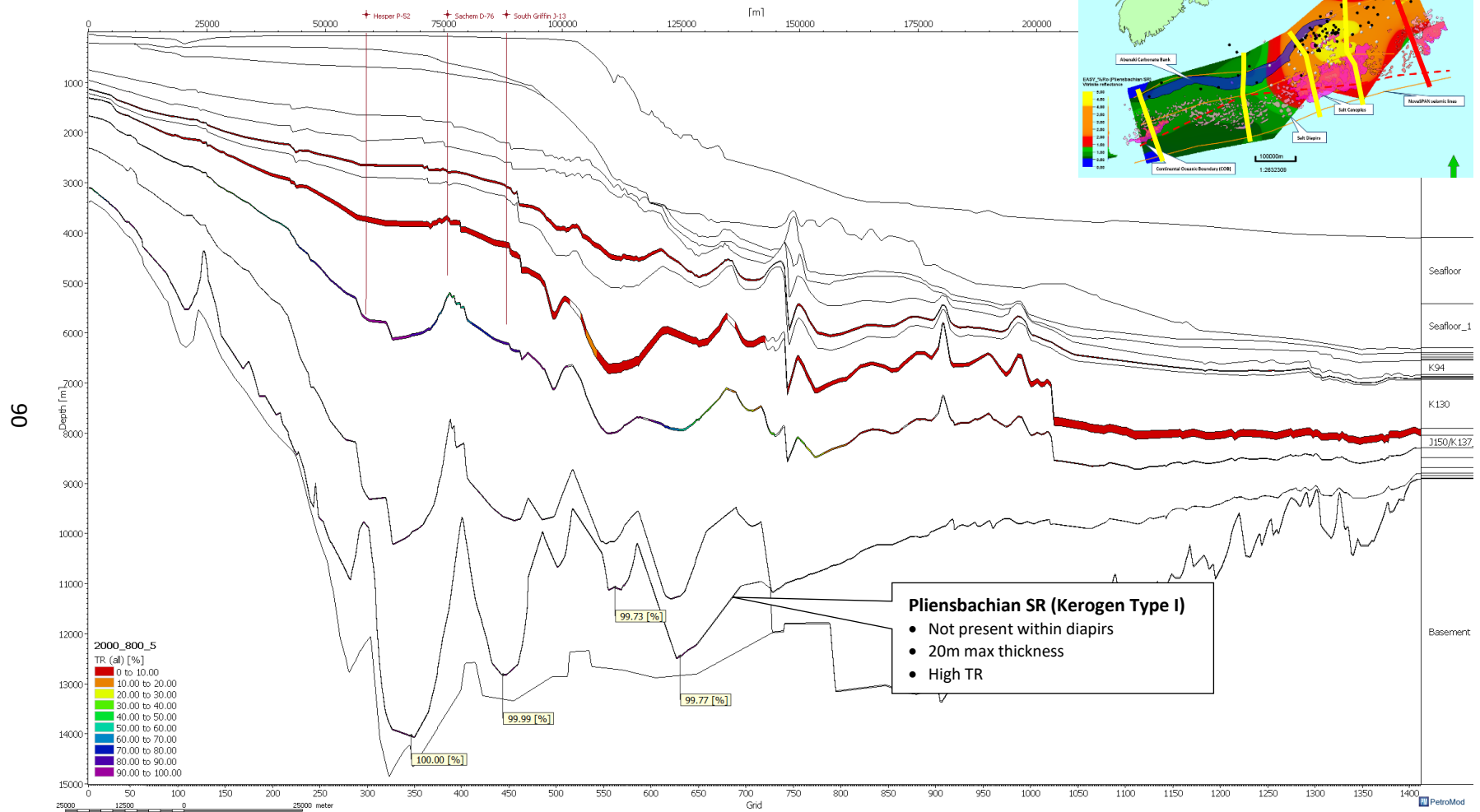


Figure 3.48: Model of transformation ratio for Pliensbachian source rock (Type I) for NovaSPAN 2000 line. Here we can observe the five different source rocks in the model; the Lower Jurassic source rock is the bottommost layer. The data points indicate the percentage of the value of hydrocarbons generated from the potential Lower Jurassic source rock layer.

NovaSPAN 2000 – Critical Moment (Pliensbachian Source Rock -Type III)

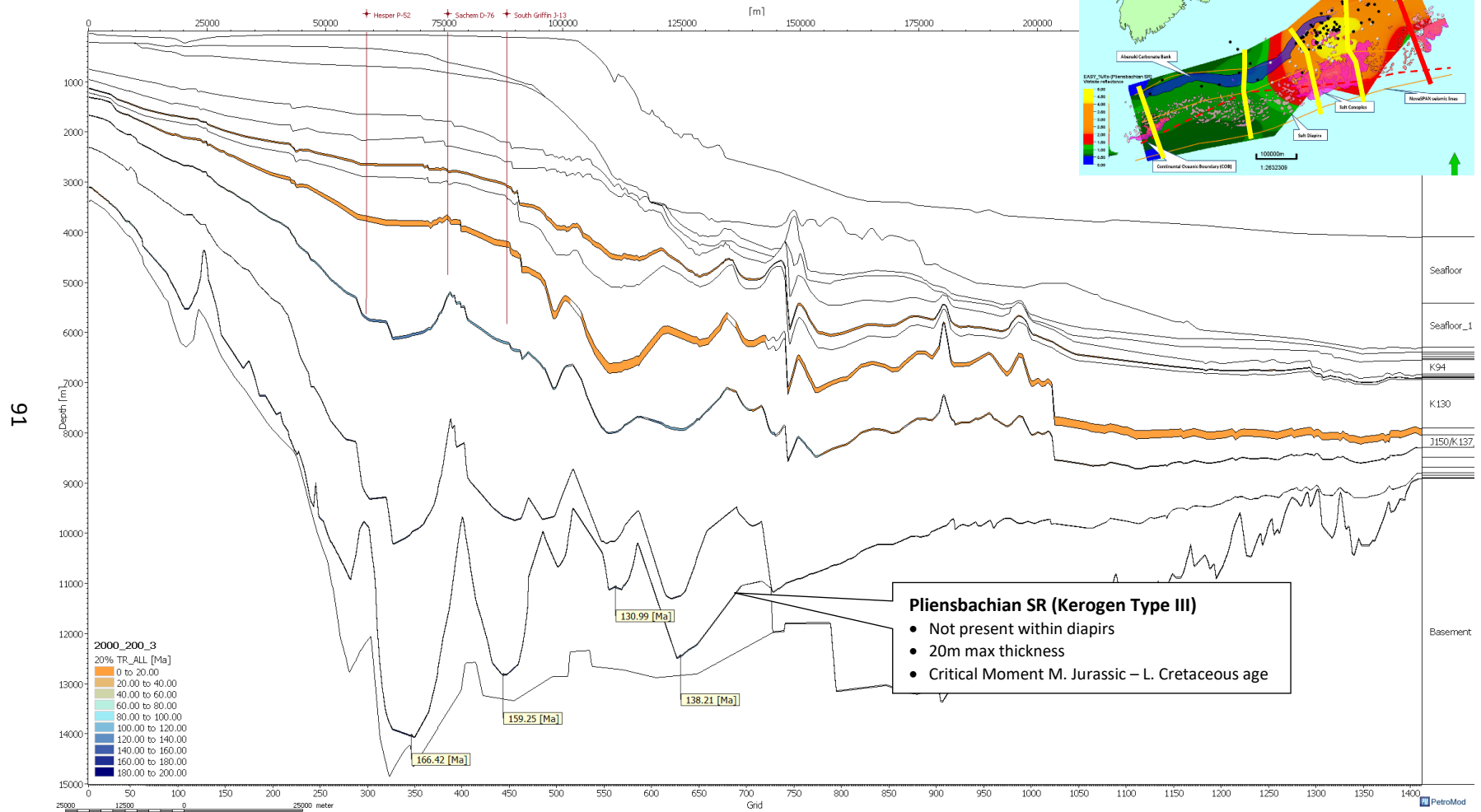


Figure 3.49: Model of the critical moment for the Pliensbachian source rock (Type III) for NovaSPAN 2000 line. Here we can observe the five different source rocks in the model; the Lower Jurassic source rock is the bottommost layer. The data points indicate the critical moment age that the potential Lower Jurassic had generated hydrocarbons exceeding the threshold.

NovaSPAN 2000 – Critical Moment (Pliensbachian Source Rock -Type II)

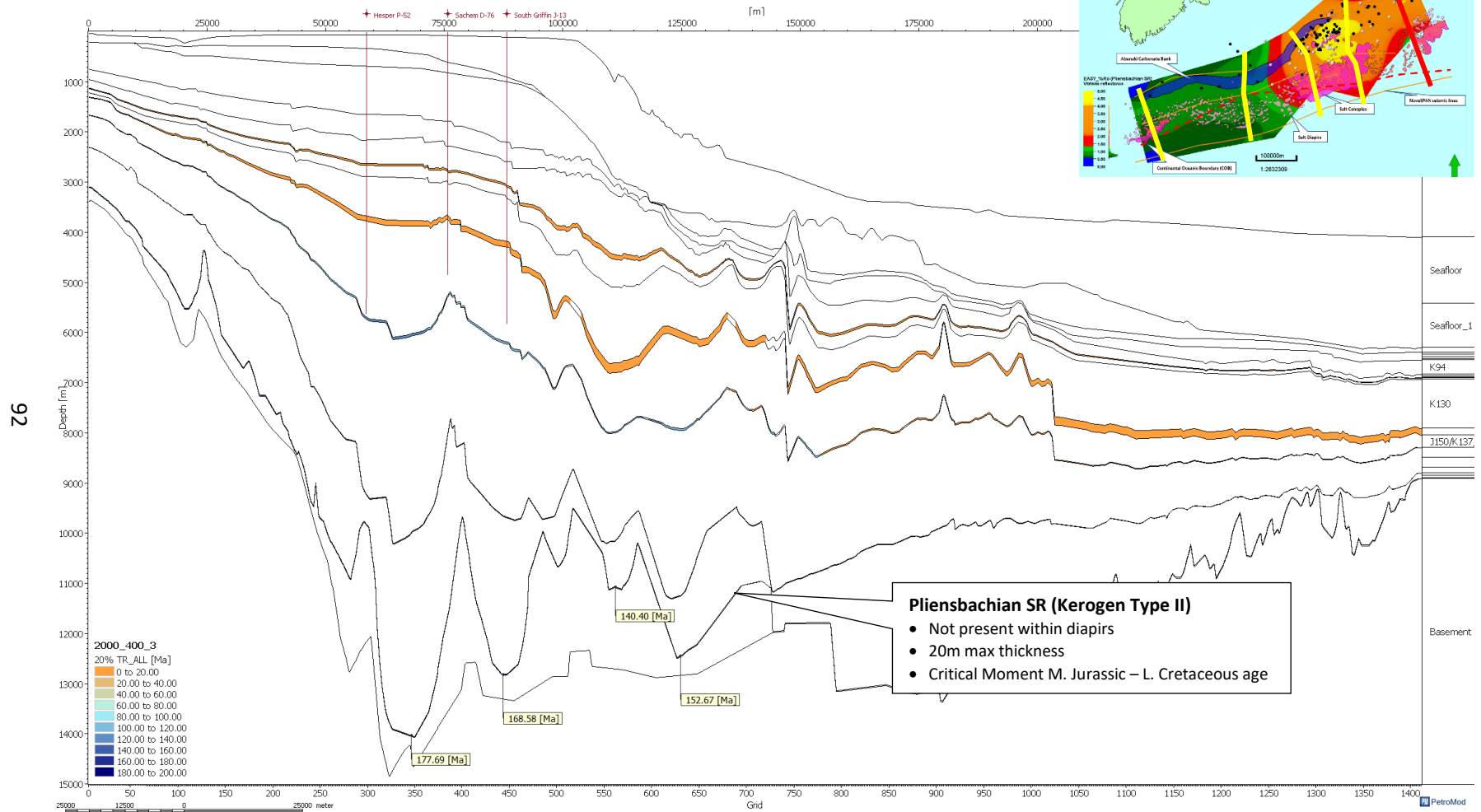


Figure 3.50: Model of the critical moment for the Pliensbachian source rock (Type II) for NovaSPAN 2000 line. Here we can observe the five different source rocks in the model; the Lower Jurassic source rock is the bottommost layer. The data points indicate the critical moment age that the potential Lower Jurassic had generated hydrocarbons exceeding the threshold.

NovaSPAN 2000 – Critical Moment (Pliensbachian Source Rock -Type I)

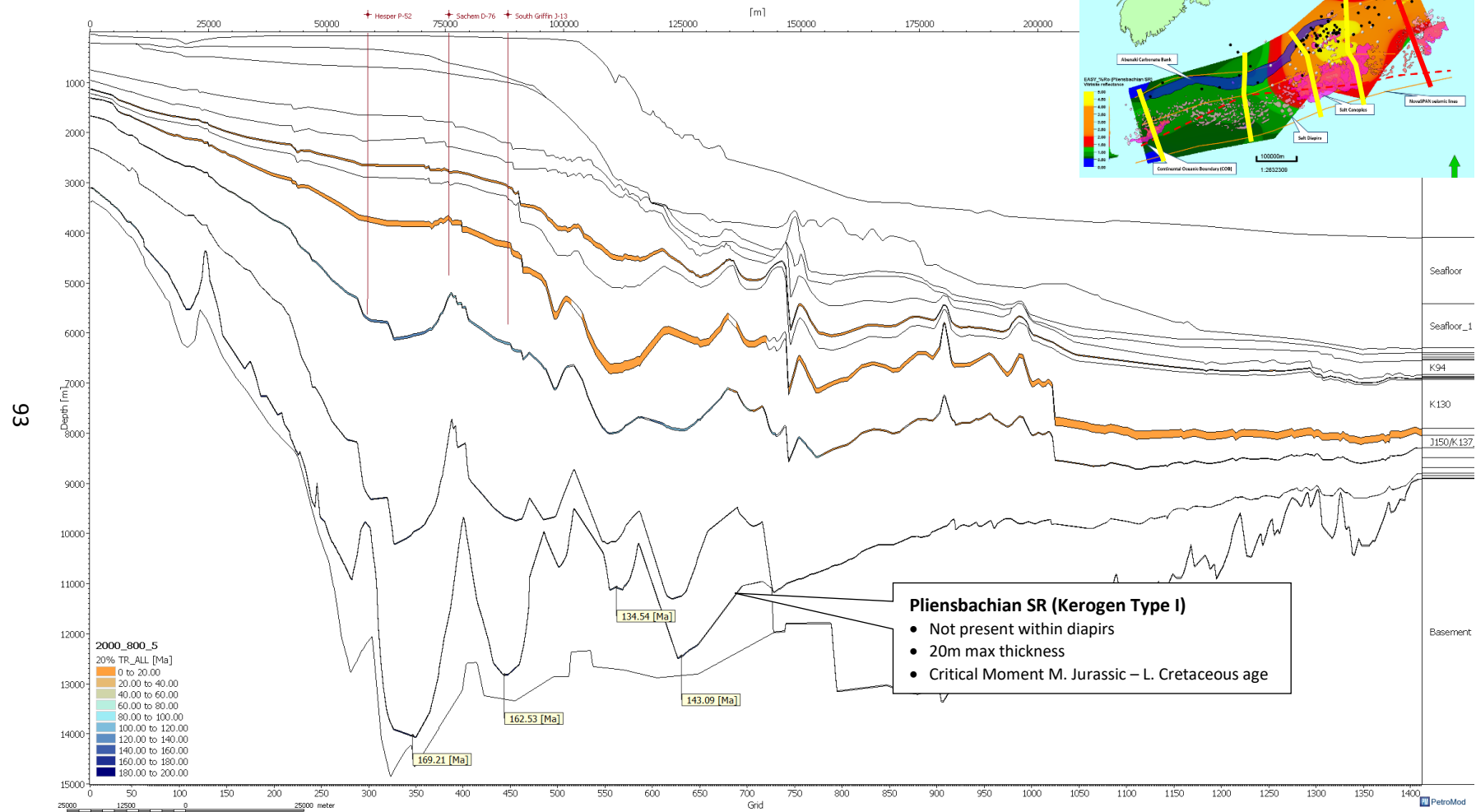


Figure 3.51: Model of the critical moment for the Pliensbachian source rock (Type I) for NovaSPAN 2000 line. Here we can observe the five different source rocks in the model; the Lower Jurassic source rock is the bottommost layer. The data points indicate the critical moment age that the potential Lower Jurassic had generated hydrocarbons exceeding the threshold.

3.7 Summary of the Base Case 2D Models

The following transformation ratio and time plot extractions are from specific locations along the 2D NovaSPAN models. These were chosen as representative locations of the shelf to slope break and the slope to abyssal region. These plots show the transformation ratio rate of the Lower Jurassic source rock (Pliensbachian SR) for each kerogen type simulated (Table 1.1). The critical moment is the age when the source rock had generated 20% of the convertible kerogen, which is the age when the transformation ratio of the source rock was 20% (dotted red line). These plots present the results for the slope and abyssal regions.

3.7.1 NovaSPAN 1100

NovaSPAN 1100 is the southernmost model; the Lower Jurassic rocks are within the oil thermal maturity window (Figure 3.18). Testing this model with the source rock parameters yielded a range of transformation ratio results (Figures 3.19 - 3.21). The Lower Jurassic source rock ranges from a low transformation ratio to a high transformation ratio, depending on the source rock kerogen type and location on the cross-section. There is also the assumption that the areas with Lower Jurassic sediments present will lie on the slope and the abyssal areas of the model and in the trough areas or mini-basins between the salt diapir. This assumption is based on that exploration on the shelf has not yielded the presence of Lower Jurassic materials. The results also show that the critical moment for the source rock interval, when it starts generating hydrocarbons. For these models, a threshold at the 20% fraction was set (Figures 3.22 - 3.24). These plots demonstrate that the Pliensbachian source rock that the critical “moment” is actually a broad range that differs on the location of the source rock within the cross-section and its kerogen type. This plot demonstrates the source rock transformation ratio at different locations along the model. The models of Lower Jurassic source rock suggests the source rock would be mature in the slope, with a late critical moment for kerogen Type I, Type II

and Type III. On the abyssal plain of the cross-section, the model suggests that the Lower Jurassic source rock would be mature for only the source rock of kerogen Type II (Table 3.1).

Table 3.1: Summary of maturity of the Lower Jurassic rocks for the model 1100. The maturity of each model is broken down into the slope and abyssal regions. The critical moment is the age when the source rock starts generating hydrocarbons. The kerogen type is the source rock type that shows maturity in the outputs.

Model	Area	Maturity	Critical Moment (Ma)	Kerogen Type
1100	Slope	Mature	80-4	Type I – Type III
	Abyssal	Mature	83	Type II

The plots from these models (Figures 3.52 and 3.53) demonstrate the transformation ratio of the Lower Jurassic source rock at the slope and abyssal plain, comparing the different types of kerogen. The transformation ratio of the three kerogen types demonstrated that on the slope the source rock of kerogen Type I, Type II and Type III has ongoing hydrocarbon generation. The difference in this model is that the source rocks of kerogen Type II has a critical moment in the Upper Cretaceous, and source rock of kerogen Type I and Type III has a later critical moment in the Pliocene. In the abyssal plain, the model demonstrates that only the source rock of kerogen Type II has reached the critical moment and it has ongoing hydrocarbon generation.

Slope

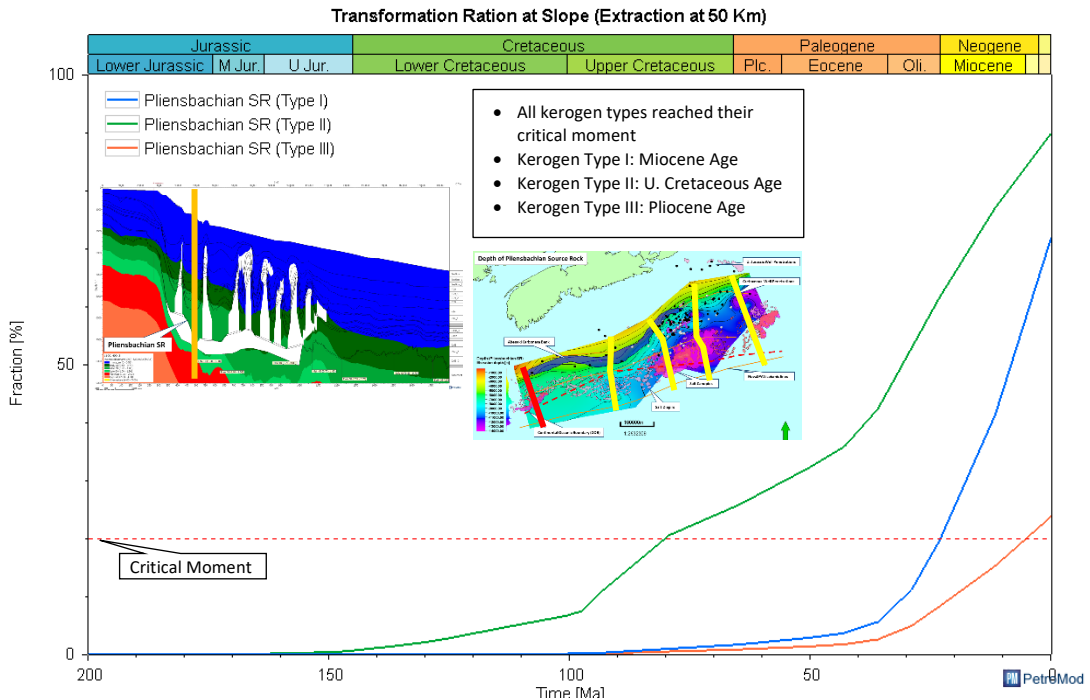


Figure 3.52: This is a 1D model extraction from the 2D NovaSPAN 1100 model at the slope region (50 Km). This plot shows the transformation ratio of the Pliensbachian source rock for each type of kerogen used in the model.

Abyssal

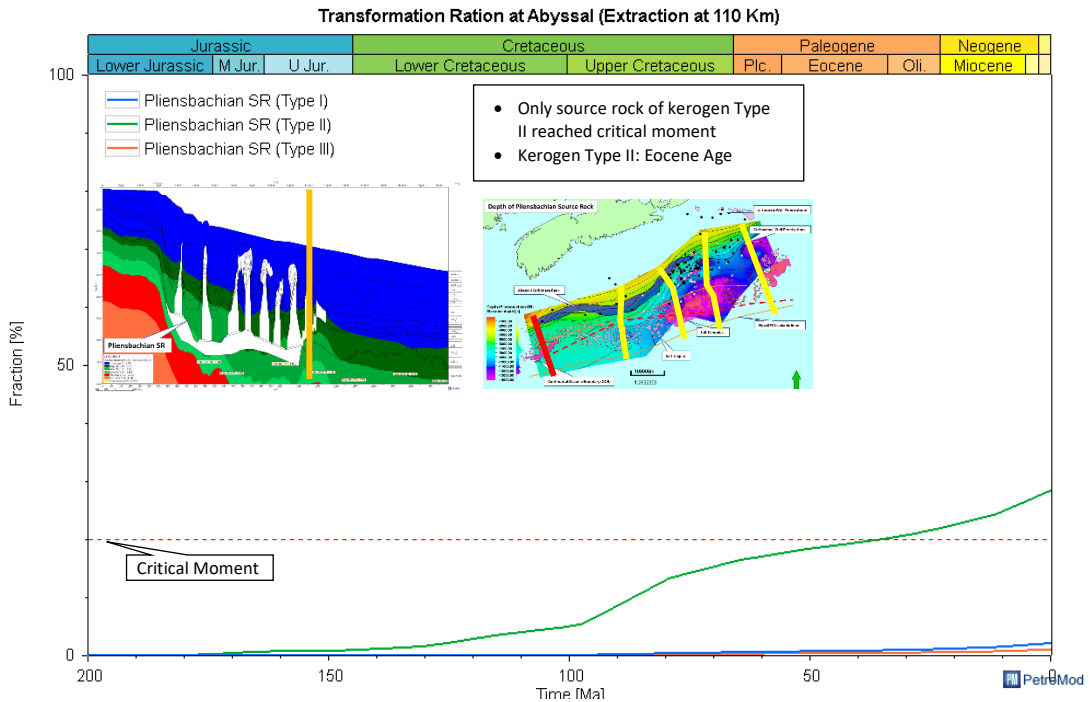


Figure 3.53: This is a 1D model extraction from the 2D NovaSPAN 1100 model in the abyssal region (110 Km). This plot shows the transformation ratio of the Pliensbachian source rock for each type of kerogen used in the model.

3.7.2 NovaSPAN 1400

The NovaSPAN 1400 is about 170 km to the north of NovaSPAN 1100; the model demonstrates the Lower Jurassic rocks within the oil thermal maturity windows (Figure 3.27). Testing this model with different kerogen types for the Lower Jurassic source rock (Table 1.1), generated a broad range of cross-section models (Figures 3.28 - 3.33). These cross-sections demonstrated that the transformation ratio of these Lower Jurassic source rock has a broad range across the slope to abyssal plain, depending on the source rock kerogen type and location along the cross-section. The following plots compare the kerogen types at two different locations along the NovaSPAN model (Figures 3.54 and 3.55).

The results from these plots (Figures 3.54 and 3.55) demonstrates that all source rock kerogen types has generated hydrocarbons at both slope and abyssal plain. Both source rocks of kerogen Type I and Type II has reached more than 90% transformation ratio and their critical moment was during the Upper to Lower Cretaceous. The source rock of kerogen Type III for which the critical moment was during the Oligocene, still has the ongoing potential to generate more hydrocarbons. From these models the Lower Jurassic source rock, if present, can be a mature source rock in the slope and abyssal plains for kerogen Type I, Type II and Type III (Table 3.2).

Table 3.2: Summary of maturity of the Lower Jurassic rocks for the model 1400. The maturity of each model is broken down into the slope and abyssal regions. The critical moment is the age when the source rock starts generating hydrocarbons. The kerogen type is the source rock type that shows maturity in the outputs.

Model	Area	Maturity	Critical Moment (Ma)	Kerogen Type
1400	Slope	Mature	135-28	Type I – Type III
	Abyssal	Mature	128-39	Type I – Type III

Slope

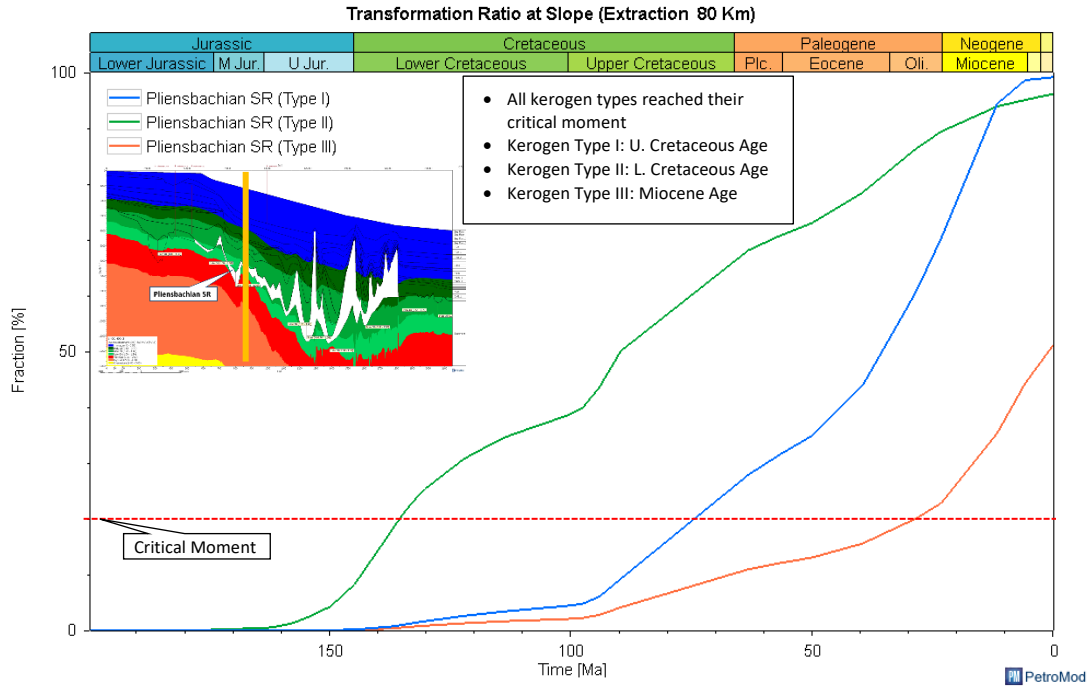


Figure 3.54: This is a 1D model extraction from the 2D NovaSPAN 1400 model at the slope region (80 Km). This plot shows the transformation ratio of the Pliensbachian source rock for each type of kerogen used in the model.

Abyssal

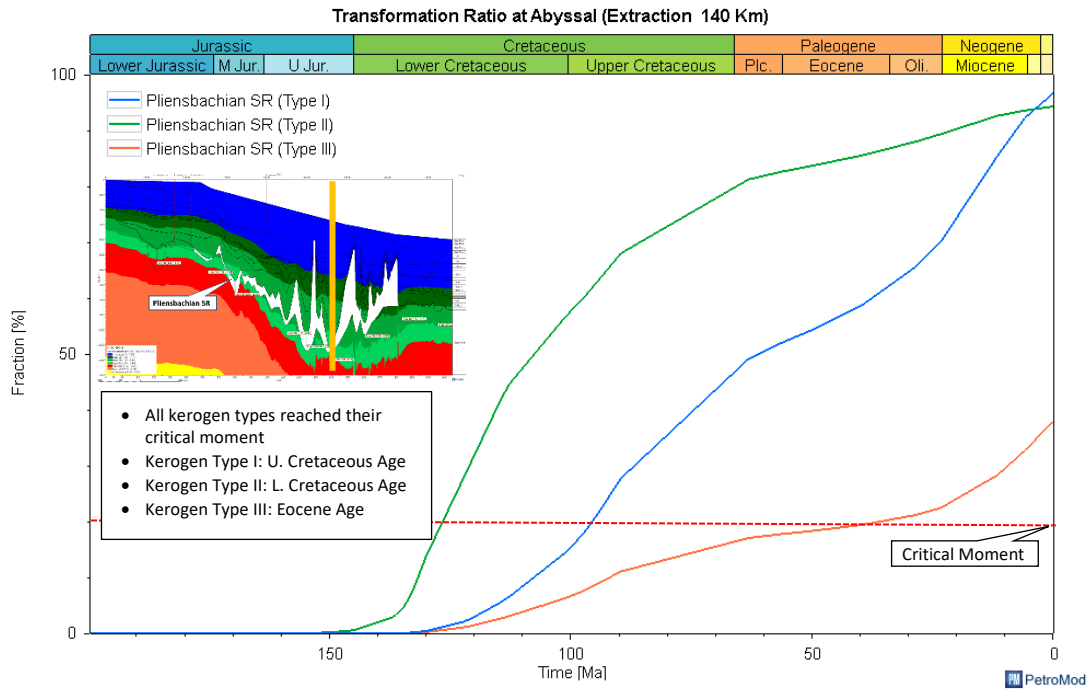


Figure 3.55: This is a 1D model extraction from the 2D NovaSPAN 1400 model in the abyssal region (140 Km). This plot shows the transformation ratio of the Pliensbachian source rock for each type of kerogen used in the model.

3.7.3 NovaSPAN 1800

This model is the north-central line of the Scotian Basin, between the NovaSPAN 1600 and NovaSPAN 2000 line. The model demonstrates that the Lower Jurassic source rock is overmature on the shelf and in the gas window on the abyssal region (Figure 3.36). The transformation ratio cross-sections for this line displays high transformation values for all source rock kerogen types (Figures 3.37 - 3.39). This model shows very thick sediment packages overlying the source rock, suggesting high depositional rates (Campbell, 2010), this high sedimentation rates may have influenced the salt mobilization and the thermal maturity of these source rocks (Goteti et al., 2013). There is evidence for multiple hydrocarbon generation pulses for the source rocks of kerogen Type III which maybe have been caused from salt mobilization and, or intervals of high sedimentation. The plots (Figures 3.40 - 3.42) demonstrates there was a fast rate of hydrocarbon generation for source rocks of kerogen Type I and Type II the Middle to Upper Jurassic. The source rock of kerogen Type III is the only type that still has ongoing potential along the NovaSPAN 1800 line. These plots demonstrated multiple hydrocarbon phase generation for source rock of Type III kerogen. This is probably from the high sedimentation influx in the basin during the Cretaceous, which also influence the salt mobilization (Figure 3.56 and Figure 3.57). From these models the Lower Jurassic source rock, if present, is overmature in the slope and abyssal plains for kerogen Type I and Type II, and source rock of kerogen Type III still has ongoing potential (Table 3.2).

Table 3.3: Summary of maturity of the Lower Jurassic rocks for the model 1800. The maturity of each model is broken down into the slope and abyssal regions. The critical moment is the age when the source rock starts generating hydrocarbons. The kerogen type is the source rock type that shows maturity in the outputs.

Model	Area	Maturity	Critical Moment (Ma)	Kerogen Type
1800	Slope	Overmature	157-152	Type I – Type II
	Abyssal	Mature	173-129	Type III

Slope

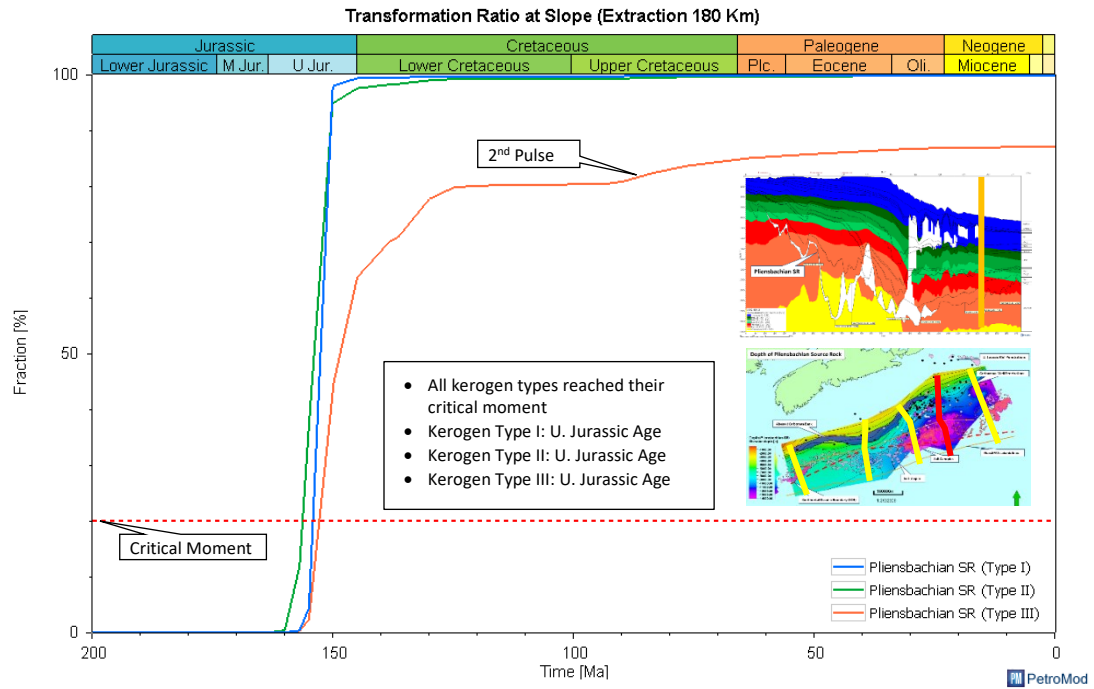


Figure 3.56: This is a 1D model extraction from the 2D NovaSPAN 1800 model at the slope region (180 Km). This plot shows the transformation ratio of the Pliensbachian source rock for each type of kerogen used in the model.

Abyssal

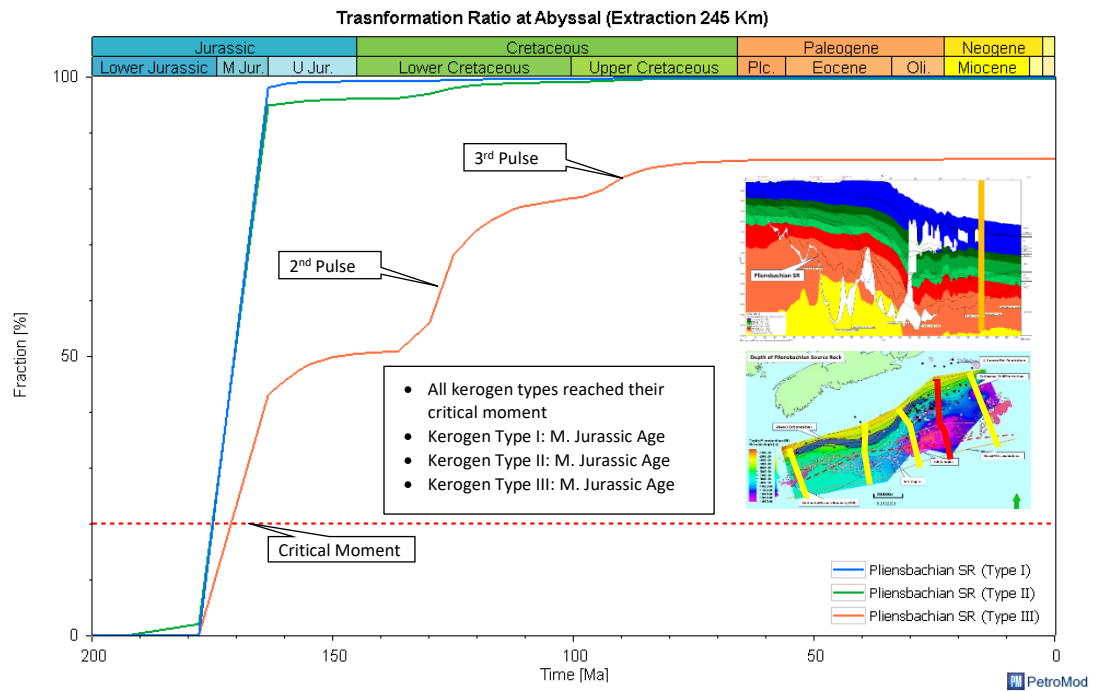


Figure 3.57: This is a 1D model extraction from the 2D NovaSPAN 1800 model in the abyssal region (245 Km). This plot shows the transformation ratio of the Pliensbachian source rock for each type of kerogen used in the model.

3.7.4 NovaSPAN 2000

The NovaSPAN 2000 is in the northernmost part of the Scotian Basin, the Lower Jurassic source rock layer in this model was truncated by the salt canopy and not modelled in the abyssal regions of this model. Interpreting the Lower Jurassic source rock underneath the salt canopy was challenging (Figure 3.45), this is due to the properties of salt attenuating the seismic signal (Jones and Davison, 2014). The maturity cross-section demonstrates that the Lower Jurassic source rock is mainly within the gas window (Figure 3.45). The transformation ration cross sections demonstrate that all the source rock kerogen types have reached high transformation ratios (Figures 3.46 - 3.48). The high transformation ratios values in this model may be probable from the fast burial rate and salt mobilization in this part of the Scotian Basin, similarly to NovaSPAN 1800 model. From these cross-sections, the Lower Jurassic source rock reached the critical moment during the Lower Cretaceous for kerogen Type I to Type III (Table 3.4). The plot (Figure 3.58), demonstrates the high transformation ratio for the source rock of kerogen Type I and Type II reaching its maximum potential during the Lower Cretaceous.

Table 3.4: Summary of maturity of the Lower Jurassic rocks for the model 2000 in the slope region. The critical moment is the age when the source rock starts generating hydrocarbons. The kerogen type is the source rock type that shows maturity in the outputs.

Model	Area	Maturity	Critical Moment (Ma)	Kerogen Type
2000	Slope	Mature	153-138	Type I – Type III

Slope

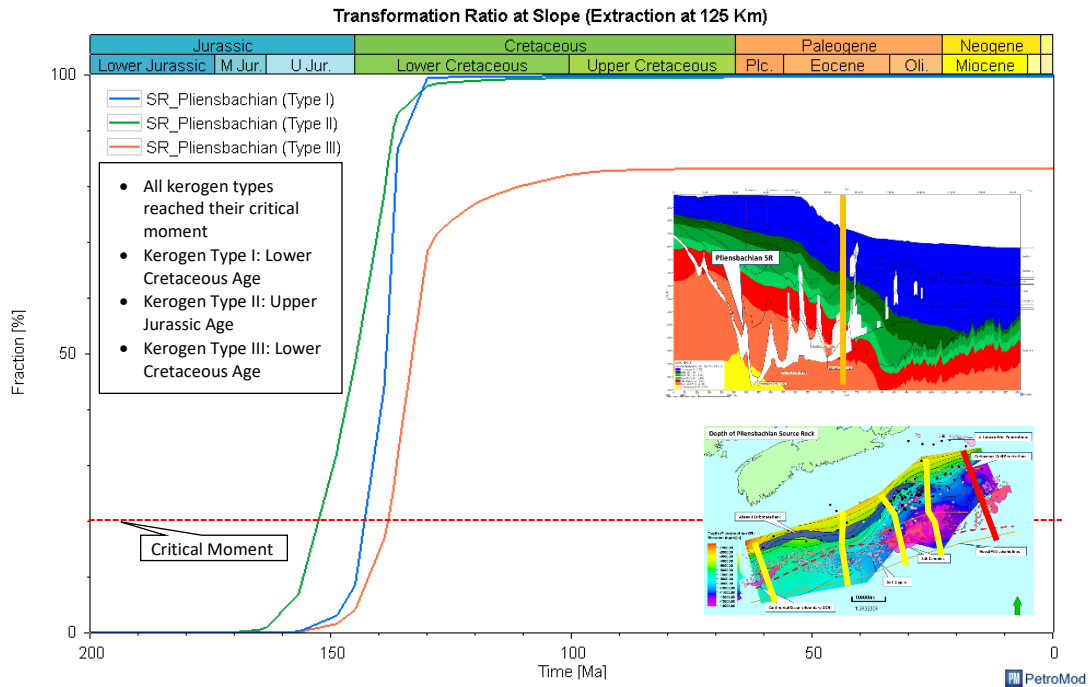


Figure 3.58: This is a 1D model extraction from the 2D NovaSPAN 2000 model at the slope region (125 Km). This plot shows the transformation ratio of the Pliensbachian source rock for each type of kerogen used in the model.

3.7.5 Extrapolation of the Lower Jurassic source rock interval

This study explored different regions of the Scotian Basin from the southernmost line of NovaSPAN 1100 to the northernmost line of NovaSPAN 2000 from the 2D models, including NovaSPAN 1600 modelled by colleague Xinyue Hu, from the Basin and Reservoir Lab. The following figures are maps extrapolated from these models. These maps are extrapolated from the models at a 1 km by 1km grid spacing. These maps demonstrate the broad range of thermal maturity of the Lower Jurassic source rock throughout the Scotian Basin.

The Lower Jurassic source rock is at a shallower depth in the southwestern part and progressively gets deeper in the northeastern part (Figure 3.59). The depth of the Lower Jurassic source rock affects the temperature (Figure 3.60). The southwestern part is much cooler than the northeastern part of the Scotian Basin. We need to take into consideration also the effects that the Argo Formation has as it mobilized on the Scotian Basin creating salt diapir and

canopies. The salt diapirs are more predominant in the southern region, while salt diapirs and canopies more common in the northern region of the Scotian Basin. The salt affects the heat flow (Goteti et al., 2013) which affects the thermal maturity of the Lower Jurassic source rock if present (Figure 3.62). The thermal maturity map shows that the Lower Jurassic rock are mature in the Scotian Basin, trending from oil window in the southwest part to the gas window in the northeastern part of the Scotian Basin (Figure 3.62). Testing this Lower Jurassic source rock with different types of kerogen types (Type I, II, and III) show us that depending on the kerogen types there are a different amount of hydrocarbon generated by them, as seen in Figure 3.63 to Figure 3.65 and also different critical moments for each kerogen type (Figure 3.66 - Figure 3.68).

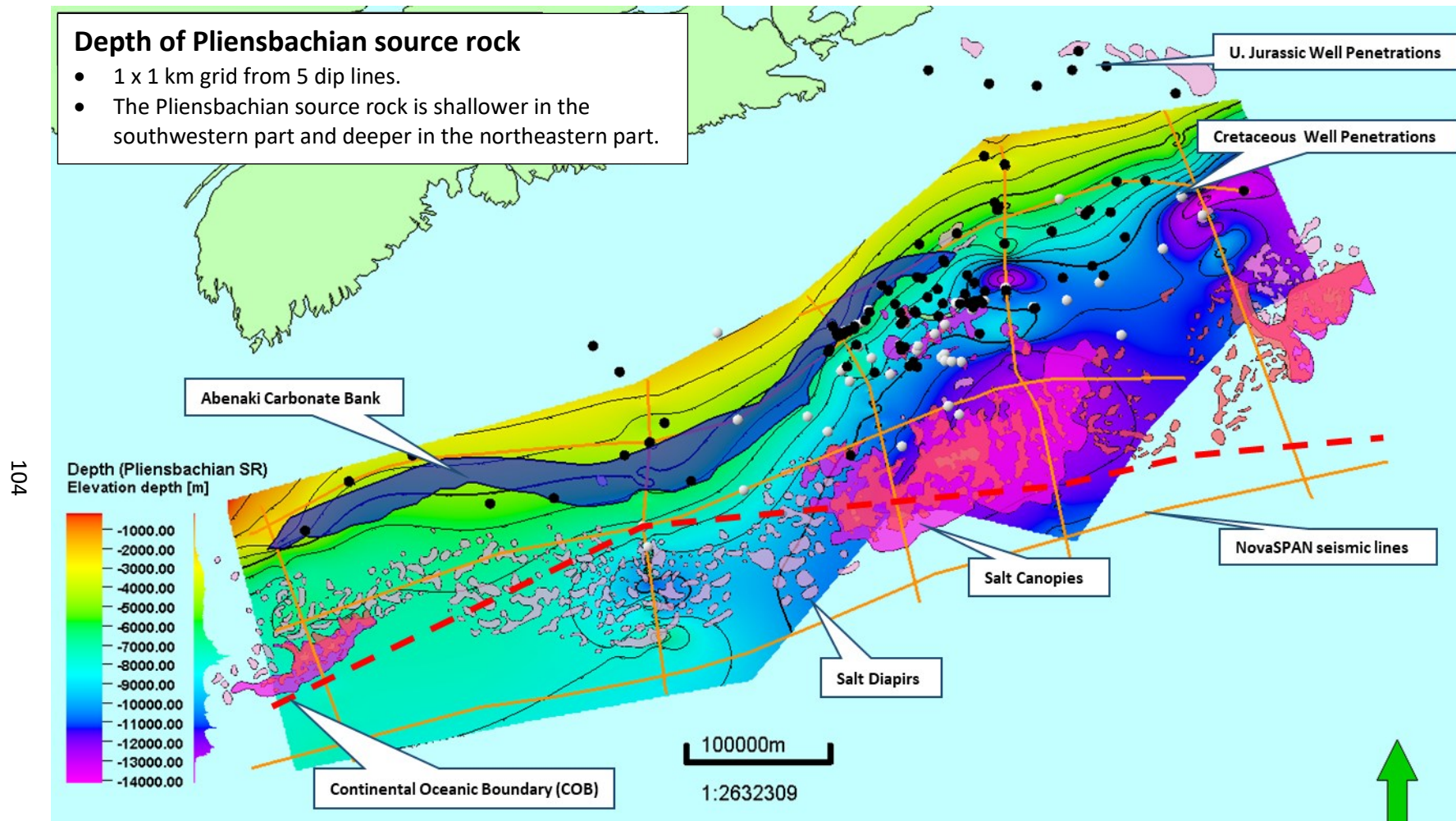


Figure 3.59: Map of depth below sea level of the Pliensbachian source rock (1 km by 1 km smooth gridded) based on NovaSPAN 1100, 1400, 1600, 1800 and 2000 models. The dark blue irregular shape is the extent of the Abenaki carbonates. The irregular pink shapes are the salt diapirs and canopies. The dots are all the boreholes in the Scotian Basin; the black dots are boreholes that penetrated the Jurassic Intervals (Middle – Upper Jurassic), the white dots are boreholes that did not penetrate the Jurassic intervals.

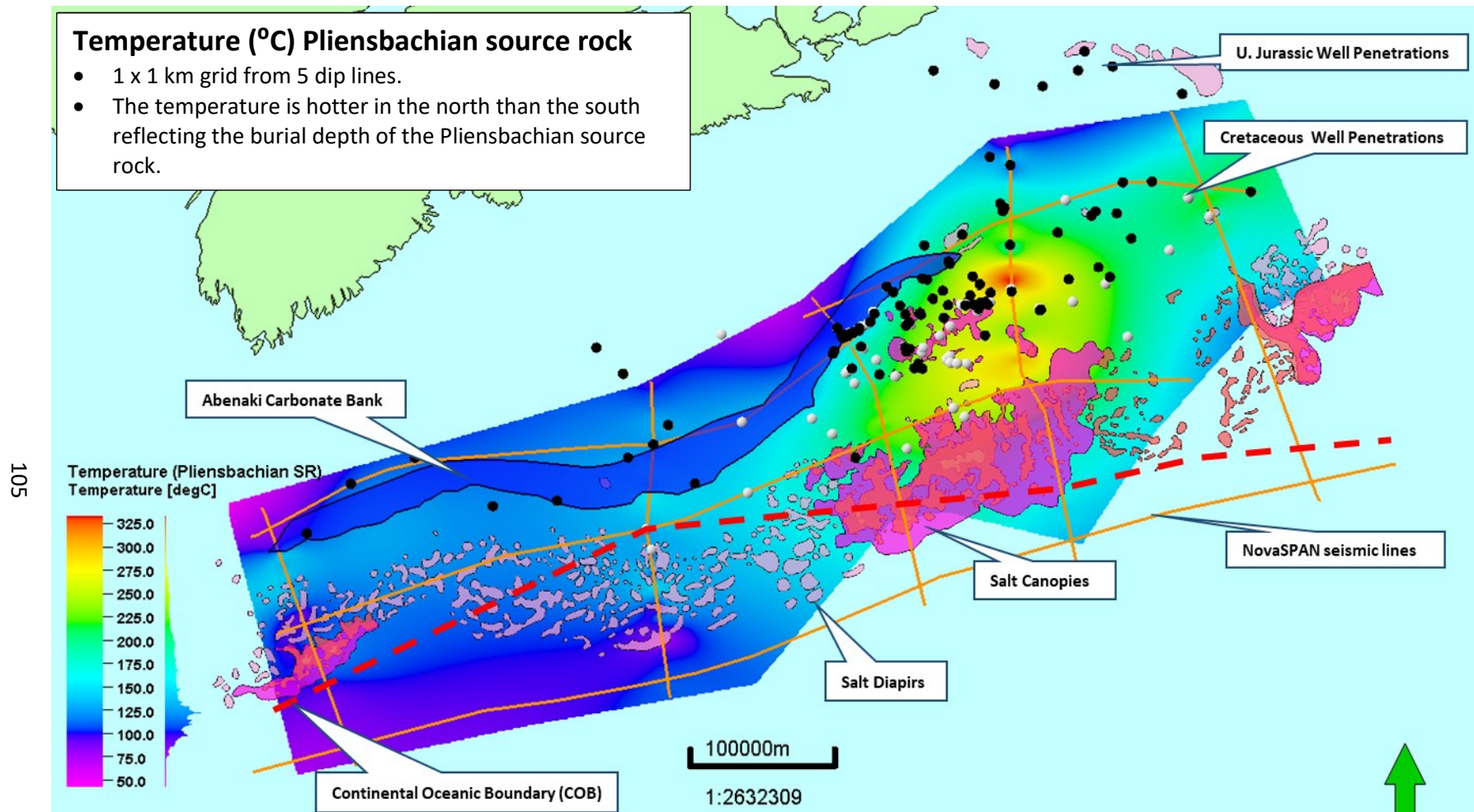


Figure 3.60: Temperature map (1 km by 1 km smooth gridded) at the top of the Pliensbachian source rock based on NovaSPAN 1100, 1400, 1600, 1800 and 2000 models. The dark blue irregular shape is the extent of the Abenaki carbonates. The irregular pink shapes are the salt diapirs and canopies. The dots are all the boreholes in the Scotian Basin; the black dots are boreholes that penetrated the Jurassic intervals (Middle – Upper Jurassic), the white dots are boreholes that did not penetrate the Jurassic internals.

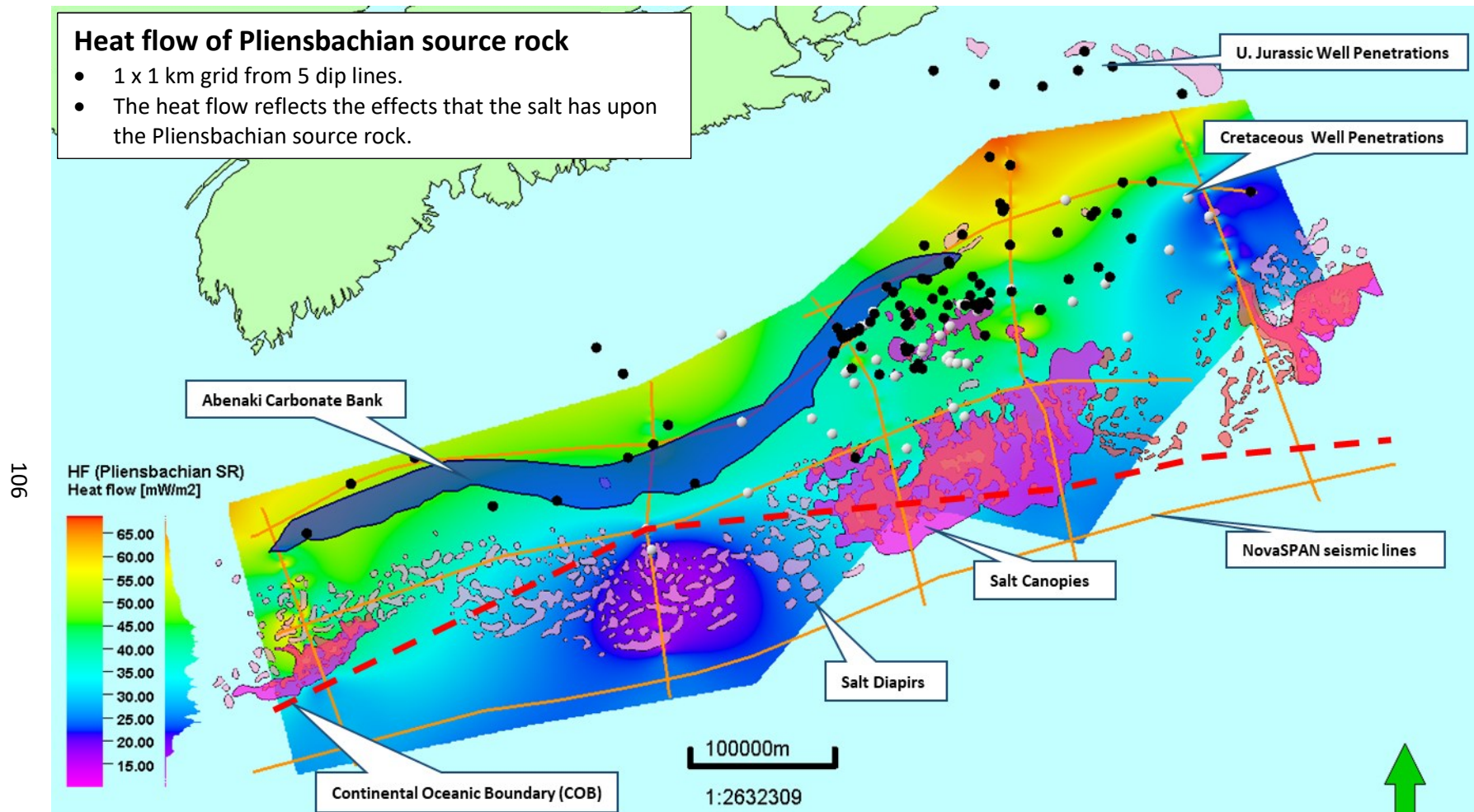


Figure 3.61: Heat flow map (1 km by 1 km smooth gridded) at the top of the Pliensbachian source rock based on NovaSPAN 1100, 1400, 1600, 1800 and 2000 models. The dark blue irregular shape is the extent of the Abenaki carbonates. The irregular pink shapes are the salt diapirs and canopies. The dots are all the boreholes in the Scotian Basin; the black dots are boreholes that penetrated the Jurassic intervals (Middle – Upper Jurassic), the white dots are boreholes that did not penetrate the Jurassic internals.

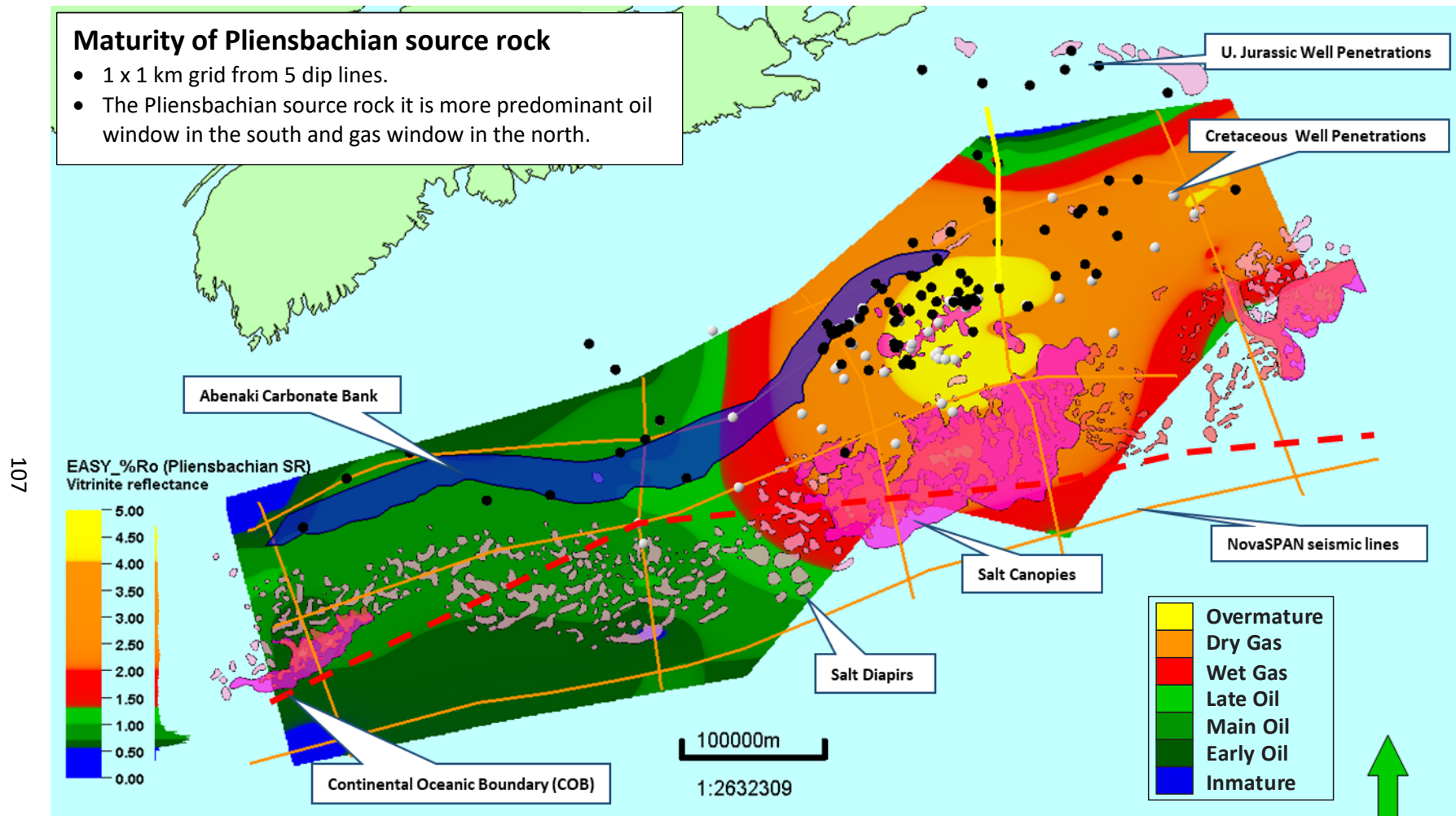


Figure 3.62: Vitrinite reflectance map (1 km by 1 km smooth gridded) at the top of the Pliensbachian source rock based on NovaSPAN 1100, 1400, 1600, 1800 and 2000 models. The dark blue irregular shape is the extent of the Abenaki carbonates. The irregular pink shapes are the salt diapirs and canopies. The dots are all the boreholes in the Scotian Basin; the black dots are boreholes that penetrated the Jurassic intervals (Middle – Upper Jurassic), the white dots are boreholes that did not penetrate the Jurassic internals. The range of vitrinite reflectance: Blue (0 – 0.55) Immature, Dark Green (0.55-0.70) Early Oil, Green (0.70-1.00) Main Oil, Light Green (1.00-1.30) Late Oil, Red (1.30 – 2.00) Wet Gas, Orange (2.00 – 4.00) Dry Gas and Yellow (4.00 – 5.00) Overmature.

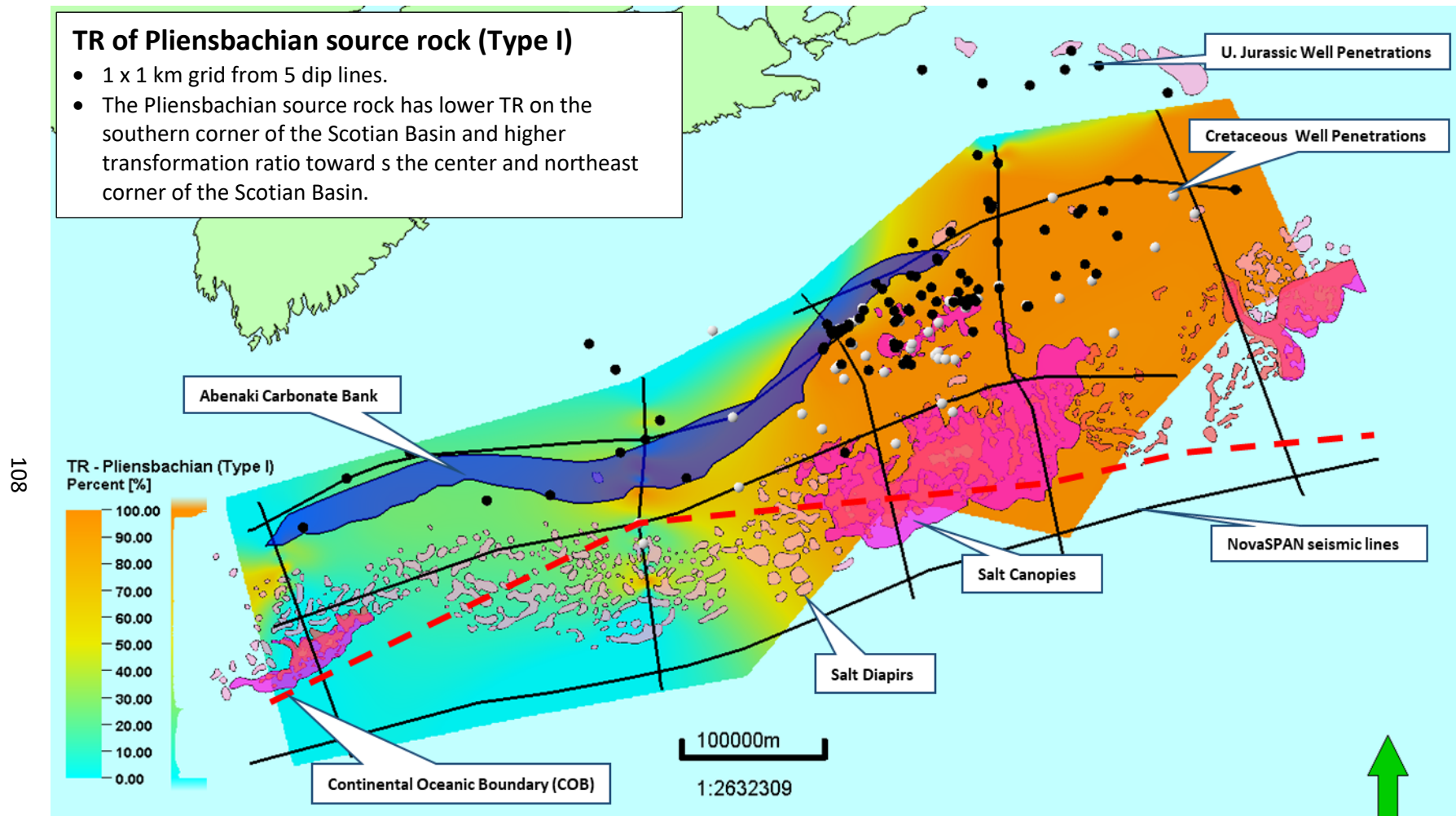


Figure 3.63: Transformation Ratio map (1 km by 1 km smooth gridded) of the Pliensbachian source rock of kerogen Type I. This particular source rock has a lower transformation ratio in the southwest corner of the Scotian Basin and a higher transformation ratio towards the northeastern corner of the Scotian Basin.

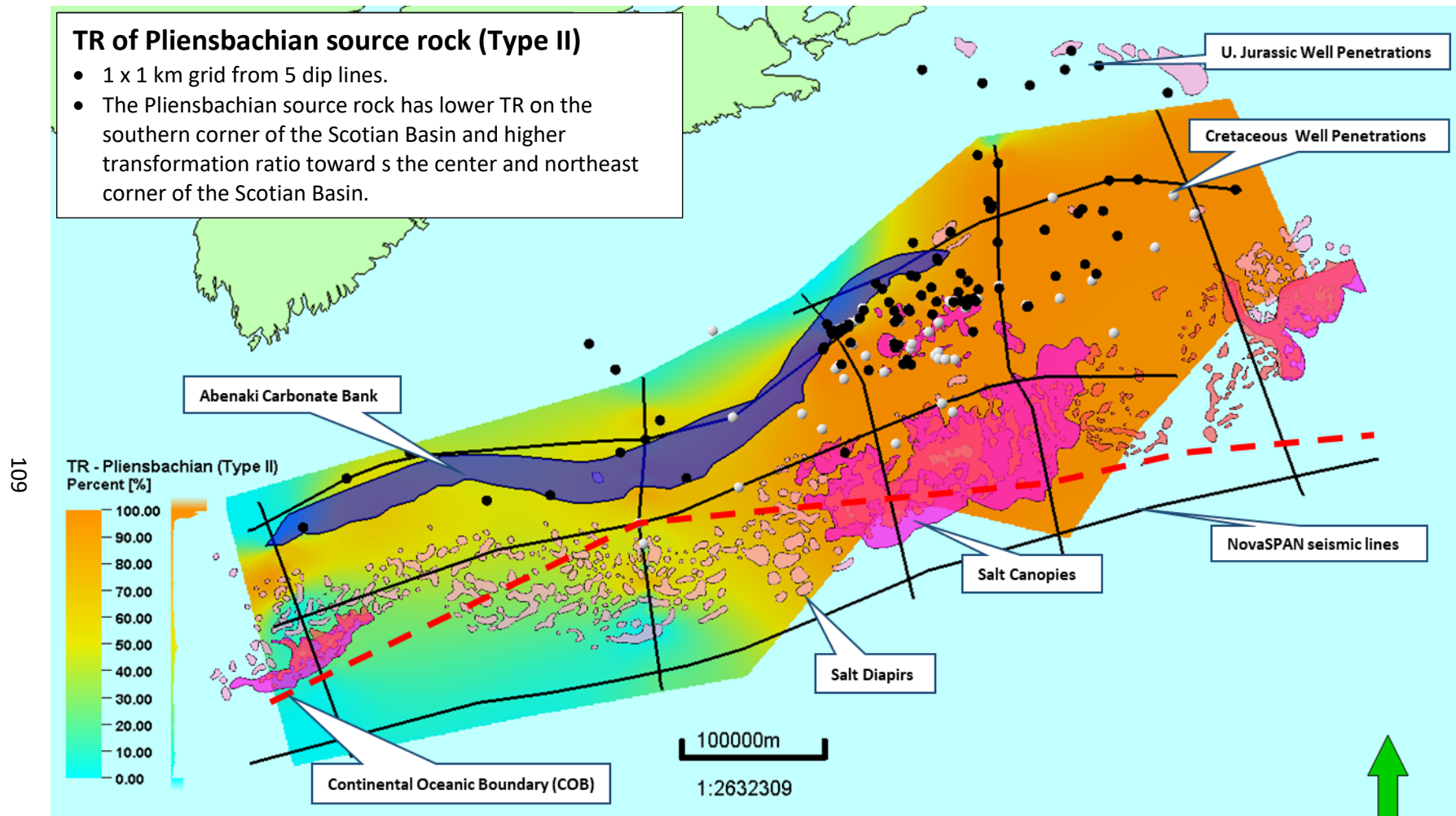


Figure 3.64: Transformation Ratio map (1 km by 1 km smooth gridded) of the Pliensbachian source rock of kerogen Type II. This particular source rock has a lower transformation ratio in the southwest corner of the Scotian Basin and progressively a higher transformation ratio towards the center to a maximum transformation ratio towards the northeastern corner of the Scotian Basin.

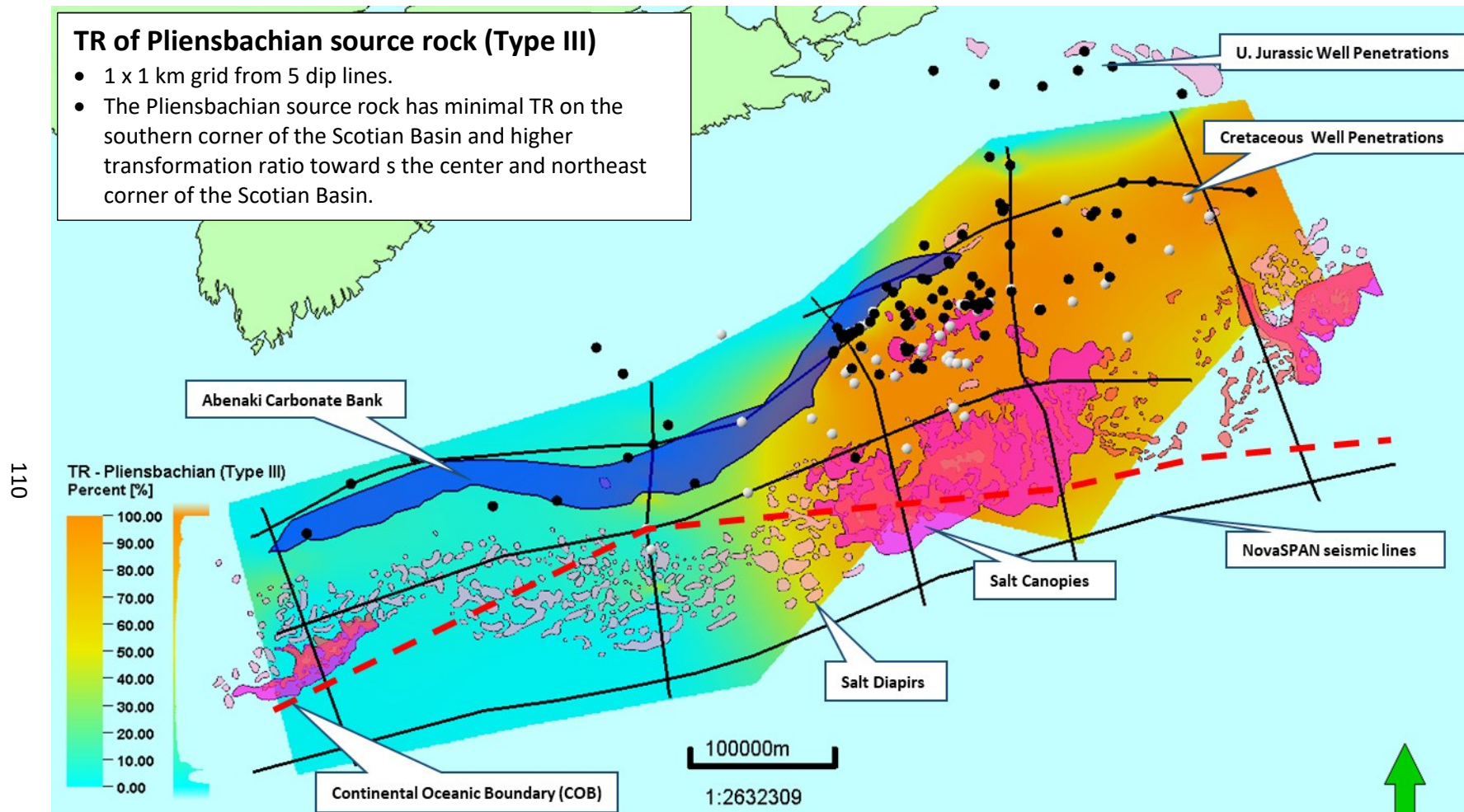


Figure 3.65: Transformation Ratio map (1 km by 1 km smooth gridded) of the Pliensbachian source rock of kerogen Type III. This particular source rock has a minimum transformation ratio in the southwest corner of the Scotian Basin and transitioning to a higher transformation ratio towards the center and the northeastern corner of the Scotian Basin.

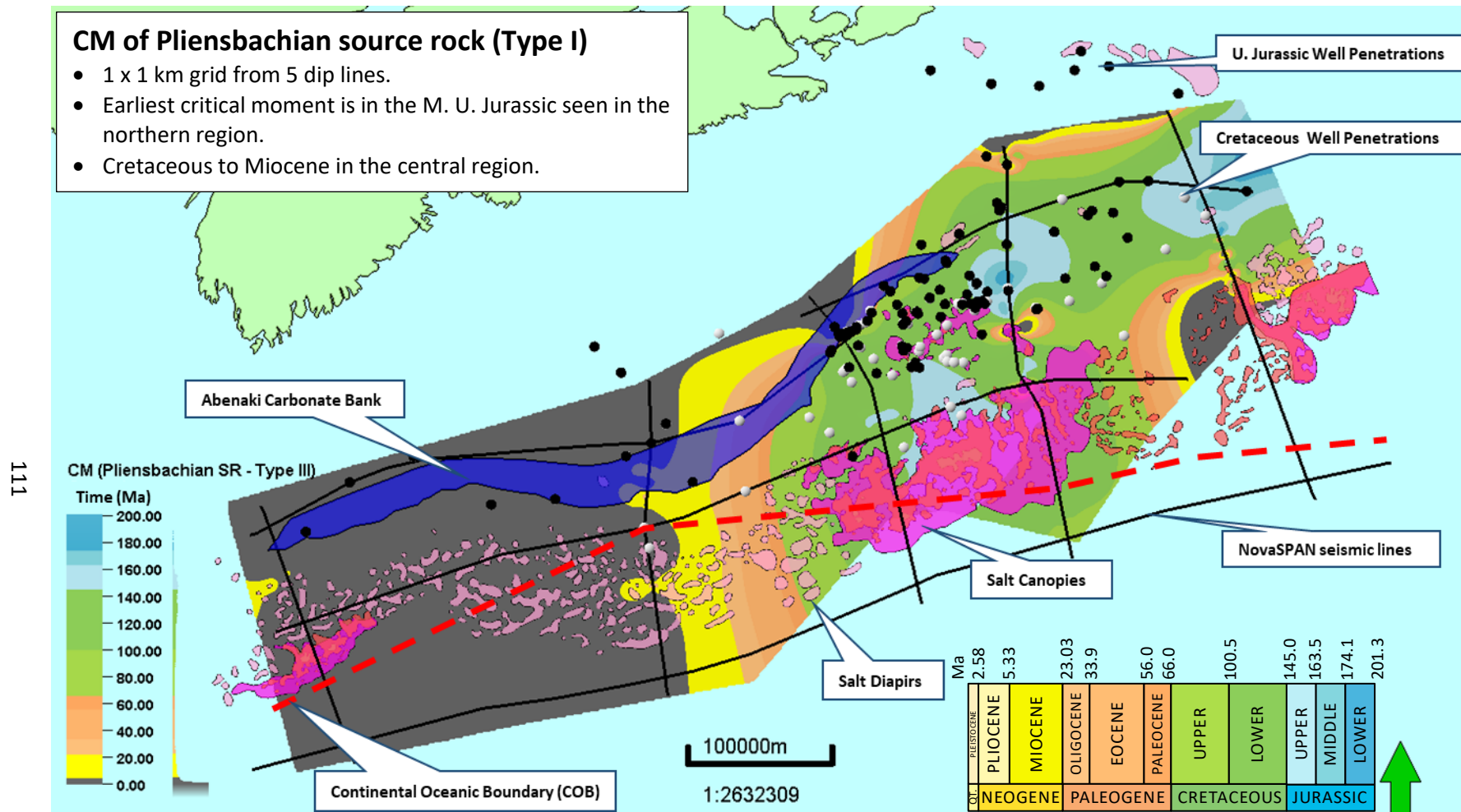
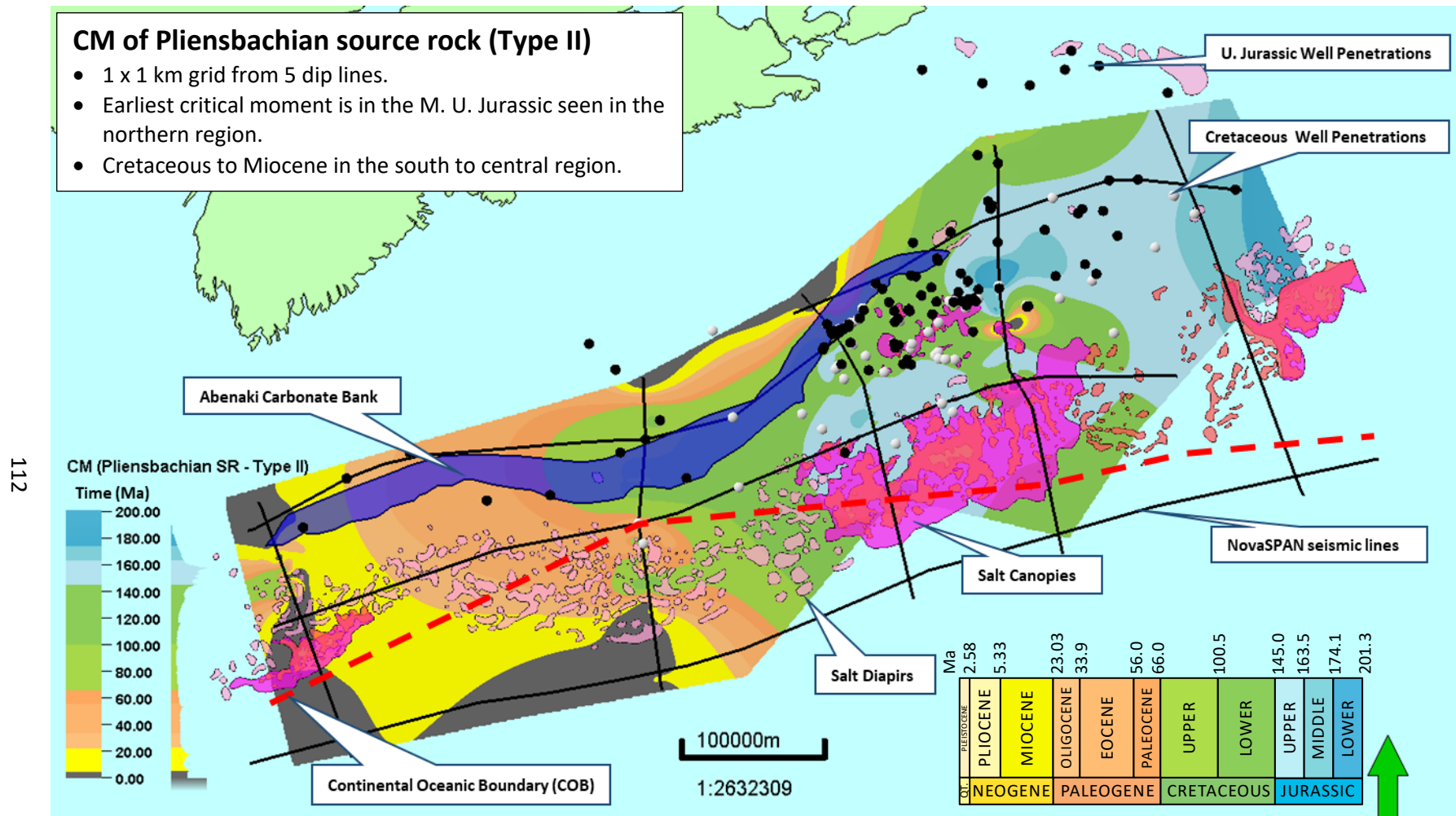


Figure 3.66: Critical Moment map (1 km by 1 km smooth gridded) of the Pliensbachian source rock of kerogen Type I. The Critical Moment is defined when the transformation ratio reached 20% of hydrocarbon generation.



112

Figure 3.67: Critical Moment map (1 km by 1 km smooth gridded) of the Pliensbachian source rock of kerogen Type II. The Critical Moment is defined when the transformation ratio reached 20% of hydrocarbon generation.

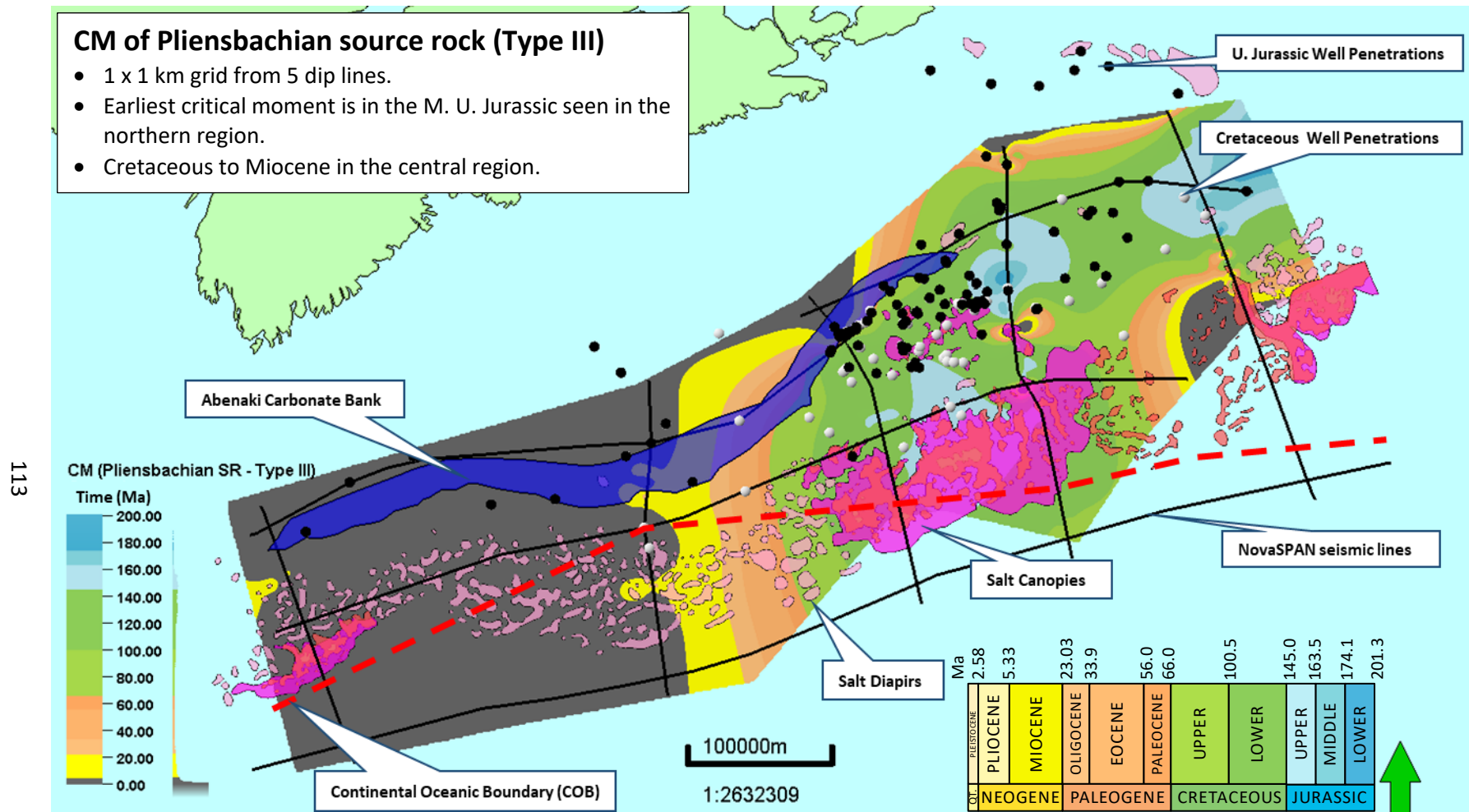


Figure 3.68: Critical Moment map (1 km by 1 km smooth gridded) of the Pliensbachian source rock of kerogen Type III. The Critical Moment is defined when the transformation ratio reached 20% of hydrocarbon generation.

3.8 Sensitivities to Base Case Model

The 2D models presented above are deterministic cases based on the Ait Moussa outcrop geochemical data with other parameters essentially the same as the 2011 PFA study. These initial models focussed on sensitivities to the PFA approach by varying geochemical parameters. In addition, sensitivities to two of the key input parameters (salt presence and Beta factor) were addressed and are presented here. These sensitivities were run by generating new versions of the five 2D cross sections, exporting the results to Petrel and remapping the resulting outputs, in particular, thermal maturity. (Figure 3.70). Furthermore, in these sensitivities the Continent Ocean Boundary was moved from a position consistent with the 2011 PFA study to a position at the outboard margin of the East Coast Magnetic Anomaly (Figure 3.69).

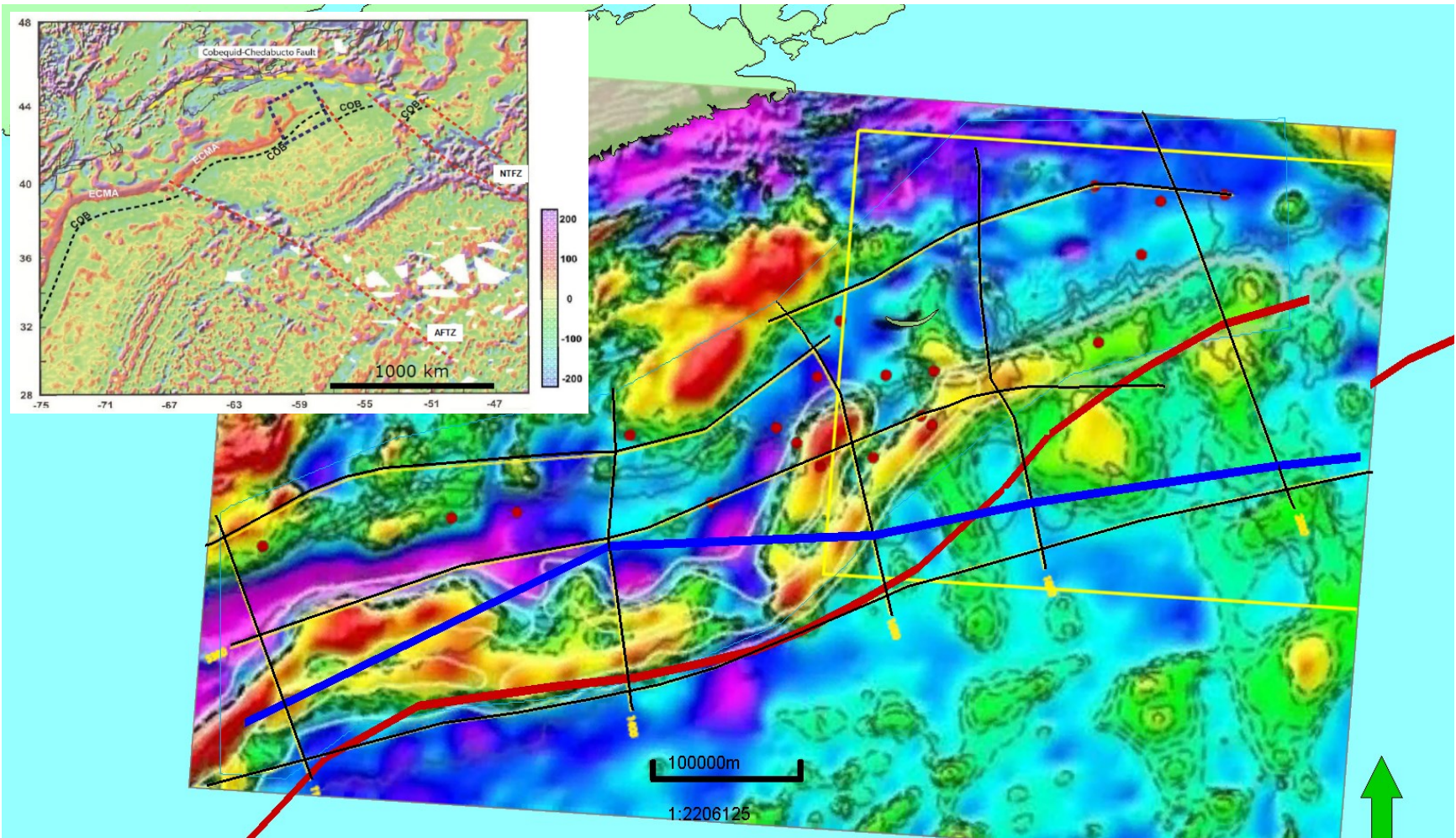


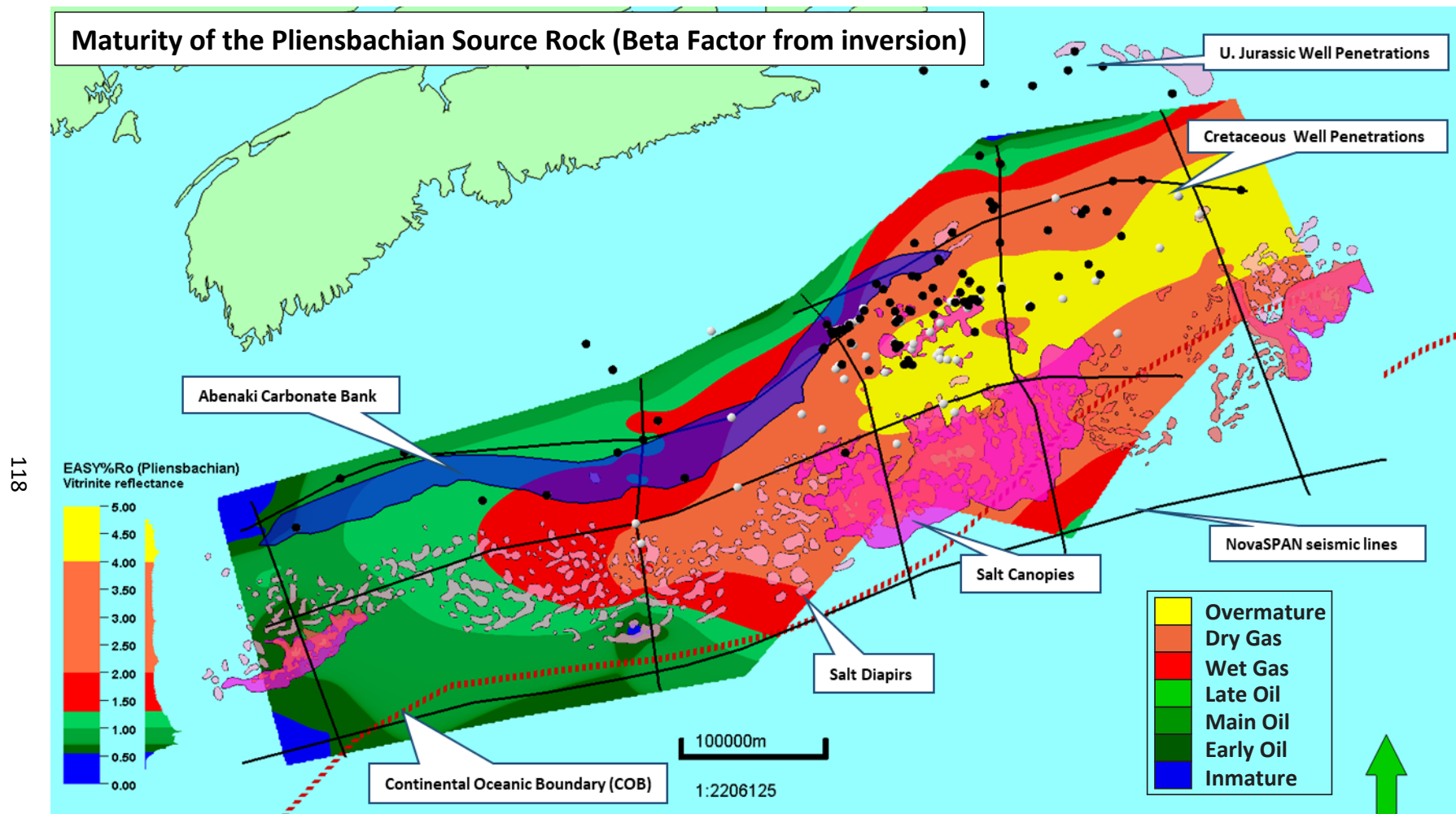
Figure 3.69: Magnetic grid of the NW Central Atlantic Ocean (Dehler, 2010; PFA 2011, PL. 2.1.2). Blue Line is Continent Ocean Boundary from the PFA (2011) 2D models (Chapter 7). Red line is Continent Ocean Boundary from inset map: magnetic anomaly map Dehler (2010) (PFA 2011, PL. 2.1.9).

Stretching factor (β), was calculated by a crustal inversion process within PetroMod in the initial models and is mapped in Figure 3.71. A new stretching factor (β) was calculated based on the depth of the Moho as interpreted from four refraction lines by Loudon, Lau, Wu et al. (2010) (Figure 3.72). This new stretching factor map (Figure 3.74) was calculated from the initial depth of the crustal lithosphere (32 km) assigned in PetroMod, the depth of the Moho as digitized from Loudon et al. (2010) and the depth of the sedimentary basement as defined in this project (Figure 3.73) from seismic interpretation. Based on refraction data Beta factor is up to three times larger at the Continent Ocean Boundary than based on inversion in PetroMod (Figure 3.75). The resulting maturity map (Figure 3.76) using the new stretching factor shows similar trends to the initial Beta factor map (Figure 3.70). The difference map shows that vitrinite reflectance via Beta from refraction data is typically 0.0-0.5 units lower than vitrinite reflectance via inversion (except on parts of the northeast NovaSPAN line) (Figure 3.77).

A thermal sensitivity test to the presence or absence of salt was also undertaken in this study. The initial suite of 2D models display a variety of salt structures observed across the Scotian Basin. In this sensitivity, salt was replaced by clastic sediment (shale) at time of deposition, and, of course, did not move in subsequent time steps. This modification enabled the 2D models to simulate a basin which has no salt deposits and to fully test two extremes of the effect of salt on thermal history in the Scotian Basin.

The salt has thermal effects on sedimentary rocks in the basin which have important implications for source rock maturity, as observed in the comparison of modelled temperature and vitrinite reflectance maps (Figure 3.78). These thermal effects are secondary to the overall trends but locally can make significant differences between types of hydrocarbons generated. The thermal implications are that salt depresses temperature at its bottom and increases temperature at its top. In the maps and models without salt it is observed that temperature is

more uniform. The absence of salt bodies (which increase heat conduction heat upwards) causes higher temperatures in the Lower Jurassic rocks in models with salt removed, and thus these models show greater maturity (Figure 3.78). The presence of salt depresses the maturity (%Ro) of Lower Jurassic rocks and temperatures are cooler compared to the map with salt absent. These differences in temperature and maturity (%Ro) are shown in Figure 3.80 and Figure 3.81.



118

Figure 3.70: Vitrinite reflectance map with COB boundary outboard of the ECMA. The dark blue irregular shape is the extent of the Abenaki carbonates. The irregular pink shapes are the salt diapirs and canopies. The dots are all the boreholes in the Scotian Basin; the black dots are boreholes that penetrated the Jurassic Intervals (Middle – Upper Jurassic), the white dots are boreholes that did not penetrate the Jurassic internals. The range of vitrinite reflectance: Blue (0 – 0.55) Immature, Dark Green (0.55-0.70) Early Oil, Green (0.70-1.00) Main Oil, Light Green (1.00-1.30) Late Oil, Red (1.30 – 2.00) Wet Gas, Orange (2.00 – 4.00) Dry Gas and Yellow (4.00 – 5.00) Overmature.

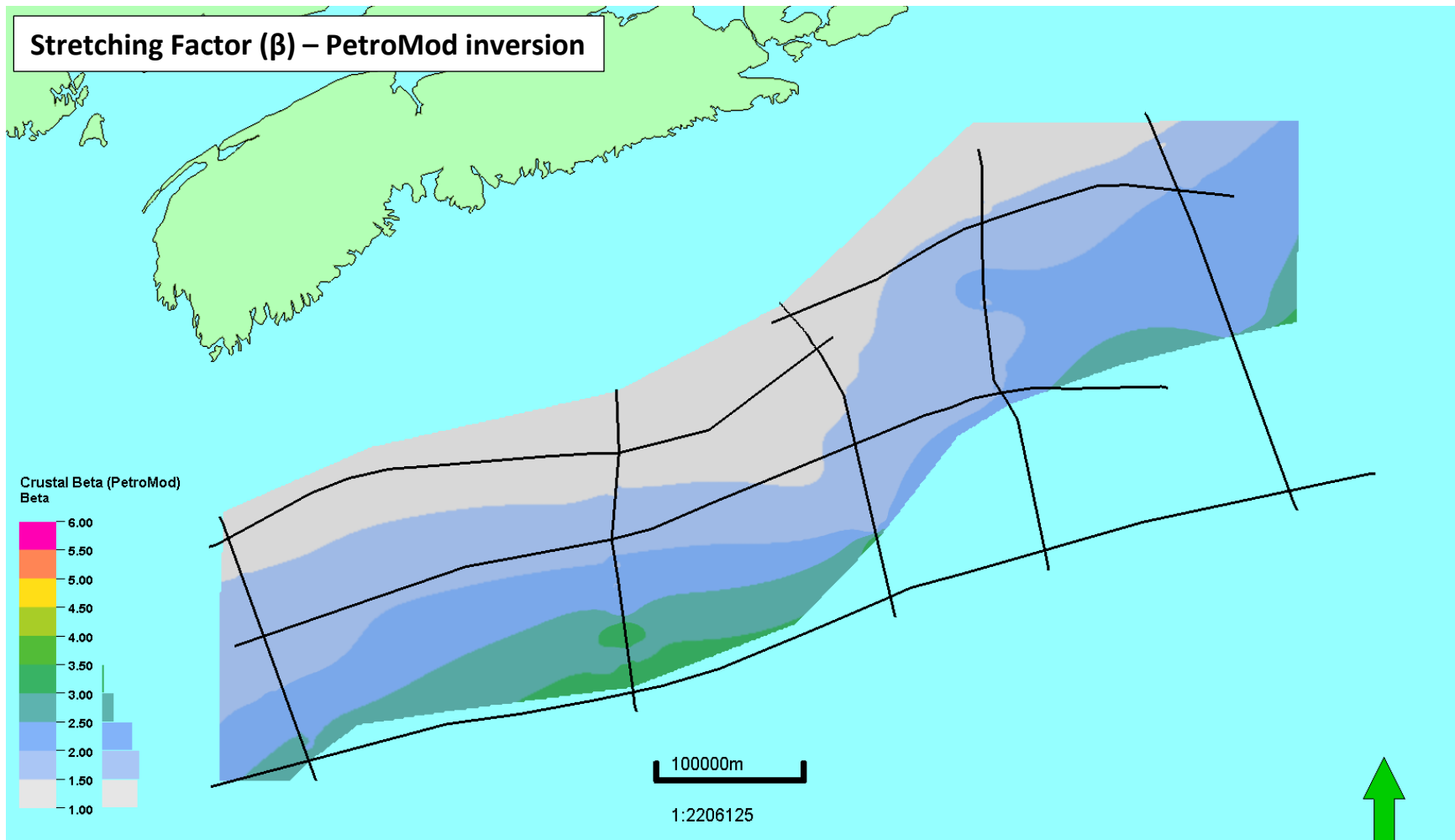


Figure 3.71: Stretching Beta factor (β) map calculated to best fit crustal inversion process by PetroMod.

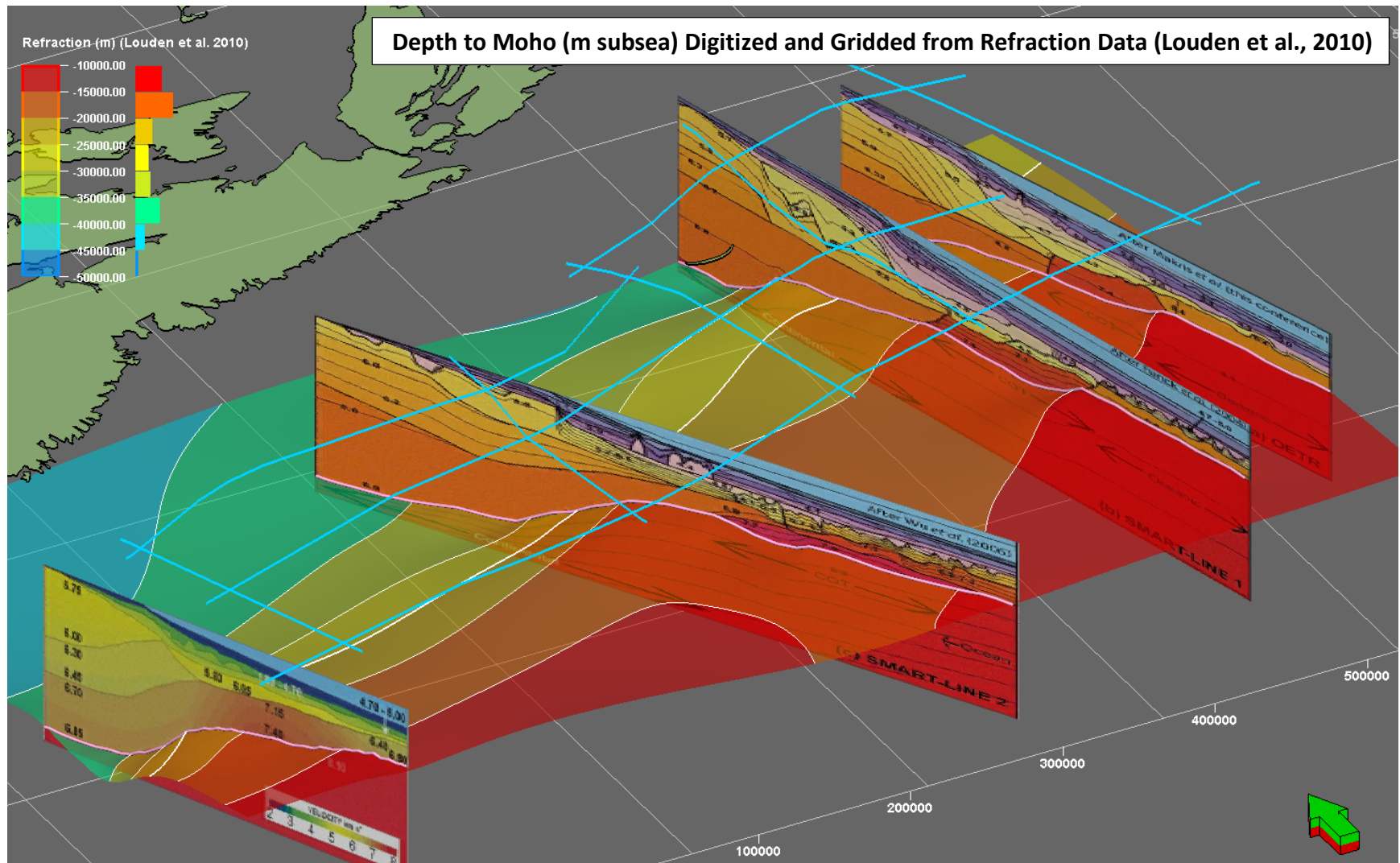


Figure 3.72: Digitized surface map of the Moho from georeferenced refraction lines from Louden et al. (2010) in Petrel. NovaSPAN lines are shown in blue lines.

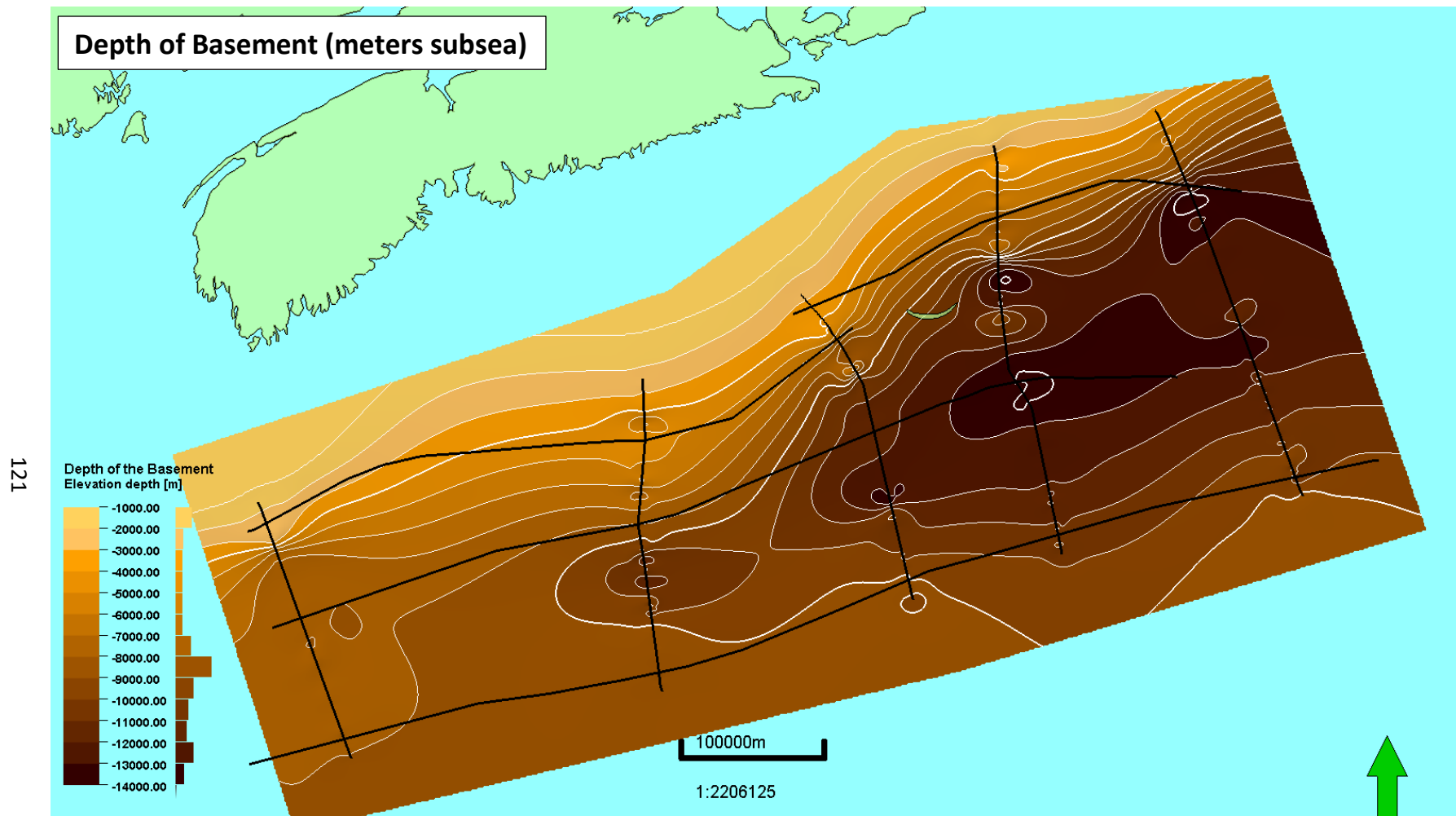


Figure 3.73: Depth of the basement from sea level based on the models from this study. NovaSPAN lines are in black lines.

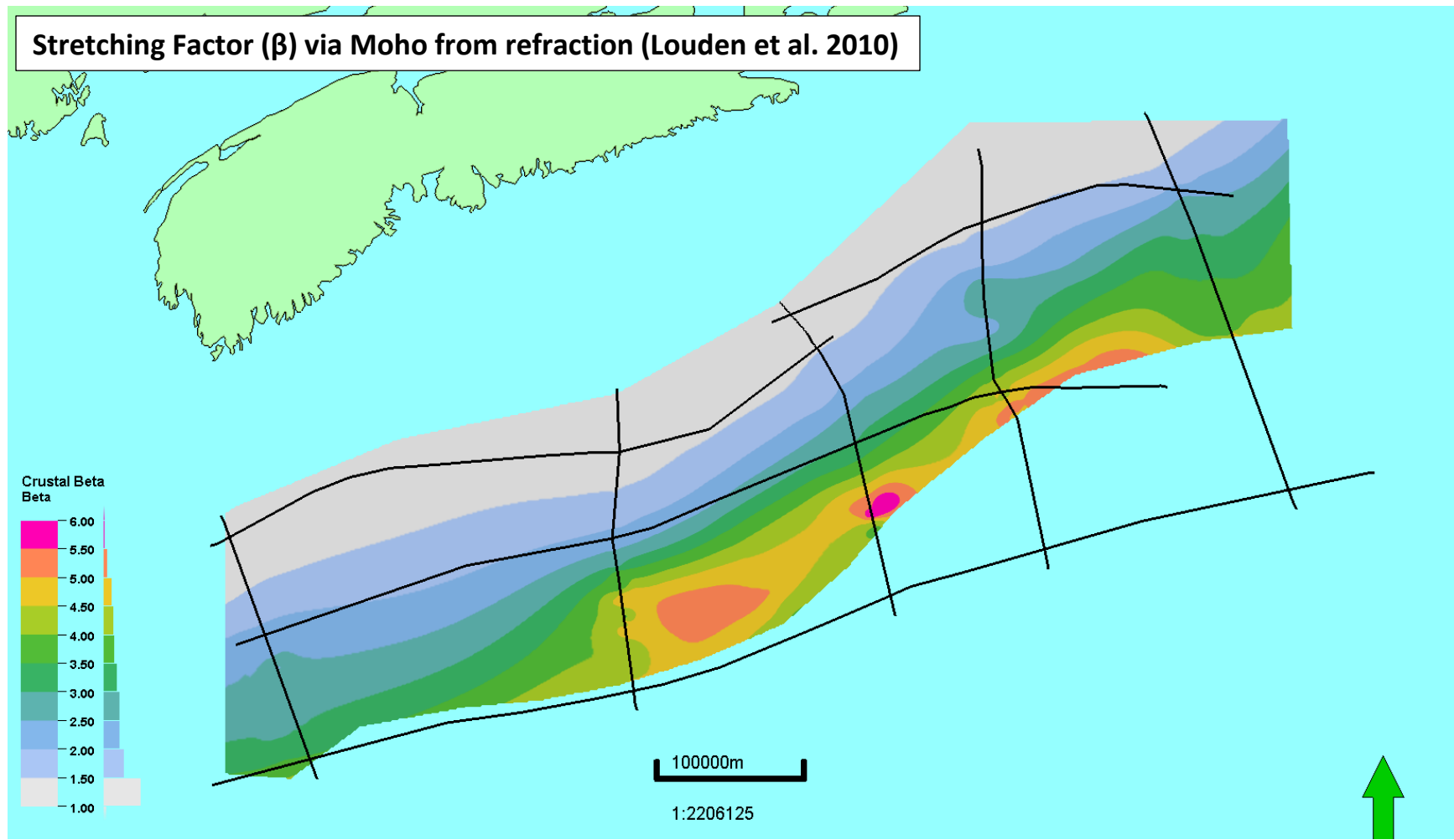


Figure 3.74: Stretching Beta factor (β) map calculated using the depth of the Moho from Louden et al. (2010) and depth to sedimentary basement as defined in this project, with an initial depth of crustal lithosphere of 32 Km.

Comparison: Beta factor using Moho depth from refraction data divided by Beta factor from inversion within PetroMod

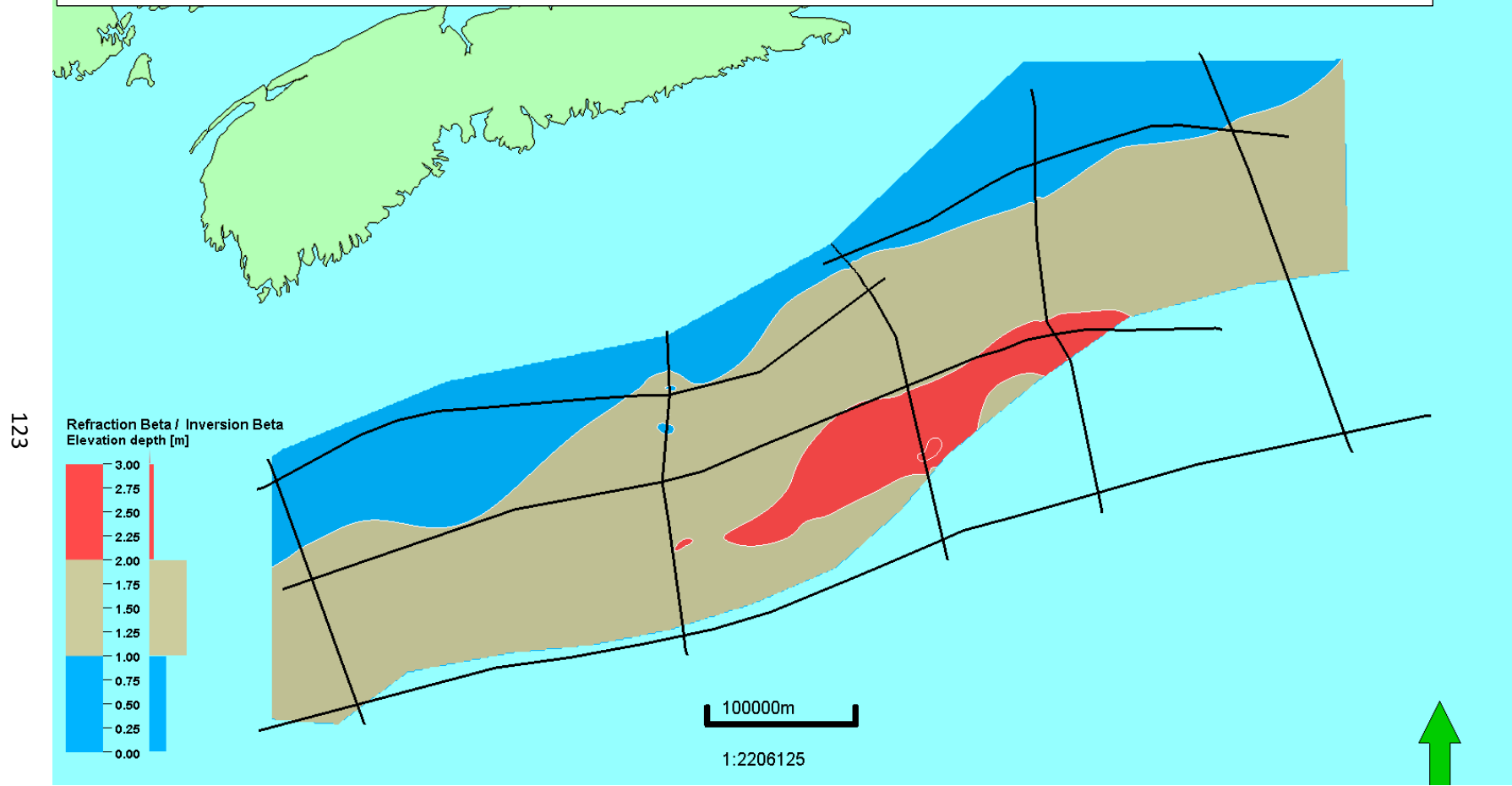


Figure 3.75: Beta factor using Moho depth from refraction data divided by Beta factor from inversion within PetroMod.

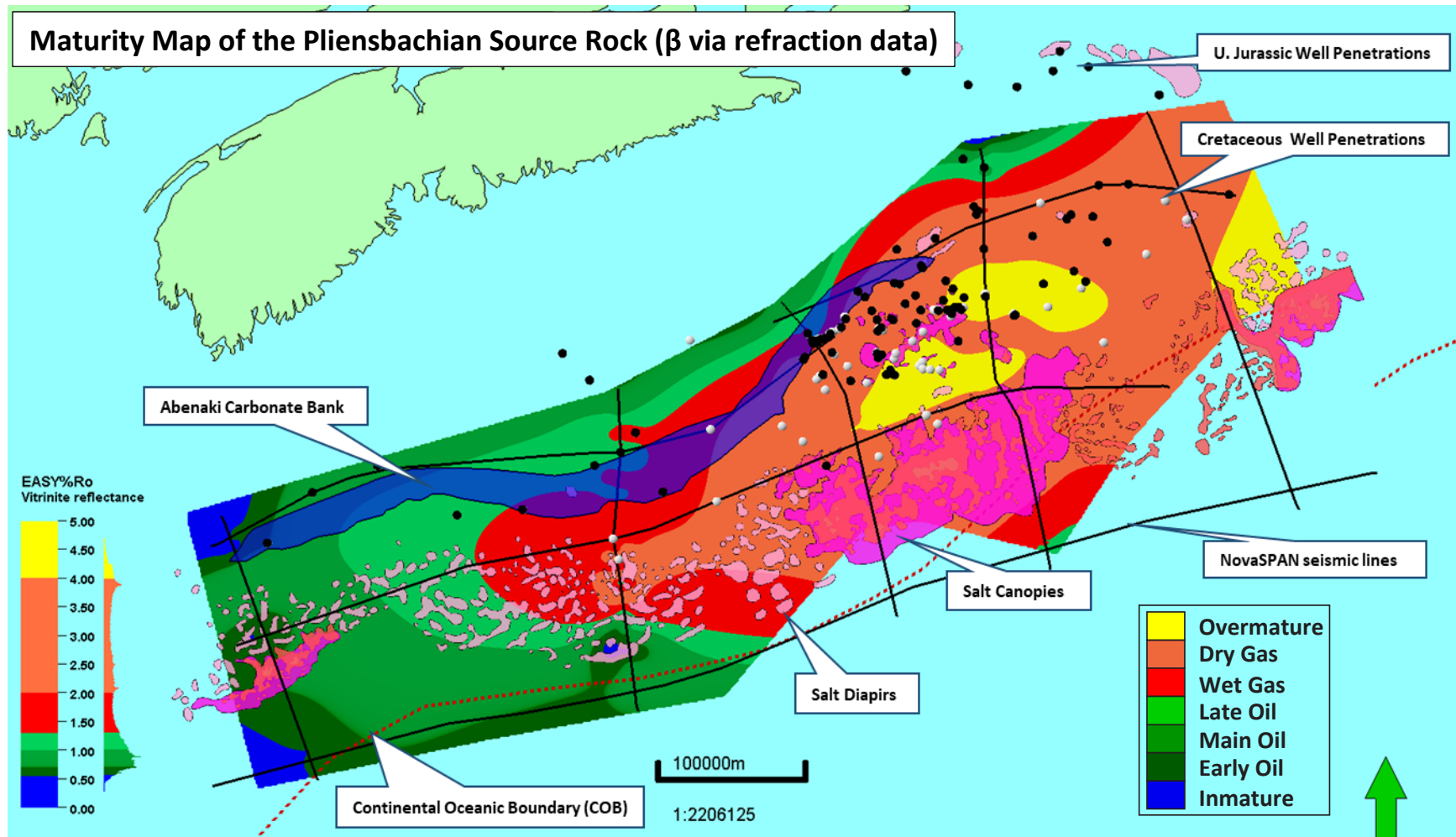


Figure 3.76: Vitrinite reflectance map based on models with calculated crustal stretching factors from refraction data (Figure 3.74). The dark blue irregular shape is the extent of the Abenaki carbonates. The irregular pink shapes are the salt diapirs and canopies. The dots are all the boreholes in the Scotian Basin; the black dots are boreholes that penetrated the Jurassic intervals (Middle – Upper Jurassic), the white dots are boreholes that did not penetrate the Jurassic intervals. The range of vitrinite reflectance: Blue (0 – 0.55) Immature, Dark Green (0.55-0.70) Early Oil, Green (0.70-1.00) Main Oil, Light Green (1.00-1.30) Late Oil, Red (1.30 – 2.00) Wet Gas, Orange (2.00 – 4.00) Dry Gas and Yellow (4.00 – 5.00) Overmature.

Vitrinite reflectance difference map: VR via beta from refraction data minus VR via beta from inversion in PetroMod

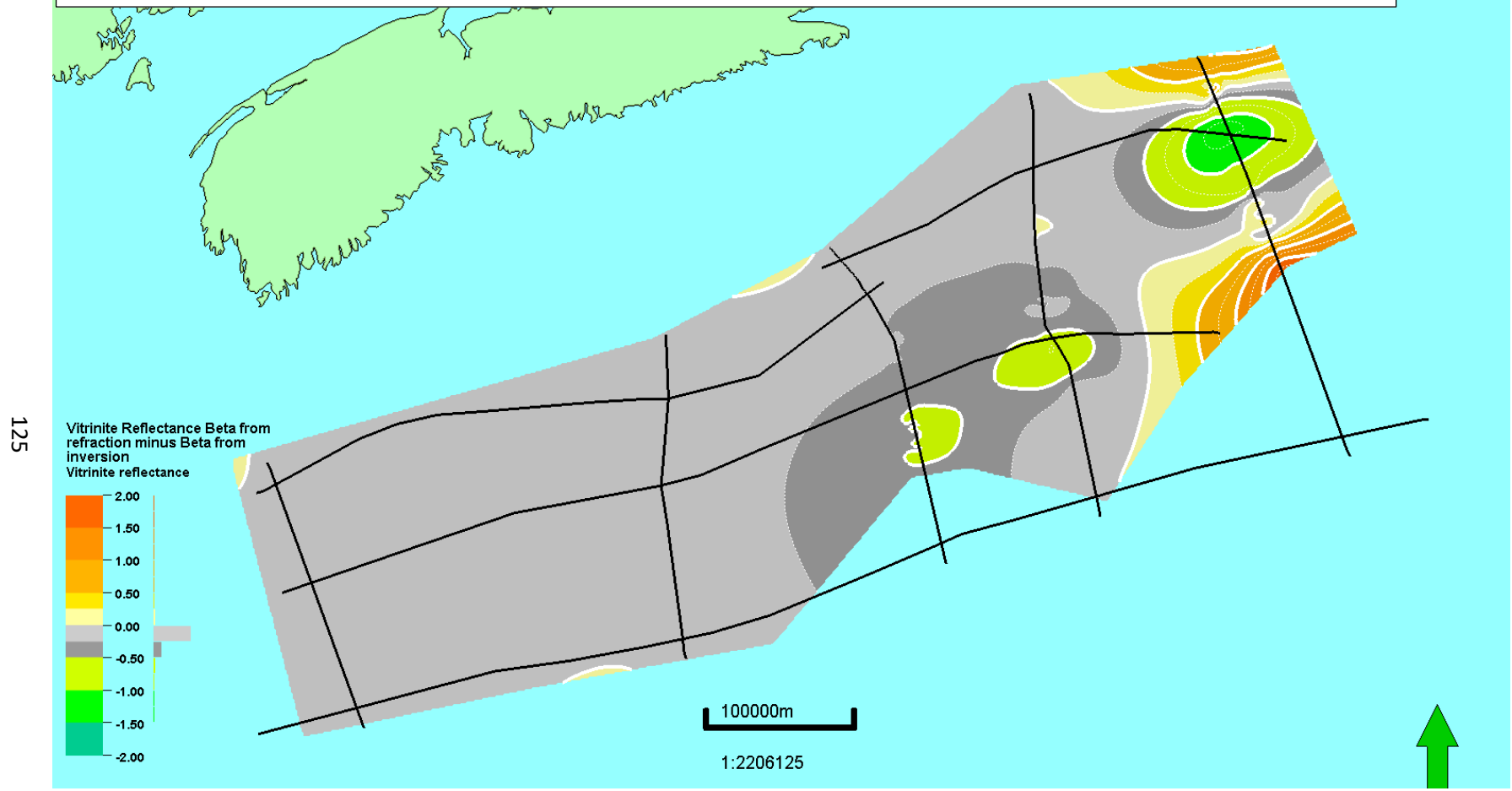


Figure 3.77: Vitrinite reflectance difference map: VR via beta from refraction data minus VR via beta from inversion in PetroMod. Grey areas indicate that maturity via refraction data is typically lower than via inversion (except on parts of the northeast NovaSPAN line).

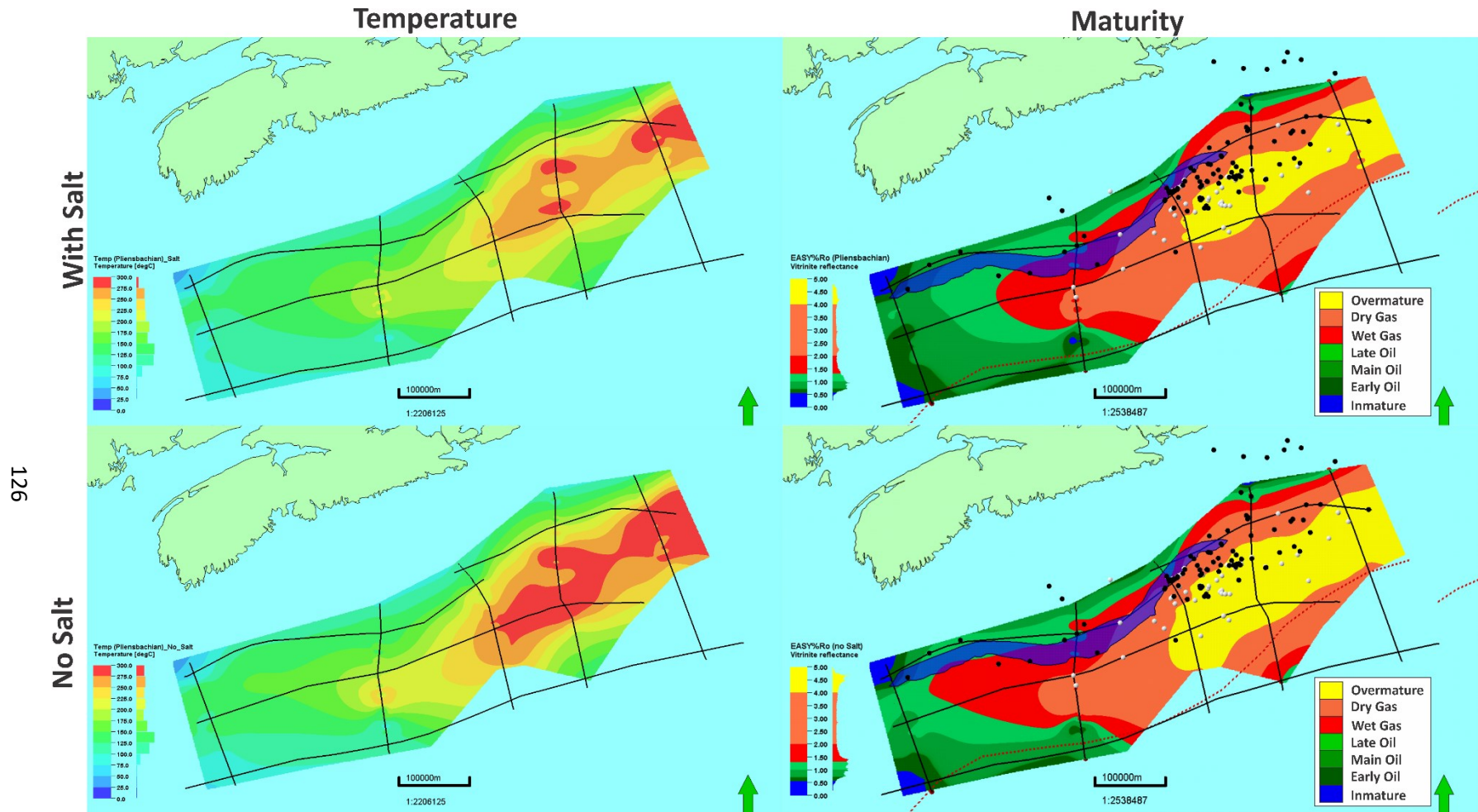
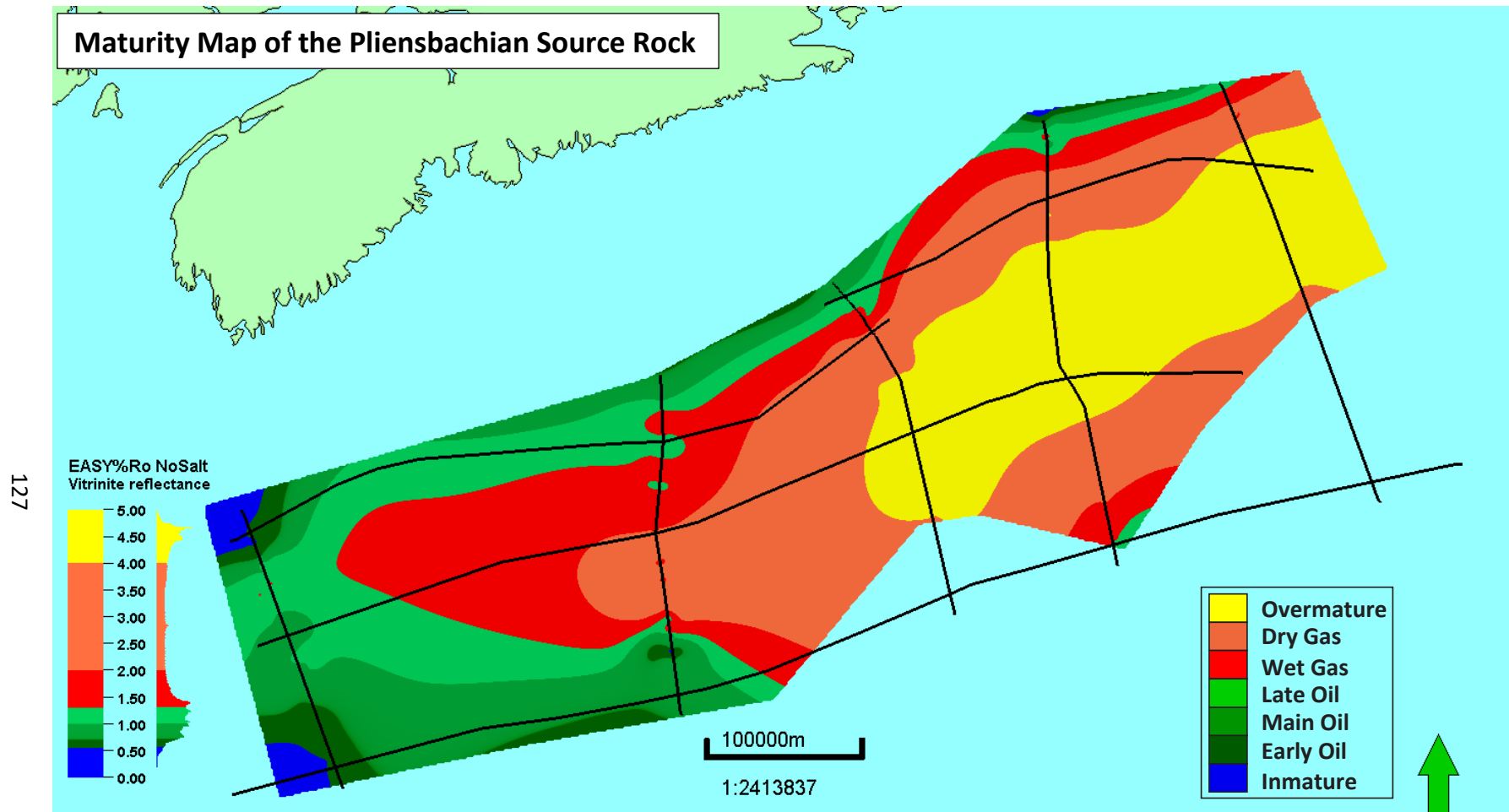
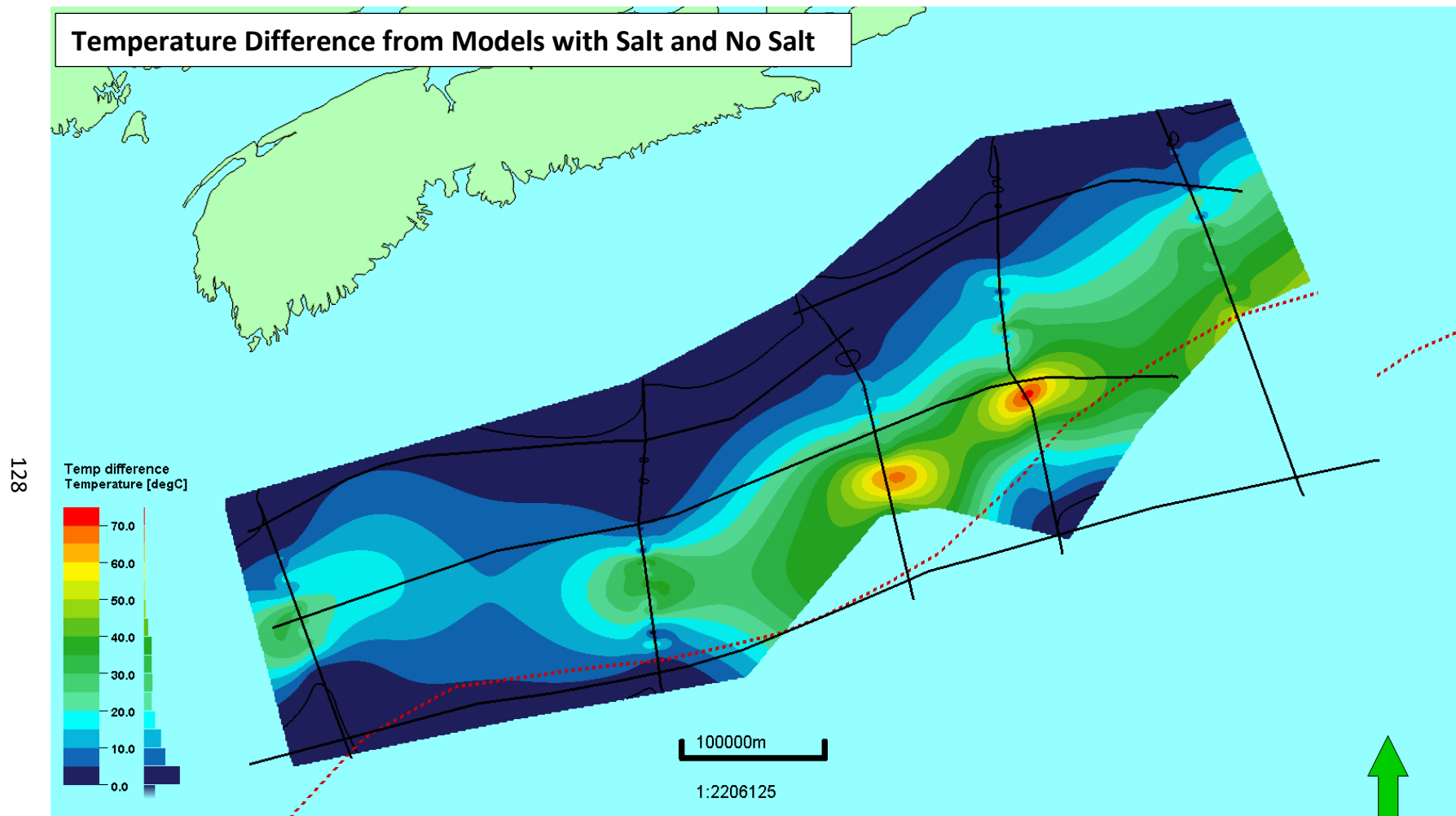


Figure 3.78: A comparison of temperature and vitrinite reflectance testing the models with salt and no salt. The temperature maps for both case scenarios, shows a similar trend towards the northeast; this is because the Lower Jurassic rocks are deeper towards the northeast regions. Although, comparing both temperature maps, it is observed that the salt structures will have significantly lower temperatures compared to the map without salt. The effects of these higher temperatures also affect the maturity of the Lower Jurassic rocks, observed in the vitrinite reflectance maps. The vitrinite reflectance maps show moderate increases in the models without salt; although the maturity trends are similar for both case scenarios. The maturity is in the oil window in the southwest towards the gas/overmature window in the northeast. Dashed red line indicates the continental oceanic boundary after Dehler (2010).



127

Figure 3.79: Thermal effect on the vitrinite reflectance map without salt deposition in the Basin. The dark blue irregular shape is the extent of the Abenaki carbonates. The irregular pink shapes are the salt diapirs and canopies. The dots are all the boreholes in the Scotian Basin; the black dots are boreholes that penetrated the Jurassic Intervals (Middle – Upper Jurassic), the white dots are boreholes that did not penetrate the Jurassic internals. The range of vitrinite reflectance: Blue (0 – 0.55) Immature, Dark Green (0.55-0.70) Early Oil, Green (0.70-1.00) Main Oil, Light Green (1.00-1.30) Late Oil, Red (1.30 – 2.00) Wet Gas, Orange (2.00 – 4.00) Dry Gas and Yellow (4.00 – 5.00) Overmature.



128

Figure 3.80: This map show the change in temperature if the salt was not present in the model. The temperature map shows a significant change in regions were the salt is present, but it has a higher change in regions where the salt is more abundant. This increase in temperature also affects the maturity (vitrinite reflectance) of the Lower Jurassic rocks; the difference is shown in the vitrinite reflectance map.

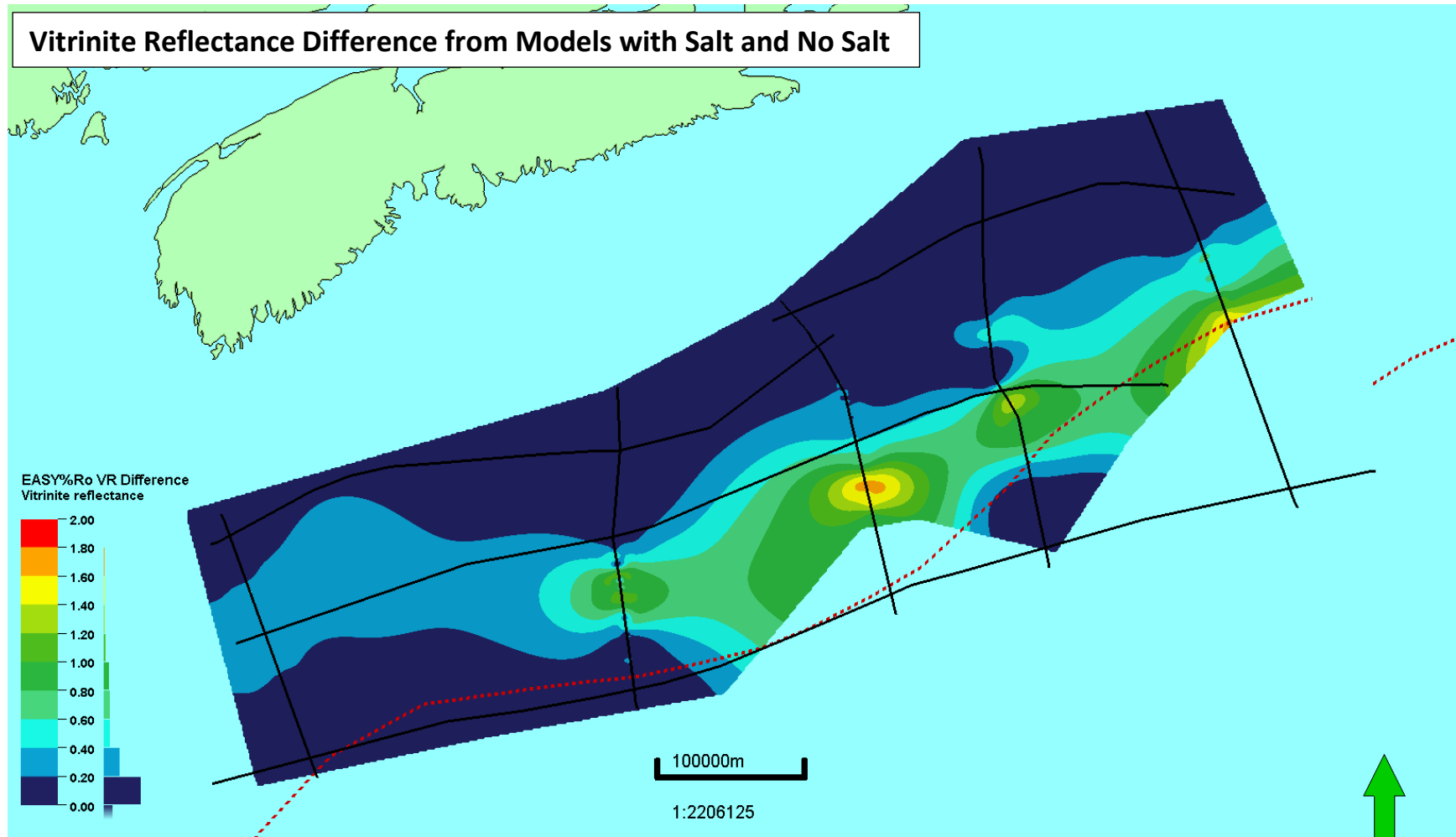


Figure 3.81: This vitrinite reflectance difference map shows the amount of %Ro that is affected by the influence of salt in the model. The map shows a significant change in regions where the salt is present, but it has a higher change in regions where the salt is more abundant.

Chapter 4: Discussion

4.1 Source Rock Parameters

The Play Fairway Analysis studies (PFA) (OERA, 2011, 2015, 2016) suggested that the Lower Jurassic successions in the southwest platform, margin, and slope of the Scotian Basin are within the thermal maturation window for hydrocarbon generation. The parameters used by the Play Fairway Analysis for the Early Jurassic Source Complex (Sinemurian – Pliensbachian – Toarcian) are defined as a kerogen Type II with a hydrogen index of 600 mgHC/gTOC and total organic carbon of either 3% or 5%. Throughout the PFA geochemistry chapter (Chapter 4) the authors state that they use a total organic carbon of 5% but in the modelling chapter (Chapter 7) their models use a total organic carbon of 3%. This leaves ambiguity in the values which were used. Also, the source rock analysis of the PFA study was based on limited data extrapolated from offshore boreholes (Nova Scotia and Morocco) and few outcrops (Morocco and Portugal) thought to be analogous to the offshore Scotian Margin. The Deep Sea Drilling Project Leg 79, site 547B (offshore Morocco) show several immature Lower Jurassic organic-rich sedimentary facies of kerogen Type III (Rullkotter, Mukhopadhyay, Schaefer et al., 1984; Wach et al., 2018). In the Play Fairway Analysis studies, the Early Jurassic Source Complex was “inferred by the analogy of source rocks recognized on the conjugate margins of Newfoundland and Nova Scotia, in Portugal and Morocco” (OERA, 2011). This thesis applies recent outcrop sampling fieldwork conducted on Aït Moussa, Morocco, which is conjugate, and it is analogous to the Scotian Basin.

Source rock parameters were derived from outcrop data samples collected from Aït Moussa, the Middle Atlas in Morocco, the outcrop is about 20 m long and is shown in panoramic photograph displays where the samples were collected (Figure 4.1). There were 11 samples collected and sent for Rock-Eval Pyrolysis and TOC. Rock-Eval pyrolysis and TOC analyses were

performed by GeoMark Research, Ltd (USA). TOC was measured using a LECO C230 instrument, calibrated with standards having known carbon contents. Total organic carbon and Rock-Eval pyrolysis results are shown in Figure 4.2.



Figure 4.1: This panoramic photograph of the outcrop of the Ait Moussa section. The outcrop is about 20 meters long. The arrows show the samples collected from the outcrop that were sent to be analyzed with Rock-Eval Pyrolysis (Figure 4.2) (Silva et al., 2017b).

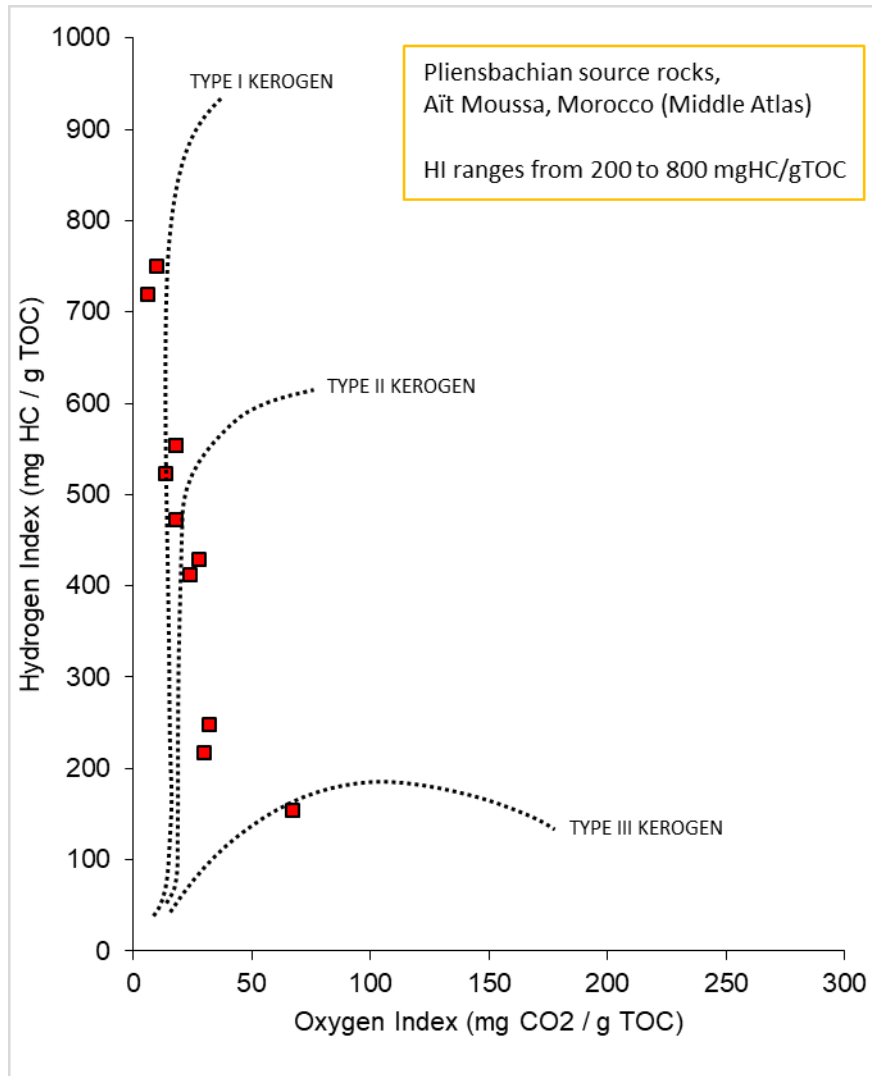


Figure 4.2: Rock-Eval Pyrolysis graph from the data collected at Ait Moussa, Morocco. This graph shows data points (red) sparse, ranging from hydrogen index (HI) of 200-800 mgHC/gTOC, Type I-Type III kerogen (Silva et al., 2017b).

Source Rock Interval

Deposition of these organic-rich intervals was associated with a $\delta^{13}\text{C}$ positive excursion, expressed in several locations around the world (see also Jenkyns, Jones, Grocke et al., 2002; Silva et al., 2011; Silva et al., 2017a). This is most likely a result due to changes of significant geological carbon storage, regional paleoenvironmental constraints governing sedimentation, and the carbon cycle. Organic matter productivity and preservation were enhanced during transgressive episodes (Hallam, 1981), affecting the carbon cycle (e.g. Jenkyns, 1988; Suan, Mattioli, Pittet et al., 2010; Silva et al., 2011; Silva, 2013; Caruthers, Smith and Grocke, 2014).

For this study, we test the Lower Jurassic source rocks with ranges of total organic carbon and hydrogen index. These parameters (Table 1.1) are based on 2016 field work by Silva and Wach, part of the Source Rock Consortia project. At Ait Moussa, Middle Atlas, Morocco. Although for the models are built and simulated with five source rock intervals (Aptian, Valanginian, Tithonian, Callovian and Pliensbachian), the focus of this study is the Lower Jurassic source rock, the Pliensbachian source rock in our models. The parameters of the other source rocks are based on the PFA study.

4.2 The Impact of Salt Tectonics

The mobilization of salt due to sediment loading created structures in the Scotian Basin. There is a distinct pattern of salt diapirs in the southern part of the Scotian Basin (Shimeld, 2004; Deptuck and Kendell, 2017) transitioning to a combination of salt diapirs and canopies in the northern part of the Scotian Basin. Similar structures are also seen in other basins such as the Gulf of Mexico, Central Santos Basin (Brazil), Tarfaya Basin (Morocco), etc. (Gemmer, Beaumont and Ings, 2005; Albertz and Ings, 2012; Deptuck and Kendell, 2012; Goteti et al., 2012; Gradmann, 2012; Goteti et al., 2013; Tari and Jabour, 2013; Peel, 2014; Deptuck and Kendell, 2017). Source rocks may be affected by the salt mobilization if the source rocks are deposited over the salt, causing the rework of the source rock. Incorporating the salt volume and dynamics into the model is essential since it has thermal implications, affecting the thermal maturity of the organic-rich interval rocks (Figure 4.3) (Zentilli and Williamson, 2004; Albertz and Ings, 2012; Goteti et al., 2013). The salt is an active heat conductor, this means it conducts the heat more efficiently than other sedimentary material (sand, shale, limestones), therefore controlling the basin heat flow (Figure 4.4). The heat flow moves quickly upwards, and this effect of heat transition affects the temperature on the sediments surrounding adjacent to salt. The

temperature increases at the cusp of the salt structures and decreases at the base of the salt (Figure 4.4).

The salt structures play a significant role in the thermal history of the Scotian Basin (Figure 4.5 and supplementary files). They can also be essential for the migration and accumulation of hydrocarbons. Salt structures can also form traps if the conditions and timing are right. Salt is impermeable at shallow depth, but its physical properties at greater depths (greater than 3.5 Km) becomes permeable (Lewis and Holness, 1996). The presence of liquid and gaseous hydrocarbons in fluid inclusions in autochthonous Argo salt is a good indicator but not proof of the existence of an effective Lower Jurassic source rock (Glooscap C-63 and Weymouth A-45) (Kettanah, Zentilli and Wielens, 2004; Kettanah and Greenough, 2013). The mechanism for emplacements of hydrocarbon fluid inclusions within the salt is beyond the scope of the study. The permeability or impermeability of salt is an ongoing area of research. End members include the effectiveness of salt in sealing hydrocarbon traps (e.g. many gas fields in the Rotliegendes sandstones of the Southern North Sea) which can be contrasted with research where it seems that salt becomes permeable when in motion, or contains anomalous textural or mineralogical features at least from experimental models (Lewis and Holness, 1996; Warren, 2017).

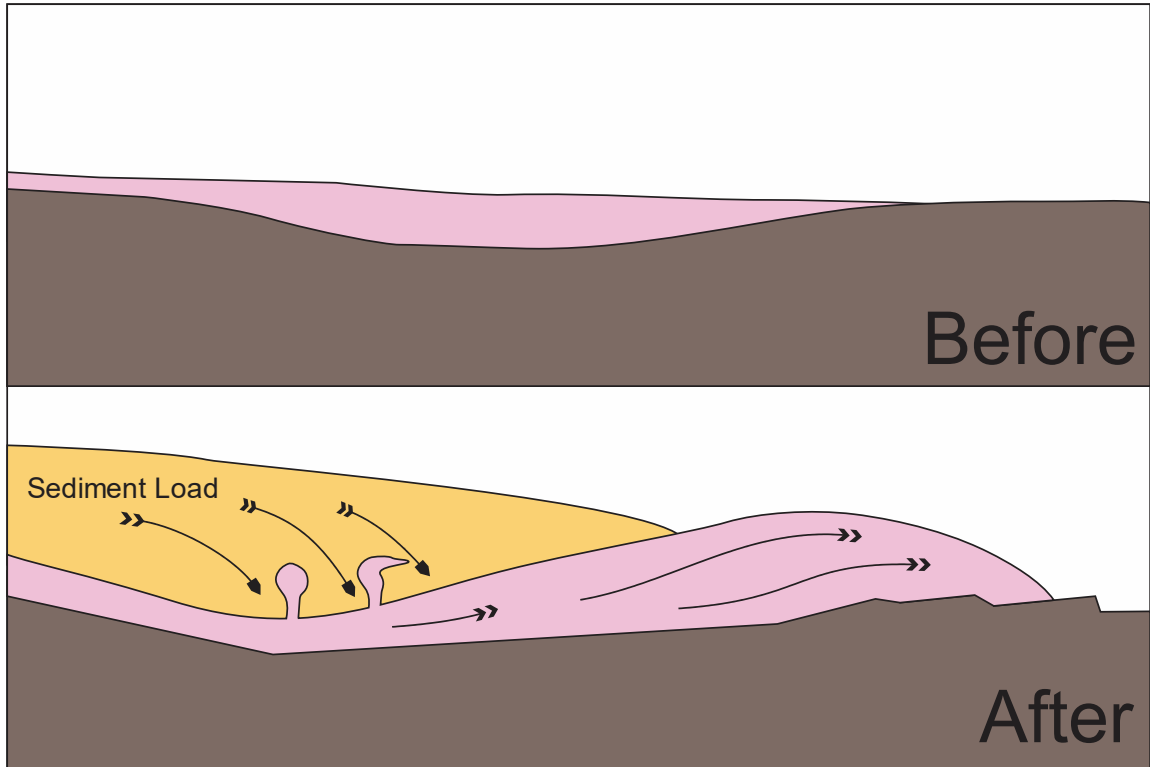


Figure 4.3: As salt is deposited it does not move until some force/weight like sediment loading is applied. Salt moves in a ductile form, like toothpaste or dough. This sediment load exerts enough pressure that triggers the salt mobilization, creating salt structures such as canopies, sheets and salt diapirs.

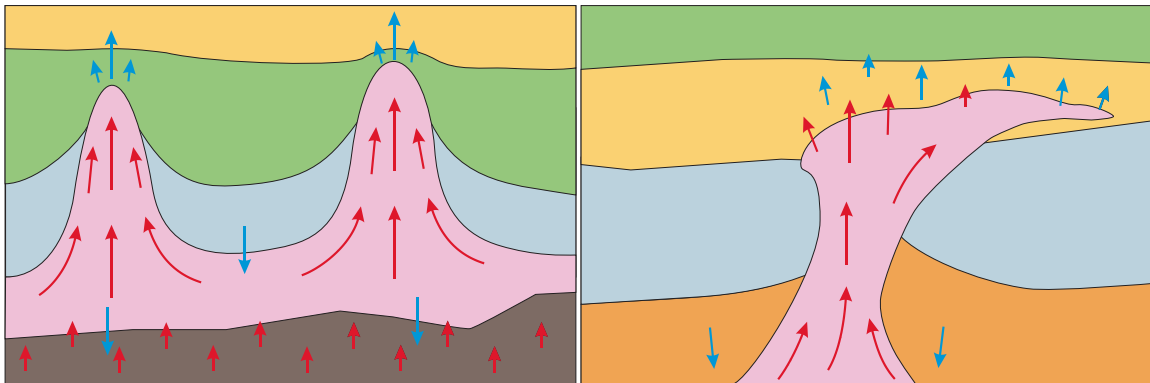


Figure 4.4: On left salt diapirs and the right a salt canopy structure, in pink. The red arrows are Heat Flow, which is the conductivity of the heat flow through the material, through the salt. The blue arrows are the temperature effects on the surrounding sediments adjacent to the salt structure.

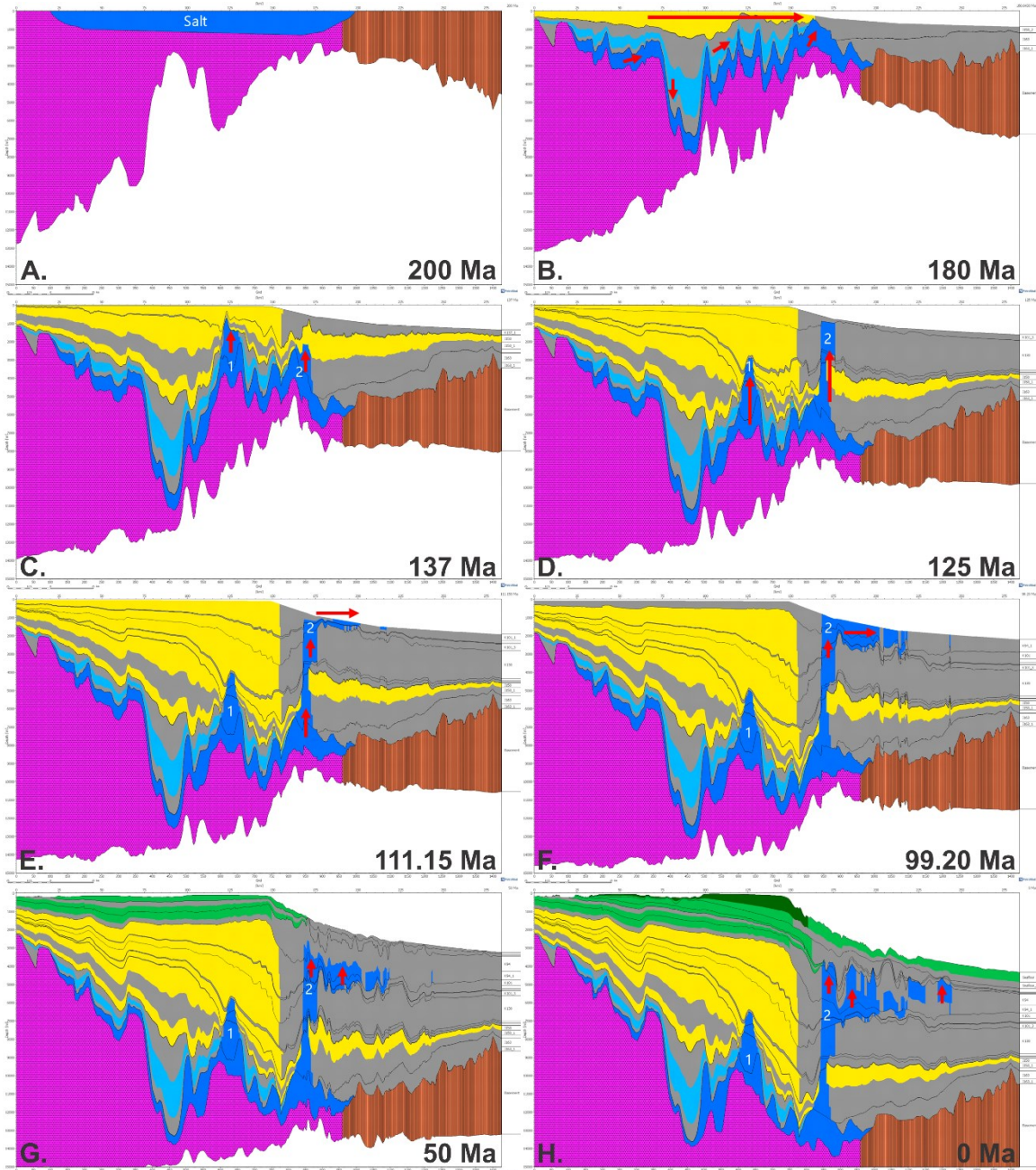


Figure 4.5: Description of salt movement through time (salt in blue layer). A. Salt Deposit during Pre-Rift . B. Salt deforming due to sediment loading, thinning in sections, moving, and thickening outboard. C. Diapirs (1) and (2) starts to form. D. Diapirs shape are more predominant, diapir (1) cease movement. E) Salt diapir (2) starts to shape into canopy, lateral movement down slope. F) More predominant canopy shape (2), possible adjacent encroachment (not seen in cross section). G) Salt canopy (2) buries due to sediment input, minor reshape due to sediment load. H) Salt canopy forms mini diapirs (2) from sediment load.

4.3 Challenges

Data Limitation

Modelling this set of NovaSPAN lines had some unique challenges, each model was built with available data, but also taking into consideration the limitations on data validation, such as the number of offshore boreholes near the seismic line and the depth penetration of boreholes (Figure 4.6).

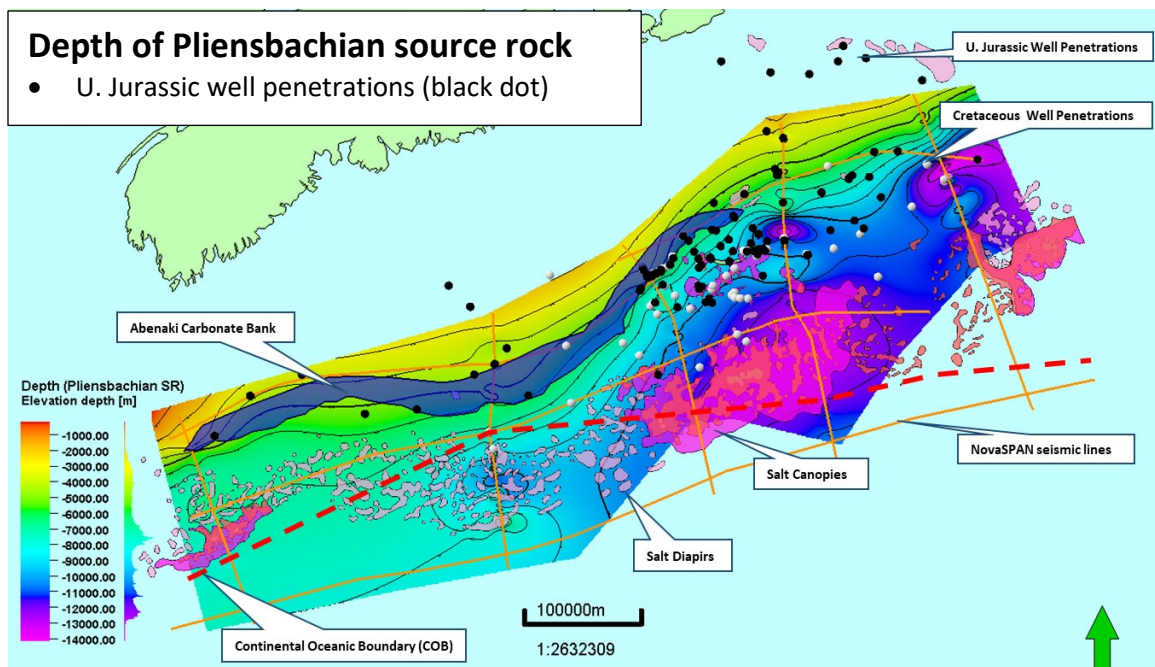


Figure 4.6: Depth smooth gridded map at the top of the Pliensbachian source rock based on NovaSPAN 1100, 1400, 1600, 1800 and 2000 models. The dark blue irregular shape is the extent of the Abenaki carbonates. The irregular pink shapes are the salt diapirs and canopies. The dots are all the boreholes in the Scotian Basin; the black dots are boreholes that penetrated the Jurassic Internals (Middle – Upper Jurassic), the white dots are boreholes that did not penetrate the Jurassic internals.

In the NovaSPAN 1100 model data was limited to only one offshore borehole, the Bonnet P-23 was the closest at 22.13 km. The other models had at least four offshore boreholes for calibration, but most of them were mainly on the shelf. Data quality from the boreholes such as vitrinite reflectance could be misleading due to the uncertainties of measuring the data. Some common errors are the incorrect identification of vitrinite reflectance, oxidation, staining, caving, reworking and mud additives. Temperatures data from the boreholes comes from log

runs and typically requires +10-+30% adjustment to actual formation temperatures, due to mud cycling when drilling cooling the formation.

Heat Flow

The Scotian Basin is located a volcanic margin, thus given a higher heat flow input than a non-volcanic margin. Towards the northeast of the Scotian Basin is the Newfoundland-Azores fault zone, which is a transition to a non-volcanic margin to the north. This northern region would have a cooler heat flow. The area modelled here is exclusively within the volcanic margin, but variations in the magnetic signature of basement (Dehler,2010) might indicate some transition in the northeast of the study area. Addressing this is a challenge for future work.

The modelling presented here does not incorporate fluid movement (advection) for two reasons: 1) computational intensity and time considerations; 2) in 2D modelling advection is often not incorporated, as it is handled much better by 3D modelling. Fluid movement should be considered in future work.

Modelling of the Salt

In this study, both methods of salt reconstruction from PetroMod were tested. The NovaSPAN 1400 line was modelled with the salt reconstruction workflow. This workflow produced a better salt reconstruction, although many challenges are present when modelling salt canopies structures. This method has a limitation due to the PetroMod software, the software does not permit irregular shapes such as salt canopies to be adequately modelled. To address this issue of modelling the salt canopies that are part of the salt structures on the Scotian Basin, the “salt piercing” tool was used in the modelling. This tool permitted the modelling of such structures, producing remarkable results for the salt diapir and salt canopies modelling. The NovaSPAN 1100, 1800 and 2000 uses the “salt piercing” tool.

4.4 Distribution of the Lower Jurassic Source Rock Maturity of the Scotian Basin

Modelling results provide an insight to maturity and transformation of potential Lower Jurassic source intervals within the Scotian Basin. Compiling the different model outputs (Tables 3.1 - 3.4) produces maturity map of potential Lower Jurassic source rock in the Scotian Basin. There is a distinct trend of maturation from the oil window in the south transitioning into a gas maturity window in the north. This trend also coincides with the type of salt tectonics observed in the Scotian Basin, demonstrating the impact of salt on the thermal maturity. Salt diapirs are predominant in the southern part of the basin, and transition to salt tongues and canopies in the north. The salt structures styles coincide with the thick sediments observed in the north. The salt canopies and tongues are common on the north where the sediment packages are thicker. The southern region where the sediments packages are thinner, salt diapir is more common (Figure 2.1).

Table 4.1: Summary the Lower Jurassic rocks maturity for the models 1100, 1400, 1600, 1800, and 2000. The maturity of each model is broken down into two different regions within the model the slope and abyssal regions. The critical moment is the age when the source rock starts generating hydrocarbons (20% Transformation Ratio). The model 1600 is not part of this study but is part of the Source Rock and Geochemistry of the Central Atlantic Margins, conducted at the Basin Reservoir Lab, Dalhousie University, which this thesis is part of (Wong, Hu, Wach in prep).

Model	Area	Maturity	Critical Moment (Ma)	Kerogen Type
1100	Slope	Mature	80-4	Type I – Type III
	Abyssal	Mature	83	Type II
1400	Slope	Mature	135-28	Type I – Type III
	Abyssal	Mature	128-39	Type I – Type III
1600	Slope	Mature	170-154	Type I – Type III
	Abyssal	Mature	175-145	Type I – Type III
1800	Slope	Overmature	157-152	Type I – Type III
	Abyssal	Mature	173-129	Type I – Type III
2000	Slope	Mature	153-138	Type I – Type III

Studies by the Play Fairway Analysis (PFA) utilized Dionisos and Temis Suit modelling software (BeicipFranlab) to model the Scotian Basin (OERA, 2011, 2015, 2016). The PFA is a 3D regional study. These studies describe the Pliensbachian source rock as kerogen Type II with 600 mgHC/gTOC with initial TOC of 5%. The PFA study modelled the sedimentation of the basin using Dionisos, to simulate sediment deposition in the basin. The output of this model was used as input for Temis 2D and 3D to test the petroleum systems of the Scotian Basin. The PFA suggests that the Pliensbachian source rock is generating oil in the southern part of the Scotian Basin and generating gas in the northern part of the Scotian Basin which is complementary to findings in this study. It was also recognized that similar patterns exist in transformation ratio of the Lower Jurassic source rock. These patterns from both studies show greater transformation ratio in the northeast of the Scotian Basin with less transformation ratio in the southwest (Figure 4.7). Finally, both studies observe similar trends in critical moment showing the critical moment occurring during the Jurassic in the northeast of the basin and during the Cretaceous in the southwest. This study also demonstrates that source rocks of different kerogen types would have different ranges of transformations ratios and critical moments for the Pliensbachian source rock within the Scotian Basin (Figure 3.63 - Figure 3.68). The PFA models does not incorporate variations in kerogen type and therefore they do not provide variations in transformations ratio and critical moment along the Scotian Basin (Table 4.2).

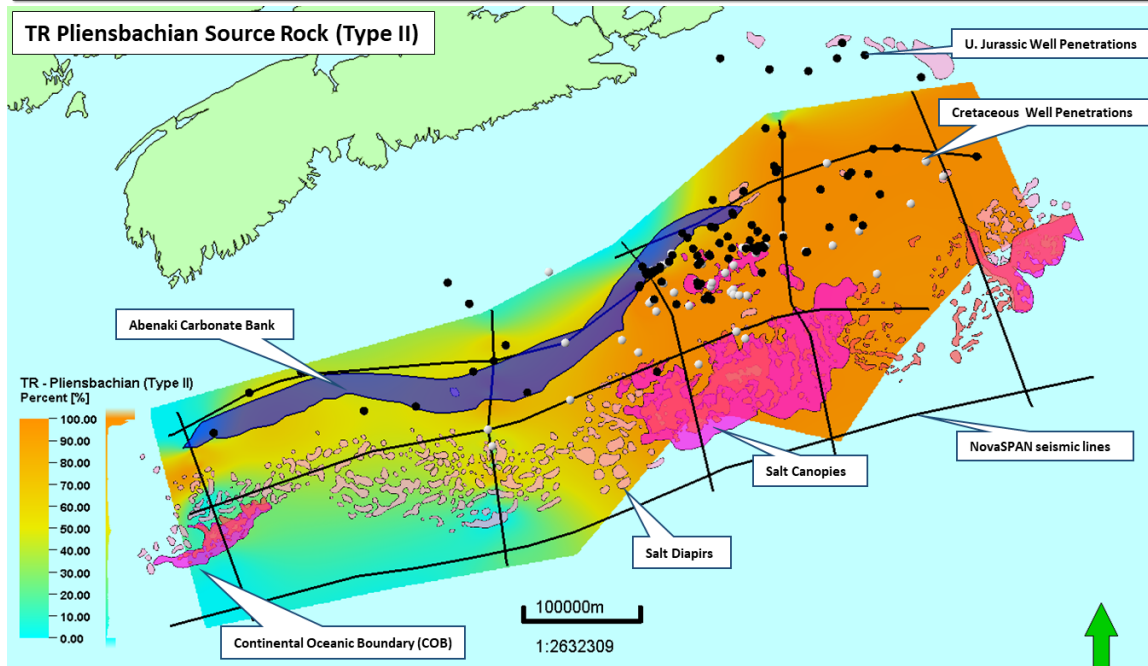
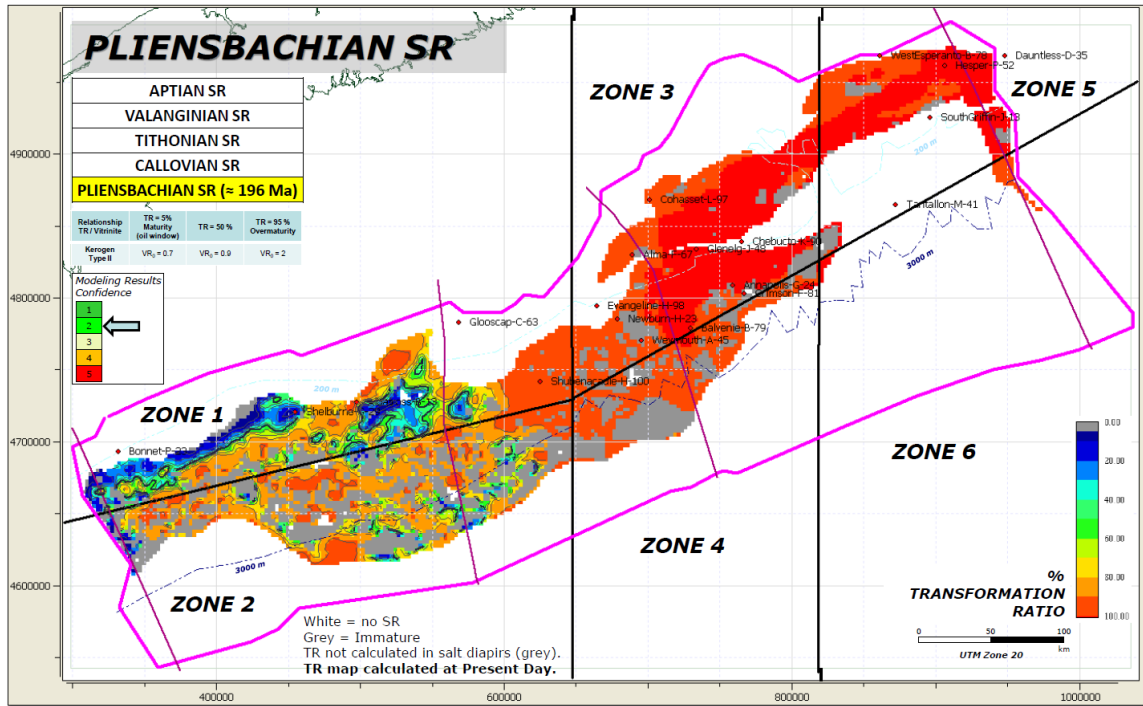


Figure 4.7: Comparison between the transformation ratio results from the PFA (OERA, 2011)(top) and this study (bottom).

Table 4.2: Modelling outcomes comparison between this study and the PFA (2011)

	PFA (2011)	This Study	Outcome
Maturity	Modelled	Modelled	Both studies demonstrates the Lower Jurassic source rocks have the same trending of oil window in the southwest towards gas/overmature towards the northeast.
Critical Moment	Modelled	Modelled	Both studies demonstrates the critical moment occurring during the Jurassic in the northeast of the basin and during the Cretaceous in the southwest .
Continental Oceanic Boundary	Ambiguity in the position of the COB	PFA (2011) and alternative position of the Continental Oceanic Boundary, different stretching factors, and the thermal effects from the salt	This study demonstrates that the COB using Dehler (2010) demonstrates warmer model and resulting in an increase of maturity level in the models (Figure 3.70).
Lower Jurassic Source Rock Parameters	Kerogen Type II	Kerogen Type I, II and III	This study demonstrates different maturity, critical moment and transformation ratio maps, depending on the source rock parameters used in this study.
Sensitivity Analyses	None	Completed	Multiple sensitivity maturity maps demonstrate the new COB location, stretching factors and thermal effects of the salt

4.5 Lower Jurassic Source Rock Maturity on the Conjugate Margin

On the conjugate margin of Morocco, in the Tarfaya Basin, a similar study by Sachse et al. (2012) suggests that the Jurassic sediments are the most important source rocks. This study uses the same software PetroMod in their 2D petroleum systems model covering both the on and offshore of the Tarfaya Basin. This study describes the Toarcian source rock with an average value of 450 mgHC/gTOC and a TOC of 4% (Sachse, Wenke, Littke et al., 2016). In their model,

the Toarcian source rock shows hydrocarbon generation occurred during the Early Cretaceous until Neogene in the offshore regions. The study suggests that the Jurassic sediments in the Tarfaya Basin are the most important source rock if they are present in the basin. Note this source rock was not adequately sampled due to its quality and availability (Sachse et al., 2016). In the Scotian Basin similar modelling constraints are present. By applying petroleum systems modelling, this study demonstrates the thermal maturity ranges of the Lower Jurassic source rocks in the Scotian Basin. In the In the Tarfaya Basin, Sachse et al. (2016) observed that the salt successions in the basin plays an essential part in the thermal maturity. In the Scotian Basin, the salt-prone Argo Formation also plays an integral part in the thermal maturity of the Lower Jurassic source rock.

4.6 Key Sensitivities

Two key sensitivities were considered; 1) the effects of salt; 2) the effect of varying of Beta factor – using a refraction-based Beta factor instead of an inversion-based Beta factor. In both cases regional trends remained similar, but locally these sensitivities could move Lower Jurassic source rocks from immature to mature and from mature to overmature.

All of the multiple inputs to thermal modelling could be exhaustively examined using sensitivity analysis. Probably the two next most important issues to address would be fluid movement (advection) and the possible consequences of a transitional area from a volcanic to non-volcanic margin in the northeast of the study area.

Chapter 5: Conclusion

The following are conclusions of this study:

1. The conjugate margins of NS and Morocco have had a parallel development from Triassic to Neogene. The presence of Lower Jurassic source rocks in the Scotian Margin has not been proven, although some indirect indications can be interpreted (see sections 1.1, 1.6, 4.1 and references Sachse et al. (2012); Fowler et al. (2016); Wach et al. (2018)). If Scotian Margin Lower Jurassic source rocks have similar lithological and geochemical characteristics to an outcrop at Ait Moussa in Morocco, then an effective Lower Jurassic hydrocarbon system should be present on the Scotian Margin.
2. This study confirms that petroleum system modelling is an effective computational tool that enables the forecasting of potential source rock maturity, from thermal history, kerogen type and basin structure. It is an economical approach to quantify and validate areas for future exploration and constrain risk.
3. The compilation of 2D models for this study, and a NovaSPAN 1600 model from my colleague Xinyue Hu, enabled the creation of Lower Jurassic maturity maps (Figure 3.62). If Lower Jurassic kerogen characteristics in the Scotian Basin are similar to the conjugate Moroccan Basin, then, depending on the location, these source rocks on the Scotian Margin may be immature (southwest), mature (northeast to southwest), or overmature (northeast).
4. Numerical model output shows that the critical moment for the petroleum generation for these rocks would range from Middle Jurassic to Miocene (Table 4.1 and Figure 3.66 - Figure 3.68).
5. The models help explain how several types of salt structures may affect the petroleum system. Salt from the Jurassic Argo Formation affects the thermal history in the surrounding

areas. The salt is more conductive to heat than other rocks hence, above the salt, sedimentary rocks are relatively hotter, and under salt, rocks tend to be relatively cooler. Since salt is relatively impermeable at shallow depths (less than 3.5 km), any escape of advective heat associated with fluid movement will be impeded and as a consequence reservoirs may be temporarily warmer.

6. The regional thermal maturity maps (Figure 3.62, Figure 3.70, Figure 3.76), suggests that the targeted Lower Jurassic rocks of this study are within the oil maturity window in the southern and central regions and within the gas to overmature window in the northern region.
7. This study complements previous work from the Play Fairway Analysis (OERA, 2011). Both studies show similar trends in temperature, maturity and critical moment. The critical moment occurs during the Jurassic in the northeast of the basin and during the Cretaceous in the southwest in both studies.
8. This study also demonstrates that two key sensitivities (Beta factor and presence/absence of salt) can have significant effect locally but regional trends are persistent. In both cases regional trends remained similar, but locally these sensitivities could move Lower Jurassic source rocks from immature to mature and from mature to overmature.

5.1 Future Work

1. There needs to be a more in-depth study of the Lower Jurassic rocks, to understand the geochemical (kerogen type) and distribution of these organic-rich rocks within the basin, especially in the slope and abyssal regions. The resolution of this question will have to await deep drilling.
2. A regional analysis of the Lower Jurassic basin morphology and oceanic circulation patterns would aid in the understanding of regional (Atlantic) source rock distribution and address the

assumption that the Moroccan and Nova Scotian margins are analogous in terms of Lower Jurassic source rock types.

3. Applying additional thermochronology techniques such as fission track (U-Th/He) would enhance the investigation of the thermal history of a sedimentary basin.
4. The area modelled here is exclusively within the volcanic margin, but variations in the magnetic signature of basement (Dehler,2010) might indicate some transition in the northeast of the study area. Addressing this is a challenge for future work.
5. Fluid movement should be considered in future work. The models presented here do not incorporate fluid movement (advection) for two reasons: 1) computational intensity and time considerations; 2) in 2D modelling advection is often not incorporated, as it is handled much better by 3D modelling.

References

- Albertz, M., and Ings, S.J. 2012. Some Consequences of Mechanical Stratification in Basin-Scale Numerical Models of Passive-Margin Salt Tectonics. Geological Society, London, Special Publications **363**(1): 303-330. doi: 10.1144/sp363.14.
- Allen, P.A., and R., A.J. 2013. Basin Analysis: Principles and Application to Petroleum Play Assessment. 3rd ed. Wiley-Blackwell. pp. 632.
- Barss, M.S., Bujak, J.P., Wade, J.A., and Williams, G.L. 1980. Age, Stratigraphy, Organic Matter Type and Colour and Hydrocarbon Occurrences in 47 Wells, Offshore Eastern Canada. Geological Survey of Canada Open File Report No.714. p. 6.
- Beaumont, C., Keen, C.E., and Boutilier, R. 1982. On the Evolution of Rifted Continental Margins: Comparison of Models and Observations for the Nova Scotian Margin. Geophysical Journal of the Royal Astronomical Society **70**(3): 667-715. doi: 10.1111/j.1365-246X.1982.tb05979.x.
- Behar, F., Vandenbroucke, M., Tang, Y., Marquis, F., and Espitalie, J. 1997. Thermal Cracking of Kerogen in Open and Closed Systems: Determination of Kinetic Parameters and Stoichiometric Coefficients for Oil and Gas Generation. Org Geochem **26**(5-6): 321-339. doi: 10.1016/s0146-6380(97)00014-4.
- Bell, J.S., and Campbell, G.R. 1990. Petroleum Resources. *In* Geology of the Continental Margin of Eastern Canada. Edited by K. M.J. and W. G.L. Geological Survey of Canada. pp. 190-238.
- Bustin, R.M. 1996. Vitrinite Reflectance as a Maturity Parameter, Applications and Limitations Edited by P. K. Mukhopadhyay and W. G. Dow; American Chemical Society Symposium Series 570; American Chemical Society: Washington, Dc, 1994; 294 Pp. Energy & Fuels **10**(3): 865-865. doi: 10.1021/ef950078e.
- Campbell, C. 2010. Salt Tectonics of the Abenaki Graben and Central Sable Subbasin: Insights from Regional Seismic Interpretation and 4d Scaled Physical Experiments. MSc. Thesis, *In* Department of Earth Sciences. Dalhousie University, Halifax, N.S. p. 195.
- Campbell, T.J. 2018. Seismic Stratigraphy and Architecture of the Jurassic Abenaki Margin, at Cohasset-Migrant, and Potential for Distal Organic-Rich Facies. MSc. Thesis, *In* Department of Earth Sciences. Dalhousie University, Halifax, N.S.
- Caruthers, A.H., Smith, P.L., and Grocke, D.R. 2014. The Pliensbachian-Toarcian (Early Jurassic) Extinction: A North American Perspective. **505**: 225-243. doi: 10.1130/2014.2505(11).
- Dehler, S.A. 2010. Initial Rifting and Break-up between Nova Scotia and Morocco: An Examination of New Geophysical Data and Models. *In* Central and North Atlantic Conjugate Margins Conference, Lisbon, Portugal.
- Deptuck, M., and Kendell, K. 2012. Contrasting Salt Tectonic Styles on the Western Versus Central Parts of the Scotian Margin, Offshore Nova Scotia. CNSOPB.

- Deptuck, M.E., and Kendell, K.L. 2017. A Review of Mesozoic-Cenozoic Salt Tectonics Along the Scotian Margin, Eastern Canada. 287-312. doi: 10.1016/b978-0-12-809417-4.00014-8.
- Dow, W.G. 1977. Kerogen Studies and Geological Interpretations. *Journal of Geochemical Exploration* **7**: 79-99. doi: 10.1016/0375-6742(77)90078-4.
- Fowler, M., Webb, J., Obermajer, M., Monnier, F., Mort, A., Luheshi, M., and MacDonald, A. 2016. Petroleum Systems of the Scotian Basin. *In AAPG, Calgary.*
- Gemmer, L., Beaumont, C., and Ings, S.J. 2005. Dynamic Modelling of Passive Margin Salt Tectonics: Effects of Water Loading, Sediment Properties and Sedimentation Patterns. *Basin Res* **17**(3): 383-402. doi: 10.1111/j.1365-2117.2005.00274.x.
- Goteti, R., Beaumont, C., and Ings, S.J. 2013. Factors Controlling Early Stage Salt Tectonics at Rifted Continental Margins and Their Thermal Consequences. *Journal of Geophysical Research: Solid Earth* **118**(6): 3190-3220. doi: 10.1002/jgrb.50201.
- Goteti, R., Ings, S.J., and Beaumont, C. 2012. Development of Salt Minibasins Initiated by Sedimentary Topographic Relief. *Earth Planet Sc Lett* **339**: 103-116. doi: 10.1016/j.epsl.2012.04.045.
- Gradmann, S. 2012. The Evolution of Deep-Water Salt-Tectonic Structures, Numerical Modeling Studies Applied to the Northwestern Gulf of Mexico. Ph.D. Dissertation *In Department of Earth Sciences. Dalhousie University, Halifax, N.S. p. 321.*
- Hafid, M., Tari, G., Bouhadioui, D., El Moussaid, I., Echarfaoui, H., Ait Salem, A., Nahim, M., and Dakki, M. 2008. Atlantic Basins. *In Continental Evolution: The Geology of Morocco. Edited by A. Michard and O. Saddiqi and A. Chalouan and D. Frizon de Lamotte. Springer Verlag, Berlin, Heidelberg.*
- Hallam, A. 1981. A Revised Sea-Level Curve for the Early Jurassic. *J Geol Soc London* **138**(Nov): 735-743. doi: DOI 10.1144/gsjgs.138.6.0735.
- Hantschel, T., and Kauerauf, A.I. 2009. *Fundamentals of Basin and Petroleum Systems Modeling.* Springer, Berlin ; London.
- Haq, B.U., Hardenbol, J., and Vail, P.R. 1987. Chronology of Fluctuating Sea Levels since the Triassic. *Science* **235**(4793): 1156-1167. doi: DOI 10.1126/science.235.4793.1156.
- Haq, B.U., and Schutter, S.R. 2008. A Chronology of Paleozoic Sea-Level Changes. *Science* **322**(5898): 64-68. doi: 10.1126/science.1161648.
- Ings, S.J. 2006. Passive Continental Margin Salt Tectonics: Numerical Modelling, Analytical Stability Analysis, and Applications to the Scotian Margin, Offshore Eastern Canada. Ph.D. Dissertation *In Department of Earth Sciences. Dalhousie University, Halifax, N.S. p. 368.*
- Ings, S.J., and Shimeld, J.W. 2006. A New Conceptual Model for the Structural Evolution of a Regional Salt Detachment on the Northeast Scotian Margin, Offshore Eastern Canada. *Aapg Bulletin* **90**(9): 1407-1423. doi: 10.1306/04060605159.

- Jansa, L.F., and Wade, J.A. 1975. Geology of the Continental Margin Off Nova Scotia and Newfoundland. *In* *Offshore Geology of Eastern Canada*. Edited by W. Van der Linden and J.A. Wade. pp. 51-106.
- Jarvis, G.T., and Mckenzie, D.P. 1980. Sedimentary Basin Formation with Finite Extension Rates. *Earth Planet Sc Lett* **48**(1): 42-52. doi: Doi 10.1016/0012-821x(80)90168-5.
- Jenkyns, H.C. 1988. The Early Toarcian (Jurassic) Anoxic Event - Stratigraphic, Sedimentary, and Geochemical Evidence. *Am J Sci* **288**(2): 101-151.
- Jenkyns, H.C., Jones, C.E., Grocke, D.R., Hesselbo, S.P., and Parkinson, D.N. 2002. Chemostratigraphy of the Jurassic System: Applications, Limitations and Implications for Palaeoceanography. *J Geol Soc London* **159**: 351-378. doi: Doi 10.1144/0016-764901-130.
- Jones, I.F., and Davison, I. 2014. Seismic Imaging in and around Salt Bodies. *Interpretation-J Sub* **2**(4): S11-S120. doi: 10.1190/Int-2014-0033.1.
- Keen, C.E., and Beaumont, C. 1990. Geodynamics of Rifted Continental Margins. *In* *Geology of the Continental Margin of Eastern Canada*. Edited by M.J. Keen and G.L. Williams. Geological Survey of Canada. pp. 391-472.
- Kettanah, Y.A., and Greenough, J. 2013. Hydrocarbon Fluid Inclusions in the Argo Salt, Offshore Canadian Atlantic Margin. *Canadian Journal of Earth Sciences* **50**(6): 607-635. doi: 10.1139/cjes-2012-0040.
- Kettanah, Y.A., Zentilli, M., and Wielens, H. 2004. Pilot Study on Fluid Inclusions in Salt (Halite) from the Osprey H-84 Well, Carson Sub-Basin, Grand Banks, Newfoundland. *In* *Atlantic Geoscience Society Annual Colloquium, Moncton, New Brunswick*. pp. 144-145.
- Kidston, A.G., Brown, D.E., Altheim, B., and Smith, B.M. 2002. Hydrocarbon Potential of the Deep-Water Scotian Slope. Halifax: Canada-Nova Scotia Offshore Petroleum Board.
- Leleu, S., Hartley, A.J., van Oosterhout, C., Kennan, L., Ruckwied, K., and Gerdes, K. 2016. Structural, Stratigraphic and Sedimentological Characterisation of a Wide Rift System: The Triassic Rift System of the Central Atlantic Domain. *Earth-Sci Rev* **158**: 89-124. doi: 10.1016/j.earscirev.2016.03.008.
- Lewis, S., and Holness, M. 1996. Equilibrium Halite-H₂O Dihedral Angles: High Rock-Salt Permeability in the Shallow Crust? *Geology* **24**(5): 431. doi: 10.1130/0091-7613(1996)024<0431:ehhoda>2.3.co;2.
- Louden, K., Lau, H., Wu, Y., and Nedimovic, M. 2010. Refraction Crustal Models and Plate Reconstruction of the Nova Scotia and Morocco Margins. OETR.
- Louden, K., Wu, Y., and Tari, G. 2013. Systematic Variations in Basement Morphology and Rifting Geometry Along the Nova Scotia and Morocco Conjugate Margins. *Geological Society, London, Special Publications* **369**(1): 267-287. doi: 10.1144/sp369.9.

- Louden, K.E., Tucholke, B.E., and Oakey, G.N. 2004. Regional Anomalies of Sediment Thickness, Basement Depth and Isostatic Crustal Thickness in the North Atlantic Ocean. *Earth Planet Sc Lett* **224**(1-2): 193-211. doi: 10.1016/j.espl.2004.05.002.
- MacDonald, C. 2009. Salt Tectonics of the Western Sable Sub-Basin: Insights from Regional Seismic Interpretation and 4d Scaled Physical Experiments. MSc. Thesis, *In* Department of Earth Sciences. Dalhousie University, Halifax, N.S. p. 238.
- MacLean, B., and Wade, J. 1993. Seismic Markers and Stratigraphic Picks in the Scotian Basin Wells: East Coast Basin Atlas Series. Geological Survey of Canada. pp. 276.
- Magoon, L.B., and Dow, W.G. 1994. The Petroleum System-from Source to Trap. American Association Of Petroleum Geologists.
- McIver, N.L. 1972. Cenozoic and Mesozoic Stratigraphy of the Nova Scotia Shelf. *Canadian Journal of Earth Sciences* **9**(1): 54-70. doi: 10.1139/e72-005.
- McKenzie, D. 1978. Some Remarks on the Development of Sedimentary Basins. *Earth Planet Sc Lett* **40**(1): 25-32. doi: 10.1016/0012-821x(78)90071-7.
- Morabet, A.M., Bouchta, R., and Jabour, H. 1998. An Overview of the Petroleum Systems of Morocco. Geological Society, London, Special Publications **132**(1): 283-296. doi: 10.1144/gsl.sp.1998.132.01.16.
- Morrison, N. 2017. Seismic Inversion and Source Rock Evaluation on Jurassic Organic Rich Intervals in the Scotian Basin, Nova Scotia. MSc. Thesis, *In* Department of Earth Sciences. Dalhousie University, Halifax, N.S. p. 196.
- Mukhopadhyay, P.K. 2006. Evaluation of the Petroleum Systems by One and Two Dimensional Numerical Modeling and Geochemical Analysis in the Area of Most Recent Exploration Wells on the Deepwater Scotian Slope, Offshore Nova Scotia. Nova Scotia Department of Energy.
- Mukhopadhyay, P.K., and Wade, J.A. 1990. Organic Facies and Maturation of Sediments from Three Scotian Shelf Wells. *Bulletin of Canadian Petroleum Geology*(38): 407-425.
- Negulic, E. 2010. Thermal Structure of the Central Scotian Slope: Seafloor Heat Flow and Thermal Maturation Models. MSc. Thesis, *In* Department of Earth Sciences. Dalhousie University, Halifax, N.S. p. 225.
- Negulic, E., and Loudon, K.E. 2017. The Thermal Structure of the Central Nova Scotia Slope (Eastern Canada): Seafloor Heat Flow and Thermal Maturation Models. *Canadian Journal of Earth Sciences* **54**(2): 146-162. doi: 10.1139/cjes-2016-0060.
- OERA. 2011. Play Fairway Analysis Atlas-Offshore Nova Scotia. Offshore Energy Research Association of Nova Scotia. Report 88-11-0004-01.
- OERA. 2015. Sw Nova Scotia Expansion Atlas. Offshore Energy Research Association of Nova Scotia.

- OERA. 2016. Central Scotian Slope Atlas. Offshore Energy Research Association of Nova Scotia.
- Olsen, P.E. 1997. Stratigraphic Record of the Early Mesozoic Breakup of Pangea in the Laurasia-Gondwana Rift System. *Annual Review of Earth and Planetary Sciences* **25**: 337-401. doi: DOI 10.1146/annurev.earth.25.1.337.
- Peel, F.J. 2014. How Do Salt Withdrawal Minibasins Form? Insights from Forward Modelling, and Implications for Hydrocarbon Migration. *Tectonophysics* **630**: 222-235. doi: 10.1016/j.tecto.2014.05.027.
- Powell, T.G. 1985. Paleogeographic Implications for the Distribution of Upper Jurassic Source Beds - Offshore Eastern Canada. *Bulletin of Canadian Petroleum Geology* **33**(1): 116-119.
- Royden, L., and Keen, C.E. 1980. Rifting Process and Thermal Evolution of the Continental-Margin of Eastern Canada Determined from Subsidence Curves. *Earth Planet Sc Lett* **51**(2): 343-361. doi: Doi 10.1016/0012-821x(80)90216-2.
- Rullkotter, J., Mukhopadhyay, P.K., Schaefer, R.G., and Welte, D.H. 1984. Geochemistry and Petrography of Organic Matter in Sediments from Deep Sea Drilling Project Sites 545 and 547, Mazagan Escarpment. **79**. doi: 10.2973/dsdproc.79.132.1984.
- Sachse, V.F., Leythaeuser, D., Grobe, A., Rachidi, M., and Littke, R. 2012. Organic Geochemistry and Petrology of a Lower Jurassic (Pliensbachian) Petroleum Source Rock from Ait Moussa, Middle Atlas, Morocco. *Journal of Petroleum Geology* **35**(1): 5-23. doi: 10.1111/j.1747-5457.2012.00516.x.
- Sachse, V.F., Wenke, A., Littke, R., Jabour, H., Kluth, O., and Zuhlke, R. 2016. 2d Petroleum System Analysis of the Tarfaya Basin, on-Offshore Morocco, North Africa. *Marine and Petroleum Geology* **77**: 1108-1124. doi: 10.1016/j.marpetgeo.2016.08.006.
- Shimeld, J. 2004. A Comparison of Salt Tectonic Subprovinces beneath the Scotian Slope and Laurentian Fan. 502-532. doi: 10.5724/gcs.04.24.0502.
- Silva, R.L. 2013. Jurassic Organic-Rich Carbonate Series of the Lusitanian Basin (Portugal): Sedimentology, Geochemistry and Palaeoenvironmental Interpretation. Universidade de Coimbra. p. 250.
- Silva, R.L., Carlisle, C.A.M., and Wach, G. 2017a. A New Toc, Rock-Eval, and Carbon Isotope Record of Lower Jurassic Source Rocks from the Slyne Basin, Offshore Ireland. *Marine and Petroleum Geology* **86**: 499-511. doi: 10.1016/j.marpetgeo.2017.06.004.
- Silva, R.L., and Duarte, L.V. 2015. Organic Matter Production and Preservation in the Lusitanian Basin (Portugal) and Pliensbachian Climatic Hot Snaps. *Global Planet Change* **131**: 24-34. doi: 10.1016/j.gloplacha.2015.05.002.
- Silva, R.L., Duarte, L.V., Comas-Rengifo, M.J., Mendonça Filho, J.G., and Azerêdo, A.C. 2011. Update of the Carbon and Oxygen Isotopic Records of the Early-Late Pliensbachian (Early Jurassic, ~187ma): Insights from the Organic-Rich Hemipelagic Series of the Lusitanian Basin (Portugal). *Chemical Geology* **283**(3-4): 177-184. doi: 10.1016/j.chemgeo.2011.01.010.

- Silva, R.L., Duarte, L.V., Gómez, J.J., Mendonça Filho, J.G., Wach, G., Sadki, D., Rodrigues, B., Carlisle, C., and Caniço, A. 2017b. Lower Jurassic Organic Matter Preservation Events, an Oceanic Anoxic Event, and Carbon Cycle Perturbations. *In* Goldschmidt, Paris, France.
- Silva, R.L., Wong, C., and Wach, G. 2015. Source Rocks and Petroleum Systems of the Scotian Basin. *CSEG Recorder*(40): 22-27.
- Suan, G., Mattioli, E., Pittet, B., Lecuyer, C., Sucheras-Marx, B., Duarte, L.V., Philippe, M., Reggiani, L., and Martineau, F. 2010. Secular Environmental Precursors to Early Toarcian (Jurassic) Extreme Climate Changes. *Earth Planet Sc Lett* **290**(3-4): 448-458. doi: 10.1016/j.epsl.2009.12.047.
- Suarez-Ruiz, I., Flores, D., Mendonca, J.G., and Hackley, P.C. 2012. Review and Update of the Applications of Organic Petrology: Part 1, Geological Applications. *Int J Coal Geol* **99**: 54-112. doi: 10.1016/j.coal.2012.02.004.
- Sweeney, J.J., and Burnham, A.K. 1990. Evaluation of a Simple Model of Vitrinite Reflectance Based on Chemical Kinetics. *AAPG Bulletin* **74**: 1559-1570.
- Tari, G., and Jabour, H. 2013. Salt Tectonics Along the Atlantic Margin of Morocco. *Geological Society, London, Special Publications* **369**(1): 337-353. doi: 10.1144/sp369.23.
- Tissot, B.P., and Welte, D.H. 1984. *Petroleum Formation and Occurrence*. 2nd, rev. and enl. ed. Springer-Verlag, Berlin; New York.
- Vandenbroucke, M., Behar, F., and Rudkiewicz, J.L. 1999. Kinetic Modelling of Petroleum Formation and Cracking: Implications from the High Pressure/High Temperature Elgin Field (UK, North Sea). *Org Geochem* **30**(9): 1105-1125. doi: Doi 10.1016/S0146-6380(99)00089-3.
- Veeken, P.C.H., and Moerkerken, B. 2013. Seismic Stratigraphic Techniques. *In* Seismic Stratigraphy and Depositional Facies Models. Houten: EAGE Publications, The Netherlands. p. 110.
- Wach, G., Silva, R.L., O'Connor, D., Wong, C., Hu, X., Carlisle, C.A.M., Sedore, P., Morrison, N., Campbell, T., and Hargreaves, A. 2018. Source Rock & Geochemistry of the Central Atlantic Margins. Basin and Reservoir Lab, Dalhousie University.
- Wade, J.A., and MacLean, B.C. 1990. The Geology of the Southeastern Margin of Canada. *In* Geology of the Continental Margin of Eastern Canada. Edited by M.J. Keen and G.L. Williams. Geological Survey of Canada. pp. 190-238.
- Warren, J.K. 2017. Salt Usually Seals, but Sometimes Leaks: Implications for Mine and Cavern Stabilities in the Short and Long Term. *Earth-Sci Rev* **165**: 302-341. doi: 10.1016/j.earscirev.2016.11.008.
- Warsitzka, M., Kukowski, N., and Kley, J. 2017. Kinematics and Dynamics of Salt Movement Driven by Sub-Salt Normal Faulting and Supra-Salt Sediment Accumulation - Combined Analogue Experiments and Analytical Calculations. *In* EGU, Vienna, Austria.

- Watts, A.B., and Ryan, W.B.F. 1976. Flexure of the Lithosphere and Continental Margin Basins. *Tectonophysics* **36**(1-3): 25-44. doi: 10.1016/0040-1951(76)90004-4.
- Weston, J.F., MacRae, R.A., Ascoli, P., Cooper, M.K.E., Fensome, R.A., Shaw, D., Williams, G.L., Dehler, S., Deptuck, M., and Karim, A. 2012. A Revised Biostratigraphic and Well-Log Sequence-Stratigraphic Framework for the Scotian Margin, Offshore Eastern Canada. *Canadian Journal of Earth Sciences* **49**(12): 1417-1462. doi: 10.1139/e2012-070.
- White, N., and McKenzie, D. 1988. Formation of the "Steer's Head" Geometry of Sedimentary Basins by Differential Stretching of the Crust and Mantle. *Geology* **16**(3): 250. doi: 10.1130/0091-7613(1988)016<0250:fotssh>2.3.co;2.
- Williamson, M.C., Courtney, R.C., Keen, C.E., and Dehler, S.A. 1995. The Volume and Rare-Earth Concentrations of Magmas Generated During Finite Stretching of the Lithosphere. *J Petrol* **36**(5): 1433-1454.
- Withjack, M.O., Schlische, R.W., and Olsen, P.E. 2012. Development of the Passive Margin of Eastern North America. 300-335. doi: 10.1016/b978-0-444-56356-9.00012-2.
- Wygrala, B.P. 1989. Integrated Study of an Oil Field in the Southern Po Basin, Northern Italy. Ph.D. Dissertation. University of Cologne, Germany. p. 217.
- Zentilli, M., and Williamson, M.C. 2004. Significance of Salt Diapirs, Magmatism and Tectonics on the Thermal History of Axel Heiberg Island, Nunavut. *In* Atlantic Geoscience Society Annual Colloquium. Atlantic Geology, Moncton, New Brunswick.

Appendix A: Borehole Information

The following tables contain the details of the offshore boreholes used. This details includes the unique well identification number (UWI), the Geological Survey of Canada borehole identifier (GSC), the date that the offshore borehole was spudded, the location within the Scotian Basin, the type of offshore borehole, the status and type of the hydrocarbon found, rotary table above sea level, water depth of the offshore borehole location, the total depth drilled; and if it was deviated the total vertical depth drilled, and the status of the offshore borehole at present day.

Table A.1: General information from the BASIN database for the boreholes used in this study. Rotatory Table (RT), Water Depth (WD), Total Depth (TD), Total Vertical Depth (TVD), and Plugged and Abandoned (P&A)

BLUENOSE G-47		BLUENOSE 2G-47	
UWI:	300 G47 44100 59150	UWI:	302 G47 44100 59150
GSC#:	D094	GSC#:	D223
Spud Date:	25-Jan-1973	Spud Date:	30-Dec-1982
Area:	Scotian Shelf	Area:	Scotian Shelf
Borehole Class:	Exploratory	Borehole Class:	Exploratory
Basin:	Scotian Basin	Basin:	Scotian Basin
Gas:	Show	Gas:	Show
Oil:	Unrated	Oil:	Unrated
RT:	29.9 m	RT:	24 m
WD:	81.4 m	WD:	85 m
TD:	4587.2 m	TD:	5797 m
TVD:	m	TVD:	m
Status:	Plugged and Abandoned	Status:	Plugged and Abandoned
HESPER I-52		HESPER P-52	
UWI:	300 I52 44500 57450	UWI:	300 P52 44500 57450
GSC#:	D162	GSC#:	D257
Spud Date:	08-May-1976	Spud Date:	31-Aug-1984
Area:	Scotian Shelf	Area:	Scotian Shelf
Borehole Class:	Exploratory	Borehole Class:	Exploratory
Basin:	Scotian Basin	Basin:	Scotian Basin
Gas:	Dry Hole	Gas:	Dry Hole
Oil:	DRY HOLE	Oil:	Dry Hole
RT:	29.9 m	RT:	40.5 m
WD:	42.1 m	WD:	44.5 m
TD:	2804.2 m	TD:	5690 m
TVD:	m	TVD:	m
Status:	Plugged and Abandoned	Status:	Plugged and Abandoned

BONNET P-23	
UWI:	300 P23 42300 65000
GSC#:	D244
Spud Date:	14-Jan-1984
Area:	Scotian Shelf
Borehole Class:	Exploratory
Basin:	Scotian Basin
Gas:	Dry Hole
Oil:	Dry Hole
RT:	25 m
WD:	133.5 m
TD:	4336 m
TVD:	m
Status:	Plugged and Abandoned

GLOOSCAP C-63	
UWI:	300 C63 43200 62000
GSC#:	D231
Spud Date:	05-Aug-1983
Area:	Scotian Shelf
Borehole Class:	Exploratory
Basin:	Scotian Basin
Gas:	Dry Hole
Oil:	Dry Hole
RT:	22.86 m
WD:	99 m
TD:	4551.5 m
TVD:	m
Status:	Plugged and Abandoned

MISSISSAUGA H-54	
UWI:	300 H54 44300 59150
GSC#:	D009
Spud Date:	26-May-1970
Area:	Scotian Shelf
Borehole Class:	Exploratory
Basin:	Scotian Basin
Gas:	Dry Hole
Oil:	Dry Hole
RT:	25.9 m
WD:	102.1 m
TD:	4202.3 m
TVD:	m
Status:	Plugged and Abandoned

MOHEIDA P-15	
UWI:	300 P15 43100 62150
GSC#:	D168
Spud Date:	18-Nov-1976
Area:	Scotian Shelf
Borehole Class:	Exploratory
Basin:	Scotian Basin
Gas:	Dry Hole
Oil:	Dry Hole
RT:	29.9 m
WD:	111.9 m
TD:	4297.7 m
TVD:	m
Status:	Plugged and Abandoned

MOHICAN I-100	
UWI:	300 I00 43000 62150
GSC#:	D074
Spud Date:	28-Dec-1971
Area:	Scotian Shelf
Borehole Class:	Exploratory
Basin:	Scotian Basin
Gas:	Dry Hole
Oil:	Dry Hole
RT:	29.9 m
WD:	153.3 m
TD:	4393.4 m
TVD:	m
Status:	Plugged and Abandoned

TORBROOK C-15	
UWI:	300 C15 42400 62150
GSC#:	D383
Spud Date:	16-Nov-2002
Area:	Scotian Slope
Borehole Class:	Exploratory
Basin:	Scotian Basin
Gas:	Dry Hole
Oil:	Dry Hole
RT:	25 m
WD:	1674.5 m
TD:	3600 m
TVD:	3599.95 m
Status:	Plugged and Abandoned

WYANDOT E-53	
UWI:	300 E53 45000 59150
GSC#:	D018
Spud Date:	07-Nov-1970
Area:	Scotian Shelf
Borehole Class:	Exploratory
Basin:	Scotian Basin
Gas:	Unrated
Oil:	SHOW
RT:	31.4 m
WD:	121 m
TD:	3049.5 m
TVD:	M
Status:	Plugged and Abandoned

SACHEM D-76	
UWI:	300 D76 44400 57300
GSC#:	D146
Spud Date:	17-May-1975
Area:	Scotian Shelf
Borehole Class:	Exploratory
Basin:	Scotian Basin
Gas:	Dry Hole
Oil:	Dry Hole
RT:	29.9 m
WD:	58.5 m
TD:	4878.6 m
TVD:	M
Status:	Plugged and Abandoned

SOUTH GRIFFIN J-13	
UWI:	300 J13 44300 58000
GSC#:	D243
Spud Date:	08-Jan-1984
Area:	Scotian Shelf
Borehole Class:	Exploratory
Basin:	Scotian Basin
Gas:	Dry Hole
Oil:	Dry Hole
RT:	39.62 m
WD:	63.4 m
TD:	5920 m
TVD:	M
Status:	Plugged and Abandoned

Appendix B: Borehole Temperature & Vitrinite Reflectance

The following tables are data collected from BASIN database; each offshore borehole has a table of temperature and vitrinite reflectance. Only Moheida P-15 and Hesper P-52 do not have vitrinite reflectance data. Each table has the measured depth (meters) and its corresponding value with the author of the provenance of the data and column describing the colour symbol in the model plots when comparing the modelled results against measured data. The BASIN database can be accessed from the Government of Canada website, Natural Resources Canada. (http://basin.gdr.nrcan.gc.ca/index_e.php).

Table B.1: Temperature data from BASIN database for Bonnet P-23. The symbol is the colour of the data point on the 1D calibration plot.

Temperature			
Measured Depth (m)	Temperature (C)	Source	Symbol
1163.0	33.0	Petro-Canada Inc	Yellow Circle
3145.0	80.0	Petro-Canada Inc	Yellow Circle
3173.0	80.0	Petro-Canada Inc	Yellow Circle
3176.0	80.0	Petro-Canada Inc	Yellow Circle
3186.0	75.0	Petro-Canada Inc	Yellow Circle
4271.0	113.0	Petro-Canada Inc	Yellow Circle
4287.0	111.0	Petro-Canada Inc	Yellow Circle
4287.0	111.0	Petro-Canada Inc	Yellow Circle
4292.0	109.0	Petro-Canada Inc	Yellow Circle
4295.0	102.0	Petro-Canada Inc	Yellow Circle
4300.0	103.0	Petro-Canada Inc	Yellow Circle
4315.0	101.0	Petro-Canada Inc	Yellow Circle
4325.0	101.0	Petro-Canada Inc	Yellow Circle

Table B.2 Vitrinite reflectance data from BASIN database for Bonnet P-23. The symbol is the colour of the data point on the 1D calibration plot.

Vitrinite Reflectance					
Measured Depth (m)	Degree	Vitrinite Standard Deviation	Source	Year	Symbol
590	0.27	0.03	Avery, M.P.	2003	Orange Diamond
830	0.30	0.03	Avery, M.P.	2003	Orange Diamond
1040	0.29	0.03	Avery, M.P.	2003	Orange Diamond
1280	0.26	0.02	Avery, M.P.	2003	Orange Diamond
1520	0.31	0.06	Avery, M.P.	2003	Orange Diamond
1760	0.34	0.04	Avery, M.P.	2003	Orange Diamond
2000	0.43	0.06	Avery, M.P.	2003	Orange Diamond
2240	0.37	0.01	Avery, M.P.	2003	Orange Diamond
2420	0.42	0.05	Avery, M.P.	2003	Orange Diamond
2750	0.40	0.02	Avery, M.P.	2003	Orange Diamond
3190	0.43	0.04	Avery, M.P.	2003	Orange Diamond
3460	0.52	0.05	Avery, M.P.	2003	Orange Diamond
1030	0.35	0.05	Petro-Canada Inc	1985	Green Diamond
1450	0.39	0.05	Petro-Canada Inc	1985	Green Diamond
1570	0.32	0.06	Petro-Canada Inc	1985	Green Diamond
1630	0.38	0.05	Petro-Canada Inc	1985	Green Diamond
1660	0.40	0.05	Petro-Canada Inc	1985	Green Diamond
1720	0.38	0.03	Petro-Canada Inc	1985	Green Diamond
1880	0.44	0.06	Petro-Canada Inc	1985	Green Diamond
1900	0.46	0.07	Petro-Canada Inc	1985	Green Diamond
1900	0.40	0.04	Petro-Canada Inc	1985	Green Diamond
2440	0.43	0.12	Petro-Canada Inc	1985	Green Diamond
2560	0.65	0.02	Petro-Canada Inc	1985	Green Diamond
2830	0.49	0.02	Petro-Canada Inc	1985	Green Diamond
2890	0.58	0.04	Petro-Canada Inc	1985	Green Diamond
3247	0.54	0.04	Petro-Canada Inc	1985	Green Diamond
3270	0.61	0.06	Petro-Canada Inc	1985	Green Diamond
3290	0.56	0.06	Petro-Canada Inc	1985	Green Diamond
3344	0.63	0.05	Petro-Canada Inc	1985	Green Diamond
3350	0.65	0.11	Petro-Canada Inc	1985	Green Diamond
3440	0.66	0.06	Petro-Canada Inc	1985	Green Diamond
3521	0.87	0.00	Petro-Canada Inc	1985	Green Diamond
3530	0.72	0.03	Petro-Canada Inc	1985	Green Diamond
3726	0.83	0.07	Petro-Canada Inc	1985	Green Diamond
3830	0.84	0.08	Petro-Canada Inc	1985	Green Diamond
3860	0.91	0.08	Petro-Canada Inc	1985	Green Diamond

Table B.3: Temperature data from BASIN database for Bluenose G-47. The symbol is the colour of the data point on the 1D calibration plot.

Temperature			
Measured Depth (M)	Temperature (C)	Source	Symbol
1194.3	25.6	ISSLER 1982	Pink Circle
2981.3	78.9	ISSLER 1982	Pink Circle
3597.6	98.8	MOBIL OIL CANADA LTD	Yellow Circle
3605.8	99.9	MOBIL OIL CANADA LTD	Yellow Circle
3624.3	104.2	ISSLER 1982	Pink Circle
3668.0	99.9	MOBIL OIL CANADA LTD	Yellow Circle
3678.9	98.8	MOBIL OIL CANADA LTD	Yellow Circle
3818.2	104.3	MOBIL OIL CANADA LTD	Yellow Circle
4075.8	102.7	MOBIL OIL CANADA LTD	Yellow Circle
4077.6	102.7	MOBIL OIL CANADA LTD	Yellow Circle
4586.0	108.8	MOBIL OIL CANADA LTD	Yellow Circle
4586.0	108.8	MOBIL OIL CANADA LTD	Yellow Circle
4586.3	108.8	MOBIL OIL CANADA LTD	Yellow Circle
4586.6	108.8	MOBIL OIL CANADA LTD	Yellow Circle
4586.9	108.8	MOBIL OIL CANADA LTD	Yellow Circle
4586.9	108.8	MOBIL OIL CANADA LTD	Yellow Circle
4587.3	118.9	ISSLER 1982	Pink Circle

Table B.4: Vitrinite reflectance data from BASIN database for Bluenose G-47. The symbol is the colour of the data point on the 1D calibration plot.

Vitrinite Reflectance					
Measured Depth (m)	Degree	Vitrinite Standard Deviation	Source	Year	Symbol
338.33	0.18		Robertson Research International Ltd	1976	Green Diamond
402.34	0.17		Robertson Research International Ltd	1976	Green Diamond
493.78	0.19		Robertson Research International Ltd	1976	Green Diamond
585.22	0.15		Robertson Research International Ltd	1976	Green Diamond
676.66	0.19		Robertson Research International Ltd	1976	Green Diamond
768.11	0.21		Robertson Research International Ltd	1976	Green Diamond
1042.43	0.25		Robertson Research International Ltd	1976	Green Diamond
1133.87	0.28		Robertson Research International Ltd	1976	Green Diamond
1313.70	0.29		Robertson Research International Ltd	1976	Green Diamond
1524.02	0.31		Robertson Research International Ltd	1976	Green Diamond
1679.47	0.36		Robertson Research International Ltd	1976	Green Diamond
1743.48	0.30		Robertson Research International Ltd	1976	Green Diamond
1798.34	0.32		Robertson Research International Ltd	1976	Green Diamond
1859.30	0.29		Robertson Research International Ltd	1976	Green Diamond
2042.18	0.37		Robertson Research International Ltd	1976	Green Diamond
2103.15	0.43		Robertson Research International Ltd	1976	Green Diamond
2164.11	0.41		Robertson Research International Ltd	1976	Green Diamond
2255.55	0.39		Robertson Research International Ltd	1976	Green Diamond
2438.43	0.40		Robertson Research International Ltd	1976	Green Diamond
2712.75	0.51		Robertson Research International Ltd	1976	Green Diamond

2834.67	0.57	Robertson Research International Ltd	1976	Green Diamond
2895.64	0.54	Robertson Research International Ltd	1976	Green Diamond
2956.60	0.43	Robertson Research International Ltd	1976	Green Diamond
3291.88	0.56	Robertson Research International Ltd	1976	Green Diamond
3413.80	0.56	Robertson Research International Ltd	1976	Green Diamond
4206.29	0.61	Robertson Research International Ltd	1976	Green Diamond
4267.25	0.65	Robertson Research International Ltd	1976	Green Diamond
2895.64	0.54	Robertson Research International Ltd	1976	Green Diamond

Table B.5: Temperature data from BASIN database for Bluenose 2G-47. The symbol is the colour of the data point on the 1D calibration plot.

Temperature			
Measured Depth (m)	Temperature (C)	Source	Symbol
3013.0	84.0	Mobil Oil Canada Ltd	Yellow Circle
3013.0	84.0	Mobil Oil Canada Ltd	Yellow Circle
3014.0	84.0	Mobil Oil Canada Ltd	Yellow Circle
3021.0	72.0	Mobil Oil Canada Ltd	Yellow Circle
3082.1	90.0	Mobil Oil Canada Ltd	Yellow Circle
3082.1	90.0	Mobil Oil Canada Ltd	Yellow Circle
4550.0	121.0	Mobil Oil Canada Ltd	Yellow Circle
4590.0	132.0	Mobil Oil Canada Ltd	Yellow Circle
4623.0	125.0	Mobil Oil Canada Ltd	Yellow Circle
4927.0	136.0	Mobil Oil Canada Ltd	Yellow Circle
4934.0	131.0	Mobil Oil Canada Ltd	Yellow Circle
4936.0	136.0	Mobil Oil Canada Ltd	Yellow Circle
4937.0	136.0	Mobil Oil Canada Ltd	Yellow Circle
4938.0	165.0	Mobil Oil Canada Ltd	Yellow Circle
5020.0	138.0	Mobil Oil Canada Ltd	Yellow Circle
5112.4	143.0	Mobil Oil Canada Ltd	Yellow Circle
5112.4	144.0	Mobil Oil Canada Ltd	Yellow Circle
5235.0	148.0	Mobil Oil Canada Ltd	Yellow Circle
5486.0	160.0	Mobil Oil Canada Ltd	Yellow Circle
5493.0	164.0	Mobil Oil Canada Ltd	Yellow Circle
5581.0	157.0	Mobil Oil Canada Ltd	Yellow Circle
5581.0	158.0	Mobil Oil Canada Ltd	Yellow Circle
5795.0	166.0	Mobil Oil Canada Ltd	Yellow Circle
5796.0	164.0	Mobil Oil Canada Ltd	Yellow Circle
5796.0	164.0	Mobil Oil Canada Ltd	Yellow Circle
5797.0	164.0	Mobil Oil Canada Ltd	Yellow Circle
5797.0	164.0	Mobil Oil Canada Ltd	Yellow Circle
5797.0	164.0	Mobil Oil Canada Ltd	Yellow Circle

Table B.6: Vitrinite reflectance data from BASIN database for Bluenose 2G-47. The symbol is the colour of the data point on the 1D calibration plot.

Vitrinite Reflectance					
Measured Depth (m)	Degree	Vitrinite Standard Deviation	Source	Year	Symbol
890.0	0.29		Avery, M.P.	1993	Orange Diamond
1100.0	0.36		Avery, M.P.	1993	Orange Diamond
1220.0	0.37		Avery, M.P.	1993	Orange Diamond
1400.0	0.42		Avery, M.P.	1993	Orange Diamond
1555.0	0.46		Avery, M.P.	1993	Orange Diamond
1675.0	0.42		Avery, M.P.	1993	Orange Diamond
1975.0	0.46		Avery, M.P.	1993	Orange Diamond
2140.0	0.47		Avery, M.P.	1993	Orange Diamond
2320.0	0.55		Avery, M.P.	1993	Orange Diamond
2500.0	0.54		Avery, M.P.	1993	Orange Diamond
2680.0	0.56		Avery, M.P.	1993	Orange Diamond
2890.0	0.65		Avery, M.P.	1993	Orange Diamond
3010.0	0.64		Avery, M.P.	1993	Orange Diamond
3250.0	0.67		Avery, M.P.	1993	Orange Diamond
3400.0	0.70		Avery, M.P.	1993	Orange Diamond
3550.0	0.74		Avery, M.P.	1993	Orange Diamond
3730.0	0.77		Avery, M.P.	1993	Orange Diamond
3930.0	0.77		Avery, M.P.	1993	Orange Diamond
4080.0	0.75		Avery, M.P.	1993	Orange Diamond
4290.0	0.82		Avery, M.P.	1993	Orange Diamond
4440.0	0.84		Avery, M.P.	1993	Orange Diamond
4620.0	1.01		Avery, M.P.	1993	Orange Diamond
4770.0	1.01		Avery, M.P.	1993	Orange Diamond
4980.0	1.17		Avery, M.P.	1993	Orange Diamond
5280.0	1.52		Avery, M.P.	1993	Orange Diamond
5490.0	1.61		Avery, M.P.	1993	Orange Diamond
5625.0	1.74		Avery, M.P.	1993	Orange Diamond
5745.0	1.82		Avery, M.P.	1993	Orange Diamond
4730.0	1.09	0.06	Avery, M.P.	1994	Orange Diamond
5050.0	1.39	0.10	Avery, M.P.	1994	Orange Diamond
5260.0	1.38	0.11	Avery, M.P.	1994	Orange Diamond
5695.0	1.52	0.11	Avery, M.P.	1994	Orange Diamond
870.0	0.43		Geochem Laboratories	1983	Green Diamond
960.0	0.57		Geochem Laboratories	1983	Green Diamond
1140.0	0.59		Geochem Laboratories	1983	Green Diamond
1230.0	0.57		Geochem Laboratories	1983	Green Diamond

1320.0	0.68	Geochem Laboratories	1983	Green Diamond
1410.0	0.61	Geochem Laboratories	1983	Green Diamond
1500.0	0.59	Geochem Laboratories	1983	Green Diamond
1590.0	0.60	Geochem Laboratories	1983	Green Diamond
1680.0	0.63	Geochem Laboratories	1983	Green Diamond
1770.0	0.64	Geochem Laboratories	1983	Green Diamond
1890.0	0.62	Geochem Laboratories	1983	Green Diamond
1950.0	0.63	Geochem Laboratories	1983	Green Diamond
2040.0	0.63	Geochem Laboratories	1983	Green Diamond
2130.0	0.64	Geochem Laboratories	1983	Green Diamond
2220.0	0.64	Geochem Laboratories	1983	Green Diamond
2340.0	0.62	Geochem Laboratories	1983	Green Diamond
2400.0	0.64	Geochem Laboratories	1983	Green Diamond
2550.0	0.64	Geochem Laboratories	1983	Green Diamond
2580.0	0.66	Geochem Laboratories	1983	Green Diamond
2670.0	0.67	Geochem Laboratories	1983	Green Diamond
2760.0	0.65	Geochem Laboratories	1983	Green Diamond
2820.0	0.61	Geochem Laboratories	1983	Green Diamond
2940.0	0.62	Geochem Laboratories	1983	Green Diamond
3030.0	0.66	Geochem Laboratories	1983	Green Diamond
3120.0	0.66	Geochem Laboratories	1983	Green Diamond
3120.0	0.65	Geochem Laboratories	1983	Green Diamond
3240.0	0.62	Geochem Laboratories	1983	Green Diamond
3330.0	0.69	Geochem Laboratories	1983	Green Diamond
3390.0	0.70	Geochem Laboratories	1983	Green Diamond
3480.0	0.69	Geochem Laboratories	1983	Green Diamond
3540.0	0.68	Geochem Laboratories	1983	Green Diamond
3570.0	0.72	Geochem Laboratories	1983	Green Diamond
3630.0	0.70	Geochem Laboratories	1983	Green Diamond
3750.0	0.68	Geochem Laboratories	1983	Green Diamond
3840.0	0.72	Geochem Laboratories	1983	Green Diamond
3930.0	0.70	Geochem Laboratories	1983	Green Diamond
4050.0	0.73	Geochem Laboratories	1983	Green Diamond
4110.0	0.67	Geochem Laboratories	1983	Green Diamond
4200.0	0.70	Geochem Laboratories	1983	Green Diamond
4290.0	0.73	Geochem Laboratories	1983	Green Diamond
4380.0	0.73	Geochem Laboratories	1983	Green Diamond
4470.0	0.75	Geochem Laboratories	1983	Green Diamond
4560.0	0.73	Geochem Laboratories	1983	Green Diamond
4650.0	0.73	Geochem Laboratories	1983	Green Diamond
4740.0	0.72	Geochem Laboratories	1983	Green Diamond

4860.0	0.80	Geochem Laboratories	1983	Green Diamond
---------------	------	----------------------	------	---------------

Table B.7: Temperature data from BASIN database for Glooscap C-63. The symbol is the colour of the data point on the 1D calibration plot.

Temperature			
Measured Depth (m)	Temperature (C)	Source	Symbol
855.0	29.5	Husky Oil Operations Ltd	Yellow Circle
2657.0	63.0	Husky Oil Operations Ltd	Yellow Circle
4442.0	118.0	Husky Oil Operations Ltd	Yellow Circle
4442.0	118.0	Husky Oil Operations Ltd	Yellow Circle
4452.0	114.0	Husky Oil Operations Ltd	Yellow Circle
4551.0	114.0	Husky Oil Operations Ltd	Yellow Circle
4551.0	114.0	Husky Oil Operations Ltd	Yellow Circle

Table B.8: Vitrinite reflectance data from BASIN database for Glooscap C-63. The symbol is the colour of the data point on the 1D calibration plot.

Vitrinite Reflectance					
Measured Depth (m)	Degree	Vitrinite Standard Deviation	Source	Year	Symbol
420.0	0.37	0.05	Avery, M.P.	1988	Green Diamond
690.0	0.31	0.05	Avery, M.P.	1988	Green Diamond
860.0	0.38	0.06	Avery, M.P.	1988	Green Diamond
1020.0	0.4	0.07	Avery, M.P.	1988	Green Diamond
1200.0	0.39	0.05	Avery, M.P.	1988	Green Diamond
1410.0	0.44	0.03	Avery, M.P.	1988	Green Diamond
1590.0	0.49	0.06	Avery, M.P.	1988	Green Diamond
1860.0	0.46	0.05	Avery, M.P.	1988	Green Diamond
2040.0	0.49	0.07	Avery, M.P.	1988	Green Diamond
2250.0	0.63	0.06	Avery, M.P.	1988	Green Diamond
2400.0	0.56	0.08	Avery, M.P.	1988	Green Diamond
2550.0	0.83	0.07	Avery, M.P.	1988	Green Diamond
2730.0	0.77	0.06	Avery, M.P.	1988	Green Diamond
3000.0	0.79	0.00	Avery, M.P.	1988	Green Diamond
3480.0	1.09	0.01	Avery, M.P.	1988	Green Diamond

Table B.9: Temperature data from BASIN database for Hesper I-52. The symbol is the colour of the data point on the 1D calibration plot.

Temperature			
Measured Depth (m)	Temperature (C)	Source	Symbol
714.8	17.8	Petro-Canada	Yellow Circle
727.3	17.8	Petro-Canada	Yellow Circle
1419.0	42.8	Issler 1982	Pink Circle
2788.0	82.7	Issler 1982	Pink Circle
2797.5	68.8	Petro-Canada	Yellow Circle
2797.5	76.6	Petro-Canada	Yellow Circle
2797.8	68.3	Petro-Canada	Yellow Circle
2798.4	70.5	Petro-Canada	Yellow Circle
2799.0	73.3	Petro-Canada	Yellow Circle

Table B.10: Vitrinite reflectance data from BASIN database for Hesper I-52. The symbol is the colour of the data point on the 1D calibration plot.

Vitrinite Reflectance					
Measured Depth (m)	Degree	Vitrinite Standard Deviation	Source	Year	Symbol
585.22	0.27	0.06	Avery, M.P.	2008	Green Diamond
1106.44	0.28	0.03	Avery, M.P.	2008	Green Diamond
1216.17	0.36	0.04	Avery, M.P.	2008	Green Diamond
1911.12	0.4	0.05	Avery, M.P.	2008	Green Diamond
2124.48	0.47	0.04	Avery, M.P.	2008	Green Diamond
2215.92	0.48	0.05	Avery, M.P.	2008	Green Diamond
2337.84	0.47	0.04	Avery, M.P.	2008	Green Diamond
2612.17	0.52	0.06	Avery, M.P.	2008	Green Diamond
2734.09	0.6	0.08	Avery, M.P.	2008	Green Diamond

Table B.11: Temperature data from BASIN database for Hesper P-52. The symbol is the colour of the data point on the 1D calibration plot. There is no available vitrinite reflectance for Hesper P-52.

Temperature			
Measured Depth (m)	Temperature (C)	Source	Symbol
3060.0	78.0	Husky Oil Operations Ltd	Yellow Circle
3064.0	74.0	Husky Oil Operations Ltd	Yellow Circle
3068.0	76.0	Husky Oil Operations Ltd	Yellow Circle
3068.0	76.0	Husky Oil Operations Ltd	Yellow Circle
3068.0	78.0	Husky Oil Operations Ltd	Yellow Circle
3070.0	74.0	Husky Oil Operations Ltd	Yellow Circle
4884.7	109.0	Husky Oil Operations Ltd	Yellow Circle
4899.0	107.0	Husky Oil Operations Ltd	Yellow Circle
4901.0	109.0	Husky Oil Operations Ltd	Yellow Circle
4913.0	107.0	Husky Oil Operations Ltd	Yellow Circle
5234.7	131.0	Husky Oil Operations Ltd	Yellow Circle
5236.0	130.0	Husky Oil Operations Ltd	Yellow Circle
5237.0	131.0	Husky Oil Operations Ltd	Yellow Circle
5237.0	131.0	Husky Oil Operations Ltd	Yellow Circle
5237.0	131.0	Husky Oil Operations Ltd	Yellow Circle
5240.0	127.0	Husky Oil Operations Ltd	Yellow Circle
5242.0	129.0	Husky Oil Operations Ltd	Yellow Circle
5676.5	147.0	Husky Oil Operations Ltd	Yellow Circle
5680.0	147.0	Husky Oil Operations Ltd	Yellow Circle
5686.0	147.0	Husky Oil Operations Ltd	Yellow Circle
5689.0	146.0	Husky Oil Operations Ltd	Yellow Circle
5689.0	147.0	Husky Oil Operations Ltd	Yellow Circle
5689.0	147.0	Husky Oil Operations Ltd	Yellow Circle
5689.0	147.0	Husky Oil Operations Ltd	Yellow Circle

Table B.12: Temperature data from BASIN database for Missisauga H-54. The symbol is the colour of the data point on the 1D calibration plot.

Temperature			
Measured Depth (m)	Temperature (C)	Source	Symbol
538.0	47.2	Issler 1982	Pink Circle
1508.2	41.1	Shell Canada Ltd	Yellow Circle
1509.0	45.3	Issler 1982	Pink Circle
2882.2	72.2	Shell Canada Ltd	Yellow Circle
3039.0	86.1	Issler 1982	Pink Circle
3040.1	81.0	Shell Canada Ltd	Yellow Circle
3973.7	19.4	Shell Canada Ltd	Yellow Circle
3974.0	97.7	Shell Canada Ltd	Yellow Circle
3974.0	103.9	Issler 1982	Pink Circle
4185.8	99.9	Shell Canada Ltd	Yellow Circle
4186.0	124.4	Issler 1982	Pink Circle
4188.0	93.2	Shell Canada Ltd	Yellow Circle

Table B.13: Vitrinite reflectance data from BASIN database for Missisauga H-54. The symbol is the colour of the data point on the 1D calibration plot.

Vitrinite Reflectance					
Measured Depth (m)	Degree	Vitrinite Standard Deviation	Source	Year	Symbol
2761.0	0.54		Hacquebard, P.A.	1973	Green Diamond
3321.0	0.56		Hacquebard, P.A.	1973	Green Diamond
3398.0	0.60		Hacquebard, P.A.	1973	Green Diamond
3477.0	0.63		Hacquebard, P.A.	1973	Green Diamond
3617.0	0.49		Hacquebard, P.A.	1973	Green Diamond
3709.0	0.66		Hacquebard, P.A.	1973	Green Diamond
3794.0	0.65		Hacquebard, P.A.	1973	Green Diamond
3820.0	0.70		Hacquebard, P.A.	1973	Green Diamond

Table B.14: Temperature data from BASIN database for Moheida P-15. The symbol is the colour of the data point on the 1D calibration plot. There is no available vitrinite reflectance for Moheida P-15.

Temperature			
Measured Depth (m)	Temperature (C)	Source	Symbol
900.8	24.2	Issler 1982	Pink Circle
1931.8	59.7	Issler 1982	Pink Circle
3517.8	114.2	Issler 1982	Pink Circle
3529.0	105.5	Petro-Canada	Yellow Circle
4280.8	125.4	Issler 1982	Pink Circle
4283.4	115.4	Petro-Canada	Yellow Circle
4290.1	122.1	Petro-Canada	Yellow Circle
4291.9	115.4	Petro-Canada	Yellow Circle
4292.2	121.0	Petro-Canada	Yellow Circle

Table B.15: Temperature data from BASIN database for Mohican I-100. The symbol is the colour of the data point on the 1D calibration plot.

Temperature			
Measured Depth (m)	Temperature (C)	Source	Symbol
2028.2	55.7	Issler, 1982	Pink Circle
3366.2	100.0	Issler, 1982	Pink Circle
4239.8	102.7	Shell Canada Ltd	Yellow Circle
4253.2	123.5	Issler, 1982	Pink Circle
4254.4	109.9	Shell Canada Ltd	Yellow Circle
4254.4	109.9	Shell Canada Ltd	Yellow Circle
4393.4	114.3	Shell Canada Ltd	Yellow Circle

Table B.16: Vitrinite reflectance data from BASIN database for Mohican I-100. The symbol is the colour of the data point on the 1D calibration plot.

Vitrinite Reflectance					
Measured Depth (m)	Degree	Vitrinite Standard Deviation	Source	Year	Symbol
640.1	0.21		Robertson Research International Ltd	1976	Green Diamond
704.1	0.22		Robertson Research International Ltd	1976	Green Diamond
768.1	0.19		Robertson Research International Ltd	1976	Green Diamond
823.0	0.23		Robertson Research International Ltd	1976	Green Diamond
951.0	0.22		Robertson Research International Ltd	1976	Green Diamond
1005.9	0.21		Robertson Research International Ltd	1976	Green Diamond
1069.9	0.24		Robertson Research International Ltd	1976	Green Diamond
1133.9	0.22		Robertson Research International Ltd	1976	Green Diamond
1316.8	0.26		Robertson Research International Ltd	1976	Green Diamond
1499.6	0.32		Robertson Research International Ltd	1976	Green Diamond
1554.5	0.37		Robertson Research International Ltd	1976	Green Diamond
1682.5	0.28		Robertson Research International Ltd	1976	Green Diamond
2164.1	0.23		Robertson Research International Ltd	1976	Green Diamond
2225.1	0.29		Robertson Research International Ltd	1976	Green Diamond
2286.0	0.37		Robertson Research International Ltd	1976	Green Diamond
2347.0	0.35		Robertson Research International Ltd	1976	Green Diamond
2590.8	0.37		Robertson Research International Ltd	1976	Green Diamond
3322.4	0.45		Robertson Research International Ltd	1976	Green Diamond
3413.8	0.52		Robertson Research International Ltd	1976	Green Diamond
3505.2	0.54		Robertson Research International Ltd	1976	Green Diamond

3596.7	0.53	Robertson Research International Ltd	1976	Green Diamond
4053.9	0.58	Robertson Research International Ltd	1976	Green Diamond
4328.2	0.57	Robertson Research International Ltd	1976	Green Diamond

Table B.17: Temperature data from BASIN database for Torbrook C-15. The symbol is the colour of the data point on the 1D calibration plot.

Temperature				
Measured Depth (m)	Temperature (C)	Source		Symbol
3150.0	48.0	Encana		Yellow Circle
3537.0	56.0	Encana		Yellow Circle
3547.0	51.0	Encana		Yellow Circle
3570.0	51.0	Encana		Yellow Circle
3570.0	51.0	Encana		Yellow Circle
3570.0	51.0	Encana		Yellow Circle
3570.0	51.0	Encana		Yellow Circle

Table B.18: Vitrinite reflectance data from BASIN database for Torbrook C-15. The symbol is the colour of the data point on the 1D calibration plot.

Vitrinite Reflectance					
Measured Depth (m)	Degree	Vitrinite Standard Deviation	Source	Year	Symbol
2665	0.29	0.06	Mukhopadhyay, P.K.	2006	Green Diamond
2955	0.32	0.05	Mukhopadhyay, P.K.	2006	Green Diamond
3125	0.34	0.04	Mukhopadhyay, P.K.	2006	Green Diamond
3245	0.35	0.05	Mukhopadhyay, P.K.	2006	Green Diamond
3495	0.37	0.08	Mukhopadhyay, P.K.	2006	Green Diamond
3535	0.36	0.06	Mukhopadhyay, P.K.	2006	Green Diamond
3600	0.36	0.05	Mukhopadhyay, P.K.	2006	Green Diamond

Table B.19: Temperature data from BASIN database for Sachem D-76. The symbol is the colour of the data point on the 1D calibration plot.

Temperature			
Measured Depth (m)	Temperature (C)	Source	Symbol
1170.4	32.2	Issler 1982	Yellow Circle
3053.8	79.4	Mobil Oil Canada Ltd	Yellow Circle
3121.4	79.4	Issler 1982	Pink Circle
4868.3	113.2	Mobil Oil Canada Ltd	Pink Circle
4869.2	103.2	Mobil Oil Canada Ltd	Yellow Circle
4874.4	110.0	Issler 1982	Yellow Circle
4876.2	105.5	Mobil Oil Canada Ltd	Yellow Circle
4876.2	112.1	Mobil Oil Canada Ltd	Yellow Circle
4876.2	112.1	Mobil Oil Canada Ltd	Yellow Circle
4876.5	103.2	Mobil Oil Canada Ltd	Yellow Circle

Table B.20: Vitrinite reflectance data from BASIN database for Sachem D-76. The symbol is the colour of the data point on the 1D calibration plot.

Vitrinite Reflectance					
Measured Depth (m)	Degree	Vitrinite Standard Deviation	Source	Year	Symbol
868.7	0.34		Davies, E.H.	1983	Green Diamond
1399.1	0.33		Davies, E.H.	1983	Green Diamond
2054.4	0.49		Davies, E.H.	1983	Green Diamond
2164.1	0.5		Davies, E.H.	1983	Green Diamond
2191.5	0.44		Davies, E.H.	1983	Green Diamond
2246.4	0.46		Davies, E.H.	1983	Green Diamond
2273.8	0.45		Davies, E.H.	1983	Green Diamond
2328.7	0.43		Davies, E.H.	1983	Green Diamond
2438.4	0.46		Davies, E.H.	1983	Green Diamond
2529.9	0.46		Davies, E.H.	1983	Green Diamond
2593.9	0.48		Davies, E.H.	1983	Green Diamond
2721.9	0.46		Davies, E.H.	1983	Green Diamond
2776.8	0.52		Davies, E.H.	1983	Green Diamond
2840.8	0.48		Davies, E.H.	1983	Green Diamond
2950.5	0.51		Davies, E.H.	1983	Green Diamond
3179.1	0.51		Davies, E.H.	1983	Green Diamond
3206.5	0.58		Davies, E.H.	1983	Green Diamond
3352.8	0.59		Davies, E.H.	1983	Green Diamond
3983.8	0.64		Davies, E.H.	1983	Green Diamond

4121.0	0.65	Davies, E.H.	1983	Green Diamond
4203.2	0.71	Davies, E.H.	1983	Green Diamond
4285.5	0.73	Davies, E.H.	1983	Green Diamond
4340.4	0.73	Davies, E.H.	1983	Green Diamond
4505.0	0.74	Davies, E.H.	1983	Green Diamond
4532.4	0.78	Davies, E.H.	1983	Green Diamond
4642.2	0.84	Davies, E.H.	1983	Green Diamond
4724.5	0.75	Davies, E.H.	1983	Green Diamond
4855.5	0.84	Davies, E.H.	1983	Green Diamond

Table B.21: Temperature data from BASIN database for South Griffin J-13. The symbol is the colour of the data point on the 1D calibration plot.

Temperature			
Measured Depth (m)	Temperature (C)	Source	Symbol
905.0	33.0	Husky Oil Operations Ltd	Yellow Circle
3076.3	58.0	Husky Oil Operations Ltd	Yellow Circle
3108.0	66.0	Husky Oil Operations Ltd	Yellow Circle
4700.0	112.0	Husky Oil Operations Ltd	Yellow Circle
4719.0	102.0	Husky Oil Operations Ltd	Yellow Circle
4719.0	112.0	Husky Oil Operations Ltd	Yellow Circle
4719.0	112.0	Husky Oil Operations Ltd	Yellow Circle
4720.0	108.0	Husky Oil Operations Ltd	Yellow Circle
4722.0	112.0	Husky Oil Operations Ltd	Yellow Circle
4727.0	110.0	Husky Oil Operations Ltd	Yellow Circle
4773.0	110.0	Husky Oil Operations Ltd	Yellow Circle
5460.0	151.0	Husky Oil Operations Ltd	Yellow Circle
5905.0	154.0	Husky Oil Operations Ltd	Yellow Circle
5905.0	154.0	Husky Oil Operations Ltd	Yellow Circle
5910.0	144.0	Husky Oil Operations Ltd	Yellow Circle
5919.0	144.0	Husky Oil Operations Ltd	Yellow Circle
5919.0	146.0	Husky Oil Operations Ltd	Yellow Circle
5919.0	146.0	Husky Oil Operations Ltd	Yellow Circle
5919.0	146.0	Husky Oil Operations Ltd	Yellow Circle
5919.0	148.0	Husky Oil Operations Ltd	Yellow Circle
5919.0	148.0	Husky Oil Operations Ltd	Yellow Circle
5919.0	148.0	Husky Oil Operations Ltd	Yellow Circle
5919.0	154.0	Husky Oil Operations Ltd	Yellow Circle

Table B.22: Vitrinite reflectance data from BASIN database for South Griffin J-13. The symbol is the colour of the data point on the 1D calibration plot.

Vitrinite Reflectance					
Measured Depth (m)	Degree	Vitrinite Standard Deviation	Source	Year	Symbol
560	0.2	0.02	Avery, M.P.	1988	Green Diamond
800	0.29	0.03	Avery, M.P.	1988	Green Diamond
1280	0.31	0.04	Avery, M.P.	1988	Green Diamond
1525	0.34	0.05	Avery, M.P.	1988	Green Diamond
2005	0.38	0.03	Avery, M.P.	1988	Green Diamond
2240	0.46	0.06	Avery, M.P.	1988	Green Diamond
2600	0.51	0.05	Avery, M.P.	1988	Green Diamond
2840	0.53	0.06	Avery, M.P.	1988	Green Diamond
3085	0.6	0.09	Avery, M.P.	1988	Green Diamond
3205	0.64	0.05	Avery, M.P.	1988	Green Diamond
3325	0.67	0.08	Avery, M.P.	1988	Green Diamond
3585	0.71	0.07	Avery, M.P.	1988	Green Diamond
3735	0.79	0.07	Avery, M.P.	1988	Green Diamond
3885	0.79	0.09	Avery, M.P.	1988	Green Diamond
4035	0.94	0.06	Avery, M.P.	1988	Green Diamond
4245	0.97	0.08	Avery, M.P.	1988	Green Diamond
4695	0.99	0.05	Avery, M.P.	1988	Green Diamond
4935	1.18	0.06	Avery, M.P.	1988	Green Diamond
5055	1.23	0.07	Avery, M.P.	1988	Green Diamond
5475	1.41	0.07	Avery, M.P.	1988	Green Diamond
5655	1.67	0.11	Avery, M.P.	1988	Green Diamond

Table B.23: Temperature data from BASIN database for Wyandot E-53. The symbol is the colour of the data point on the 1D calibration plot.

Temperature			
Measured Depth (m)	Temperature (C)	Source	Symbol
781.4	29.6	Issler 1982	Pink Circle
1562.4	43.2	Issler 1982	Pink Circle
2368.3	53.3	Shell Canada Ltd	Yellow Circle
2790.4	76.4	Issler 1982	Pink Circle
2792.9	67.7	Shell Canada Ltd	Yellow Circle
2881.0	70.5	Shell Canada Ltd	Yellow Circle
3047.1	73.3	Shell Canada Ltd	Yellow Circle
3047.4	82.8	Issler 1982	Pink Circle

3048.0	75.5	Shell Canada Ltd	Yellow Circle
3048.0	78.3	Shell Canada Ltd	Yellow Circle
3048.0	78.3	Shell Canada Ltd	Yellow Circle

Table B.24: Vitrinite reflectance data from BASIN database for Wyandot E-53. The symbol is the colour of the data point on the 1D calibration plot.

Vitrinite Reflectance					
Measured Depth (m)	Degree	Vitrinite Standard Deviation	Source	Year	Symbol
940.0	0.36		Hacquebard, P.A.	1973	Green Diamond
1078.0	0.35		Hacquebard, P.A.	1973	Green Diamond
1284.0	0.36		Hacquebard, P.A.	1973	Green Diamond
1609.0	0.37		Hacquebard, P.A.	1973	Green Diamond

Appendix C: Python Code

This python code was written to read the Canstrat borehole logs. The program loads the Canstrat lithology well logs type XXXXXXXXXXXXXXXXXXXX_YYYYYYY_CS_MAIN.LAS (Example of the filename: 300C634320062000_EC00185_CS_MAIN.LAS) and uses the Canstrat lithology code RTC_ID values to calculate the ratio between two depths from the lithology log, and outputs it the console and saves the results in a text file under the borehole name.

```
__author__ = 'Carlos Wong'
# Python Script to read Canstrat CS_main.las type files to get lithology ratio
# between depth A and B.  Outputs file as
# text under well name.  For more info contact carlos.wong@dal.ca
# input_file = "300C634320062000_EC00185_CS_main.las"
# for test and development
# RTC_ID DICTIONARY values are from CANSTRAT from CS_main las file.
RTC_ID = {"1.00": "Igneous Basic",
          "2.00": "Igneous Acidic",
          "3.00": "Metamorphic",
          "4.00": "Volcanic",
          "8.00": "Siderite",
          "9.00": "Glacial Till",
          "12.00": "Conglomerate",
          "13.00": "Breccia",
          "16.00": "Chert",
          "17.00": "Sandstone",
          "18.00": "Siltstone",
          "19.00": "Clay",
          "20.00": "Shale",
          "22.00": "Bentonite",
          "24.00": "Coal",
          "26.00": "Marlstone",
          "27.00": "Limestone",
          "30.00": "Dolomite",
          "35.00": "Anhydrite",
          "37.00": "Salt",
          "39.00": "Gypsum",
          "40.00": "Phosphate",
          "-999.25": "NULL NULL NULL"}
# RTC_Cnt DICTIONARY counter for the Range of query
RTC_Cnt = {"1.00": 0,
           "2.00": 0,
           "3.00": 0,
           "4.00": 0,
           "8.00": 0,
           "9.00": 0,
           "12.00": 0,
```

```

        "13.00": 0,
        "16.00": 0,
        "17.00": 0,
        "18.00": 0,
        "19.00": 0,
        "20.00": 0,
        "22.00": 0,
        "24.00": 0,
        "26.00": 0,
        "27.00": 0,
        "30.00": 0,
        "35.00": 0,
        "37.00": 0,
        "39.00": 0,
        "40.00": 0,
        "-999.25": 0}

well = ""
# get user FILENAME and RANGE of section to query section
fileName = raw_input("Enter CanStrat filename (filename.las): ")
flag = True
#open file to get well name
f = open(fileName, "r")
for line in f:
    wordlist = line.split()
    if wordlist[0] == 'WELL.':
        wordlist = [x for x in wordlist if x != 'WELL. ']
        wordlist = [x for x in wordlist if x != ':Well']
        wordlist = [x for x in wordlist if x != 'Name']
        well = " ".join(wordlist)
        print "Well : %s" % well
    if wordlist[0] == '~A': # DATA section of LAS
        break
f.close()
print "NOTE: CanStrat is in m unit depth, check your depth unit"
print "Enter the range (round it up to xxx.10 not xxx.13: "
print "Type exit to quit script"
# file open a file to write results, file saved under wellname.txt.
fo = open(well+".txt", "w")
fo.write("***** %s *****\n\n" % well)
#repeat until user types "exit" to quit script
while flag:
    temp = raw_input("Top range : ")
    if temp.lower() != "exit":
        TopRange = float(temp)
    else:
        exit("Program Ended")
    temp = raw_input("Bottom range : ")
    if temp.lower() != "exit":
        BtmRange = float(temp)
    else:
        exit("Program Ended")
    print "The Thickness is: %s" % (BtmRange - TopRange)
# OPEN the LAS FILENAME
f = open(fileName, "r")
# f = open(input_file, "r") # for test and development only

```

```

# read LAS file line by line
flag2 = False # reading the data section
Npkg = 0 # total N numbers of the range
for line in f:
    wordlist = line.split()
    if wordlist[0] == '~A': # DATA section of LAS
        flag2 = True
        continue
    if flag2:
        if (float(wordlist[0]) >= TopRange) and (float(wordlist[0]) <=
BtmRange):
            Npkg += 1 # increment by 1 the counter
            RTC_Cnt[wordlist[1]] += 1
            if (float(wordlist[0]) > BtmRange): # Break/EXIT for loop at end
of range
                break
    print ""
    print "Range from %s to %s (n = %s):" % (TopRange, BtmRange, Npkg)
    print "==== Lithology Mix ====="
    fo.write("Range from %s to %s (n = %s):\n" % (TopRange, BtmRange, Npkg))
    fo.write("The Thickness is: %s \n" % (BtmRange - TopRange))
    fo.write("==== Lithology Mix =====\n")
    for key in RTC_Cnt:
        if RTC_Cnt[key] > 0:
            print "%s: %s %" % (RTC_ID[key], float(RTC_Cnt[key]) / Npkg *
100)
                fo.write("%s: %s %%\n" % (RTC_ID[key], float(RTC_Cnt[key]) / Npkg
* 100))
    print "==== END =====\n"
    fo.write("==== END =====\n\n")
    #reset RTC_Cnt counter
    for key in RTC_Cnt:
        RTC_Cnt[key] = 0
    f.close()
fo.close()

```

Appendix D: Uncertainty Tests with Petro Risk

D.1 Calibration

To calibrate this model with the input heat flow, so it closely matches our measured data from the borehole. An uncertainty analysis simulation was run with PetroRisk, a module within PetroMod. This module allows uncertainties in geologic input data that are being used for the construction of the model (e.g. lithofacies properties and distributions, heat flow, source rocks, and boundary conditions such as erosion and tectonic influences) to be defined and the effects of these uncertainties on the outcome of the model to be quantified and statistically evaluated. We ran a Monte Carlo (MC) simulation on this model, which sample points are selected without considering the previously generated sample points sampling distribution, which is a random sampling. Each model was tested with a Monte Carlo simulation 100 times, and the resulting output displays the confidence interval of the probability distribution for the modelled borehole. This confidence interval is represented in percentiles of 10 percentile (P10) and 90 percentile (P90) pink lines in the resulting outputs represent the confidence interval.

Using PetroRisk in PetroMod, we test some uncertainties on the model. The model has tested two parameters:

3. **Heat flow uncertainty:** Values are drawn from a probability distribution shift the heat flow trend of the model. In this study, we use a normal distribution with a confidence interval of 10% and 90%.with uncertainty time frame of 225 Ma to 0 Ma with a 10 and 90 percentile.
4. **Heat flow time shift uncertainty:** The heat flow trend of the model is shifted in geological time according to a probability distribution. For this study, we use a normal

distribution with a set the time shift to be a 10 and 90 percentile of a normal distribution (-6.4 Ma to 6.4 Ma).

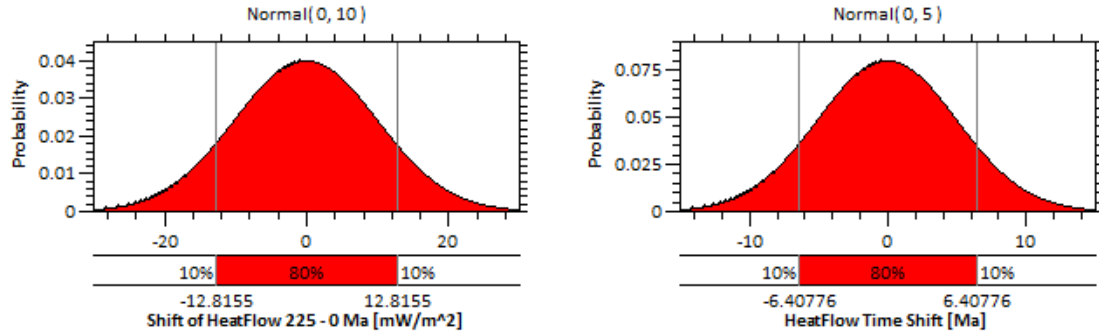


Figure D.2: The uncertainties parameters used to test the model, left is the shift of heat flow from 225 Ma to 0 Ma and right is the heat flow time shift.

D.2 NovaSPAN 1100

Bonnet P-23

After running the Monte Carlo simulation, the following results were acceptable when comparing our simulated model runs (Figure D. and Figure D.4).

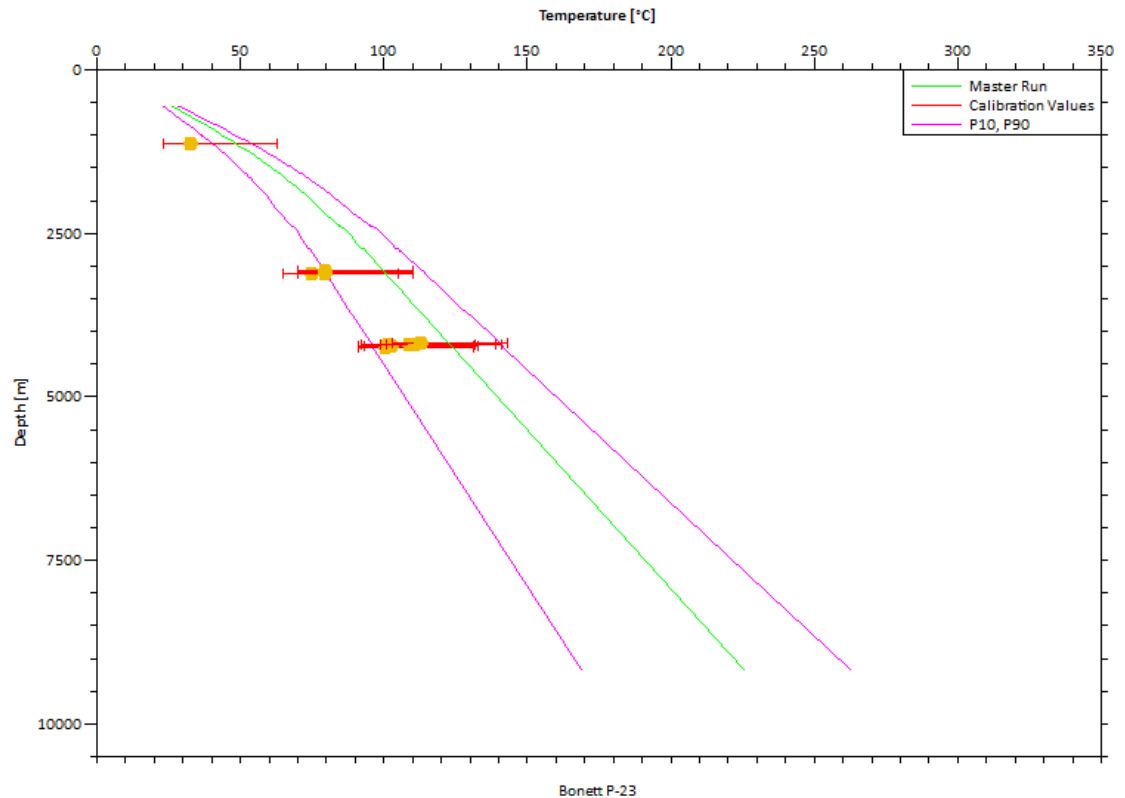


Figure D.3: Temperature plot Bonnet P-23. P10 and P90 confidence lines are in pink. We can see that the modelled line (green) is within the confidence range. The yellow circles are measured data from the borehole.

The temperature model from the Monte Carlo run shows us that the model is within the temperatures parameters. The pink lines are the P10 and P90 based on the heat flow uncertainty parameter, and the green line is the model run (Figure 2.4). The vitrinite reflectance falls within an acceptable range. Here we see two different datasets in the borehole reports. One data set is from Petro-Canada (1985) and the second is from Avery (2003).

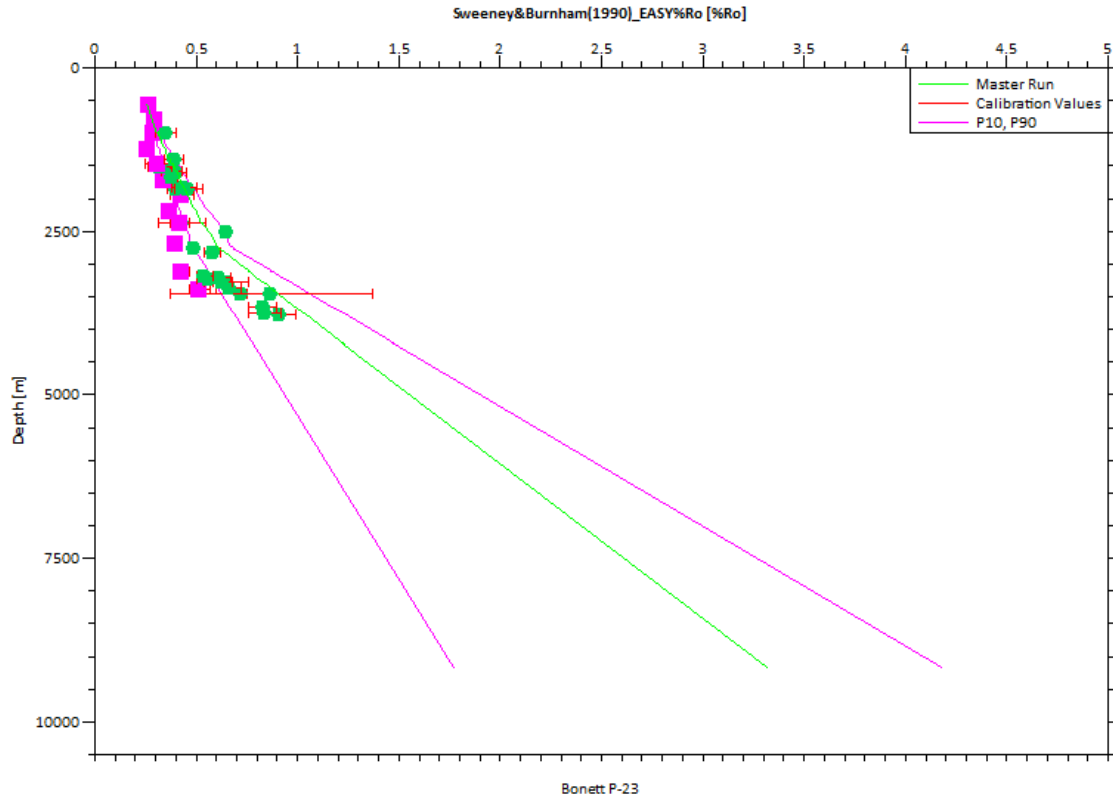


Figure D.4: Vitrinite Reflectance plot of Bonnet P-23. P10 and P90 confidence lines are in pink. We can see that the modelled line (green) is within the confidence range. The pink squares (Avery, M.P., 2003) and green circles (Petro-Canada, 1985) are measured data from the borehole.

D.3 NovaSPAN 1400

The model results with these uncertainties parameters (Figure D.) shows that the vitrinite reflectance and temperature values are within the uncertainty parameters test. The sensitivity tests show a positive result that the Moheida P-15 and Torbrook C-15 borehole vitrinite reflectance and temperature graph matches the borehole data. This means that the model is valid within the parameters used during the simulations (Figure D.5 and Figure D.6). We use Moheida P-15 and Torbrook C-15 boreholes to calibrate the model because these boreholes are not offset from the NovaSPAN seismic line.

Moheida P-15

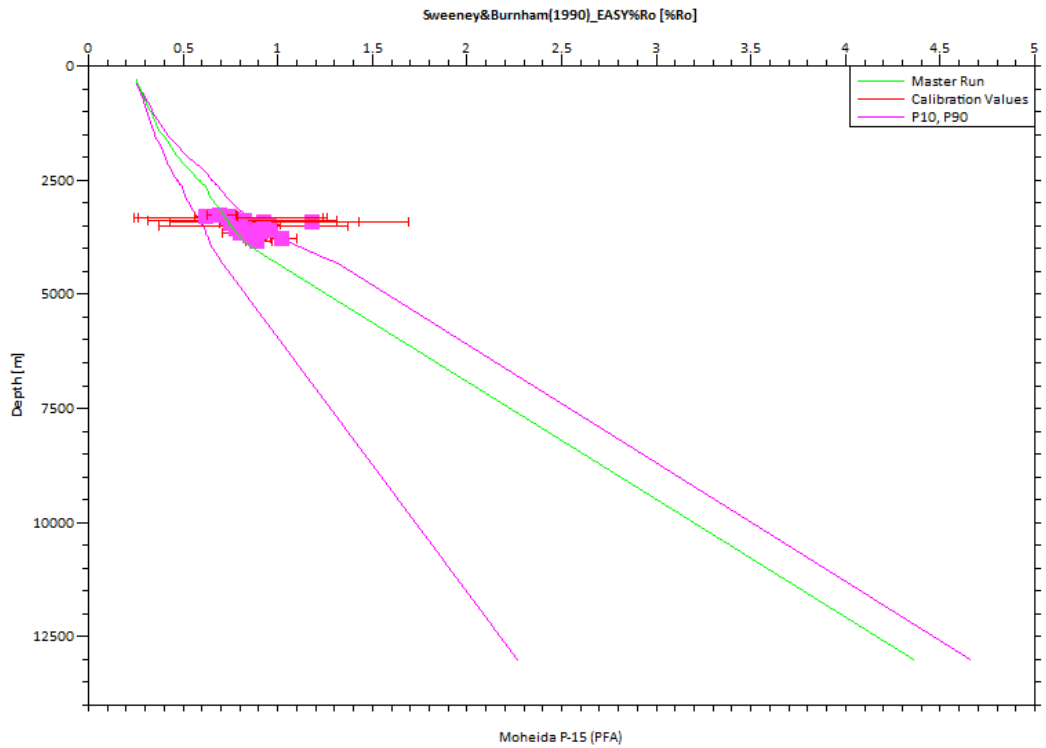
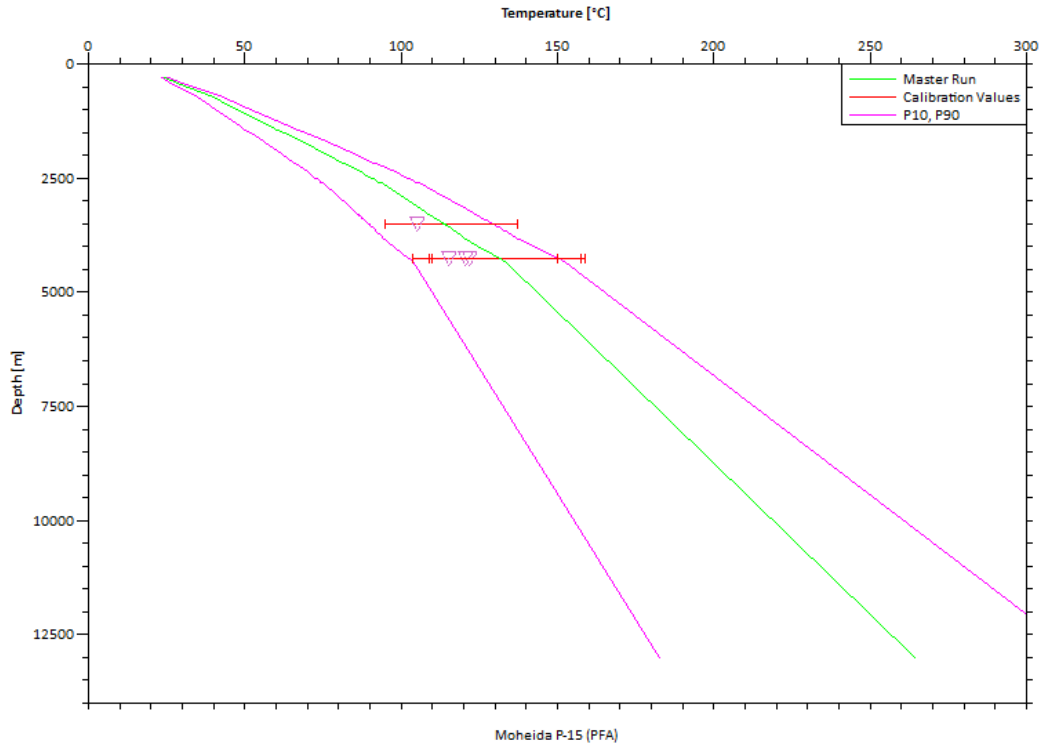


Figure D.5: Uncertainty test results from Monte Carlo Simulation for Moheida P-15. The green line is the modelled line, and pink lines are P10 and P90.

Torbrook C-15

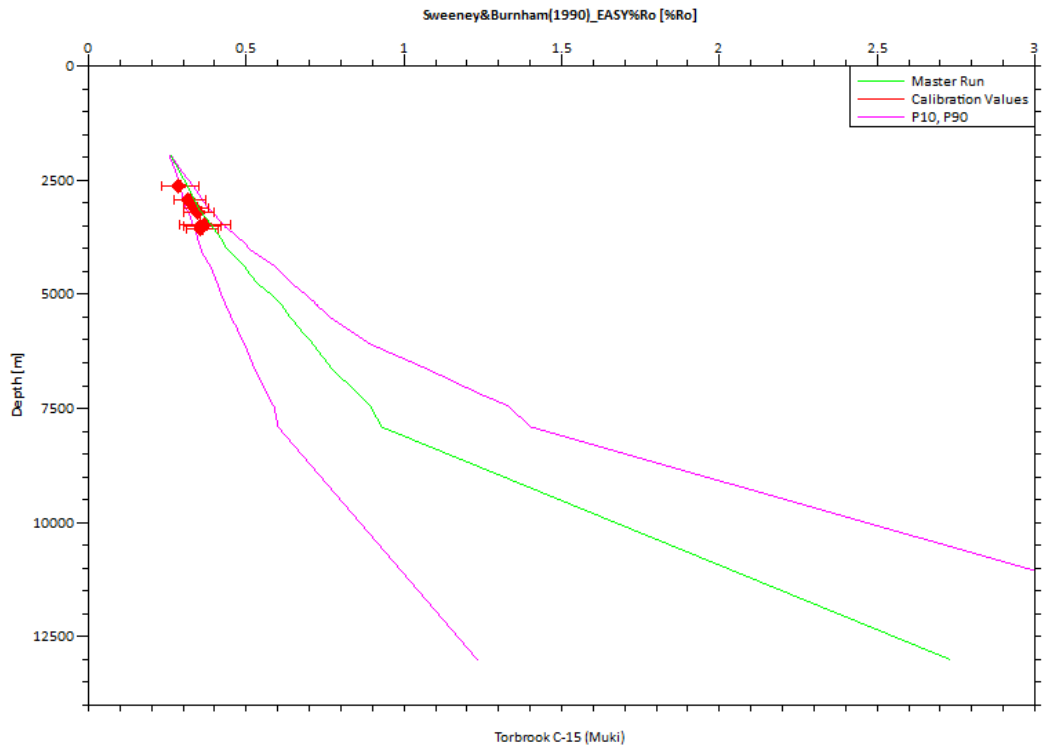
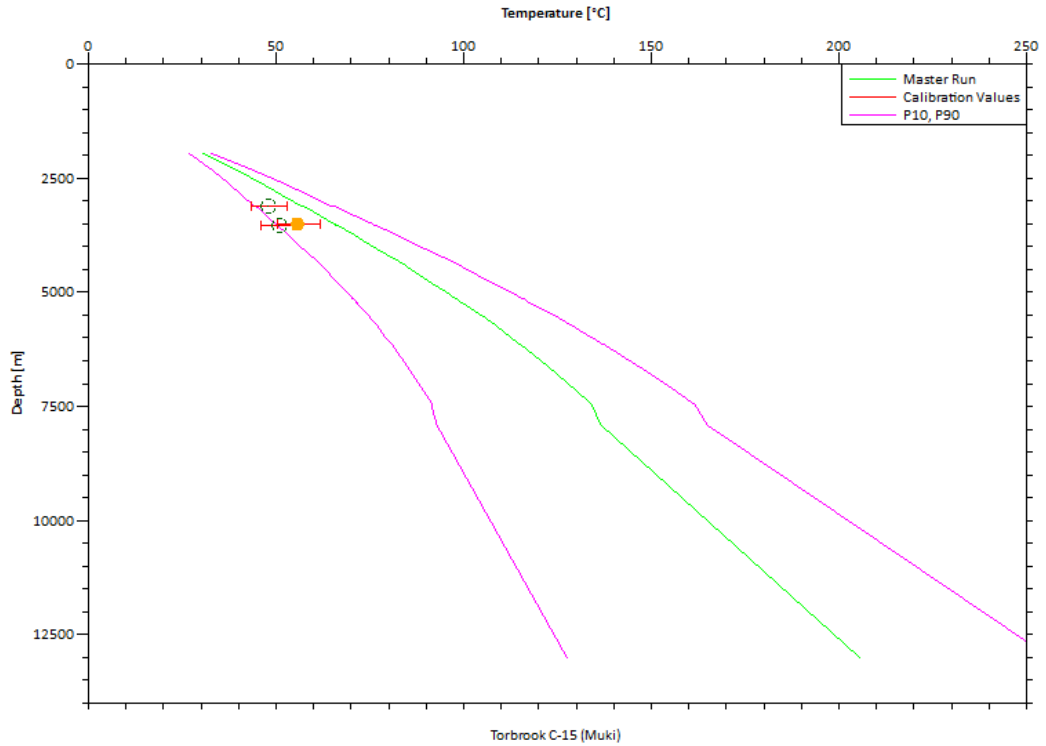


Figure D.6: Uncertainty test results from Monte Carlo simulation for Torbrook C-15. The green line is the modelled line, and pink lines are P10 and P90.

D.4 NovaSPAN 1800

The model results with these uncertainties parameters (Figure D.) shows that the vitrinite reflectance and temperature values are within the uncertainty parameters test.

Bluenose G-47

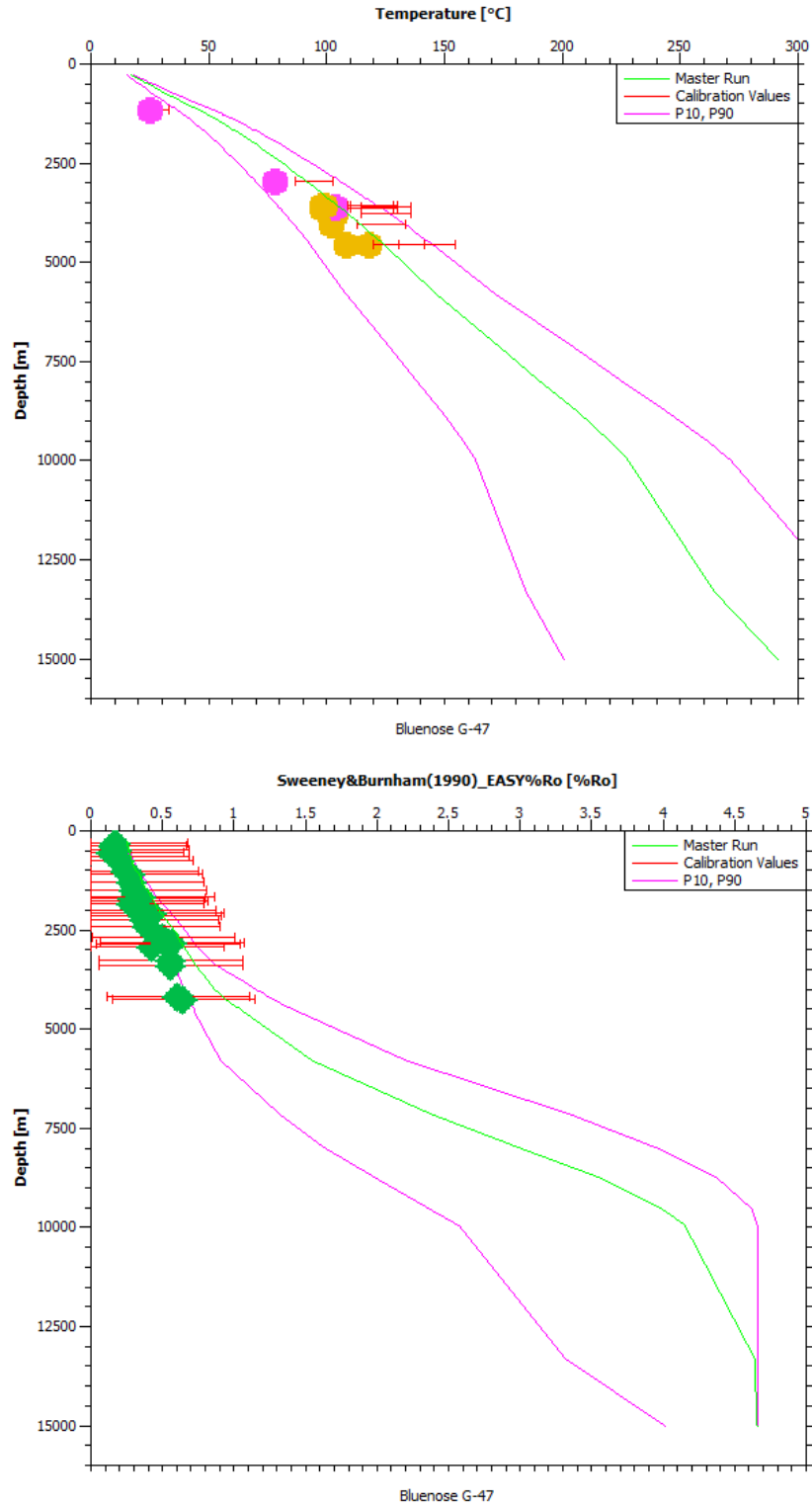


Figure D.7: Uncertainty test results from Monte Carlo Simulation for Bluenose G-47. The green line is the modelled line, and pink lines are P10 and P90.

Bluenose 2G-47

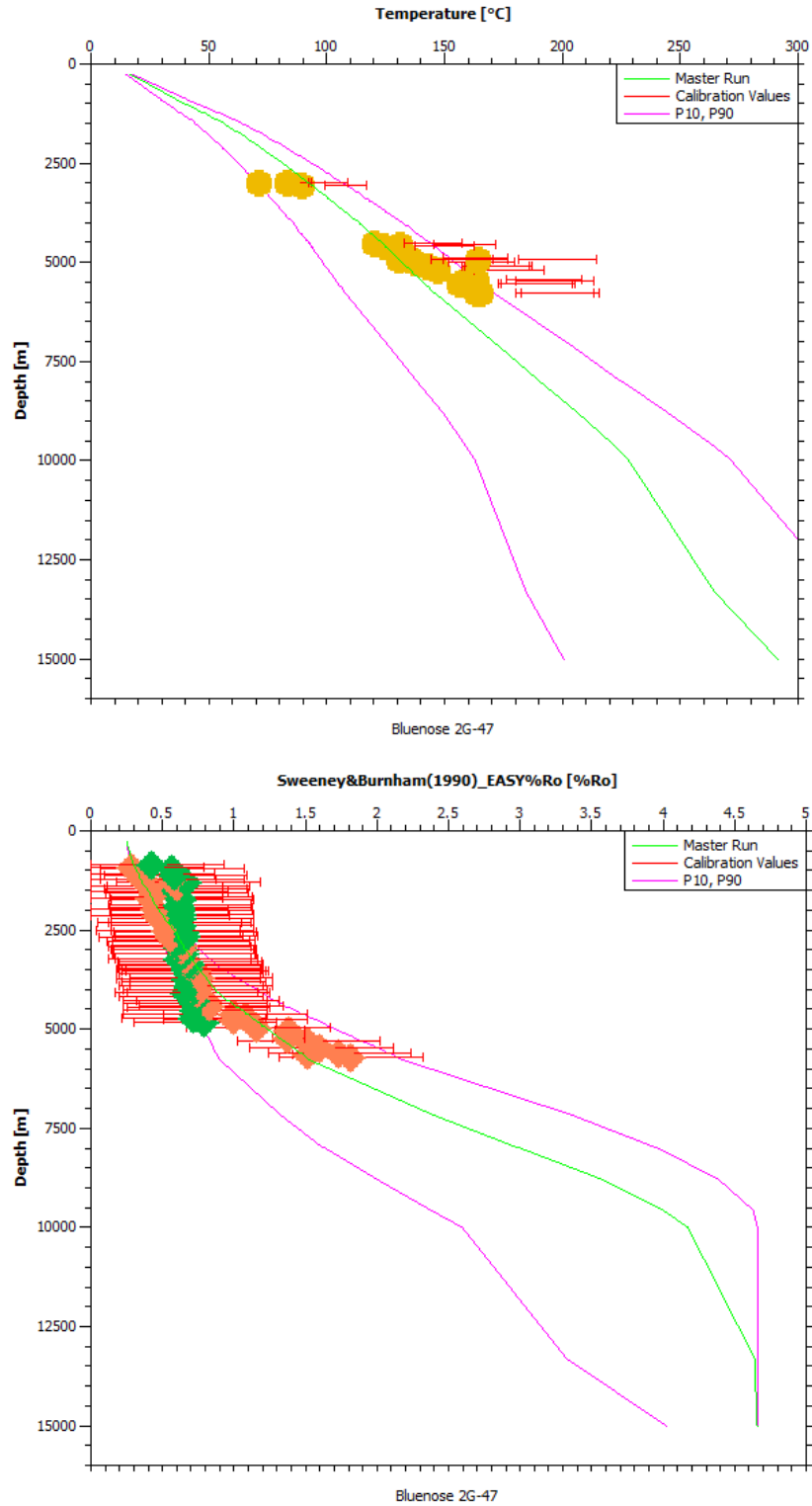


Figure D.8: Uncertainty test results from Monte Carlo Simulation for Bluenose 2G-47. The green line is the modelled line, and pink lines are P10 and P90.

D.5 NovaSPAN 2000

The results from this model would show differences between the model and the calibration data (Figures 0.90 - 0.11).

Hesper I-52

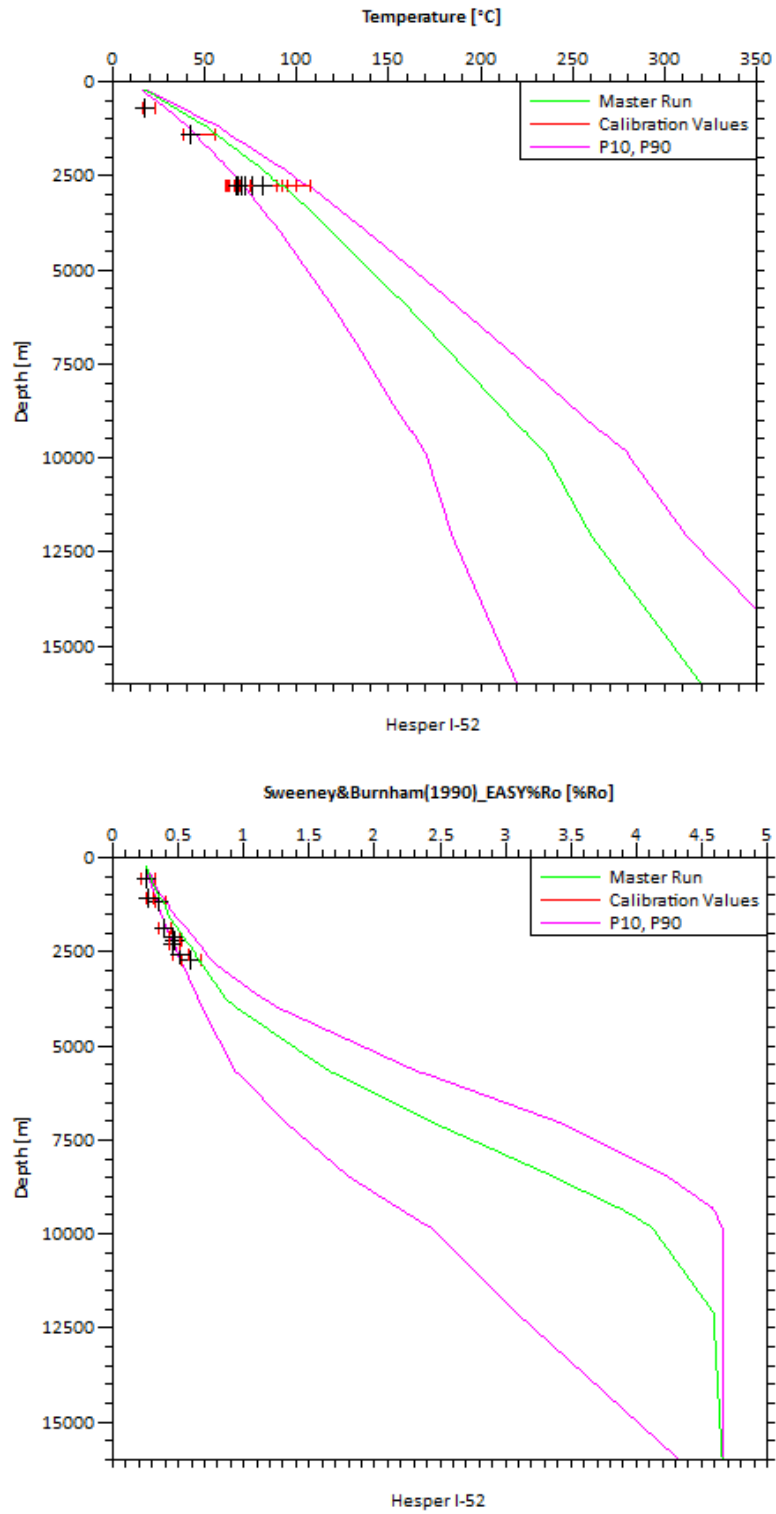


Figure D.9: Uncertainty test results from Monte Carlo Simulation for Hesper I-52. The green line is the modelled line, and pink lines are P10 and P90.

Hesper P-52

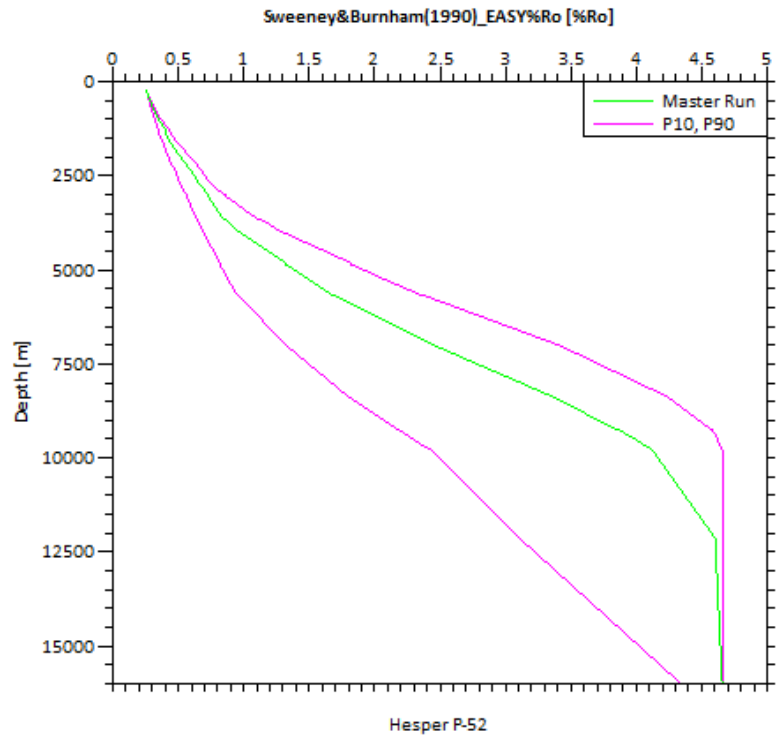
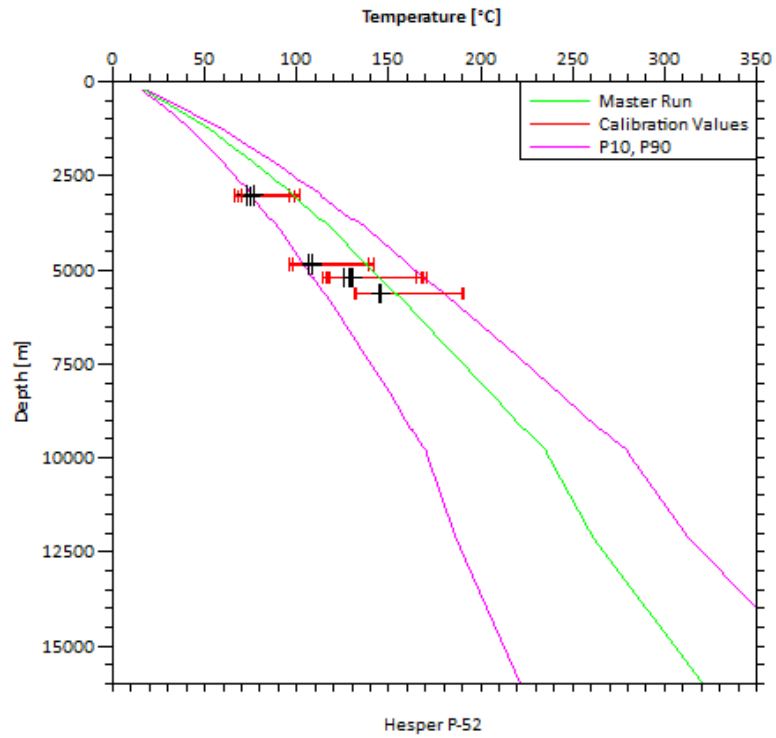


Figure D.10: Uncertainty test results from Monte Carlo Simulation for Hesper P-52. The green line is the modelled line, and pink lines are P10 and P90.

Sachem D-76

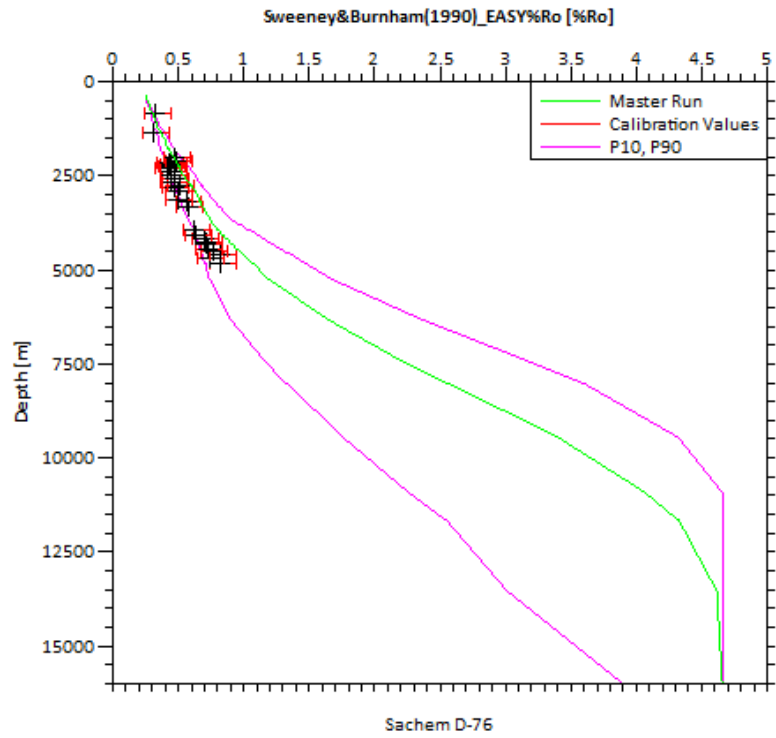
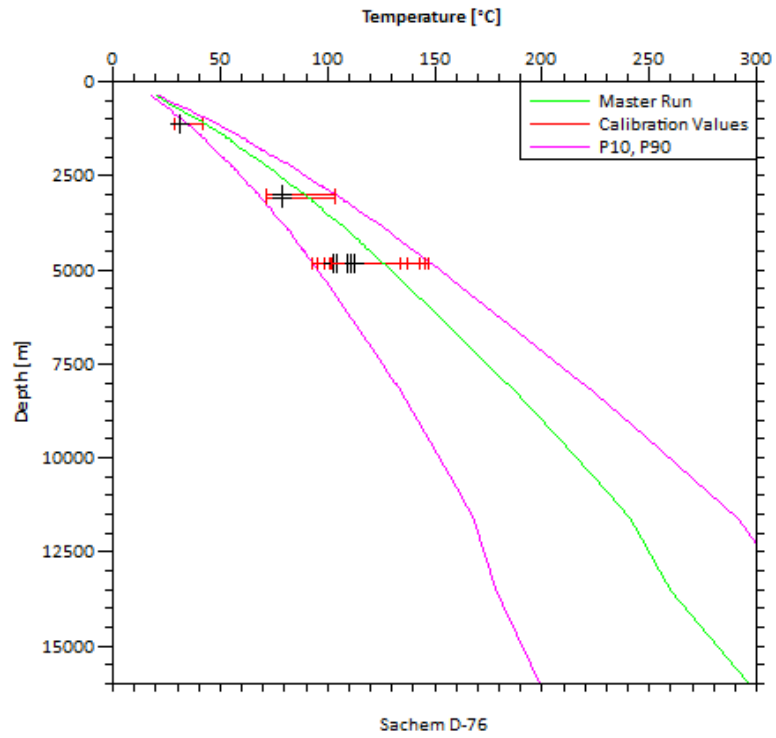


Figure D.11: Uncertainty test results from Monte Carlo Simulation for Sachem D-76. The green line is the modelled line, and pink lines are P10 and P90.